Therapeutic Approaches to Insulin Resistance and Type 2 Diabetes

Siobhán Leonard, B.Sc.

A thesis submitted to National University of Ireland, Maynooth

for the degree of Doctor of Philosophy

October 2015

Biology Department,

National University of Ireland, Maynooth

Supervisor: Prof. John Findlay

Head of Department: Prof. Paul Moynagh

Contents

Declaration

I hereby declare that the contents of this thesis are entirely my own work and that it has not been previously submitted as an exercise for a degree to this or any other university. The work and information of others have been acknowledged and cited in the text.

Signature: Siobhán Leonard

Date: 10/05/16

Acknowledgements

I would first and foremost like to thank my supervisor Professor John Findlay. I would not have gotten to this stage without the advice, support and encouragement he has given to me over the last four years. I would also like to thank Dr. Donal O'Gorman for his guidance as I began this project. I am sincerely grateful to the Higher Education Authority for funding this research under the PRTLI Cycle 5 BioAT Programme.

To all my colleagues at NUIM, especially the members of the Membrane Protein Lab, thank you for your support and for sharing your expertise. Kate, Pam, Adam, Gemma, Darren, Conor and Elisa, I would have been lost without your help and guidance.

To my amazing friends that have been there through it all, Helen, Susan, Thérèse, Zita, Fiona, and Jen, I can't thank you enough, the chats, coffee and chocolate kept me going. Nikki, thank you for listening to my endless rants, for dragging me out of my thesis cave and for being a constant source of entertainment.

To my family, my Mam and Dad, my sisters, Audrey and Fiona and my brothers, Martin and Peter, you have supported me in more ways than words can describe. I know I wouldn't have gotten this far without you and for that I am so grateful.

Finally, Karl, thank you for being there, for believing in me when I couldn't, for understanding that five more minutes in the lab never meant five more minutes and for always knowing how to make me smile. I can't imagine doing anything without you and this was no exception.

Abstract

Type 2 diabetes is a chronic metabolic disorder primarily caused by a systemic insulin resistant state to which obesity is a major contributor. Increasing visceral adipose tissue augments adipokine secretion provoking an enduring low-grade inflammatory response that negatively impacts on the insulin signalling cascade. In an intervention study of a murine diet-induced model of type 2 diabetes, a novel compound, RTC-1, designed to reduce serum levels of one such adipokine, RBP, improved glucose handling and prevented weight gain. This compound also had a direct positive effect on glucose uptake *in vitro*, independent of its predicted mode of action. Through cellular analysis this study has established the mechanism by which this is achieved. RTC-1 was found to inhibit complex I of the mitochondrial respiratory chain (NADH:ubiquinone oxidoreductase), leading to a likely increase in the AMP to ATP ratio and the consequential activation of the cellular energy regulator, AMPK. This in turn stimulated the signalling pathway which enhanced the incorporation of the glucose transporter, GLUT4, into the plasma membrane. RTC-1 was also found to prevent adipogenesis and induced osteogenesis in an AMPK dependent manner. Additionally, RTC-1 was observed to provoke an increase in insulin sensitivity.

In a separate project, the signalling capabilities of an orphan GPCR, GPR21, were investigated. Knockout studies have suggested a role for this receptor in macrophage infiltration into adipose tissue to augment insulin resistance through an unknown mechanism. Overexpression studies revealed GPR21 to be a constitutively active receptor, which couples $G\alpha_q$ type G proteins leading to the activation of the MAP kinases. Overexpression of GPR21 markedly attenuated insulin signalling and

promoted macrophage migration. Interestingly, the effect of GPR21 on insulin signalling lessened in the presence of increasing concentrations of serum, inferring the possibility of a native regulatory ligand. Homology modelling and ligand docking studies led to the identification of a novel compound that interacted with GPR21. Its effects offered the potential as an anti-diabetic therapy as it was found to regulate GPR21-induced macrophage migration and to counteract the influence of GPR21 on the insulin signalling pathway.

Abbreviations

ACC	Acetyl CoA carboxylase
ADP	Adenosine 3', 5'-diphosphate
AICAR	5-Aminoimidazole-4-carboxamide ribonucleotide
AID	Auto-inhibitory domain
AMP	Adenosine 3', 5'-monophosphate
AMPK	AMP-activated protein kinase
ANOVA	Analysis of variance
ASK1	Apoptosis signal regulating kinase 1
AS160	Akt Substrate of 160 kDa
ATP	Adenosine 3', 5'-triphosphate
BMDM	Bone marrow derived macrophage
bp	Base pair
BSA	Bovine serum albumin
CaMKKβ	Ca^{2+}/calmodulin dependent protein kinase kinase beta
cAMP	Cyclic AMP
CBM	Carbohydrate binding molecule
CBS	Cystathionine-beta-synthase
cDNA	Complementary DNA
CPM	Counts per minute

CRTC2	CREB-regulated transcription co-activator 2
CT	Crossing threshold
Cys	Cysteine
C-terminal	COOH terminal
DAG	1,2-diacylglycerol
DD	Death domain
DHPO	2-(3,4-Dihydro-2H-pyrrolium-1-yl)-3oxoindan-1-olate
DMEM	Dulbecco's Modified Eagle's Medium
DMSO	Dimethylsulphoxide
DNA	Deoxyribonucleic acid
DPBS	Dulbecco's phosphate buffered saline
DPP-4	Dipeptidyl peptidase 4
dsDNA	Double-stranded DNA
ECH1	Delta (3,5)-delta(2,4)-dienoyl-CoA isomerase
ECL	Enhanced chemiluminescence
EDTA	Ethylenediamine tetraacetic acid
eGFP	Enhanced green fluorescent protein
EGTA	Ethylene glycol tetraacetic acid
ELISA	Enzyme-Linked Immunosorbent Assay
eNOS	Endothelial nitric oxide synthase
ER	Endoplasmic reticulum
Erk	Extracellular signal regulated kinase

E. coli	*Escherichia coli*
$FADH_2$	Flavin adenine dinucleotide
FBS	Foetal bovine serum
FITC	Fluorescein isothiocyanate
FoxO1	Forkhead transcription factor of O group 1
FRET	Fluorescence resonance energy transfer
g	Gravitational force
G	Gram
GAP	GTPase-accelerating protein
GDP	Guanosine-5'-diphosphate
GEF	Guanine nucleotide exchange factors
GIP	Glucose-dependent insulinotropic polypeptide
GLP-1	Glucagon-like peptide 1
GLP-1R	Glucagon-like peptide 1 receptor
GLUT4	Glucose transporter type 4
G protein	Guanine nucleotide-binding protein
GPCR	G protein coupled receptor
GP-130	Glycoprotein 130
GRK	G protein coupled receptor kinase
GRP-1-GST	General receptor for phosphoinositides 1 containing a glutathione S-transferase tag
GSK3	Glycogen synthase kinase 3

GSV	GLUT4 storage vesicles
GTP	Guanosine-5'-triphosphate
GTPase	Guanosine triphosphatase
h	Hour
H	Hydrogen
HDAC	Class IIa histone deacetylases
HEPES	4-(2-Hydroxyethyl)piperazine-1-ethanesulfonic acid, N-(2-Hydroxyethyl)piperazine-N′-(2-ethanesulfonic acid)
hERG	Human ether-à-go-go-related gene
HFD	High fat diet
HFHS	High fat high sugar
HMGR	3-hydroxy-3-methylglutaryl-CoA reductase
HPLC	High performance liquid chromatography
HRP	Horseradish peroxidase
HRPT	Hypoxanthine guanine phosphoribosyltransferase
HTRF	Homogeneous Time Resolved Fluorescence
IBMX	Isobutylmethylxanthine
IC_{50}	Half maximal inhibitory concentration
IFN-γ	Interferon-gamma
IgG	Immunoglobulin G
IKKβ	I-kappa-B kinase beta
IL	Interleukin

iNOS	Inducible nitric oxide synthase
IP_1	Inositol 1-phosphate
IP_2	Inositoldiphosphate
IP_3	Inositol 1,4,5-triphosphate
IP_6	Inositol hexaphosphate
IP6K	IP_6 kinase
IP_7	Diphosphoinositol pentakisphosphate
IRAK	IL-1 receptor-associated kinases
IRS1	Insulin receptor substrate 1
JAK	Janus kinase
JNK	c-Jun N-terminal kinase
kb	Kilo base
kDa	Kilo Dalton
KO	Knockout
KRB	Krebs ringer buffer
KRBG	Krebs ringer buffer containing glucose
L	Litre
LB	Lysogeny Broth
LDL-C	Low-density lipoprotein cholesterol
LE	Long exposure
LKB1	Liver kinase B1

LTB4	Leukotriene B4
M	Molar
MAP	Mitogen activated protein
MAPK	MAP kinase
MAPKK	MAPK kinase
MAPKKK	MAPKK kinase
MCP-1	Monocyte chemoattractant protein-1
MEKK1	MAP/Erk kinase kinase 1
mg	Milligram
mGPG	Mitochondrial glycerophosphate dehydrogenase
min	Minute
MKK4/7	MAPK kinase 4/7
ml	Millilitre
mm	Millimetre
mM	Millimolar
MO25	Mouse protein-25
mpc	Mitochondria pyruvate carrier
mRNA	Messenger RNA
MSC	Mesenchymal stromal cells
mTORC	Mammalian target of rapamycin complex
Myc-tag	10 amino acid affinity tag with the sequence EQKLISEEDL
MyD88	Myeloid differentiation factor 88
Mϕ	Macrophage

NAD	Nicotinamide adenine dinucleotide
NADH	Nicotinamide adenine dinucleotide with Hydrogen attached
NF-κB	Nuclear factor kappa B
ng	Nanogram
NLRP3	NOD like Receptor 3
nm	Nanometre
nM	Nanomolar
Nrf2	Nuclear Factor-Erythroid 2 p45–related factor 2
N-terminal	NH_2 terminal
PBS	Phosphate buffered saline
PCR	Polymerase chain reaction
PDK1	Phosphoinositide-dependent protein kinase 1
PFKFB3	6-phosphofructo-2-kinase/fructose-2,6-biphosphatase 3
PGC1α	Proliferator-activated receptor gamma co-activator 1 alpha
PH	Pleckstrin homology
PIP_2	Phosphatidylinositol 3,4,5-bisphosphate
PIP_3	Phosphatidylinositol 3,4,5-triphosphate
PI3K	Phosphatidylinositide 3 kinase
PKA	Protein kinase A
PKB	Protein kinase B
PKC	Protein kinase C
PLC	Phospholipase C
pM	Picomolar

PMSF	Phenylmethylsulfonyl fluoride
PPARγ	Peroxisome proliferator-activated receptor gamma
PP2	Protein phosphatase 2
PVDF	Polyvinylidenedifluoride
qRT-PCR	Quantitative Real Time PCR
RBP	Retinol binding protein
RGS	Regulators of G protein signalling
RhoGEF	Rho guanine nucleotide exchange factor
RIP1	Receptor interacting protein 1
RNA	Ribonucleic acid
ROS	Reactive oxygen species
RT	Room temperature
RPM	Revolutions per minute
RPMI-1640	Roswell Park Memorial Institute 1640
SDS	Sodium Dodecyl Sulphate
SDS-PAGE	Sodium Dodecyl Sulphate Polyacrylamide Gel Electrophoresis
SE	Short exposure
SEM	Standard error of the mean
Ser	Serine
SH2	Src homology 2
SGLT2	Sodium-glucose co-transporter 2

SOC	Super optimal broth with catabolite repression
SOCS	Suppressors of cytokine signalling
SREBP1C	Sterol regulatory element-binding protein 1C
STAT	Signal transducers and activators of transcription
STRA6	Stimulated by retinoic acid 6
STRAD	Sterile-20-related adaptor
SUR	Sulfonylurea receptor
SVF	Stromal vascular fraction
SV40	Simian virus 40
TAE	Tris-acetate-EDTA
TAK1	TGF-beta-activated kinase 1
TBS	Tris buffered saline
TBST	Tris-buffered saline containing Tween-20
TEMED	N, N, N', N'-Tetramethylethylene-diamine
TGR5	Takeda G protein coupled receptor 5
Thr	Threonine
TIFIA	RNA polymerase I-associated transcription factor
TIR	Toll/IL-1 receptor
TLR4	Toll like receptor 4
TMB	3,3′,5,5′-Tetramethylbenzidine
TNF-α	Tumour necrosis factor alpha
TNP	N2-(m-(trifluoromethyl)benzyl) N6-(p-nitrobenzyl) purine
TRADD	Tumour necrosis factor receptor associated death domain

TRAF	Tumour necrosis factor receptor associated factor
TTR	Transthyretin
Tyr	Tyrosine
Ulk	Unc-51-like kinase
UV	Ultraviolet
v/v	Volume per volume
w/v	Weight per volume
ZDF	Zucker Diabetic Fatty
αMEM	Minimal Essential Medium alpha
β2AR	Beta-adrenergic receptor
µCi	Microcurie
µg	Microgram
µl	Microlitre
µm	Micrometre
µM	Micromolar

List of Figures

Chapter 1 Introduction

Chapter 2 Materials and Methods

Chapter 3 Elucidating the Mechanism of Action of A Novel Anti-Diabetic Compound

List of Tables

Chapter 1 Introduction

Chapter 2 Materials and Methods

Chapter 4 GPR21, A Novel Target for Obesity-Associated Type 2 Diabetes

Chapter 1

Introduction

1.1 Diabetes

Type 2 diabetes accounts for more than 90 % of diabetic cases and has steadily become one of the greatest modern public health threats in terms of human, social and economic costs. According to the World Health Organization (2014), 371 million people are currently estimated to suffer with the disease, while a staggering 552 million people are predicted to be affected by 2030. The chronic complications of diabetes; diabetic retinopathy, nephropathy, neuropathy and macrovascular disease, contribute to the enhanced risk of morbidity and mortality in individuals with this condition. In 2012, diabetes accounted for approximately 1.5 million deaths worldwide.

Type 1 and type 2 diabetes develop as a consequence of defective production and action of insulin. Type 1 diabetes is an autoimmune disease caused by a combination of genetic and non-genetic factors, which lead to the destruction of insulin secreting pancreatic β-cells. Type 2 diabetes, however, is a progressive disease, primarily caused by insulin resistance. The global prevalence of type 2 diabetes has been attributed to a rise in obesity associated with genetic, epigenetic and societal factors (Chen, Magliano and Zimmet, 2012). In 2014, 39 % of adults worldwide were classed as overweight, approximately 13 % were obese, while the dangerous rise in childhood and adolescent obesity is further contributing to this epidemic (Singh *et al.,* 2008, Reinehr, 2013, World Health Organization, 2014).

1.2 Insulin

Under normal physiological conditions, insulin, along with its primary counter-regulatory hormone glucagon, regulate blood glucose homeostasis through sophisticated signalling cascades (Aronoff *et al.,* 2004). Insulin is a peptide hormone synthesised in the β-cells of the islets of Langerhans in the pancreas, the biosynthesis and secretion of which is controlled by gene transcription, translation, post-translational modifications and regulatory factors that impact on its release from mature secretory granules. While glucose is the primary regulator of insulin secretion, other factors including acetylcholine, amino acids, fatty acids, glucose-dependent insulinotropic polypeptide (GIP) and glucagon-like peptide-1 (GLP-1) can influence its release (Wilcox, 2005). As blood glucose levels rise above 3.3 mmol/l postprandially, insulin secreted by pancreatic β-cells binds to its plasma membrane receptor, present in all cells, to stimulate glucose uptake and inhibit glucagon secretion from pancreatic α-cells, thus preventing hepatic glucose production (Gerich, 1993).

1.2.1 The Insulin Signalling Pathway

Insulin initiates its action by binding to its receptor, a heterotetrameric membrane-bound glycoprotein consisting of two extracellular α-subunits and two intramembraneous β-subunits linked by disulphide bonds (Fig. 1.1). Upon binding the α-subunit, insulin induces a conformational change that allows ATP to interact with the intracellular face of the β-subunit, triggering the rapid autophosphorylation of the receptor at a number of tyrosine residues, including $Tyr^{1150/1151}$ in the regulatory loop of the receptor (Tornqvist *et al.,* 1987, Wilcox, 2005, Hubbard, 2013). The phosphotyrosine-binding domain of insulin receptor substrates, such as insulin receptor substrate 1 (IRS1) then interact with the receptor, which in turn phosphorylates the

substrate at numerous tyrosine residues (White, 1997). The phosphorylated tyrosine residues are recognised by the Src homology 2 (SH2) domain of the p85 regulatory subunit of the lipid kinase phosphatidylinositol 3 kinase (PI3K). This interaction translocates PI3K to the plasma membrane where the activated catalytic subunit, p110, phosphorylates its substrate phosphatidylinositol 3,4,5-bisphosphate (PIP_2) on the 3′ position of the inositol ring, producing the lipid second messenger phosphatidylinositol 3,4,5-triphosphate (PIP_3) (Shepherd *et al.,* 1998, Pirola *et al.,* 2004). PIP_3 recruits pleckstrin homology (PH) domain containing proteins such as phosphoinositide-dependent protein kinase 1 (PDK1) and Akt, also known as protein kinase B (PKB), to the plasma membrane. PDK1 then relays its signal potential by phosphorylating Akt at Thr^{308} in the catalytic domain, while mammalian target of rapamycin complex 2 (mTORC2), which is activated by ribosomes in response to PI3K signalling, is believed to phosphorylate Akt at Ser^{473} in the carboxyl terminal hydrophobic domain (Zinzalla *et al.,* 2011, Vadlakonda *et al.,* 2013, Mackenzie and Elliott, 2014).

Once activated, Akt can regulate glucose homeostasis through a multitude of signalling cascades. Akt phosphorylates and deactivates glycogen synthase kinase 3 (GSK3) resulting in the activation of glycogen synthase, which leads to the conversion of glucose to glycogen (Rayasam *et al.,* 2009). Akt also suppresses forkhead transcription factor of O group 1 (FoxO1) transactivation, promoting its relocation outside of the nucleus, thereby inhibiting the expression of gluconeogenic genes and stimulating that of glycolytic genes (Zhang *et al.,* 2006). Furthermore, Akt directly influences glucose uptake through the Akt substrate of 160 kDa (AS160), also known as TBC1D4, phosphorylation of which facilitates the translocation of glucose transporter 4 (GLUT4) to the plasma membrane. AS160 is a Rab GTPase-accelerating protein (Rab GAP). Rab proteins bind transport vesicles and influence their localisation based on its

nucleotide-bound state. GLUT4 storage vesicles (GSV) are associated with a number of Rab proteins, which in their inactive GDP-bound state hold the vesicle in the cytosol. AS160, catalyses the hydrolysis of any bound GTP to GDP sustaining the Rab in its inactive state. Akt phosphorylates AS160 at a number of key residues including Thr^{642} and Ser^{588}, leading to its dissociation from GSVs. This allows GTP to associate with one or more Rab proteins to facilitate the trafficking of GSVs to the plasma membrane (Sano, 2003, Larance *et al.,* 2005, Hutagalung and Novick, 2011). Defects in this tightly regulated signalling cascade have been attributed to the development of type 2 diabetes (Fröjdö *et al.,* 2009).

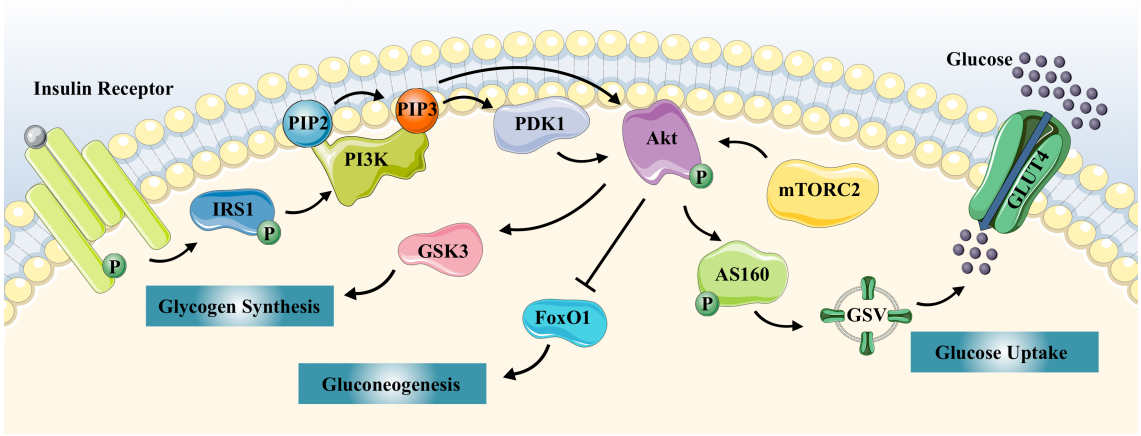

Figure 1.1 The insulin signalling pathway.

Upon autophosphorylation triggered by the binding of insulin, the insulin receptor recruits and phosphorylates IRS1, which interacts with the p85 regulatory subunit of PI3K, targeting this enzyme to the plasma membrane where the p110 catalytic subunit generates PIP_3. PIP_3 recruits PH domain containing proteins such as Akt and PDK1 to the plasma membrane. Akt is then phosphorylated by the now activated PDK1, in conjunction with mTORC2. Once activated, Akt can regulate glucose homeostasis by promoting glycogen synthesis, preventing gluconeogenesis and stimulating glucose uptake.

1.3 Obesity-Induced Inflammation

Adipose tissue functions as a multicellular endocrine organ composed of adipocytes, stromal-vascular cells and immune cell populations. The expansion of white adipose tissue associated with overnutrition leads to hypoxia, cell death, changes in fatty acid metabolism, altered adipose tissue specific cytokine (adipokine) secretion and pro-inflammatory immune cell infiltration, which can lead to development of insulin resistance (McArdle *et al.,* 2013). Since visceral adipose tissue accumulates more pro-inflammatory cells in obesity, it is more metabolically damaging than subcutaneous adipose tissue (O'Rourke and Metcalf, 2009). As obesity progresses, adipocytes secrete chemotactic cytokines such as monocyte chemotactic protein-1 (MCP-1) and leukotriene B4 (LTB4) recruiting monocytes into the adipose tissue where they differentiate into macrophages (Osborn and Olefsky, 2012).

1.3.1 Macrophage Infiltration into Adipose Tissue

Macrophages infiltrating adipose tissue undergo polarisation, switching from the anti-inflammatory M2 type subset to the pro-inflammatory M1 type subset under the influence of interferon-gamma (IFN-γ) as well as interleukin 17 (IL-17), secreted by resident pro-inflammatory T cells (Fig. 1.2) (Lumeng *et al.,* 2007, Winer *et al.,* 2009). M1 macrophages secrete a repertoire of pro-inflammatory cytokines including IL-1β, IL-6, and tumour necrosis factor-alpha (TNF-α) to further stimulate obesity-associated inflammation (Chawla *et al.,* 2012). Increased levels of circulating free fatty acids, produced as a consequence of augmented lipolysis, have also been reported to trigger macrophage secretion of the pro-inflammatory cytokines MCP-1, IL-6, IL-1β and TNF-α *in vitro* (Nguyen *et al.,* 2007). Several studies have demonstrated the central role M1 macrophages play in the promotion of insulin resistance, since deletion of this subset of

macrophages reduces adipose tissue inflammation and normalises insulin sensitivity (Patsouris *et al.,* 2008).

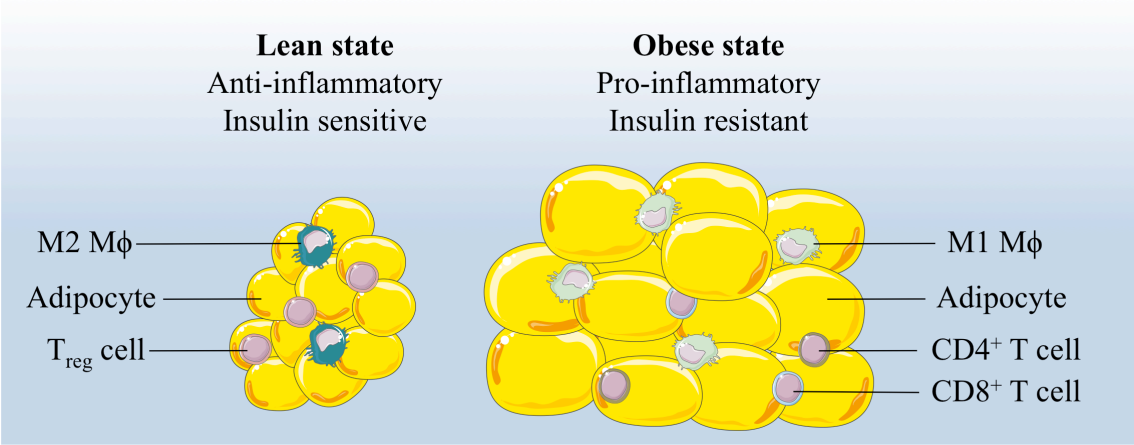

Figure 1.2 Adipose tissue in lean and obese states.

In the lean state, M2 macrophages (M2 Mϕ) and regulatory T cells (T_{reg}) reside in the adipose tissue and stem inflammation. In the case of obesity, where adipocytes increase in number and in mass, the inflammasome is triggered by saturated free fatty acids and pro-inflammatory cytokines resulting in the secretion of MCP-1 to promote the infiltration of pro-inflammatory M1 macrophages (M1 Mϕ) into adipose tissue. M1 macrophages recruit effector ($CD8^+$) and memory ($CD4^+$) T cells, which release pro-inflammatory cytokines further contributing to the development of insulin resistance (Kanneganti and Dixit, 2012).

1.4 Insulin Resistance

Insulin resistance is characterised by a diminished capacity for insulin to act on its receptor in peripheral tissues, leading to hyperglycaemia and hyperinsulinaemia as pancreatic β-cells produce excessive amounts of insulin to control blood glucose homeostasis. As the condition progresses, β-cell function deteriorates exacerbating hyperglycaemia, leading to the development of type 2 diabetes and its associated complications (Wilcox, 2005). Augmented adipokine secretion associated with obesity is now recognised as a major cause of this pathophysiological defect.

1.4.1 Pro-inflammatory Cytokines and Insulin Resistance

Chronic low-grade inflammation induced by obesity negatively impacts on the insulin signalling pathway largely through the increased production of the pro-inflammatory cytokines IL-1β, IL-6 and TNF-α.

1.4.1.1 IL-1β

Pro-IL-1β is cleaved by caspase-1 to form mature IL-1β (Lopez-Castejon and Brough, 2011) chronic exposure to which reduces IRS1 expression, leading to a decrease in AS160 phosphorylation and GLUT4 translocation in a manner dependent on the mitogen activated protein kinase (MAPK), extracellular signal related kinase (Erk) (Jager *et al.,* 2007). Receptor-mediated effects of IL-1β have been observed to trigger the activation of I-kappa-B kinase beta (IKKβ) (Section 1.4.1.4.1) and the MAPKs (Section 1.4.1.4.2), which negatively impact on the insulin signalling pathway. Furthermore, the NOD like Receptor 3 (NLRP3)-caspase-1 inflammasome, which induces caspase-1 activity to produce IL-1β (Martinon *et al.,* 2002), also has been implicated in the development of insulin resistance. A decrease in NLRP3 expression is

associated with improved insulin sensitivity, while NLRP3 deficient mice display decreased obesity-induced inflammation and an increase in insulin-stimulated phosphorylation of Akt (Vandanmagsar *et al.,* 2011).

1.4.1.2 IL-6

A two to three-fold increase in circulating IL-6 is observed in obese and type 2 diabetic patients (Kern *et al.,* 2001). Exposure of HepG2 cells and primary murine hepatocytes to this pro-inflammatory cytokine has been found to inhibit insulin receptor signal transduction (Senn *et al.,* 2002), through a mechanism now believed to involve the JAK-STAT signalling pathway (Section 1.4.1.4.3). However, the effect of IL-6 on insulin signalling occurs with elevated levels of the cytokine only, as Wallenius and colleagues (2002), observed an obesogenic phenotype in IL-6 deficient mice, to which low doses of centrally administered IL-6 increased energy expenditure, demonstrating anti-obesity effects. Carey and colleagues (2006), attributed this to the influence of IL-6 on the cellular energy regulator AMP activated protein kinase (AMPK) (Section 1.5), as glucose disposal was enhanced in an AMPK-dependent manner in healthy humans exposed to recombinant IL-6.

1.4.1.3 TNF-α

TNF-α is by far the most well-established pro-inflammatory cytokine contributing to insulin resistance, with triple the amount of this protein secreted from the adipose tissue of obese subjects (Kern *et al.,* 2001). Neutralisation and deletion of TNF-α, which is also markedly upregulated in the adipose tissue of experimental models of obesity, has been found to significantly improve insulin sensitivity (Hotamisligil and Spiegelman, 1994, Uysal *et al.,* 1997). Receptor-mediated effects of TNF-α have been observed to trigger the activation of IKKβ, the MAPKs and the JAK-STAT pathway to promote

insulin resistance making it the most prominent of the pro-inflammatory cytokines to impede the insulin signalling pathway.

1.4.1.4 Cytokine Signalling and Insulin Resistance

TNF-α and IL-1β transiently activate both IKKβ and the MAPK c-Jun N-terminal kinase (JNK), which have been directly implicated in the development of insulin resistance through multiple mechanisms (Fig. 1.3) (Solinas and Karin, 2010). Ablation of IKKβ (Yuan *et al.*, 2001) and JNK (Hirosumi *et al.*, 2002) has been shown to protect mice from the development of insulin resistance. Additionally, TNF-α and IL-6 can trigger the activation of suppressors of cytokine signalling 3 (SOCS3) through the JAK-STAT pathway, deletion of which prevents obesity-induced insulin resistance in skeletal muscle (Jorgensen *et al.,* 2013).

1.4.1.4.1 IKKβ

Phosphorylation of IKK at the β-subunit can be induced by the RIP1-TRADD-TRAF2 complex formed at the death domain of the activated TNF-α receptor and through IL-1β signal transduction involving MyD88, IRAK and TRAF6 (Karik *et al.,* 2004). IKKβ has been proposed to phosphorylate IRS1 at multiple serine residues, which prevents insulin-induced tyrosine phosphorylation of its substrate, rendering the insulin signalling pathway inactive (Gao *et al.,* 2002). However, the primary role of IKKβ in the development of insulin resistance is believed to be through its influence on nuclear factor kappa B (NF-κB) to promote pro-inflammatory gene expression (Cai *et al.,* 2005).

1.4.1.4.2 MAPKs

Downstream of TNF-α and IL-1β receptor activation, TRAF2 and TRAF6 also activate the MAPK cascade (Fig. 1.4) to trigger the phosphorylation of JNK. Activation of MAP/Erk kinase kinase 1 (MEKK1) and apoptosis signal regulating kinase 1 (ASK1), leads to the stimulation of MAPK kinases 4 and 7 (MKK4/7), highly specific activators of JNK (Liu *et al.,* 1996, Tournier *et al.,* 2001). Since JNK deficient mice display reduced expression of pro-inflammatory cytokines, this protein is believed to exacerbate metabolic inflammation through the phosphorylation of the downstream transcription factor c-Jun (Tuncman *et al.,* 2006). However, the most notable mechanism by which JNK induces insulin resistance is through the phosphorylation of IRS1 at Ser^{307}, which prevents insulin from acting upon its substrate, impeding the insulin signalling cascade (Aguirre *et al.,* 2000).

The other MAPKs, which can be activated by TNF-α receptor signalling, p38 and Erk (Sabio and Davis, 2014), have also been observed to influence the insulin signalling cascade. Mice lacking the δ isoform of p38 are protected from obesity-induced insulin resistance and oxidative stress-stimulated β-cell failure as a result of the increased activation of protein kinase D, a positive regulator of insulin secretion (Sumara *et al.,* 2009). Furthermore, mice overexpressing p38α exhibit reduced insulin-stimulated IRS1 tyrosine phosphorylation as a result of increased serine phosphorylation, while liver specific expression of dominant negative p38α in *ob/ob* mice has been found to improve glucose tolerance (Hemi *et al.,* 2011).

Pharmacological inhibition of Erk attenuates the effect of IL-1β on IRS1 (Jager *et al.,* 2007) and enhances the transcriptional activity of the redox sensitive transcription factor

Nuclear Factor-Erythroid 2 p45–related factor 2 (Nrf2), preventing oxidative stress-induced insulin resistance (Tan *et al.,* 2011). However, an opposing role has been suggested for this MAPK, as inhibition of Erk has been found to promote insulin resistance in *Drosophila* as a result of decreased insulin receptor expression (Zhang *et al.,* 2011).

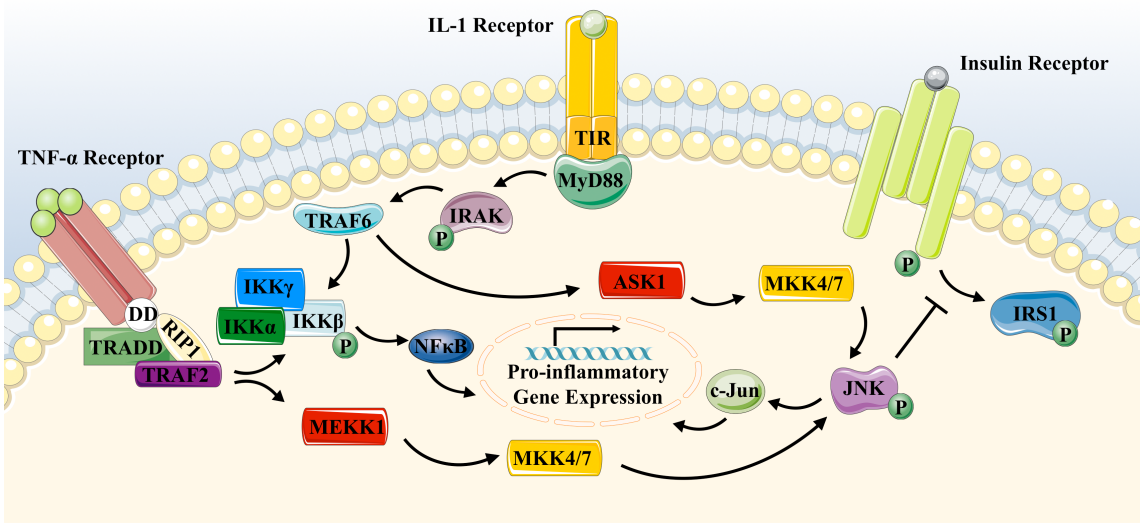

Figure 1.3 The effects of TNF-α and IL-1β-mediated activation of IKKβ and JNK on the insulin signalling pathway.

The TNF-α receptor undergoes trimerisation following ligand binding, allowing the scaffolding protein, receptor interacting protein 1 (RIP1), to initiate complex formation with the intracellular death domain (DD) of the receptor, the adaptor protein, TNF receptor associated death domain (TRADD), and TNF receptor associated factor 2 (TRAF2). In response to activation by IL-1β, the Toll/IL-1 receptor (TIR) domain of the IL-1 receptor interacts with the TIR domain of myeloid differentiation factor 88 (MyD88), which transduces the signal to a family of IL-1 receptor-associated kinases (IRAKs). IRAKs undergo phosphorylation by other IRAKs inducing the activation of TNF receptor-associated factor 6 (TRAF6). Both TRAF2 and TRAF6 phosphorylate IKKβ and lead to the activation of the JNK MAPK cascade. IKKβ and JNK provoke further expression of pro-inflammatory genes such as TNF-α, pro-IL-1β and IL-6 through NF-κB and c-Jun respectively. IKKβ and JNK also directly attenuate insulin signalling by phosphorylating IRS1 at serine residues, which prevents insulin-induced tyrosine phosphorylation of this protein. Adapted from (Karik *et al.,* 2004).

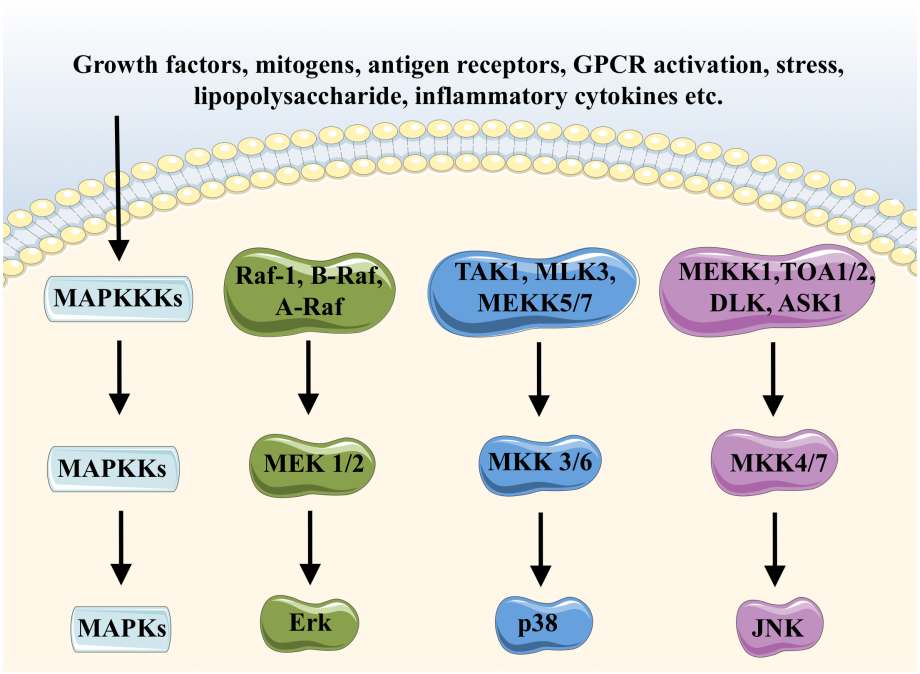

Figure 1.4 MAPK signalling cascades.

The three-tiered MAPK cascades can be activated by a multitude of factors including mitogens, cytokines, growth factors, cellular stresses and guanine nucleotide binding protein coupled receptor (GPCR) signal transduction. An activate MAPK kinase kinase (MAPKKK) triggers a MAPK kinase (MAPKK) to specifically phosphorylate one of the MAPKs Erk, p38 and JNK. Once activated MAPKs can target intracellular proteins or enter the nucleus to trigger transcription factor activation (Jeffrey *et al.,* 2007).

1.4.1.4.3 SOCS3

Cytokine binding to its receptor can also lead to the activation of the JAK-STAT-SOCS pathway, which negatively influences insulin signalling (Fig. 1.5). TNF-α receptor stimulation leads to the recruitment of one or more Janus kinases (JAK), which phosphorylate the receptor, creating docking sites for signal transducers and activators of transcription (STAT) (Ehlting *et al.,* 2007). Upon phosphorylation STATs form homo- or heterodimeric complexes that translocate to the nucleus and activate the transcription of target genes. Upon interaction with its ligand, the IL-6 receptor associates with the signalling receptor glycoprotein 130 (GP-130), which dimerises leading to the activation of the JAK-STAT pathway (Heinrich *et al.,* 1998, Sommer *et al.,* 2005). TNF-α and IL-6-induced activation of this pathway can lead to the transcription of SOCS3 (O'Sullivan *et al.,* 2007). SOCS3 has been observed to bind Tyr^{960} of the insulin receptor, partially impairing receptor autophosphorylation. As Tyr^{960} is a critical recognition site for IRS1, cytokine-induced activation of SOCS3 also suppresses IRS1 signalling, attenuating insulin-induced glycogen synthesis (Ueki *et al.,* 2004). However, more recently Sachithanandan and colleagues (2010), demonstrated liver specific deletion of SOCS3 to improve insulin sensitivity yet promote lipogenesis leading to obesity, increased inflammation and the development of nonalcoholic fatty liver disease. Furthermore, Pedroso and colleagues (2014), found that inactivation of SOCS3 improved insulin sensitivity, while having no effect on diet-induced obesity. These studies and countless others highlight obesity-induced type 2 diabetes as a multifactorial disease, to which the contributory factors may be differentially regulated in any given case, and therefore unlikely to be curtailed by targeting any one element alone.

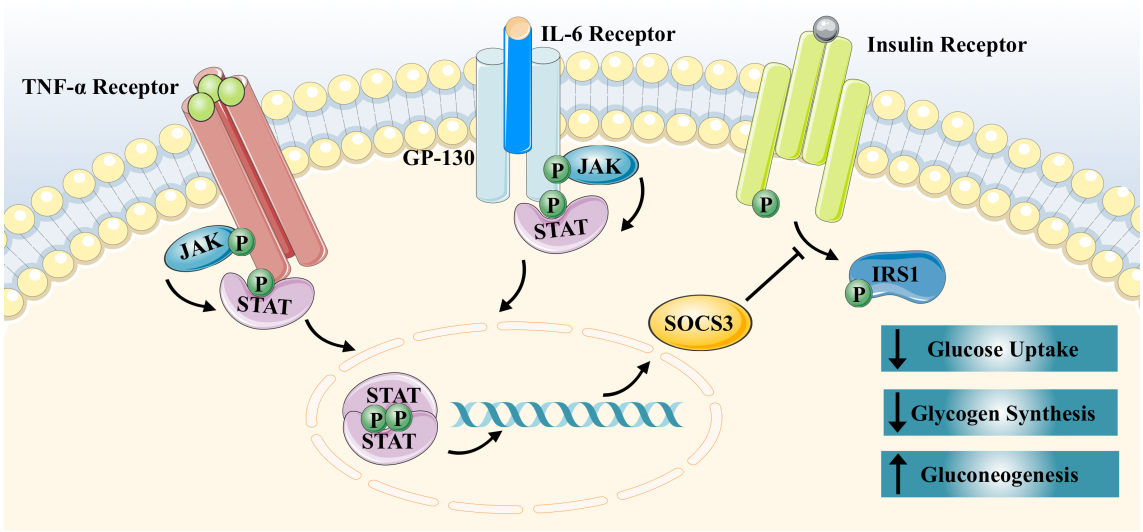

Figure 1.5 Cross talk between the JAK-STAT pathway and the insulin signalling pathway.

TNF-α and IL-6-induced receptor activation triggers JAK to phosphorylate the cytoplasmic domain of the receptor creating a docking site for STAT. Once phosphorylated, STATs dimerise and enter the nucleus to activate the transcription of SOCS3. SOCS3 inhibits tyrosine phosphorylation of IRS1 decreasing glucose uptake and glycogen synthesis and increasing gluconeogenesis.

1.4.2 Retinol Binding Protein and Insulin Resistance

Retinol binding protein (RBP) facilitates the transport of hydrophobic retinol (vitamin A) from its primary storage site, the liver, to target tissues (Kanai *et al.,* 1968). Retinol-bound RBP circulates in the bloodstream bound to transthyretin (TTR), which prevents the glomerular filtration and excretion of RBP due to the increased mass of the RBP-TTR complex (Goodman, 1984, van Bennekum *et al.,* 2001). At the target tissue, retinol is transported across the cell membrane via the RBP receptor, stimulated by retinoic acid 6 (STRA6), which competes with TTR to bind RBP (Heller, 1975, Sivaprasadarao and Findlay, 1988a, 1988b, Kawaguchi *et al.,* 2007). STRA6 then mediates the transfer of retinol to the cellular retinol binding protein (Sundaram *et al.,* 1998). As retinol-free RBP does not bind TTR, it is then easily excreted by the kidney. While liver is the primary site of RBP secretion, adipose tissue, amongst others, has also been found to contribute to circulating RBP levels (Tsutsumi *et al.,* 1992).

This adipokine has been implicated in the genesis of obesity-related insulin resistance as serum RBP levels are elevated in obese subjects. Furthermore, the characteristic insulin resistant state of the adipose tissue specific GLUT4 knockout mouse is associated with a significant increase in adipose tissue secretion of RBP (Yang *et al.*, 2005). Continuing on from this, Yang and colleagues (2005), found mice injected with recombinant human RBP to be insulin resistant and glucose intolerant, while RBP knockout mice displayed increased insulin sensitivity. Additionally, treatment with fenretinide, a synthetic retinoid that inhibits RBP binding to TTR, promoting RBP excretion, was found to improve glucose tolerance in obese insulin resistant mice. However, fenretinide treatment also demonstrated beneficial effects in obese, insulin resistant RBP knockout mice, suggesting an RBP-independent response. Nonetheless,

the improvement in glucose disposal associated with weight loss also correlates with a decrease in RBP levels, demonstrating the significant role this adipokine may play in obesity-related insulin resistance (Graham *et al.,* 2006).

Conflicting reports have emerged as to how RBP contributes to the development of insulin resistance. Berry and Noy (2012), suggest retinol-bound RBP induces the phosphorylation of STRA6, which activates a JAK-STAT pathway, involving JAK2 and STAT5, to upregulate SOCS3 expression, thereby inhibiting insulin signalling. However, when Muenzner and colleagues (2013), exposed control and STRA6 overexpressing cells to RBP, in the presence or absence of retinol, no change in STAT5 phosphorylation was observed. Furthermore in mice overexpressing RBP in the liver, the increased serum levels of retinol-bound RBP were not associated with a change in SOCS3 mRNA expression in the adipose tissue. Norseen and colleagues (2012), suggest RBP acts independently of STRA6 to incite an immune response that contributes to the development of insulin resistance. Direct stimulation of adipose tissue macrophages with RBP led to an increase in IL-6, IL-1β, TNF-α and MCP-1 expression and a reduction in the negative regulator of inflammation, peroxisome proliferator-activated receptor gamma (PPARγ). This effect was triggered with retinol-free RBP just as proficiently as with retinol-bound RBP. RBP was also found to activate the NFκB, p38, Erk and JNK signalling pathways in macrophages. RBP demonstrated a reduced effect on MCP-1 and IL-6 expression in JNK deficient macrophages and in Toll like receptor 4 (TLR4) deficient macrophages. However, the effect of RBP was not completely inhibited, suggesting other signalling pathways may be involved in RBP-induced insulin resistance. More recently Young and colleagues (2015), in this laboratory, found retinol-bound RBP to decrease levels of protein

phosphatase 1β, a regulator of the rate limiting enzymes involved in glycogen metabolism, in C2C12 muscle cells. As a consequence of the observed decrease in glycogen synthase activity a detrimental effect on insulin stimulated glycogen production was observed. The reduced ability to store glucose as glycogen and the attenuated capacity to utilise glycogen stores can contribute to the development of insulin resistance and may account for the influence of elevated RBP levels on this condition.

1.4.3 Adipose Tissue Hormones and Insulin Resistance

The perturbed release of hormones from adipose tissue has also been found to contribute to the pathogenesis of insulin resistance. The secretion of resistin is markedly upregulated in murine models of genetic and diet-induced obesity and has been found to play a central role in the production of inflammatory molecules such as TNF-α and IL-6 through the activation of NF-κB (Codoñer-Franch and Alonso-Iglesias, 2015). Leptin release is also upregulated in obese subjects (Silha *et al.,* 2003). Under normal physiological conditions, leptin regulates energy balance by suppressing food intake and increasing fatty acid oxidation through the action of AMPK (Minokoshi *et al.,* 2002, Klok *et al.,* 2007). However, with obesity, subjects are essentially resistant to the positive effects of leptin, as the increased levels of SOCS3 associated with obesity impair leptin-induced activation of AMPK (Yang *et al.,* 2012). Conversely, the expression of adiponectin is significantly decreased with obesity, this adipokine also enhances fatty acid oxidation through AMPK, suppresses TNF-α and IFN-γ production and improves insulin sensitivity (Carbone *et al.,* 2012). These hormones play a pivotal role in the regulation of energy homeostasis, the impact of both leptin and adiponectin on AMPK to maintain this balance, stresses the importance of this kinase in the regulation of a fundamental aspect of the type 2 diabetic phenotype.

1.5 AMP Activated Protein Kinase (AMPK)

AMPK is a highly conserved metabolic master switch present in all eukaryotes, which responds to fluctuations in ADP:ATP and AMP:ATP ratios to restore energy homeostasis by regulating pathways involved in glucose metabolism, lipid metabolism, protein synthesis and mitochondrial biogenesis (Sanders *et al.*, 2007, Xiao *et al.*, 2011, O'Neill, Holloway and Steinberg, 2013). Although cellular processes are driven by the hydrolysis of ATP to ADP and a free phosphate, adenylate kinases rapidly catalyse two ADP molecules to generate one ATP and one AMP molecule (Zeleznikar *et al.,* 1990), giving great emphasis to this ratio as an indicator of energy status in times of enhanced cellular stress.

1.5.1 AMPK Structure

AMPK is a heterotrimeric kinase consisting of a catalytic α-subunit and regulatory β and γ subunits. In mammals AMPK is encoded by seven genes for the specific isoforms of each subunit (α1, α2, β1, β2, γ1, γ2, γ3; α1, γ2 and γ3 isoforms also have splice variants) (Table 1.1) (Steinberg and Kemp, 2009, Viollet *et al.,* 2010, Hardie, 2011). Combinations of the diverse isoforms lead to the formation of at least 12 different complexes which confer defined properties to the kinase in terms of localisation and signalling functions (Viollet *et al.,* 2010). The subunits of AMPK are generally unstable when expressed individually, with co-expression of all three necessary for kinase activity (Hardie, 2011).

Table 1.1 Tissue distribution of AMPK subunits.

Subunit	Tissue Distribution
α1	**Adipose tissue**, lung, brain, liver, kidney, spleen**,** pancreas, heart, skeletal muscle
α2	**Heart**, **skeletal muscle**, kidney, liver, brain, lung, adipose tissue, spleen**,** pancreas
β1	Widespread
β2	**Skeletal muscle**, **heart**
γ1	Widespread
γ2	Widespread; **brain**, **placenta**, **heart**, **skeletal muscle**
γ3	Skeletal muscle

Key: **High expression**, low expression

The catalytic α-subunit of AMPK is a 63 kDa protein containing a serine/threonine kinase domain. The phosphorylation of Thr^{172} confers activation (Hawley *et al.,* 1996, Stein *et al.,* 2000), whereas that of Ser^{485} triggered by Akt and potentially through autophosphorylation, renders the kinase inactive (Horman *et al.,* 2006, Hurley *et al.,* 2006). The α-subunit also comprises an auto-inhibitory domain (AID) at the N-terminus, while the C-terminus contains binding domains for the β and γ subunits. The β-subunit has a central carbohydrate binding molecule (CBM) and a C-terminal region that binds the α and γ subunits. The N-terminal region of the γ-subunit is followed by Bateman domains; regulatory adenine nucleotide-binding sites composed of four highly conserved cystathionine-beta-synthase (CBS) sequence repeats (Kemp, 2004). The CBS motifs gather such that there are four sites where adenine nucleotides can potentially bind (Fig. 1.6).

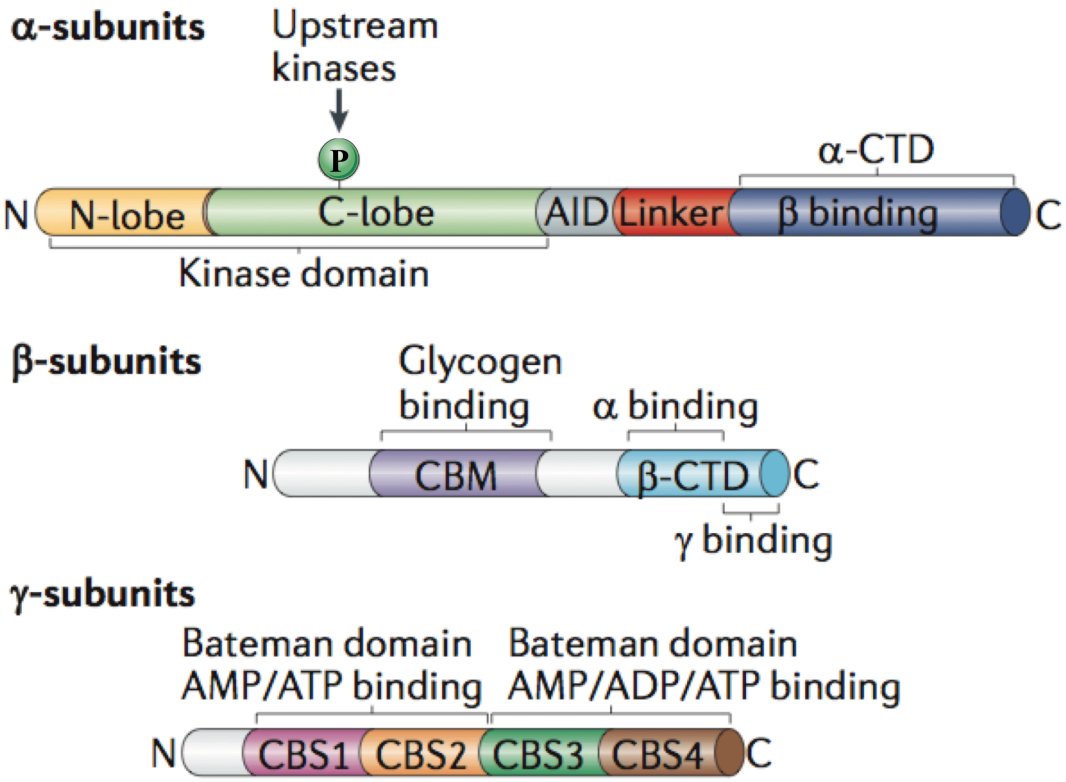

Figure 1.6 Domain map of AMPK.

The α and γ subunits come together at the β-subunit carboxy-terminal domain (β-CTD) to form the AMPK complex. Image from (Hardie, Ross and Hawley, 2012).

1.5.2 AMPK Activation

In its inactive state, AMPK is bound to ATP, until a change in cellular energy balance allows AMP to compete with ATP to occupy the kinase at the CBS1 and CBS3 sites, while ADP appears to bind to CBS3 only. Nucleotide exchange at these two CBS motifs triggers a conformational change that provokes AMPK activation through three main mechanisms (Fig. 1.7) (Corton *et al.,* 1994, Davies *et al.,* 1995, Hawley *et al.,* 1996).

1. Under moderate stress, AMP or ADP bind to CBS3 to promote the phosphorylation of Thr^{172} by upstream kinases, conferring more than 200-fold increased activity.
2. The replacement of ATP at CBS3 also stimulates an association between the N-terminal lobe of the kinase domain and the CBM of the β-subunit to protect against Thr^{172} dephosphorylation.
3. Under more severe stress, AMP displaces ATP at CBS1 to allosterically activate previously phosphorylated AMPK, adding a further 10-fold activation status to the kinase.

The CBS4 site contains a permanently bound AMP molecule, whereas CBS2 appears to be always vacant, potentially due to the lack of an aspartate residue which interacts with the ribose ring of a bound nucleotide in the other three CBS sites (Viollet *et al.,* 2010, Hardie, 2011, Xiao *et al.,* 2011, Carling and Viollet, 2015).

In addition to IL-6, adiponectin and leptin as previously mentioned, pharmacological agents, hormones and cellular stresses such as glucose starvation, ischemia, hypoxia and exercise can all initiate specific signalling cascades that lead to the activation of AMPK.

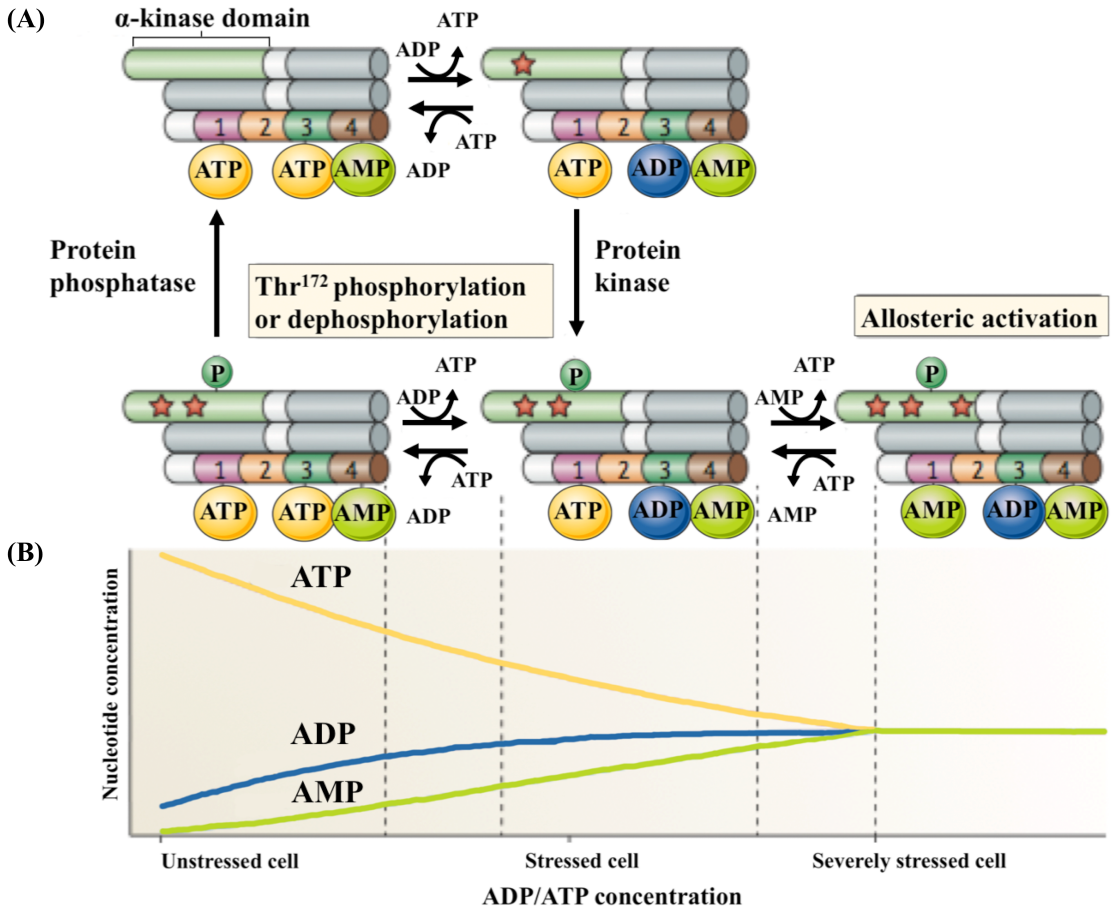

Figure 1.7 Model of AMPK activation.

(A) A mechanistic model for the activation states of AMPK governed by nucleotide binding, regulatory kinases and phosphatases. As ADP can readily bind to the CBS3 site, it can promote and maintain the phosphorylation of AMPK at Thr^{172}. However, ADP cannot bind to CBS1 and therefore cannot allosterically activate phosphorylated AMPK to trigger the greater than 2000-fold increase in kinase activity, emphasising the critical role AMP plays in the regulation of this protein. (B) Predicted nucleotide concentrations under various levels of cellular stress. Image adapted from (Hardie, Ross and Hawley, 2012).

1.5.2.1 Pharmacological Activation of AMPK

A number of pharmacological agents have been reported to activate AMPK through direct and indirect mechanisms. 5-Aminoimidazole-4-carboxamide riboside (AICAR), which is phosphorylated into the AMP analog ZMP by adenosine kinase, was the first compound identified to directly activate AMPK. ZMP mimics AMP as it binds the γ-subunit of AMPK inducing allosteric activation, which facilitates the phosphorylation of Thr^{172} by upstream kinases (Sullivan *et al.,* 1994, Corton *et al.,* 1995). PT1 allosterically activates AMPK *in vitro* and is believed to interact with the α-subunit near the autoinhibitory domain to directly relieve autoinhibition (Pang *et al.,* 2008). Salicylate (Hawley *et al,*. 2012) and the small-molecules A769662 (Scott *et al.,* 2008) and 991 (Xiao *et al.,* 2013), have also been observed to directly activate AMPK as they stabilise the AMP-induced interaction between the CBM of the β-subunit and the kinase domain of the α-subunit to protect against the dephosphorylation of Thr^{172}. Several activators of AMPK such as biguanides, of which metformin is the first line of treatment for type 2 diabetes (Bridges *et al.,* 2014, Matsuzaki and Humphries, 2015), berberine (Turner *et al.,* 2008) and the novel compound R419 (Jenkins *et al.,* 2013) have been observed to indirectly activate AMPK by inhibiting complex I of the mitochondrial respiratory chain.

1.5.2.1.1 Inhibition of NADH:ubiquione oxidoreductase

The mitochondrial respiratory chain comprises five complexes, complex I (NADH:ubiquinone oxidoreductase), complex II (succinate:ubiquinone oxidoreductase), complex III (ubiquinol:cytochrome c oxidoreductase), complex IV (cytochrome c oxidoreductase) and complex V (ATP synthase) (Fig. 1.8). Oxidative phosphorylation begins as electrons are donated from NADH to NADH:ubiquinone

oxidoreductase or from $FADH_2$ to succinate:ubiquinone oxidoreductase. NADH:ubiquinone oxidoreductase establishes the proton gradient as it releases two hydrogen ions for every one electron across the matrix into the intermembrane space, while the other complexes release one hydrogen for every electron processed (Wikström, 1984). Furthermore, ubiquinol:cytochrome c oxidoreductase and cytochrome c oxidoreductase form a supramolecular association with NADH:ubiquinone oxidoreductase, creating respirasomes which confer a kinetic advantage to NAD-linked respiration (Genova and Lenaz, 2014).

Electrons are sequentially transferred to cytochrome c oxidoreductase where they interact with molecular oxygen and hydrogen ions to generate a water molecule. The energy associated with the proton gradient is then exploited by ATP synthase to generate ATP from ADP and inorganic phosphate (Fernández-Vizarra *et al.,* 2009). Inhibition of NADH:ubiquinone oxidoreductase perturbs this energy generation leading to a significant decrease in ATP synthesis, as NADH:ubiquinone oxidoreductase is believed to provide 40 % of the protons required for ATP production (Efremov *et al.,* 2010). The resultant build-up of ADP may then directly interact with AMPK, or is subject to the action of adenylate kinase to increase cellular AMP levels, all of which enhance AMPK activation.

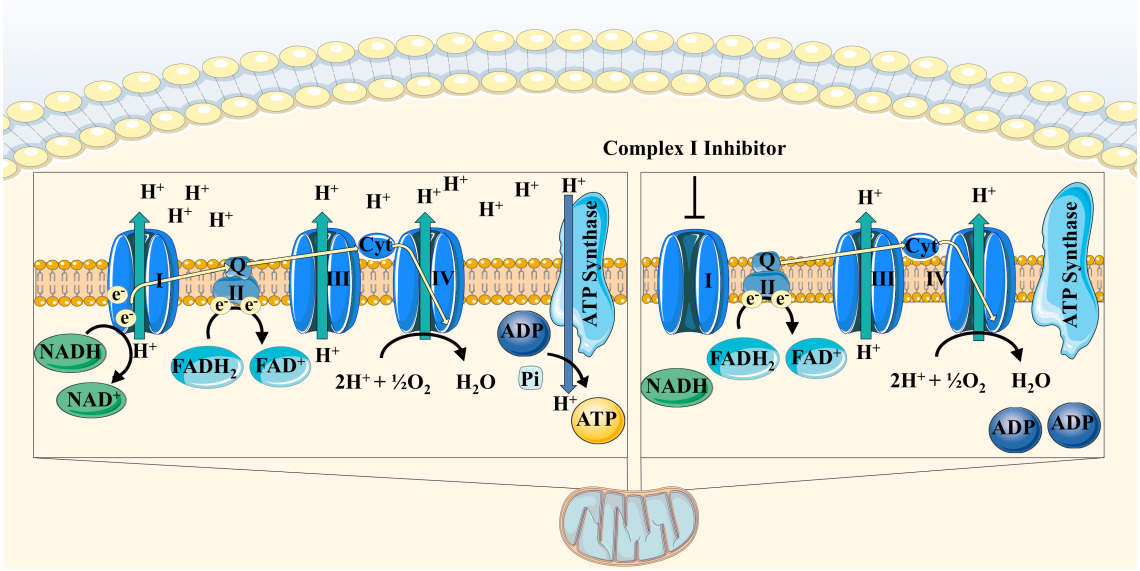

Figure 1.8 The mitochondrial respiratory chain.

Electrons generated from NADH and $FADH_2$ are passed through the complexes of the mitochondrial respiratory chain with the aid of the carrier molecules, ubiquinone (Q) and cytochrome c (Cyt) leading to the reduction of molecular oxygen to water. The energy liberated during respiration through the creation of the H^+ gradient is used by ATP synthase to catalyse the condensation of ADP and inorganic phosphate (Pi) into ATP. Inhibition of NADH:ubiquinone oxidoreductase leads to a significant decrease in energy production which is sensed by AMPK.

The naturally occurring phytochemicals quercetin and resveratrol also activate AMPK as they inhibit ATP synthase to alter cellular energy balance (Zheng and Ramirez, 2000). Numerous other natural and synthetic compounds with anti-diabetic and anti-obesogenic properties have also been observed to influence AMPK activity including, DHPO (Kandadi *et al.,* 2010), curcumin (Kim *et al.,* 2010) and tangeretin (Kim *et al.,* 2012) however, the mechanism by which this occurs remains elusive.

1.5.2.2 Exercise-Induced Activation of AMPK

As well as through a decrease in ATP production, AMPK can be activated by an increase in ATP consumption through the more physiological condition of metabolic stress that is exercise. The rise in cellular ADP and AMP as a consequence of intense muscle contraction and prolonged low impact exercise leads to the activation of one of the three AMPK complexes expressed in human skeletal muscle; α1β2γ1, α2β2γ1 and α2β2γ3 (Richter and Ruderman, 2009). As the potent AMPK activator AICAR regulates glucose and lipid metabolism in a similar manner to contraction in skeletal muscle, AMPK is believed to mediate many of the beneficial effects of exercise (Merrill *et al.,* 1997). Furthermore, exercise induces the release of IL-6 which has been found to activate the kinase (Kelly *et al.,* 2004).

The leptin-receptor-deficient Zucker Diabetic Fatty (ZDF) rat displays the importance of AMPK and exercise in the management of the type 2 diabetic phenotype as treadmill training of the ZDF rat, which displays decreased AMPK activity, markedly improves glucose tolerance and insulin sensitivity (Becker-Zimmermann *et al.,* 1982, Yu *et al.,* 2004). Furthermore, AMPKβ1β2 (O'Neill *et al.,* 2011) and AMPKα1α2 (Lantier *et al.,* 2014) skeletal muscle specific knockout mice have reduced exercise capacity while β1β2 knockout mice display significantly reduced contraction-stimulated glucose

uptake. These studies also proposed a role for AMPK in exercise-induced stimulation of mitochondrial biogenesis to expand the mitochondrial network within muscle cells, increasing the capacity for aerobic ATP provision (Hood, 2009).

1.5.2.3 Regulation of AMPK Phosphorylation

Once bound by AMP or ADP the phosphorylation of AMPK at Thr^{172} can be regulated (Fig. 1.9). AMPK is primarily phosphorylated by a complex formed between liver kinase B1 (LKB1) and two accessory subunits, the pseudokinase sterile-20-related adaptor (STRAD) and the scaffolding protein, mouse protein-25 (MO25) (Hawley *et al.,* 2003, Woods *et al.,* 2003). STRAD induces LKB1 relocalisation from the nucleus to the cytoplasm with the aid of the histone/protein deacetylase, sirtuin 1 (Lan *et al.,* 2008). STRAD then stimulates the catalytic activity of LKB1 and promotes interaction with MO25, which stabilises the activation loop of LKB1 in a conformation necessary for it to catalyse the phosphorylation of AMPK (Zeqiraj *et al.,* 2009). Although tissue-specific deletion of LKB1 has demonstrated the central role this protein plays in the phosphorylation of AMPK, kinase activation can also be modulated by Ca^{2+}/calmodulin dependent protein kinase kinase β (CaMKKβ) in a Ca^{2+} dependent manner. This action is particularly important in neurons, endothelial cells and T lymphocytes (Hawley *et al.,* 2005, Shackelford and Shaw, 2009). Furthermore, the effects of leptin (Park *et al.,* 2013) and adiponectin (Lee and Shao, 2012) on AMPK activity are proposed to be mediated through the action of CaMKKβ.

Other proteins that play a role in AMPK activity include the protein phosphatases 2 A (PP2A) and C (PP2C) (Davies *et al.,* 1995), and the MAPKKK TGF-beta-activated kinase 1 (TAK1) (Momcilovic *et al.,* 2006). Both PP2A and PP2C suppress AMPK activity in the absence of ADP and AMP through dephosphorylation, while TAK1 has

been found to increase AMPK phosphorylation at Thr^{172} *in vitro*.

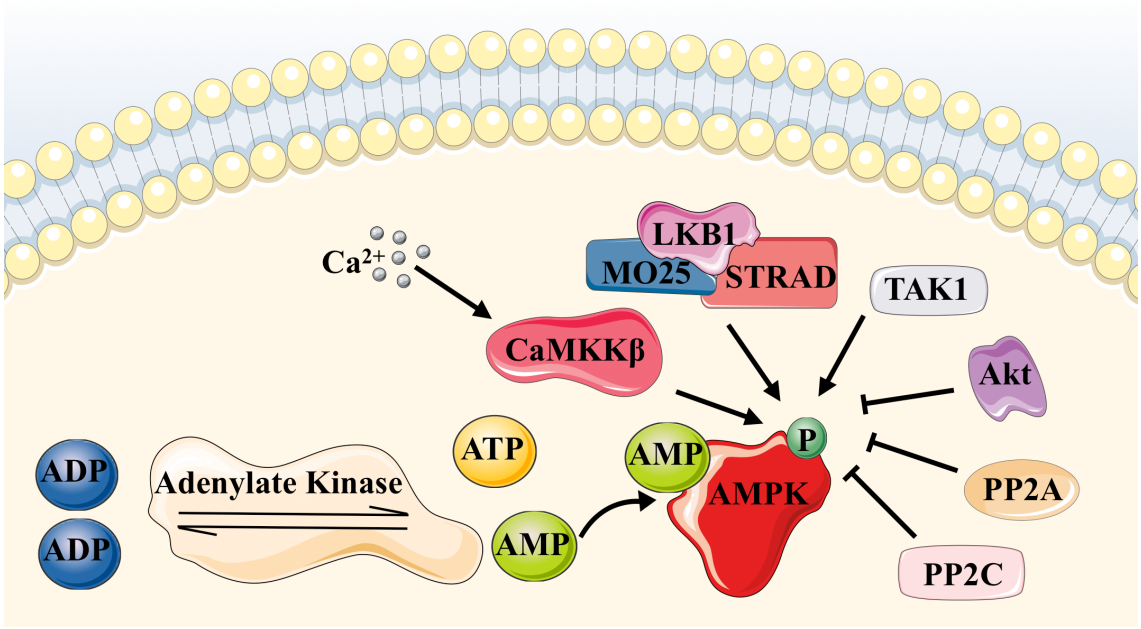

Figure 1.9 The regulation of AMPK phosphorylation.

Alterations in cellular energy balance lead to an increase in intracellular ADP that is promptly converted into ATP and AMP through the action of adenylate kinase. The increasing levels of AMP and ADP displace ATP bound to the CBS domain of the γ-subunit of AMPK. The resultant conformational change allows AMPK to be phosphorylated at Thr^{172} within the activation loop of the α-subunit by the LKB1 complex, CaMKKβ and TAK1. ADP as well as AMP binding stabilises AMPK in an active conformation preventing its dephosphorylation by PP2A and PP2C. Activated Akt stimulates AMPK phosphorylation at Ser^{485} to impede phosphorylation at Thr^{172}.

1.5.3 Downstream Effects of AMPK Activation

Once activated, AMPK restores cellular energy balance by switching on ATP generating pathways and switching off ATP consuming pathways, a response that has been found to counteract many of the cellular abnormalities of type 2 diabetes (Fig. 1.10) (Kahn *et al.,* 2005).

1.5.3.1 Lipid Metabolism

The primary role attributed to AMPK, which aided its discovery, was as a regulator of key enzymes involved in lipid metabolism (Munday *et al.,* 1988, Hardie *et al.,* 1989). Activated AMPK phosphorylates 3-hydroxy-3-methylglutaryl-CoA reductase (HMGCR) to suppress cholesterol synthesis, while AMPK-induced phosphorylation of acetyl-CoA carboxylase (ACC) influences fatty acid synthesis and oxidation. Phosphorylation of ACC at Ser^{79} halts its enzymatic activity leading to a decrease in malonyl CoA, a key substrate for fatty acid synthesis. The fall in malonyl-CoA content leads to a subsequent increase in fatty acid oxidation by heightening carnitine palmitoyltransferase 1 in skeletal muscle (Winder and Hardie, 1996, Ruderman *et al.,* 1999). AMPK also prevents the cleavage and activation of sterol regulatory element-binding protein 1C (SREBP1C)-induced triglyceride synthesis (Li *et al.,* 2011).

1.5.3.2 Glucose Metabolism

Consistent with a role in maintaining energy homeostasis AMPK exploits glucose metabolism, promoting catabolism and suppressing anabolism to restore cellular ATP levels. AMPK converges with the insulin signalling pathway to promote glucose uptake through GLUT4 translocation in an AS160 dependent manner (Treebak *et al.,* 2006). The CBM domain of the AMPK β-subunit has been postulated to facilitate its

interaction with glycogen-associated proteins such as glycogen synthase (Hardie *et al.,* 2012). In fact, AMPK has been observed to phosphorylate glycogen synthase, inhibiting the process of glycogen synthesis in favour of glycolysis, yet whether this is dependent on a CBM-mediated interaction remains unclear (Bultot *et al.,* 2012). AMPK also acts on 6-phosphofructo-2-kinase and 6-phosphofructo-2-kinase/fructose-2,6-biphosphatase 3 (PFKFB3), a key regulator of the glycolytic enzyme phosphofructokinase-1 to inhibit the process of glycolysis (Marsin *et al.,* 2000, 2002, Bando, 2005, Doménech *et al.,* 2015). Furthermore, AMPK reduces gluconeogenesis as it phosphorylates CREB-regulated transcription co-activator 2 (CRTC2) (Koo *et al.,* 2005), and Class IIa histone deacetylases (HDACs) (Mihaylova *et al.,* 2011).

1.5.3.3 Mitochondrial Biogenesis

The expression of peroxisome proliferator-activated receptor-gamma co-activator 1 alpha (PGC1α), which enhances the activity of mitochondrial gene transcription factors, can be augmented by AMPK-induced phosphorylation to stimulate mitochondrial biogenesis, promoting ATP production (Jäger *et al.,* 2007).

1.5.3.4 Protein Synthesis

To maintain intracellular ATP levels, activated AMPK phosphorylates the RNA polymerase I-associated transcription factor (TIFIA), preventing the assembly of transcription complexes necessary for the synthesis of ribosomal RNA (Hoppe *et al.,* 2009). In addition to this, AMPK phosphorylates key components of mTORC1; tuberous sclerosis 1 (Inoki *et al.,* 2003) and the regulatory associated protein of mTOR (Gwinn *et al.,* 2008) to suppress protein synthesis.

1.5.3.5 Autophagy

As a consequence of reduced mTORC1 signalling, AMPK alleviates the inhibitory effect of the complex on unc-51-like kinase 1 (Ulk1) and Ulk2 to promote autophagy and mitophagy, the specific engulfment of damaged mitochondria by autophagosomes. AMPK has also been postulated to directly phosphorylate Ulk1/2, however, the results remain inconsistent (Alers *et al.,* 2012).

The impact of AMPK on autophagy demonstrates a cytoprotective response, modulating some of the damaging effects of type 2 diabetes (Gonzalez *et al.,* 2011). Hyperglycaemia associated with type 2 diabetes, causes an imbalance in the antioxidant capacity of the cell leading to organelle damage. The insulin secreting β-cells rely on autophagosomes to sequester and recycle misfolded pro-insulin, defective secretory granules and dysfunctional mitochondria to maintain normal cell function (Lee, 2014). Impairments in this system have been observed to attenuate these protective effects as hepatic suppression of the murine autophagy related gene 7 results in increased endoplasmic reticulum stress and insulin resistance (Yang *et al.,* 2010).

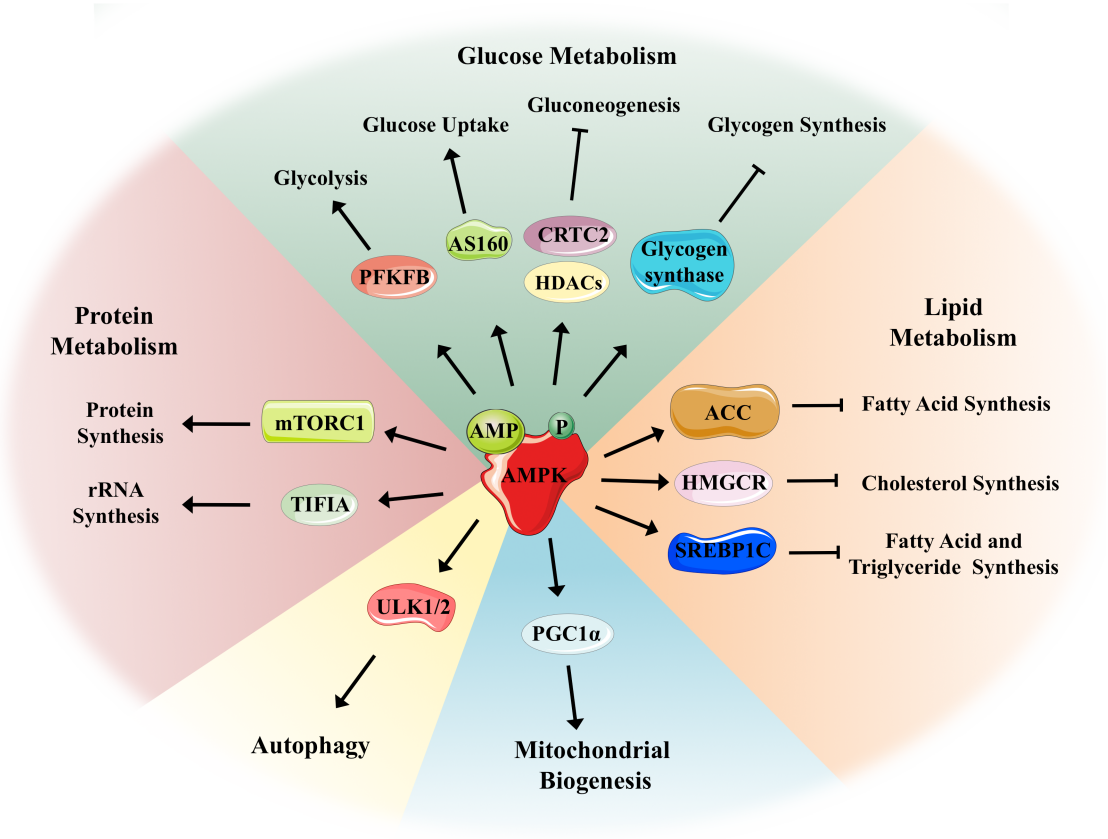

Figure 1.10 Downstream targets of activated AMPK.

AMPK regulates cellular energy balance by switching on ATP generating catabolic processes; glucose metabolism, fatty acid oxidation, mitochondrial biogenesis and autophagy and by switching off ATP consuming anabolic processes; fatty acid synthesis, triglyceride synthesis, cholesterol synthesis, protein synthesis, gluconeogenesis, glycogen synthesis and ribosomal RNA synthesis. Image adapted from (Hardie, Ross and Hawley, 2012).

1.6 Therapeutic Interventions for Type 2 Diabetes

Given the beneficial effects of AMPK on many of the hallmarks of type 2 diabetes, it is unsurprising that some anti-diabetic drugs target this kinase to regulate glycaemic control. Although the beneficial effects of exercise and weight loss on insulin sensitivity are undisputed (Henriksen, 2002, Kopp *et al.,* 2005), perseverance often proves difficult (Gage, 2012). Failing dietary intervention, the AMPK activator metformin is the primary drug of choice to control type 2 diabetes, which may be used in conjunction with a range of other therapies if treatment goals are not met (Inzucchi *et al.,* 2015).

1.6.1 Metformin

Anti-hyperglycaemic effects have been observed in response to many guanidine-containing compounds. However, metformin is the only drug of its class, the biguanides, available as a therapeutic intervention, as the more potent effects of phenformin and buformin carry a higher risk for lactic acidosis (Rena *et al.,* 2013). Metformin has been in use for over 50 years, however, some understanding of its mechanism of action has only been gained in recent years and remains an area of dynamic research. The anti-diabetic effects of metformin originate with the suppression of hepatic gluconeogenesis and glucagon signalling and the promotion of glucose uptake. Metformin is believed to enter the cell through the organic cation transporter 1, which demonstrates high levels of expression in the liver and kidney (Pernicova and Korbonits, 2014). Metformin then inhibits NADH:ubiquinone oxidoreductase increasing cellular ADP and AMP, leading to the activation of AMPK and the consequential downstream effects (Rena *et al.,* 2013). However the glucose-lowering influence of metformin has also been observed to occur through an AMPK independent

mechanism. Miller and colleagues (2013), proposed that metformin-induced increases in AMP inhibit adenylate cyclase to reduce the accumulation of cyclic AMP (cAMP), thus attenuating the signalling capabilities of glucagon. Binding of glucagon to its receptor activates adenylate cyclase, consequently stimulating the cAMP dependent kinase, protein kinase A (PKA), to phosphorylate downstream targets that increase hepatic glucose production.

In circumstances where metformin is contraindicated, gastrointestinal complications prove problematic (Bailey *et al.,* 1996), or treatment goals are not met, one of the second line anti-diabetics may be prescribed, yet these often have more undesirable side effects.

1.6.2 Thiozolidinediones

Initially the thiazolidinediones were thought to activate PPARγ to modulate the transcription of essential genes involved in lipid metabolism, reducing pro-inflammatory cytokines to attenuate insulin resistance. However, like metformin the thiazolidendiones have been found to exert a cohort of their effects through the action of AMPK (LeBrasseur *et al.,* 2006). More recently, these compounds been found to bind to the mitochondria pyruvate carrier 1 (mpc1) and mpc2, to modulate the entry of pyruvate into the tricarboxylic acid cycle (Colca *et al.,* 2013). The thiazolidendiones may therefore regulate mitochondrial fatty acid synthesis and branched-chain amino acid levels to modulate insulin sensitivity, as a change in the supply of branched-chain amino acids has been proposed to activate mTOR, a negative regulator of insulin action and β-cell function. Side effects of this class of anti-diabetics include weight gain, osteoporosis, heart failure and increased low-density lipoprotein cholesterol (LDL-C) (Colca *et al.,* 2014).

1.6.3 Sulfonylureas

The sulfonylureas comprise the oldest anti-diabetic therapy. However, these drugs have been phased out due to a high incidence of adverse reactions. The second generation of sulfonylureas represent the next most commonly prescribed drugs after metformin for the treatment of type 2 diabetes. These compounds bind to the sulfonylurea receptor (SUR), a major component of K_{ATP} channels in pancreatic β-cells, mimicking the effect of ATP binding to close the channels. This depolarises the β-cell membrane, opening Ca^{2+} channels, which stimulates the fusion of insulin secretory vesicles with the cell membrane. Sulfonylureas have also been observed to promote insulin secretion as they bind the exchange protein directly activated by cAMP, which interacts with the Rap1 protein to increase vesicle fusion. However, as a consequence of augmented insulin secretion, the sulfonylureas often cause hypoglycaemia, which is associated with an increased risk of cardiovascular events. Furthermore, SUR isoforms are also found on cardiomyocytes and help mediate adaptations to cardiac ischemia by increasing K^+ efflux, although this predisposes malignant ventricular arrhythmias. Sulfonylureas may therefore confer antiarrhythmic properties but may enlarge infarct size (Thulé and Umpierrez, 2014).

1.6.4 Metaglitinides

The meglitinides function in a similar way, yet with a different molecular binding site to the sulfonylureas, as they close β-cell membrane K_{ATP} channels to promote insulin secretion. These compounds have a shorter duration of action and thus a reduced but not eliminated risk of hypoglycaemia (Stein, Lamos and Davis, 2013).

1.6.5 α-Glucosidase Inhibitors

The α-glucosidase inhibitors attenuate intestinal α-glucosidase to delay the absorption of consumed carbohydrates resulting in a reduction in blood glucose levels. Side effects are minimal, however, gastrointestinal complications and frequent dosing regimes significantly reduce compliance (Stein, Lamos and Davis, 2013).

1.6.6 Dopamine-2 Agonists

The dopamine-2 agonist bromocriptine is believed to alter the hypothalamic circadian rhythm to offset an insulin resistant state. Taken within two hours of waking, bromocriptine reduces the increased prolactin levels typically associated with type 2 diabetics in a state of fasting hyperglycaemia. As a consequence, the dopamine-2 agonist is believed to restore dopaminergic activity, decreasing plasma levels of glucose, triglycerides and free fatty acids. Furthermore, bromocriptine reduces uncoupled inducible nitric oxide synthase (iNOS)- and endothelial NOS (eNOS)-stimulated generation of reactive oxygen species to protect against atherogenesis in the high fat–fed spontaneously hypertensive rat. It has been observed to also decrease major cardiac events in human subjects (Defronzo, 2011). However, these anti-diabetic agents seem to exert a modest influence on glycaemic control with associated reports of nausea, dizziness, fatigue and rhinitis (Inzucchi *et al.*, 2015).

1.6.7 Sodium-Glucose Co-Transporter 2 Inhibitors

The sodium-glucose co-transporter 2 (SGLT2) is solely expressed in the apical domain of the epithelial cells in the early proximal convoluted tubule of the kidney, where this protein couples the transport of glucose with sodium against a concentration gradient. SGLT2 inhibitors block the action of the transporters, enhancing the excretion of

glucose to improve glycaemic control. Mild side effects include genitourinary infections, polyuria, hypotension and increased LDL-C and creatinine levels (Idris and Donnelly, 2009, Inzucchi *et al.,* 2015)**.**

1.6.8 Amylin Agonists

Amylin is a pancreatic β-cell glucoregulatory hormone, co-released with insulin. Upon binding to its receptor, a GPCR in the brain, amylin reduces glucagon release from the pancreas, suppresses appetite and modulates gastric emptying. The amylin agonist, pramlintide exhibits a similar biological effect to amylin. However, frequent administration is required and side effects including hypoglycaemia and gastrointestinal problems have been observed (Hay *et al.,* 2015).

1.6.9 Bile Acids Sequesterants

The bile acids sequesterant, colesevelam binds bile acids in the intestine forming a complex that cannot be reabsorbed through the enterohepatic circulation. As a consequence bile acid synthesis increases, facilitated by the nuclear farnesoid X receptor, while incretin hormones are also augmented through the action of the GPCR, TGR5. As a result, gastric emptying is delayed, hepatic glucose metabolism improves, insulin secretion is enhanced and glucose absorption is reduced. Complications of these drugs include gastrointestinal complaints, an increase in triglycerides and compromised absorption of other medications (Hansen *et al.,* 2014).

1.6.10 Incretin Based Therapies

As observed with bile acid sequesterants, targeting the incretin system is a promising approach to attenuate the effects of type 2 diabetes. The incretin hormones GIP and GLP-1 are secreted in response to nutrients entering the gut. Upon binding to their

receptors, GPCRs in β-cells, GLP-1 and GIP induce a signalling cascade to increase insulin secretion before being rapidly inactivated by dipeptidyl peptidase 4 (DPP-4). This effect is responsible for 50 – 70 % of insulin secretion, yet is markedly reduced and sometimes absent in subjects with type 2 diabetes. The GLP-1 receptor agonists exhibit increased resistance to DPP-4 degradation to markedly improve insulin secretion, decrease glucagon release, delay gastric emptying and increase satiety (Garber, 2011). However, as this is an injectable therapy, training is required and may be disconcerting. Apprehension also surrounds this therapy as cases of acute pancreatitis have been reported with implications for pancreatic cancer, while medullary thyroid tumors have been observed in animals (Nauck and Friedrich, 2013).

The DPP-4 inhibitors reduce the degradation of both GIP and GLP-1. However, the hypoglycaemic efficacy is less than that of GLP-1 agonists as concentrations cannot rise above physiological levels. The DPP-4 inhibitors also demonstrate no effect on satiety or gastric emptying. Concerns have been raised regarding the safety of these compounds as cases of acute pancreatitis and seronegative polyarthropathy have been reported (Tomkin, 2014).

1.7 Guanine Nucleotide Binding Protein Coupled Receptors

The actions of dopamine-2, amylin, GIP, GLIP-1 and bile acids to modulate glycaemic control through the action of GPCRs emphasises the importance of these receptors in the regulation of a multitude of cellular functions that may contribute to the development of type 2 diabetes. GPCRs comprise the largest protein superfamily in mammalian genomes, with more than 800 genes encoding for these versatile receptors in humans (Fredriksson *et al.,* 2003). GPCRs are characterised by the presence of seven membrane spanning α-helical segments separated by alternating intracellular and extracellular loop regions. These membrane-bound receptors recognise a variety of extracellular stimuli, such as photons, ions, small molecules, peptides and proteins and propagate this signal potential across the membrane over a distance of 50 Å to elicit intracellular responses (Stevens *et al.,* 2013). With each GPCR highly specific to a particular signal, these receptors mediate most cellular responses to hormones and neurotransmitters, as well as being responsible for vision, olfaction and taste (Rosenbaum *et al.,* 2009). Based on their sequence and structural similarity, GPCRs are commonly divided into five families named Glutamate, Rhodopsin, Adhesion, Frizzled/taste receptor 2 and Secretin (GRAFS) (Fig. 1.11) (Fredriksson *et al.,* 2003).

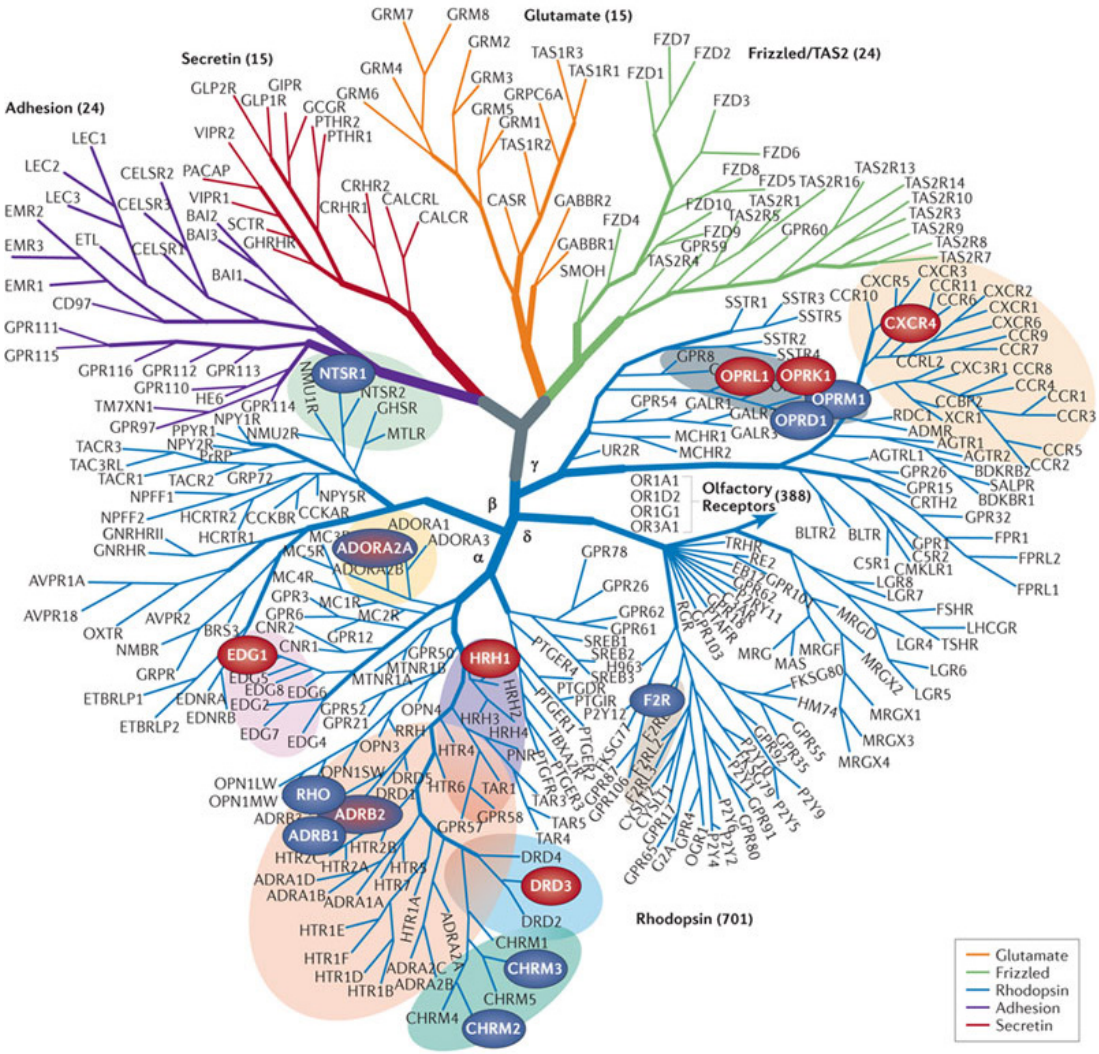

Figure 1.11 The GRAFS Classification of GPCRs.

The GRAFS classification system places more than 800 human GPCRs into five major families: Rhodopsin (class A); Secretin and Adhesion (class B); Glutamate (class C); and Frizzled/taste receptor 2 (TAS2), based on their sequence and structural similarity. Image from (Stevens *et al.*, 2013)**.**

1.7.1 Guanine Nucleotide Binding Proteins

Despite these resounding similarities, GPCRs employ diverse and complex regulatory processes to convey extracellular signals to the internal environment of the cell. Classically, GPCRs were solely believed to achieve this by coupling the binding of an agonist to the activation of multiple heterotrimeric guanine nucleotide binding protein (G protein) subtypes (Rosenbaum *et al.,* 2009). G proteins are composed of an αβγ trimer from the various combinations of the 21 α, 6 β and 12 γ subunits (Downes and Gautam, 1999). The α-subunit is GDP-bound and complexed to a Gβγ heterodimer, which acts as a guanine nucleotide dissociation inhibitor, stabilising the protein in the inactive GDP-bound state (Higashijima *et al.,* 1987). Based on sequence similarity of the α-subunit, which confers similar downstream signalling mechanisms, G proteins are divided into four families (Table 1.2) (Strathmann and Simon, 1991, Kimple *et al.,* 2014).

Table 1.2 G protein families.

G protein family	Family members	Effector protein
G_s	G_s, G_{olf}	Adenylate Cyclase
G_i	G_{i1}, G_{i2}, G_{i3}, G_{o1}, G_{o2}, G_z. G_t, G_{gust}	Adenylate Cyclase
G_q	G_q, G_{11}, G_{14}, $G_{15/16}$	Phospholipase C
$G_{12/13}$	G_{12}, G_{13}	RhoGEF

1.7.2 Canonical GPCR Signalling

The binding of an agonist to a GPCR promotes a change in the relative positioning of transmembrane α-helices III and VI which leads to reorientation of the third intracellular loop of the receptor to uncover previously cryptic G protein binding sites (Wess, 1997, Kobilka, 2002). The Gβγ heterodimer serves to target Gα to the membrane (Rehm, 1997) and present it to the receptor in the appropriate conformation (Oldham and Hamm, 2006, Smrcka, 2008). Upon interaction, the receptor acts as a guanine nucleotide exchange factor (GEF), inducing the release of GDP from the α-subunit of the G protein in favour of GTP. The active GTP-bound α-subunit dissociates from the receptor and the Gβγ dimer to interact with effector proteins with 20 – 100 fold higher affinity than in their GDP-bound state (Hamm, 1998, Knall and Johnson, 1998). The now independent Gβγ dimer relays signals from the GPCR to a number of target proteins including; adenylate cyclase isoforms, phospholipase isoforms, ion channels, PI3K, and MAPKs (Khan *et al.,* 2013). The α-subunits of the G_s and G_i subfamily members regulate adenylate cyclase to stimulate (G_s) or inhibit (G_i) the production of cAMP, which influences PKA (Krebs, 1989). $G\alpha_q$ activates phospholipase C (PLC) to modulate intracellular levels of 1,2-diacylglycerol (DAG) and inositol 1,4,5 triphosphate (IP_3) (Birnbaumer *et al.,* 1990, Rhee, 2001). DAG signals directly to protein kinase C (PKC) (Kishimoto *et al.,* 1980), whereas IP_3 binds to its receptor in the endoplasmic reticulum to trigger the release of Ca^{2+} (Berridge and Irvine, 1984). $G\alpha_{12/13}$ stimulates the activation of Rho guanine nucleotide exchange factors (RhoGEFs) which initiate Rho-dependent signalling cascades through Rho-associated coiled-coil containing protein kinases (Hart *et al.,* 1998, Siehler, 2009) (Fig. 1.12). The activation of these secondary messengers imparts the signal potential of the GPCRs to regulate a multitude of specific cellular cascades throughout the cell (Offermanns,

2003).

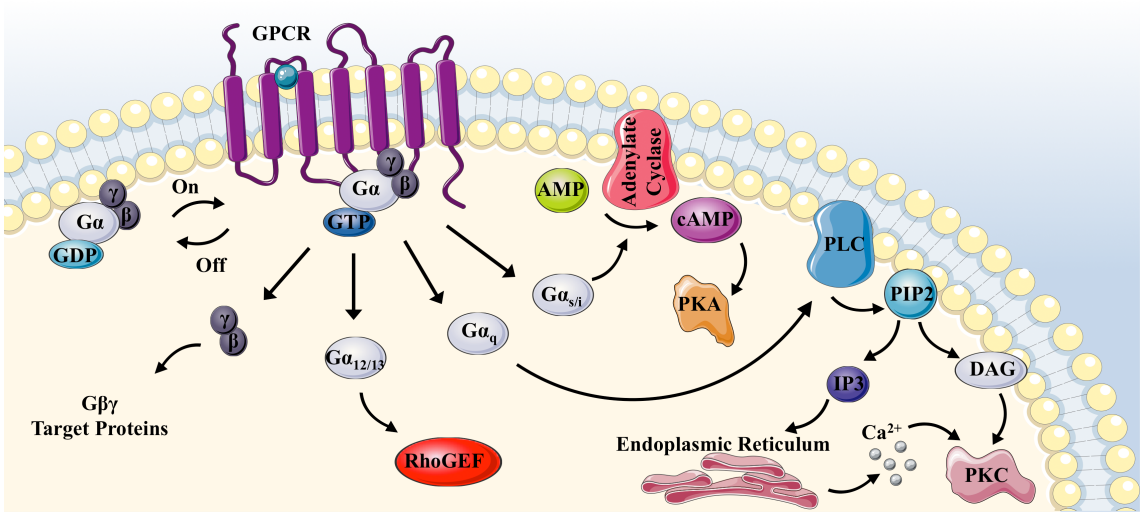

Figure 1.12 GPCR signal transduction through G proteins.

Upon ligand binding a GPCR undergoes a conformational change to recruit and activate a specific G protein by exchanging GDP for GTP at the α-subunit. The now independent Gβγ dimer targets specific effector proteins while the four classes of GTP-bound Gα proteins transmit signal potential to family dependent target proteins.

1.7.3 GPCR Signal Termination

The duration of one cycle of receptor activation of an effector can be dictated by the intrinsic guanosine triphosphatase (GTPase) activity of Gα as the hydrolysis of GTP to GDP promotes reconstitution and membrane localisation of the Gαβγ heterotrimer (Neer, 1995). This step is often influenced by regulators of G protein signalling (RGS) that bind Gα and accelerate GTP hydrolysis (Fig. 1.13) (Siderovski and Willard, 2005, Oldham and Hamm, 2008).

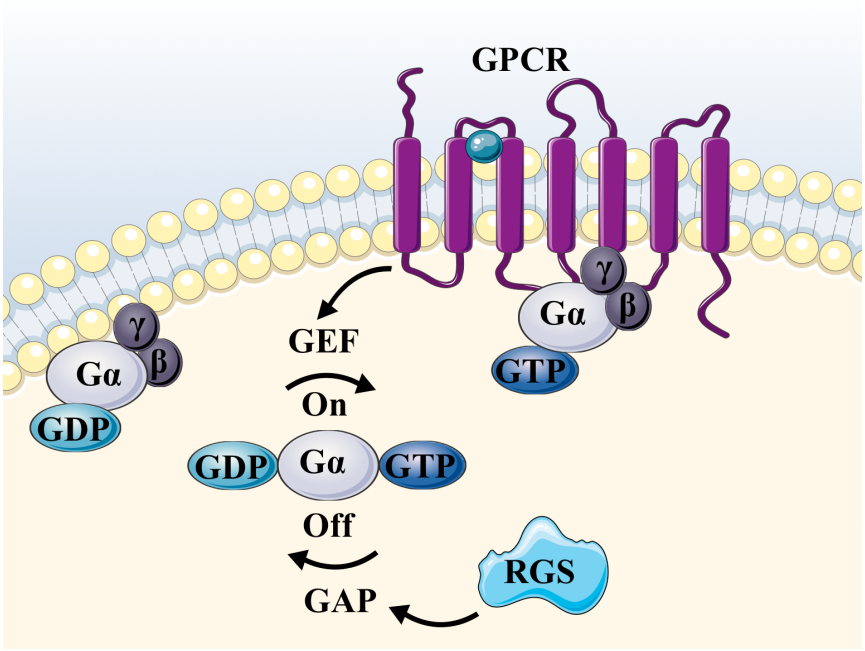

Figure 1.13 Regulation of G protein activity.

Focusing on the G protein α-subunit, ligand occupied GPCRs act as GEFs, facilitating GDP release and the subsequent binding of GTP to activate the G protein. RGS proteins act as GTPase-accelerating proteins (GAPs) for Gα, dramatically enhancing their core rate of GTP hydrolysis to terminate GPCR signal transduction.

However, GPCRs have been found to have more complex signalling behaviour beyond the control of G proteins alone. To rapidly terminate activation, negative feedback loops uncouple GPCRs from heterotrimeric G proteins through covalent modifications of the receptor as a consequence of phosphorylation by intracellular kinases (Thompson and Findlay, 1984, Premont *et al.,* 1995). G protein coupled receptor kinase (GRK) association is promoted by Gβγ dimers (Daaka *et al.,* 1997), whereas second messenger dependent kinases; PKA and PKC are stimulated by cAMP and IP_3 as a consequence of $G\alpha_{i/s}$ and $G\alpha_q$ respective activation (Tobin, 2008). The phosphorylated receptor has increased affinity for cytosolic cofactor proteins called β-arrestins, which more effectively uncouple the receptor from the G protein by sterically inhibiting interactions (Lohse *et al.,* 1990). The β-arrestin-receptor complex becomes associated with clathrin-coated pits which shape rounded vesicles in the cytoplasm for intracellular handling (Goodman *et al.*, 1996). The receptor can then be trafficked to lysosomes for degradation or to recycling endosomes which dephosphorylate and reprocess the GPCR back to the plasma membrane (Fig. 1.14) (Pierce *et al.,* 2002).

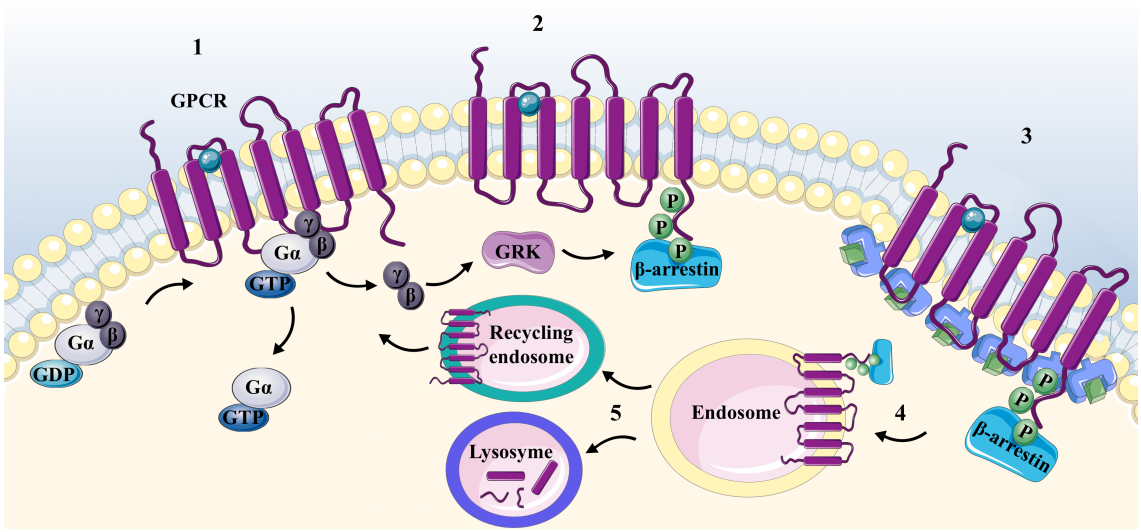

Figure 1.14 GPCR desensitisation.

(1) Ligand binding recruits a G protein to the GPCR, which becomes activated through receptor-induced exchange of GDP for GTP. The free Gβγ dimer and Gα subunits signal to downstream effector proteins eventually initiating a negative feedback loop to desensitise the receptor to the bound ligand. (2) Activation of PKA, PKC and GRK leads to GPCR phosphorylation and the recruitment of β-arrestin. (3) The GPCR-β-arrestin complex binds with high affinity to clathrin. (4) Clathrin-coated pits lead to receptor internalisation. (5) The receptor is then processed by endosomes (Pierce *et al.,* 2002).

1.7.4 Non-Canonical GPCR Signalling

Activation of GPCR signalling may also go beyond the classical function of coupling an agonist to a G protein to modulate a downstream effector. Functional studies of the β-adrenergic receptor (β2AR), the most well characterised GPCR, demonstrate constitutive activity of the receptor which can be blocked by an inverse agonist (Chidiac *et al.,* 1994). Furthermore, a β2AR mutant incapable of G protein activation was found to activate MAPK pathways in a β-arrestin dependent manner (Shenoy *et al.,* 2006). As this multifaceted behaviour has been observed for many different GPCRs (Pierce and Lefkowitz, 2001, Tao, 2008), a complex picture of GPCR activation has emerged, while the structural changes associated with activation may be similar, the mechanism by which these changes are evoked is quite different.

1.7.5 Kinetics of GPCR Activation

Natural and synthetic ligands acting on GPCRs are classified into full agonists, partial agonists, inverse agonists and antagonists. A number of kinetic models have been developed to describe the response of a GPCR to ligand binding to transition between active and inactive states (Bouvier, 2013).

In the classical two-state model (Leff ,1995) (Fig. 1.15A), GPCRs are thought to exist in equilibrium between two states; resting (R) and activated (R*). In the absence of a ligand the equilibrium of most receptors favours the R state while few, like rhodopsin, demonstrating constitutive activity, lie in the R* state. The efficacy of a ligand reflects its ability to alter the equilibrium between these two states (Kobilka, 2007). Inverse agonists stabilise the R state favouring the transition toward inactive conformations to reduce the level of basal or constitutive activity below that of the resting receptor, while

agonists preferentially bind the active conformations to amplify receptor activity.

In the three state model (Fig. 1.15B), in the absence of a ligand, the receptor is in an intermediate state (R*), showing some level of activity. Inverse agonists favour inactive conformations (R), transitioning receptor equilibrium towards this state, whereas agonists favour active conformations (R**). Full agonists maximally stimulate the biological responses of the receptor while partial agonists are unable to elicit full activity even at saturating concentrations. Fully active conformations are promoted by GPCR coupling to multiple G proteins based on the specificity of the ligand (Leff *et al.,* 1997).

A revised model (Fig 1.15C), proposes that the unliganded receptor is largely in an inactive conformation promoted by inverse agonists. Agonists favour intermediate states (R*), while unique fully activated conformational states (R**, $R^{\#\#}$ and R'') are promoted by specific signalling effectors such as G proteins, kinases and β-arrestins (Kenakin, 2003). Antagonists have equal affinity for inactive, intermediate and active states and therefore have no effect on the signalling potential of the receptor but can prevent other ligands from binding (Rosenbaum *et al.,* 2009).

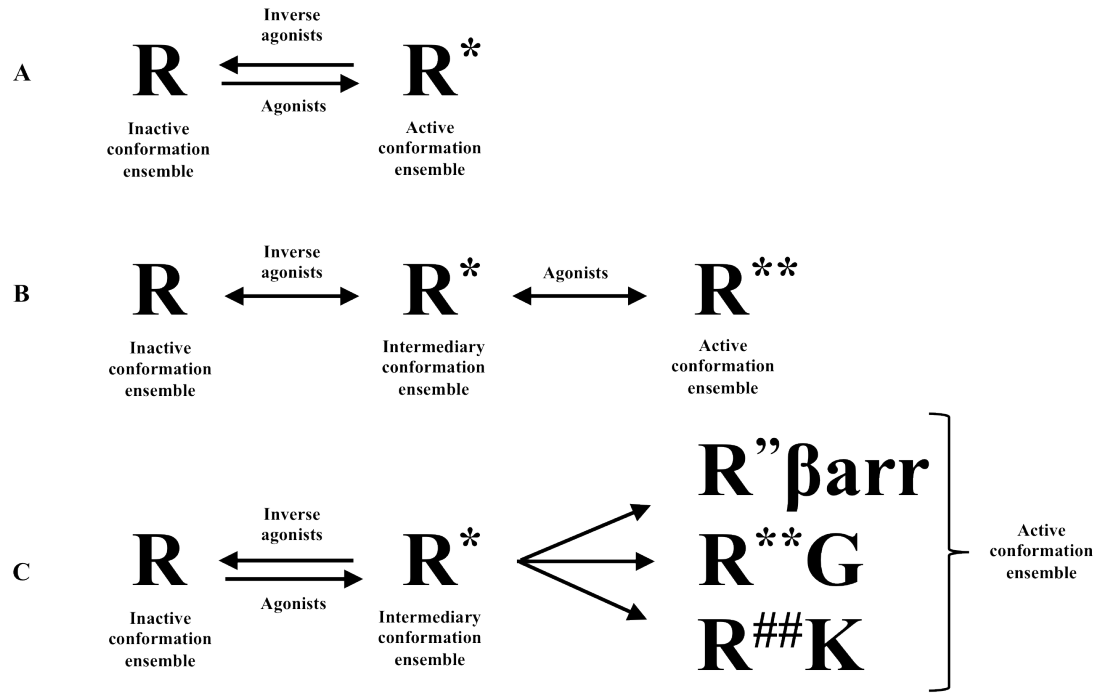

Figure 1.15 Active and inactive states of GPCRs.

(A) The two state model of GPCR kinetics. (B) The three state model of GPCR kinetics. (C) The adapted three state model which considers agonist stabilisation of unique fully activated conformational states promoted by specific signalling effectors such as G proteins (R**G), kinases ($R^{\#\#}K$) and β-arrestins (R”βarr). Image adapted from (Bouvier, 2013).

1.7.6 GPCRs and Type 2 Diabetes

The diverse GPCR superfamily plays a key role in the overall homeostasis of complex organisms making them important physiological regulators of many disease states. The ability of GPCRs to transduce extracellular signals into intracellular effector pathways makes them appealing drug targets with 30 – 40 % of marketed drugs affecting these versatile receptors (Ma and Zemmel, 2002, Lappano and Maggiolini, 2011, Tautermann, 2014). Moreover, the specific impact of GPCRs on immune responses, appetite, insulin secretion and energy homeostasis makes them attractive for the treatment of type 2 diabetes (Table 1.3). In addition to targeting GPCRs with known ligands and downstream effects, several of the more than 140 orphan receptors (Tang *et al.,* 2012), have been found to regulate key aspects of the diabetic phenotype, as evidenced by knockout and knockin studies (Matsuda and Aiba, 2004).

Table 1.3 GPCRs and type 2 diabetes.

GPCR	Effects mediated by receptor	References
Adrenergic Receptors		
β2AR	Regulates energy metabolism and glycogenolysis during exercise	(Chruscinski *et al.,* 1999)
α-(2A)AR	Contributes to defective insulin secretion in diabetic patients	(Robertson *et al.,* 1976) (Rosengren *et al.,* 2010)
Arginine Vasopressin Receptor		
AVPR2	Maintains water homeostasis; loss of function causes nephrogenic diabetes insipidus	(van der Ouweland *et al.,* 1992)
Bombesin Receptors		
NMBR	Female specific role in the regulation of energetic homeostasis, with female KO mice partially resistance to diet-induced obesity	(Paula *et al.,* 2010)
GRPR	Regulates satiety and participates in the termination of meals	(Ladenheim *et al.,* 2002)
BRS3	Regulates body weight, satiety and glucose/insulin homeostasis	(Ohki-Hamazaki *et al.,* 1997)

Table 1.3 GPCRs and type 2 diabetes.

GPCR	Effects mediated by receptor	References
Cannabinoid Receptors		
GPR55	Increases calcium transients and insulin secretion stimulated by glucose	(Romero-Zerbo *et al.,* 2011)
CB1	Modulates the endocrine hypothalamic-peripheral endocrine axes to regulate appetite and energy balance	(Ravinet Trillou *et al.,* 2004)
CB2	Modulates Tnf and Ccl2 expression to promote insulin resistance and liver inflammation	(Deveaux *et al.,* 2009)
Cholecystokinin Receptors		
CCK-AR	Inhibits short-term food intake	(Kopin *et al.,* 1999)
CCK-BR	Regulates digestion and absorption	(Nagata *et al.,* 1996)
Estrogen Receptors		
GPR30	Induces insulin secretion	(Sharma and Prossnitz, 2011)
Fatty Acid Receptors		
GPR41	Regulator of host energy balance through effects that are dependent upon the gut microbiota	(Samuel *et al.,* 2008)
GPR43	Inhibits lipolysis, regulates plasma lipid profiles and is involved neutrophil chemotaxis	(Ge *et al.,* 2008)
GPR40	Enhances glucose-stimulated insulin secretion. Conflicting KO studies have showed this receptor to protect mice from obesity-induced hyperinsulinemia and exacerbate insulin resistance	(Steneberg *et al.,* 2005) (Shapiro *et al.,* 2005) (Kebede *et al.,* 2008)
GPR84	Regulates IL-4 production by activated T lymphocytes	(Venkataraman and Kuo, 2005)
GPR120	Induces secretion of GLP1 and GIP. Inhibits inflammatory signalling in macrophages	(Oh *et al.,* 2010)
GPR119	Important for incretin and insulin secretion	(Lan *et al.,* 2009)
Ghrelin Receptors		
GHS-R	Stimulates growth hormone secretion, modulates glucose sensing and insulin sensitivity	(Sun *et al.,* 2008)
GPR39	Regulates body weight and endocrine function	(Tremblay *et al.,* 2007) (Holst *et al.,* 2009)

Table 1.3 GPCRs and type 2 diabetes.

GPCR	Effects mediated by receptor	References
Glucagon Receptor		
GCGR	Regulates insulin sensitivity and β cell function	(Sørensen *et al.,* 2006)
Hydroxycarboxylic Acid Receptors		
GPR109a	Mediates anti-lipolytic effects of ketone bodies, activates immune cells	(Taggart *et al.,* 2005)
GPR109b	Anti-lipolytic effects, activates immune cells	(Ahmed *et al.,* 2009)
GPR81	Mediates anti-lipolytic effects of insulin	(Cai *et al.,* 2008)
Incretin Receptors		
GLP-1R	Regulates glucose production and the action of insulin	(Ayala *et al.,* 2010)
GIPR	Stimulates insulin release	(Miyawaki *et al.,* 2002)
Lysophospholipid Receptors		
GPR12	Regulates weight gain and energy expenditure	(Bjursell *et al.,* 2006a)
Melanin Concentrating Hormone Receptors		
MCH1	Regulates insulin sensitivity and/or secretion via a mechanism not dependent on decreased body weight	(Bjursell *et al.,*2006b)
Melanocortin Receptors		
MC3R	Regulates energy homeostasis playing a critical role in weight regulation	(Lee *et al.,* 2002)
MC4R	Regulates energy homeostasis and food intake	(Huszar et al., 1997)
Melatonin Receptors		
MT1	Regulates glucose metabolism. KO mice display increased insulin resistance	(Contreras-Alcantara *et al.,* 2010)
GPR50	Regulates thermogenesis and torpor. *ob/ob* mice display reduced receptor expression	(Bechtold *et al.,* 2012)
Metastin Receptor		
GPR54	Regulates endocrine function, weight gain and energy expenditure primarily in female mice	(Tolson *et al.,* 2014)
Muscarinic Acetylcholine Receptors		
M3	Regulates food intake. Mice lacking the receptor display reduced food intake, reduced body weight and low leptin and insulin serum levels	(Yamada *et al.,* 2001)
Neuropeptide Receptors		
NPY Receptors	Control appetite and regulate insulin secretion	(Chamorro *et al.,* 2002)

Table 1.3 GPCRs and type 2 diabetes.

GPCR	Effects mediated by receptor	References
Neuropeptide Receptors		
Orexin receptors	Regulate appetite	(Rodgers *et al.,* 2002)
GPR7	Regulates energy homeostasis in male mice. KO male mice develop adult-onset obese phenotype exacerbated with a HFD	(Ishii *et al.,* 2003)
Orphan Receptors		
GPR21	Coordinates macrophage pro-inflammatory activity. KO mice have improved glucose tolerance, insulin sensitivity and a modest lean phenotype	(Gardner *et al.,* 2012) (Osborn *et al.,* 2012)
GPR26	Regulates energy homeostasis; GPR26 deficiency in the hypothalamus is associated with high genetic susceptibility to the onset of obesity	(Chen, Liu, *et al.,* 2012)
GPR116	Regulates systemic energy homeostasis; adipose tissue specific KO mice displayed glucose intolerance and insulin resistance	(Nie *et al.,* 2012)
Serotonin Receptors		
5HT2C	Regulates appetite. KO mice are overweight as a result of abnormal control of feeding behaviour	(Tecott *et al.,* 1995)
5HT1A	Regulates satiety. The receptor agonist stimulates food intake in lean control rats but inhibits feeding in obese rats up to 6 months of age	(Voigt *et al.,* 2002)
Somatostatin Receptors		
SSTR2	Regulates hypoglycaemia-stimulated glucagon and corticosterone release in diabetic rats	(Yue *et al.,* 2012)
SST5	Regulates pancreatic insulin secretion and contributes to the regulation of glucose homeostasis and insulin sensitivity	(Strowski *et al.,* 2003)
UDP Glucose Receptors		
GPR105	Regulates insulin secretion and immune cell chemotaxis. Conflicting reports on the consequences of receptor deletion on insulin signalling	(Xu *et al.,* 2012) (Meister *et al.,* 2014)

1.7.6.1 GPR21

GPR21, an orphan GPCR has recently emerged as a novel target for the treatment of type 2 diabetes (Gardner *et al.,* 2012, Osborn *et al.,* 2012). Gardner and colleagues found GPR21 knockout mice fed on a high fat diet (HFD) to have a modest lean phenotype, increased insulin sensitivity, improved glucose tolerance and a reduction in pro-inflammatory markers when compared to wild type littermates. In a simultaneous study, the Olefsky group (Osborn *et al.,* 2012), reiterated these findings and proposed the involvement of GPR21 in coordinating macrophage pro-inflammatory activity in the context of obesity-induced insulin resistance. In wild type mice, GPR21 mRNA was highly induced in the stromal vascular fraction (SVF) of adipose tissue from HFD mice but not in the lean counterparts, while knockout mice had a reduced percentage of M1 macrophages in both control and HFD states. Increased expression of GPR21 was observed in wild type M1 macrophages with lower expression in the anti-inflammatory M2 macrophages of the SVF. Furthermore, the essential cytoskeletal reorganisation required for transmigration was absent in GPR21 knockout macrophages. Overall, knockout mice demonstrated a decrease in pro-inflammatory gene expression and an increase in anti-inflammatory genes with a concurrent increase in insulin-stimulated Akt phosphorylation in liver and adipose tissue. Moreover, wild type mice that received bone marrow transplantations from knockout mice demonstrated a similar phenotype to the GPR21 deficient mice. Receptors such as GPR21 open new avenues for the discovery of next generation drugs to effectively treat obesity-induced type 2 diabetes.

1.8 Computational Drug Discovery

A major challenge in targeting GPCRs for the development of novel anti-diabetic therapies is the lack of experimentally elucidated high-resolution crystal structures. This proves even more irksome in the case of orphan receptors for which no endogenous ligands have yet been identified. However, advances in homology modelling and ligand docking studies have vastly improved the development of targeted therapies towards such GPCRs (Stockert and Devi, 2015).

1.8.1 Homology Modelling

Homology modelling involves the development of a model of a protein of interest based on its amino acid sequence and a template protein structure of related homologous proteins. A template is chosen using a BLASTP search of the Protein Data Bank (www.rcsb.org) (Altschul *et al.,* 1990) with three criteria considered, the structure resolution, ligand type and percentage sequence identity to the target (Xiang, 2006).

As crystal structures are available for less than 20 unique receptors in the rhodopsin-like class, the family in which GPR21 resides, (Fredriksson and Schio, 2005, Latek *et al.,* 2013), it is very difficult to achieve a sequence identity above 30 % with most GPCRs. Therefore, when working with these receptors, it is more important to have a high sequence identity between the template and target in the conserved seven transmembrane region, as this is likely to be a ligand binding region, while decreased sequence similarity in the external loops should not affect the success of the model (Bhattacharya *et al.,* 2013). The use of multiple templates may also increase the rate of success in these challenging cases (Latek *et al.,* 2013).

Once a template has been selected, the next step is to align it with the target to identify regions that may be a consequence of functional, structural or evolutionary relationships between the sequences using an alignment tool such as Clustal W (Larkin *et al.,* 2007). It is then important to satisfy the spatial restraints of the model, more specifically the modelling of loops using a database of loops or by *ab initio* methods, to resolve regions of the target sequence that are not aligned to a template. These regions are most susceptible to errors, especially when there is a low sequence identity between the target and template (Michalsky *et al.,* 2003). The resulting structure is then analysed with a range of computational tools to determine the quality of the model (Fanelli and De Benedetti, 2011).

1.8.2 Molecular Docking

When a satisfactory homology model has been constructed molecular docking can be employed to predict the predominant binding mode of a possible ligand with the protein. In order to achieve this, it must be assumed that small molecules interact with the receptor and the binding site has been conserved in the template used to generate the model. In the case of orphan receptors, blind docking can be undertaken with programmes such as LigPrep to prepare high quality, all atom, 3D structures which can be inputted into a docking tool such as Glide (Grid-based ligand docking with energetics) from the Schrödinger product suite (www.schrodinger.com). The simplest approach to take is rigid-rigid docking where the protein and ligands are kept static. Glide searches for favourable interactions between the ligand and the homology model. Ranked ligands can then be screened through flexible docking to get a better representation of the possible interactions. Once a clear picture is established, ligands can be altered to improve affinity and prevent clashes with the protein, and finally screened in a biological assay. These methods have been successful in identifying

potent and selective ligands for numerous GPCRs (Evers and Klabunde, 2005, Dong *et al.,* 2013, Jacobson 2013, Pappalardo *et al.,* 2014, Stockert and Devi, 2015).

1.9 Aims and Objectives

Type 2 diabetes is a multifaceted metabolic disorder developing as a consequence of distorted cellular signalling. This project aimed to identify novel therapeutic avenues for the treatment of this disease by elucidating the underlying mechanism of action of a successful, novel anti-diabetic compound, RTC-1, and by exposing the signalling mechanisms of a recently identified target, GPR21.

Solidifying the mechanism of action of a novel compound is essential to the development of a prospective therapy for type 2 diabetes. RTC-1 was designed to clear serum RBP levels in an attempt to modulate the development of insulin resistance. However, *in vitro* analysis revealed the ability of this compound to stimulate glucose uptake, an effect its predicted mechanism of action would not account for. Through cellular analysis, the effects of RTC-1 were explored in respect to key aspects modified with the development of type 2 diabetes, namely glucose uptake, insulin resistance, adipogenesis and osteogenesis. While a comparative study with the most common anti-diabetic therapy, metformin, gave context to the influence of RTC-1.

In a separate study, the signalling capabilities of a novel diabetic target, GPR21, were investigated with the hope of regulating its proposed effect on macrophage migration. In order to fully appreciate this GPCR in the context of insulin resistance, the G protein to which GPR21 couples to amplify signal potential was assessed, while the downstream consequences of receptor activation on insulin signalling, glucose uptake and macrophage migration were explored. In addition to this, the influence of a novel compound designed through a computational approach to bind GPR21 was evaluated to determine if attenuating the effects of the receptor could prevent the development of insulin resistance through a previously unexplored mechanism.

Chapter 2

Materials and Methods

2.1 Materials

All chemicals used were from Sigma-Aldrich unless otherwise stated.

2.2 Cell Culture

All cell culture materials and reagents were kept sterile and used in a Class II biological safety cabinet. All cell lines were maintained at 37 °C in a sterile, humidified, 5 % CO_2 atmosphere. Foetal Bovine Serum (FBS) and horse serum were heat inactivated at 56 °C for 30 minutes prior to use, to inactivate complement.

2.2.1 Culture of Adherent Cells

Adherent cell lines (Table 2.1) were maintained in high glucose (4500 mg/ml) Dulbecco's Modified Eagle's Medium (DMEM) containing 100 µg/ml penicillin/streptomycin, 2 mM L-glutamine (complete medium) and 10 % (v/v) FBS. Cryo-preserved cells were rapidly thawed in a 37 °C water bath, washed with 10 ml complete medium containing 10 % (v/v) FBS and centrifuged to remove the cryo-protectant, DMSO. Cells were resuspended in complete medium supplemented with 10 % (v/v) FBS and cultured in a T75 flask (Sarstedt) at 37 °C, in a humidified, 5 % CO_2 environment. When 80 % confluency was reached, non-adherent cells were washed away with Dulbecco's phosphate buffered saline (DPBS) (Gibco). Remaining cells were detached from the flask by incubating with 0.25 % (v/v) trypsin-1 mM EDTA solution (Thermo Fisher Scientific), for 5 minutes at 37 °C. Protease action was neutralised with the addition of complete medium supplemented with 10 % (v/v) FBS. Trypsin-EDTA was removed by centrifugation, cells were resuspended in complete medium with 10 % (v/v) FBS and counted using a haemocytometer. Cells were seeded at an optimal density, as recommended by the supplier, and incubated at 37 °C with 5 %

CO_2 until 80 % confluent. Cells were then passaged once more, cryo-preserved or differentiated if required.

Table 2.1 Adherent cell lines.

Cell line	Description	Culture medium
C2C12	Myoblast cell line from mouse skeletal muscle	High glucose DMEM (Thermo Fisher Scientific) 10 % FBS (Thermo Fisher Scientific) 2 mM L-glutamine (Thermo Fisher Scientific) 100 µg/ml penicillin/streptomycin (Thermo Fisher Scientific)
3T3-L1	Murine pre-adipocytes	High glucose DMEM (Thermo Fisher Scientific) 10 % FBS (Thermo Fisher Scientific) 2 mM L-glutamine (Thermo Fisher Scientific) 100 µg/ml penicillin/streptomycin (Thermo Fisher Scientific)
SH-SY5Y	Human neuroblastoma	High glucose DMEM (Thermo Fisher Scientific) 10 % FBS (Thermo Fisher Scientific) 2 mM L-glutamine (Thermo Fisher Scientific) 100 µg/ml penicillin/streptomycin (Thermo Fisher Scientific)
HEK293T	Immortalised Human embryonic kidney cell line containing the SV40 Large T-antigen	High glucose DMEM (Sigma-Aldrich) 10 % FBS (Sigma-Aldrich) 2 mM L-glutamine (Thermo Fisher Scientific) 100 µg/ml penicillin/streptomycin (Thermo Fisher Scientific)
BMDM	Immortalised murine bone marrow derived macrophage	High glucose DMEM (Sigma-Aldrich) 10 % FBS (Sigma-Aldrich) 2 mM L-glutamine (Thermo Fisher Scientific) 100 µg/ml penicillin/streptomycin (Thermo Fisher Scientific)
J774	Murine BALB/cN monocyte/macrophage	High glucose DMEM (Sigma-Aldrich) 10 % FBS (Sigma-Aldrich) 2 mM L-glutamine (Thermo Fisher Scientific) 100 µg/ml penicillin/streptomycin (Thermo Fisher Scientific)
CHO	Chinese Hamster Ovary cell line	Ham's F-12 Nutrient mixture (Sigma-Aldrich) 10 % FBS (Sigma-Aldrich) 2 mM L-glutamine (Thermo Fisher Scientific) 100 µg/ml penicillin/streptomycin (Thermo Fisher Scientific)
COS-1	Kidney cell line from African green monkey	High glucose DMEM (Sigma-Aldrich) 10 % FBS (Sigma-Aldrich) 2 mM L-glutamine (Thermo Fisher Scientifc) 100 µg/ml penicillin/streptomycin (Thermo Fisher Scientific)

Table 2.1 Adherent cell lines.

Cell line	Description	Culture medium
A549	Human alveolar basal epithelial cell line	Ham's F-12 Nutrient mixture (Sigma-Aldrich) 10 % FBS (Sigma-Aldrich) 2 mM L-glutamine (Thermo Fisher Scientific) 100 µg/ml penicillin/streptomycin (Thermo Fisher Scientific)
HepG2	Human cell line from a liver hepatocellular carcinoma	High glucose DMEM (Thermo Fisher Scientific) 10 % FBS (Thermo Fisher Scientific) 2 mM L-glutamine (Thermo Fisher Scientific) 100 µg/ml penicillin/streptomycin (Thermo Fisher Scientific)
MSC	Murine mesenchymal stromal cells isolated from the femur and tibia of 6 – 8 week old female BALB/c mice	Minimal Essential Medium alpha (αMEM) (Sigma-Aldrich) 10 % FBS (Thermo Fisher Scientific) 10 % Horse Serum (Gibco) 2 mM L-glutamine (Thermo Fisher Scientific) 100 µg/ml penicillin/streptomycin (Thermo Fisher Scientific)

2.2.1.1 C2C12 Cell Culture and Differentiation

C2C12 cells were purchased from Sigma-Aldrich (91031101), seeded at a density of $2x10^3$ cells/cm^2 and maintained as described in Section 2.2.1. When 80 % confluent, differentiation into myotubes was induced with complete medium supplemented with 2 % (v/v) horse serum (Gibco) for 3 days. Fully differentiated cells were washed once with DPBS and stimulated with various compounds in complete medium supplemented with 0.1 % (v/v) horse serum. Rotenone (R8875-5G), metformin (04635) and wortmannin (W3144) were obtained from Sigma-Aldrich. TNF-α (315-01A) was supplied by PeproTech and Compound C (171264) was from Merck Millipore. Insulin (Sigma-Aldrich, I9278) stimulations were carried out in filter sterilised (0.2 µm) Krebs Ringer Buffer containing glucose (KRBG); 136 mM NaCl, 20 mM HEPES, 4.7 mM KCl, 1 mM $MgSO_4$, 1 mM $CaCl_2$, 4.05 mM Na_2HPO_4, 0.95 mM NaH_2PO_4, 5 mM glucose, pH 7.4.

2.2.1.2 3T3-L1 Cell Culture and Differentiation

3T3-L1 cells were obtained from ATCC® (CL-173), seeded at a density of $2x10^4$ cells/cm^2 and maintained as described in Section 2.2.1. When 80 % confluent, differentiation into adipocytes was induced with complete medium supplemented with 10 % (v/v) FBS, 10 µg/ml insulin, 0.5 mM IBMX and 1 µM dexamethasone. After 2 days, the medium was changed to complete medium containing 10 % (v/v) FBS and 10 µg/ml insulin. Every 2 days following, medium was changed to complete medium containing 10 % (v/v) FBS until 80 % of cells formed intracellular lipid droplets.

Differentiated 3T3-L1 cells were stained for lipid accumulation as described by Kuri-Harcuch and Green (1978). Cells were washed twice with phosphate buffered saline (PBS) before fixing with 10 % (v/v) formalin for 20 minutes. Cells were then washed three times with PBS and incubated for 20 minutes with filtered (0.2 µm) 1.5 mg/ml Oil Red O, prepared in 1:1 isopropanol:PBS. Excess stain was removed by washing once with PBS and cells were visualised with an inverted light microscope. To quantify lipid accumulation, Oil Red O was extracted with isopropanol and absorbance was measured at 520 nm with an ELx800TM microplate reader (Kasturi and Joshi, 1982).

2.2.1.3 Murine Mesenchymal Stromal Cell (MSC) Culture and Differentiation

MSC isolated from the femur and tibia of 6 – 8 week old female BALB/c mice were kindly donated as a live culture courtesy of Dr. Karen English. Cells were maintained in complete αMEM supplemented with 10 % (v/v) FBS and 10 % (v/v) horse serum as described in Section 2.2.1 with an optimal seeding density of $1x10^5$ cells/cm^2. When 80 % confluent cells were differentiated into fat or bone cells.

Adipogenic differentiation was induced with MSC culture medium containing 5 µg/ml insulin, 50 µM indomethacin, 1 µM dexamethasone and 0.5 µM IBMX. Fresh medium was added every 3 days for 21 days. On day 21, cells were stained for lipid accumulation with Oil Red O (Section 2.2.1.2).

Osteoblast differentiation was induced with MSC culture medium supplemented with 1 mM dexamethasone, 20 mM β-glycerolphosphate, 50 µM L-ascorbic acid-2 phosphate and 50 ng/ml L-thyroxine sodium pentahydrate. Fresh medium was added every 3 days. After 21 days, cells were stained for calcium deposition with Alizarin Red S prepared in dH_2O (20 mg/ml). Cells were washed twice with PBS before fixing with 10 % (v/v) formalin for 20 minutes. Cells were then washed three times with PBS and incubated with Alizarin Red S for 20 minutes. Excess stain was removed by washing once with PBS and cells were visualised with an inverted light microscope. Calcium deposition was quantified as described by Tavakol and colleagues (2012). Alizarin Red S was extracted with 800 µl 10 % (v/v) acetic acid and agitated for 30 minutes at room temperature, cells were then scraped into a 1.5 ml tube and vortexed for 30 seconds. The solution was covered with 500 µl mineral oil, incubated for 10 minutes at 85 °C, then cooled on ice for 5 minutes. Samples were centrifuged at 20,000 x g for 15 minutes. 500 µl of the supernatant was added to 200 µl 10 % (v/v) ammonium hydroxide and absorbance was read at 405 nm on an ELx800TM microplate reader.

2.2.2 Culture of RAW 264.7 Semi-Adherent Cells

RAW 264.7 semi-adherent macrophages derived from murine blood were kindly donated as a live culture courtesy of Dr. Sinead Miggin. When 80 % confluent, adherent cells were detached with a cell scraper, centrifuged and resuspended in DMEM

supplemented with 10 % (v/v) FBS, 100 µg/ml penicillin/streptomycin and 2 mM L-glutamine at a density of $3x10^4$ cells/cm^2.

2.2.3 Culture of THP-1 Suspension Cells

THP-1, a human monocyte cell line was kindly donated as a live culture courtesy of Prof. Paul Moynagh. Cells were seeded at a density of $2x10^5$ cells/ml in RPMI-1640 supplemented with 100 µg/ml penicillin/streptomycin, and 10 % (v/v) FBS. Flasks were tilted at a 45° angle in the CO_2 incubator to provide an optimal environment for growth. When a density of $8x10^5$ cells/ml was reached, cells were sub-cultured by centrifugation and resuspension at a density of $2x10^5$ cells/ml.

2.2.4 Cryo-preservation of Mammalian Cells

Following sub-culture, cell pellets were gently resuspended at a density of $2x10^6$ cells in 1 ml complete medium containing 10 % (v/v) FBS and 10 % (v/v) DMSO. The cell suspension was transferred into Cryo-tubes (Nunc) and placed in a Mr. Frosty™ freezing container (Thermo Fisher Scientific) at -80 °C for 24 hours, which allowed a cooling rate of approximately -1 °C/minute. Cryo-tubes were then placed in liquid nitrogen for long-term storage.

2.3 Animals

Male C57BL/6J mice, aged 4 weeks (n=6) provided by Charles River, Calco, Lecco, Italy, were maintained on a pellet diet for 1 week, then randomly divided into two groups: normal diet (control, n=3) or a high fat high sugar diet (HFHS, 45 % kcal fat, 35 % kcal carbohydrates and 20 % kcal protein, n=3) for 16 weeks. Animals were housed at the University of Turin in a temperature-controlled environment with a 12 hour light/dark cycle. Mice were sacrificed by cervical dislocation, epididymal fat pads were

removed and snap frozen in liquid nitrogen. Samples were received on dry ice and stored at -80 °C until required. Protocols were approved by the 'Animal Use and Care Committee' of the University of Turin and subsequently by the ethics committee of the National University of Ireland, Maynooth (BSRESC-2014-008). Protocols were in accordance with the European Directive 2010/63/EU on the protection of animals used for scientific purposes.

2.4 Molecular Biology Methods

2.4.1 RNA Isolation and cDNA Synthesis

2.4.1.1 RNA Isolation

Total RNA was extracted using TRIzol® Reagent (Invitrogen) according to the manufacturer's protocol. Tissue samples were homogenised in 1 ml TRIzol® using a handheld T10 Basic Homogeniser (IKA) and stored at -20 °C until required. Samples were thawed on ice and 100 µl 1-bromo-3-chloropropane was added to each. Samples were vortexed for 20 seconds and incubated at room temperature for 5 minutes. Samples were then centrifuged at 12,000 x g at 4 °C for 15 minutes resulting in the formation of three distinct layers. The clear, aqueous upper layer containing the RNA was removed, ensuring the interphase containing DNA and the lower organic phase containing proteins were not disturbed. RNA was precipitated with 500 µl isopropanol, samples were mixed by inversion, incubated at room temperature for 10 minutes and centrifuged at 12,000 x g at 4 °C for 15 minutes. The resulting RNA pellet was washed twice with 1 ml 75 % (v/v) ethanol and centrifuged at 7,500 x g for 5 minutes at 4 °C. The supernatant was aspirated and the pellet was allowed to air dry before resuspension with 20 µl nuclease free water. RNA concentration was determined using a Nanodrop 2000 spectrophotometer (Thermo Fisher Scientific), which calculates absorbance at 260

nm and 280 nm. A ratio between 1.8 and 2.0 indicated sufficient purity, samples outside this range were discarded and remaining samples were stored at -80 °C until required.

2.4.1.2 DNase Treatment of RNA

To recover RNA contaminated with genomic DNA, samples were treated with DNase I (Invitrogen) as outlined by the manufacturer. 1 µl of amplification grade DNase I and 1 µl of 10X DNase I reaction buffer were incubated with 2 µg RNA for 15 minutes at room temperature. 1 µl 25 mM EDTA was added and samples were incubated in a GS1 Thermal Cycler (G-Storm) at 65 °C for 10 minutes, followed by cooling on ice to inactivate the DNase. RNA was then reverse transcribed into cDNA.

2.4.1.3 First Strand cDNA Synthesis

5X All-In-One RT MasterMix (Applied Biological Materials Inc.) was added to the RNA template and mixed by pipetting. cDNA was synthesised by incubating samples in a GS1 Thermal Cycler (G-Storm) for 50 minutes at 42 °C. The reaction was terminated by heating samples at 85 °C for 5 minutes followed by chilling on ice. Samples were stored at -20 °C until required.

2.4.2 Polymerase Chain Reaction (PCR)

2.4.2.1 PCR to Confirm Synthesis of cDNA

A PCR using primers specific to the house keeping gene HPRT (Table 2.2) was used to confirm synthesis of cDNA. A reaction mix was set up in a 0.2 ml PCR grade tube containing:

5 µl 5X MyTaq Reaction Buffer (Bioline)

0.5 µl Forward primer (4 pM)

0.5 µl Reverse primer (4 pM)

0.3 µl MyTaq DNA Polymerase (Bioline)

17.7 µl Nuclease free H_2O

1 µl cDNA (500 ng)

Samples were run in a GS1 Thermal Cycler (G-Storm) for 2 minutes at 95 °C followed by 40 cycles of 95 °C for 45 seconds, 58 °C for 45 seconds and 72 °C for 45 seconds. Samples were then incubated at 72 °C for 10 minutes followed by cooling on ice. To visualise nucleic acid products, samples were run on a 0.8 % (w/v) agarose gel.

2.4.2.2 Agarose Gel Electrophoresis of DNA

0.8 % (w/v) agarose was dissolved in TAE buffer (40 mM Tris-acetate, 1 mM EDTA, pH 8.4) by heating in a microwave at a medium setting. The solution was allowed to cool before the addition of the DNA visualisation agent, SYBR® Safe (Invitrogen, S33102), gels were left to set for 1 hour at room temperature prior to use. Nucleic acid samples were mixed with a loading buffer (Thermo Fisher Scientific, R0631) and electrophoresed in TAE buffer at 100 volts constant. DNA was visualised under UV light (254 nm) once sufficient migration and separation had occurred. A 1 kb GeneRuler™ DNA ladder (Thermo Fisher Scientific, SM0313) (Fig. 2.1) was used to estimate fragment length.

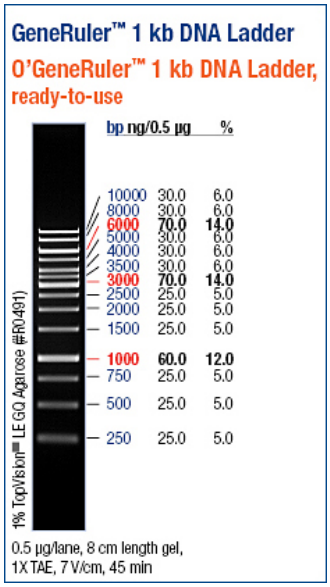

Figure 2.1 Distribution of DNA ladder used with DNA electrophoresis.

2.4.2.3 Quantative Real Time PCR (qRT-PCR)

Template cDNA was used for qRT-PCR with specific primers (Table 2.2) to detect a gene of interest using the following reaction mixture:

5 µl Fast start Universal SYBR Green Master - ROX (Roche)

1 µl Forward primer (4 pM)

1 µl Reverse Primer (4 pM)

2 µl Nuclease Free H_2O

The reaction mixture was added to a specialised optical 96 well plate (Applied Biosystems) along with 1 µl template cDNA at 500 ng and sealed with an optically clear adhesive cover. The plate was incubated at 95 °C for 5 minutes in the Applied Biosystems Step One™ real-time PCR instrument, accumulation of gene-specific products was measured continuously by means of fluorescence detection over 40 cycles. Each cycle consisted of a denaturing step of 95 °C for 15 seconds, an annealing step at

the appropriate temperature (Table 2.2) for 30 seconds, then extension at 72 °C for 30 seconds. This was followed by a melt curve cycle of 95 °C for 15 seconds, 55 °C for 15 seconds and 95 °C for a final 15 seconds. Intercalation of SYBR green into the dsDNA product was monitored after each step of primer annealing and elongation. Melt curve analysis demonstrating one single melting peak eliminated the possibility of primer-dimer associations, confirming the amplification of one specific product. Relative quantification of target gene expression was evaluated using the delta Crossing Threshold (ΔCT) method. The Applied Biosystems Step One™ software generated the CT value for each sample, which records the cycle when sample fluorescence exceeds a chosen threshold above background fluorescence. The ΔCT value was determined by subtracting the CT value of HPRT, the housekeeping gene, for each sample from the CT value of the target gene. Fold change in the relative expression of the target was determined by calculating $2^{-(\Delta CTSample-\Delta CTControl)}$.

Table 2.2 Primers.

Gene	Forward Primer 5'-3' Reverse Primer 3'-5'	Annealing Temperature (°C)
HPRT	AGGGATTTGAATCACGTTTG TTTACTGGCAACATCAACAG	58
TNF-α	GGATGAGAAGTTCCCAAATG TGAGAAGATGATCTGAGTGTG	57
F4/80	TTTCAAATGGATCCAGAAGG CAGAAGGAAGCATAACCAAG	58.9

2.4.3 Transformation of Competent *Escherichia coli* Cells

Competent TOP10 *E. coli* cells supplied by Invitrogen (C4040-03) were transformed with plasmid DNA according to the manufacturer's protocol by heat shock. 5 µl of plasmid DNA was added to 50 µl of competent cells and incubated on ice for 30

minutes. Cells were incubated at 42 °C for 30 seconds then placed on ice again. After 2 minutes, 250 µl of pre-warmed (37 °C) SOC medium was added (5 % (w/v) tryptone 0.5 % (w/v) yeast extract, 10 mM NaCl, 2.5 mM KCl, 10 mM $MgCl_2$, 10 mM $MgSO_4$, 20 mM glucose). Cells were incubated at a 45° angle at 37 °C for 1 hour with constant shaking of 200 – 250 rpm. Cells were then plated on Lysogeny Broth (LB) agar plates (1 % (w/v) tryptone, 0.5 % (w/v) yeast extract, 1 % (w/v) NaCl, 1 % (w/v) agar, pH 7.0), with the appropriate antibiotic for selection and left at 37 °C overnight.

All vectors used (Table 2.3) confer ampicillin or kanamycin resistance to *E. coli* transformants. Ampicillin was added to both liquid and solid medium at a final concentration of 100 µg/ml for selection and maintenance. Kanamycin was added at a final concentration of 50 µg/ml.

Table 2.3 Vectors.

cDNA Clone	Vector	Antibiotic Resistance	5' Restriction Site	3' Restriction Site	Insert Size (bp)
eGFP	pcDNA3	Ampicillin	XhoI	XbaI	700
GPR21	pCMV6-Entry	Kanamycin	SgfI	MluI	1050
$G\alpha_q$	pcDNA3.1+	Ampicillin	KpnI	XhoI	1085
$G\alpha_{14}$	pcDNA3.1+	Ampicillin	KpnI	XhoI	1075
$G\alpha_{15/16}$	pcDNA3.1+	Ampicillin	KpnI	XhoI	1130

2.4.4 Small Scale Isolation of DNA from *E. coli*

Successful colonies were isolated, transferred to 3 ml LB medium (1 % (w/v) tryptone, 0.5 % (w/v) yeast extract, 1 % (w/v) NaCl, pH 7.0) with the appropriate antibiotic and incubated overnight at a 45° angle at 37 °C with shaking. 2 ml of each respective culture was centrifuged at 6,800 x g for 2 minutes and DNA was extracted from the bacteria using the GeneJET Plasmid Miniprep Kit (Thermo Fisher Scientific, K0503).

DNA concentration was assessed by reading absorbance at 260 nm and 280 nm using the Nanodrop 2000 spectrophotometer (Thermo Fisher Scientific), where absorbance of 1 unit at 260 nm is ~50 µg/ml. The purified plasmid was then digested using the appropriate restriction enzyme to assess the presence of the desired insert.

2.4.5 Diagnostic Restriction Digest

To confirm production of plasmid DNA incorporating the gene of interest a diagnostic restriction digest was performed. 1 µg of plasmid DNA was digested using 0.5 µl of each restriction enzyme. Enzymes were used at a final concentration of 0.1 U/µl, in 1X reaction buffer with 100 ng/ml bovine serum albumin (BSA) (Enzymes and buffers were supplied by New England Biolabs). The reaction was incubated overnight at 37 °C. The digested plasmid was then electrophoresed using a 0.8 % (w/v) agarose gel as described in Section 2.4.2.2. The relative structure of the plasmid could then be confirmed, based on the observed banding pattern.

2.4.6 Large Scale Isolation of DNA from *E. coli*

Plasmids were propagated by inoculating 50 ml LB medium containing the required selection antibiotic with 50 µl of the small scale *E. coli* culture (Section 2.4.4). Cultures were grown at 37 °C for 16 hours with shaking. Plasmids were purified using the S.N.A.P. Midiprep kit (Invitrogen, K1910-01), as per the manufacturer's instructions. DNA was eluted with 750 µl sterile MilliQ water and DNA concentration was assessed using the Nanodrop 2000 spectrophotometer (Thermo Fisher Scientific) reading absorbance at wavelengths of 260 nm and 280 nm. DNA was aliquoted and stored at -20 °C until required.

2.4.7 Preparation of Glycerol Stocks

For long term storage, liquid cultures of *E. coli* transformed with the plasmid of interest were mixed with sterile glycerol (4:1, glycerol:*E. coli*) and frozen at -80 °C.

2.5 Genetic Manipulation of Mammalian Cells

2.5.1 Transient Transfection of HEK293T Cells

Cells were transfected with eGFP plasmid DNA using Lipofectamine® 2000 (Invitrogen) according to the manufacturer's protocol and visualised on an inverted Olympus CKX41 fluorescent microscope to determine optimal transfection conditions. HEK293T cells were seeded at $2.5x10^5$ cells/ml in a 6 well plate and allowed to adhere for 24 hours at 37 °C. For each well of a 6 well plate 2 µg plasmid DNA, or 1 µg of each plasmid DNA if co-transfecting, was incubated with 250 µl Opti-MEM® (Gibco). 4 µl Lipofectamine® 2000 was incubated with 250 µl Opti-MEM® in a separate tube for 5 minutes at room temperature. The Lipofectamine® 2000/Opti-MEM® and DNA/Opti-MEM® mix were then combined. After a 20 minute incubation at room temperature, the solution was added drop-wise to the cells and left for 24 hours at 37 °C to allow incorporation of the plasmid DNA.

2.5.2 Transient Transfection of 3T3-L1 Cells

Cells were transfected with eGFP plasmid DNA using Lipofectamine® 3000 (Invitrogen) according to the manufacturer's protocol and visualised with an inverted Olympus CKX41 fluorescent microscope to determine optimal transfection conditions. 3T3-L1 pre-adipocytes were seeded at $1.25x10^5$ cells/ml in a 6 well plate and allowed to adhere for 24 hours at 37 °C. For each well of a 6 well plate, 2.5 µg plasmid DNA, or 1.25 µg of each plasmid DNA if co-transfecting, was incubated with 125 µl Opti-

MEM® (Gibco) and 10 µl P3000. 7 µl Lipofectamine® 3000 was incubated with 125 µl Opti-MEM® in a separate tube for 5 minutes at room temperature. The Lipofectamine® 3000/Opti-MEM® and DNA/P3000/Opti-MEM® mix were combined. After a 5 minute incubation at room temperature the solution was added drop-wise to the cells. Cells were left for 24 hours at 37 °C to incorporate the plasmid DNA then differentiated into adipocytes as described in Section 2.2.1.2.

2.5.3 Transient Transfection of RAW 264.7 Cells

Cells were transfected with eGFP plasmid DNA using Lipofectamine® 3000 to determine optimal transfection conditions. RAW 264.7 cells were seeded at a density of $5x10^5$ cells/ml in a 6 well plate and allowed to settle for 24 hours at 37 °C. Cells were transfected with 4 µg plasmid DNA or 2 µg of each plasmid DNA if co-transfecting, per well of a 6 well plate as outlined in Section 2.5.2.

2.6 Biochemical Techniques

2.6.1 Protein Extraction

Cell culture vessels were placed on ice, medium removed and cells were washed three times with ice-cold PBS. Cells were then scraped into 1 ml ice-cold PBS, transferred to a 1.5 ml tube and centrifuged at 650 x g for 5 minutes. The PBS was aspirated and cell pellets were resuspended in HEPES lysis buffer; 50 mM HEPES pH 7.5, 150 mM NaCl, 10 mM Na_2HPO_4, 50 mM NaF, 1 mM EDTA, 1.5 mM $MgCl_2$, 2 mM Na_3VO_4, 1 mM $Na_4P_2O_7$, 1X SigmaFAST protease inhibitor cocktail (Sigma-Aldrich), 10 % (v/v) glycerol, 1 mM PMSF and 1 % (v/v) Triton x-100.

Frozen murine epididymal fat pads were homogenised in ice-cold HEPES lysis buffer at a ratio of 1:5 (w:v) using a T10 Basic handheld homogeniser (IKA).

Crude extracts were incubated for 1 hour at 4 °C with constant agitation. Lysates were centrifuged at 17,000 x g for 10 minutes at 4 °C. The insoluble pellet was discarded and the protein concentration of the supernatant was determined using the Pierce protein assay (Section 2.6.2.1).

2.6.2 Protein Assays

As some chemicals are known to react with the components of a protein assay, two different protein assays were employed, depending on the buffer used to isolate protein samples. A standard protein curve was prepared using BSA at 0, 50, 100, 200, 400, 600, 800, and 1000 µg/ml. Samples were diluted as required and 10 µl of each sample or standard was used in triplicate in a 96 well plate. Absorbance values obtained for each sample were compared to that of the standard curve to ascertain protein concentration.

2.6.2.1 Pierce Protein Assay

150 µl of the Pierce protein assay reagent (PN22660) was added to each standard and sample in a 96 well plate and incubated at room temperature for 5 minutes with agitation. The plate was analysed using a BIO-TEK EL800 plate reader at 630 nm.

2.6.2.2 Bicinchoninic Acid Protein Assay

The bicinchoninic acid protein assay was carried out as described by Smith and colleagues (1985). Copper sulphate was diluted 1:50 into bicinchoninic acid and 200 µl of this solution was added to each standard and sample in a 96 well plate. The plate was incubated at 37 °C for 30 minutes and subsequently read using a BIO-TEK EL800 plate reader at 562 nm.

2.6.3 Sodium Dodecyl Sulphate Polyacrylamide Gel Electrophoresis (SDS-PAGE)

SDS-PAGE was conducted using the Hoefer system according to the methods described by Laemmli (1970), to separate proteins by molecular mass weight. Samples were diluted 1:4 in Laemmli buffer (300 mM Tris-HCl, 50 % (v/v) glycerol, 10 % (w/v) SDS, 0.02 % (w/v) bromophenol blue, 10 % (v/v) β-mercaptoethanol, pH 6.8) and boiled at 95 °C for 5 minutes before loading into the wells of an appropriate percentage polyacrylamide gel (Table 2.4) sufficiently covered with SDS running buffer (0.1 % (w/v) SDS, 25 mM Tris-Base and 192 mM glycine). Samples of equal protein concentration were electrophoresed at 19 mA for approximately 2 hours along with a protein molecular weight marker (Thermo Fisher Scientific, SM1811) (Fig. 2.2).

Table 2.4 Polyacrylamide gels.

Stock Solution	**10 % Resolving Gel – For proteins above 30 kDa**	**8 % Resolving Gel – For proteins above 100 kDa**	**6 % Resolving Gel – For proteins above 200 kDa**	**5 % Stacking Gel**
dH_2O	4 ml	4.6 ml	5.3 ml	3.4 ml
30 % acrylamide/bisacrylamide (ProtoGel)	3.3 ml	2.7 ml	2 ml	830 µl
1.5 M Tris-HCl, pH 8.8	2.5 ml	2.5 ml	2.5 ml	-
1 M Tris-HCl, pH 6.8	-	-	-	630 µl
10 % (w/v) SDS	100 µl	100 µl	100 µl	50 µl
10 % (w/v) ammonium persulfate	100 µl	100 µl	100 µl	50 µl
TEMED	4 µl	6 µl	8 µl	5 µl
Total volume per gel	10 ml	10 ml	10 ml	5 ml

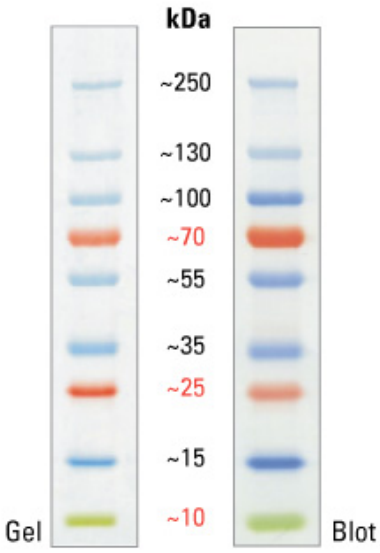

Figure 2.2 Distribution of molecular weight marker used with SDS-PAGE.

2.6.3.1 Coomassie Brilliant Blue Staining

To visualise proteins, SDS-PAGE gels were fixed for 15 minutes in 40 % (v/v) ethanol, 10 % (v/v) acetic acid for 15 minutes with agitation, this was repeated once. Gels were then incubated with agitation for a minimum of 2 hours with 40 % (v/v) ethanol, 10 % (v/v) acetic acid, 0.1 % (w/v) Coomassie Brilliant Blue G250 (Ams Biotechnology, 17524). Gels were destained for 5 minutes in 40 % (v/v) ethanol, 10 % (v/v) acetic acid then immersed in 20 % (v/v) ethanol, 10 % (v/v) acetic acid until completely destained. Gels were washed in dH_2O before imaging.

2.6.3.2 Semi-Dry Electroblotting

Alternatively, separated proteins were transferred from SDS-PAGE gels onto a PVDF membrane (GE Healthcare) in a semi-dry transfer unit (Cleaver Scientific Ltd). The PVDF membrane was pre-soaked in methanol, followed by ice-cold transfer buffer (48 mM Tris-Base, 39 mM glycine, 0.375 % (w/v) SDS, 20 % (v/v) methanol) for 10 minutes. Gels were washed once with dH_2O and soaked in ice-cold transfer buffer for 5

minutes before proteins were transferred to the membrane at 150 mA per gel for 30 minutes.

2.6.3.2.1 Western Blotting

Membranes were blocked with 5 % (w/v) BSA or non-fat dry milk (Marvel) in Tris-buffered saline containing Tween-20 (TBST); 150 mM NaCl, 20 mM Tris-HCl, pH 7.6, 0.1 % (v/v) Tween-20 for 1 hour at room temperature to prevent antibodies binding non-specifically. Membranes were subsequently incubated with a primary antibody at an optimised dilution (Table 2.5) overnight at 4 °C. The membranes were washed 3 times with TBST, 5 minutes each time, to remove unbound antibody, before incubating with the appropriate secondary antibody conjugated with HRP for 2 hours at room temperature. Membranes were then washed 3 times, 5 minutes each, with TBST and incubated with enhanced chemiluminescence (ECL) (Roche, 11500694001) for 2 minutes. Immunoreactive protein bands were visualised on UltraCruz™ Autoradiography Film (Santa Cruz Biotechnology).

Table 2.5 Western blotting antibodies.

Antibody	Dilution	Diluent	Company
Insulin Receptor β	1:1000	5% Milk TBST	Abcam (ab69508)
Phospho-Insulin Receptor β $Tyr^{1150/1151}$	1:1000	5% Milk TBST	Cell Signaling (3024)
IRS1	1:1000	5% Milk TBST	Cell Signaling (3407)
Phospho-IRS1 Tyr^{612}	1:1000	5% BSA TBST	Life Technologies (44-816G)
Akt	1:1000	5% BSA TBST	Cell Signaling (9272)
Phospho-Akt Ser^{473}	1:1000	5% BSA TBST	Cell Signaling (9271)
AS160	1:1000	5% BSA TBST	Cell Signaling (2670)
Phospho-AS160 Ser^{588}	1:1000	5% BSA TBST	Cell Signaling (8730)
Phospho-AS160 Thr^{642}	1:1000	5% Milk TBST	Cell Signaling (8881)
AMPKα	1:750	5% BSA TBST	Cell Signaling (2532)
Phospho-AMPKα Thr^{172}	1:750	5% BSA TBST	Cell Signaling (2531)
ACC	1:1000	5% BSA TBST	Cell Signaling (3662)
Phospho-ACC Ser^{79}	1:1000	5% BSA TBST	Cell Signaling (3661)
JNK	1:1000	5% BSA TBST	Cell Signaling (9258)
Phospho-JNK Thr^{183}/Tyr^{185}	1:1000	5% BSA TBST	Cell Signaling (4668)
Erk	1:1000	5% BSA TBST	Cell Signaling (4695)
Phospho-Erk Thr^{202}/Tyr^{204}	1:1000	5% BSA TBST	Cell Signaling (4370)
p38	1:1000	5% BSA TBST	Cell Signaling (9212)
Phospho-p38 Thr^{180}/Tyr^{182}	1:1000	5% BSA TBST	Cell Signaling (4511)
β-actin	1:40000	5% Milk TBST	Abcam (ab8226)
Myc	1:5000	5% Milk TBST	Cell Signaling (2276)
GPR21	1:1000	5% Milk TBST	Abcam (ab139654)
F4/80	1:1000	5% Milk TBST	Abcam (ab74383)
Anti-Rabbit IgG HRP Conjugate	1:2000	TBST	Dako (P0448)
Anti-Mouse IgG HRP Conjugate	1:5000	TBST	Promega (W4021)

2.6.3.2.2 Re-probing PVDF Membranes

When optimising antibody concentrations or when investigating more than one protein, it was possible to reuse membranes once the initial primary antibody was removed. Membranes were incubated with Restore™ Western Blot Stripping Buffer (Thermo Fisher Scientific, 21059) for 15 minutes with agitation, and then washed 3 times for 5 minutes with TBST to remove any remaining stripping buffer. To determine complete removal of antibody, membranes were incubated with ECL and exposed to X-ray film. If the procedure was successful, membranes were washed once with TBST and re-blocked in 5 % (w/v) BSA or milk in TBST for 1 hour at room temperature. Membranes were then probed with an alternative antibody following the procedure outlined in Section 2.6.3.2.1.

2.6.4 PI3K Enzyme-Linked Immunosorbent Assay (ELISA)

A PI3K ELISA (Merck Millipore, 17-493) was used to assess the direct effect of compounds on the activity of the four class I PI3Ks (p110α, p110β, p110γ and p120δ). All reagents used were supplied with the kit. Each class I PI3K was incubated with each compound (1 µM wortmannin, 10 µM RTC-1, 10 µM RTC-15, 500 µM metformin) for 10 minutes at room temperature. 5 µl of the 5X kinase reaction buffer was added to each well of a glutathione coated 96 well plate followed by 5 µl (50 µM) PIP_2. 5 µl of the kinase/compound mix was then added to the plate and incubated for 1 hour at room temperature. Wells containing no kinase acted as a buffer control, while wells containing no compounds acted as a positive control for kinase activity. 25 µl of biotinylated-PIP_3/EDTA (diluted 1:18 in TBST) was added to each well, excluding buffer control wells, followed by 50 µl of the capture protein, general receptor for phosphoinositides (GRP-1) containing a glutathione-s-transferase (GST) tag, (diluted

1:1000 in TBST) and incubated for 1 hour at room temperature. The plate was washed 4 times with 200 µl TBST then incubated with 50 µl/well streptavidin-HRP conjugate (diluted 1:2000 in TBST) for 1 hour at room temperature. Wells were washed 5 times with 200 µl TBST then incubated with 100 µl TMB for no more than 20 minutes in the dark. When a blue colorimetric change appeared, the reaction was stopped with the addition of 100 µl/well of a stop solution included in the kit. Absorbance was read at 450 nm using a BIO-TEK EL800 plate reader. To calculate the percentage of PIP_3 relative to the biotinylated-PIP_3 tracer, the absorbance values of positive wells containing the tracer only were set to 100. All other signals were divided by the biotinylated-PIP_3 average then multiplied by 100 to show the relative percentage to the positive signal. As the capture protein, GRP-1, binds either PIP_3 generated as part of the kinase reaction or the biotinylated-PIP_3 tracer, a lower signal was indicative of higher kinase activity.

2.7 Functional Assays

2.7.1 Analysis of NADH:ubiquinone oxidoreductase Activity

2.7.1.1 Isolation of Mitochondria from Rat Liver

Mitochondria were isolated from rat liver as outlined by Chappell and Hansford, (1972). The liver was washed three times with ice-cold isolation buffer (250 mM sucrose, 5 mM Tris-HCl, 1 mM EGTA, pH 7), then minced in fresh, ice-cold isolation buffer and transferred to a glass potter (Potter S Homogeniser, Sartorius). A Teflon pestle was used at 1,600 rpm to homogenise the liver in an ice-bath. The resulting homogenate was centrifuged at 750 x g for 5 minutes at 4 °C, the supernatant was retained and centrifuged at 12,000 x g for 10 minutes at 4 °C. The resulting pellet was resuspended in ice-cold isolation buffer supplemented with 2 % (w/v) fatty acid free BSA and

centrifuged at 12,000 x g for 10 minutes at 4 °C. Supernatant was discarded and the pellet was resuspended in a minimal volume of isolation buffer. Mitochondrial concentration was determined using the bicinchoninic acid procedure (Section 2.6.2.2). Mitochondria were stored at -20 °C until required.

2.7.1.2 NADH:ubiquinone oxidoreductase Activity

Immediately before the assay, mitochondria were diluted in a hypotonic buffer (25 mM K_2HPO_4, 5 mM $MgCl_2$) and permeabilised with three cycles of freezing in liquid nitrogen and thawing at room temperature. The assay was carried out in a temperature controlled Shimadzu UV-2550 UV-VIS spectrophotometer, at 30 °C in a 1 ml cuvette (Spinazzi *et al.,* 2012). Permeabilised mitochondria were incubated with 50 mM K_2HPO_4 pH 7.5, 3 mg/ml fatty acid free BSA, 300 μM KCN and 100 μM NADH, baseline activity was measured at 340 nm for 1 minute. The reaction was initiated with the addition of 60 μM ubiquinone and the resulting decrease in absorbance was followed for 3 minutes. Varying concentrations of compounds of interest were then added and absorbance was measured for a further 3 minutes. To determine the percentage activity of NADH:ubiquinone oxidoreductase, the slope of the line obtained with the addition of ubiquinone was divided by the slope of the line produced with the addition of the compound to be tested. This value was then expressed as a percentage relative to the value calculated for the vehicle control, DMSO, and the protein concentration of the mitochondrial sample. Specificity of the assay was confirmed with the addition of rotenone, a known inhibitor of NADH:ubiquinone oxidoreductase.

2.7.2 Analysis of Intracellular ATP Levels

A luminescent ATP detection assay (Abcam, ab113849) was performed according to the manufacturer's instructions. C2C12 cells were cultured in a black, clear bottomed

96 well plate at a density of $1x10^3$ cells/100 µl. Differentiated cells were stimulated with compounds of interest for various time points in triplicate. Rotenone was used as a reference inhibitor, as it is known to significantly decrease ATP levels. ATP standards were also prepared in the 96 well plate, in triplicate, with concentrations ranging from 250 pM to 10 µM. Cells were lysed with the addition of 50 µl of a detergent solution and incubated for 5 minutes at room temperature on an orbital shaker at 700 rpm. 50 µl of reconstituted substrate buffer (containing D-luciferin and luciferase) was added to the cells and incubated in the dark for 15 minutes on an orbital shaker at 700 rpm before luminescence was read on BMG labtech plate reader. ATP concentration was determined via the ATP standard curve.

2.7.3 Analysis of Glucose Transport

2.7.3.1 Radioactive Glucose Uptake

Cellular glucose uptake was measured by scintillation counting of cellular [^{3}H]-2-deoxyglucose with slight modifications to the method described by Yun and colleagues (2009). Cells were washed once with Krebs Ringer Buffer (KRB); 136 mM NaCl, 20 mM HEPES, 4.7 mM KCl, 1 mM $MgSO_4$, 1 mM $CaCl_2$, 4.05 mM Na_2HPO_4, 0.95 mM NaH_2PO_4, pH 7.4 warmed to 37 °C. Cells were then incubated with 1 µCi/ml [^{3}H]-2-deoxyglucose (PerkinElmer, NET328A001MC) in KRB at 37 °C for 10 minutes. To terminate the assay cells were washed 3 times with ice-cold KRB, then lysed in 0.1 % (w/v) SDS at 37 °C for 30 minutes. Cell lysates were diluted 1:4 in β-scintillation fluid (Beta-Plate Scint, PerkinElmer). Cellular incorporation of [^{3}H]-2-deoxyglucose was quantified by a 1450 Microbeta Liquid Scintillation Counter (PerkinElmer), which expressed results in counts per minute (CPM). Total protein content of each sample

was determined by the bicinchoninic acid procedure (Section 2.6.2.2) to define results as CPM/mg.

2.7.3.2 Flow Cytometry Analysis of GLUT4 Translocation

C2C12 myotubes were dissociated with trypsin-EDTA solution as described in Section 2.2.1. Trypsin-EDTA was neutralised with complete medium containing 10 % (v/v) FBS and cells were centrifuged at 300 x g for 5 minutes. Cell pellets were resuspended in Fc buffer (PBS containing 1 % (w/v) BSA and 1 mM EDTA), counted and further diluted to yield a density of $1x10^5$ cells/100 µl. Cells were pre-incubated with 1 µl Mouse BD Fc Block™ (BD Biosciences, 553142) for 30 min at 4 °C to prevent non-specific binding. Samples were divided into two tubes, 5 µl anti-GLUT4 (Santa Cruz Biotechnology, SC-1606) was added to one sample set. The other sample set served as the negative control, used to monitor non-specific binding of the secondary antibody, and was incubated with buffer alone. Cells were incubated for 30 minutes at 4 °C then washed by centrifuging at 300 x g for 5 minutes and resuspending the pellet in 100 µl Fc buffer. All samples were incubated with 1.2 µl anti-goat IgG-FITC (Sigma-Aldrich F7367) for 30 minutes at 4 °C and washed twice before analysis by flow cytometry with an Accuri® C6 Flow Cytometer (BD Biosciences).

2.7.4 Homogeneous Time Resolved Fluorescence (HTRF) Assays

2.7.4.1 PIP_3 HTRF Assay

A PIP_3 HTRF assay (Merck Millipore, 17-495) was used to establish the effect of compounds of interest on the production of PIP_3 in differentiated C2C12 cells. After stimulation, cells were incubated with 500 µl 0.5 M trichloroacetic acid for 5 minutes on ice to precipitate cellular debris. The cell suspension was centrifuged at 17,000 x g for 5 minutes at 4 °C, and the resulting pellet was washed with 500 µl 5 % (v/v)

trichloroacetic acid, 1 mM EDTA. Neutral lipids were extracted by incubating the pellet with 1 ml 2:1 methanol:chloroform for 10 minutes at room temperature followed by centrifugation at 17,000 x g for 5 minutes at 4 °C. This step was repeated once. Acidic lipids were then extracted by incubating the pellet with 500 µl 40:80:1 chloroform:methanol:12 M HCl for 15 minutes at room temperature. 180 µl chloroform was added to each sample followed by 320 µl 0.1 M HCl. Samples were vortexed, then centrifuged at 17,000 x g for 5 minutes at 4 °C resulting in the formation of two distinct layers. The lower phase was transferred to a clean tube and 30 µl of methanol containing 0.1 M ammonium hydroxide was added. Samples were dried in a vacuum evaporator and resuspended in 60 µl lipid recovery buffer supplied with the HTRF kit. To aid the resuspension process, samples were vortexed for 30 seconds then sonicated in a cooled sonication bath for 15 seconds. The PIP_3 detection solution was prepared as outlined in the manufacturer's instructions and incubated at room temperature for 30 minutes in the dark. Standards and samples were added to a black 96 well plate in triplicate (25 µl/well) followed by 25 µl of the detection solution, the plate was sealed and incubated at room temperature for 4 hours with agitation. The plate was then read on a BMG labtech plate reader with excitation at 340 nm and measurements of emission at 615 nm and 665 nm. The fluorescence resonance energy transfer (FRET) ratios (665 nm/615 nm) were converted to PIP_3 concentrations by interpolating values from the PIP_3 standard curve.

2.7.4.2 IP_1 HTRF Assay

Cellular inositol 1-phosphate (IP_1) levels were measured using an IP-one HTRF assay kit (Cisbio, 62IPAPEC) (Trinquet *et al.,* 2006). Sub-confluent HEK293T cells were detached from the cell culture dish by trypsinisation (Section 2.2.1) and resuspended in the appropriate volume of the assay stimulation buffer (10 mM HEPES, 1 mM $CaCl_2$,

0.5 mM $MgCl_2$, 4.2 mM, KCl, 146 mM NaCl, 5.5 mM glucose, 50 mM LiCl, pH 7.4) warmed to 37 °C, to achieve a concentration of $6x10^6$ cells/ml. 7 µl of the cell suspension was added to each well of a white half volume 384 well plate (Greiner, 781080) along with 7 µl of the compound to be tested, prepared at a 2X concentration. Triplicate samples were incubated at 37 °C for 2 hours. 3 µl IP-one-d_2 conjugate (diluted 1:20 in IP-one lysis buffer) was added to each well followed by 3 µl anti-IP-one cryptate Tb conjugate (diluted 1:20 in IP-one lysis buffer), and incubated in the dark for 1 hour at room temperature. The plate was read on a BMG labtech plate reader with an excitation at 340 nm and emissions at 615 nm and 665 nm respectively. The FRET ratios (665 nm/615 nm) were converted to IP_1 concentrations by interpolating values from an IP_1 standard curve.

2.7.5 Macrophage Migration Assay

RAW 264.7 cells were detached from the culture vessel using a cell scraper and centrifuged at 600 x g for 5 minutes. Cell pellets were resuspended in complete DMEM supplemented with 2 % (v/v) FBS at a density of $5x10^5$ cells/ml. 750 µl of 2 % (v/v) FBS DMEM was added to a well of a 24 well plate and a 6.5 mm Transwell® insert with a 5.0 µm pore polycarbonate membrane (Corning®) was placed into the well. 250 µl of the cell suspension was added to the upper chamber of the Transwell® insert and cells were incubated at 37 °C for 1 hour to acclimatise. Medium was removed from the lower chamber and replaced with 3T3-L1 adipocyte conditioned medium, cells were then incubated for 4 hours at 37 °C. To determine the migratory capacity of the cells, medium was removed from the Transwell® insert, which was subsequently washed twice with PBS then incubated in cold (-20 °C) methanol for 5 minutes to fix the migrating cells. The polycarbonate membrane was then removed from the Transwell®

insert using a scalpel and incubated with 0.05 % (w/v) crystal violet dissolved in 0.1 M disodium tetraborate, pH 9.0 containing 2 % (v/v) ethanol for 20 minutes. The membrane was washed three times with PBS before the crystal violet stain was eluted using 10 % (v/v) acetic acid with a 5 minute incubation. The resulting solution was transferred to a 96 well plate and absorbance was read at 560 nm on an ELx800TM microplate reader.

2.8 Statistical Analysis

Data are presented as mean ± the standard error of the mean (SEM). The unpaired Student's *t*-test was used to determine significance between two experimental groups. One-way analysis of variance (ANOVA) with a post-hoc Tukey test was used to determine significance among three or more groups. One-way ANOVA with a post-hoc Dunnett test was used when comparing two or more groups to a control group. GraphPad Prism® 5 software was used to carry out the analysis. Significance was denoted as $p < 0.05$; *, $p < 0.01$; **, $p < 0.001$; ***.

Chapter 3

Elucidating the Mechanism of Action of a Novel Anti-Diabetic Compound

3.1 Introduction

The emerging limitations of current anti-diabetic strategies stress the need for novel therapeutics with well-defined mechanisms of action (Rochester and Akiyode, 2014). This study focuses on securing the mode of action of a novel compound, RTC-1 (Fig. 3.1A), which demonstrated anti-diabetic properties in a murine dietary-induced model of type 2 diabetes. RTC-1 was developed following on from work conducted by Campos-Sandoval and colleagues (2011), where novel retinoid analogues were found to interrupt RBP interactions with TTR and STRA6 in a superior way to fenretinide *in vitro*. This action holds potential as an anti-diabetic therapy as we propose that unbound RBP may be readily excreted, thus preventing the proposed negative effects of the protein on the insulin signalling pathway. Through *in silico* screening of commercial databases, Dr. Gemma Kinsella found RTC-1, a non-retinoid compound, to interact with RBP. Surface plasmon resonance analysis (Fig. 3.1B) then demonstrated the ability of this compound to inhibit RBP-TTR interactions, prompting *in vivo* analysis of the effects of the compound on the type 2 diabetic phenotype.

(A)

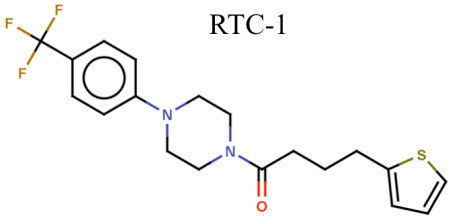

(B)

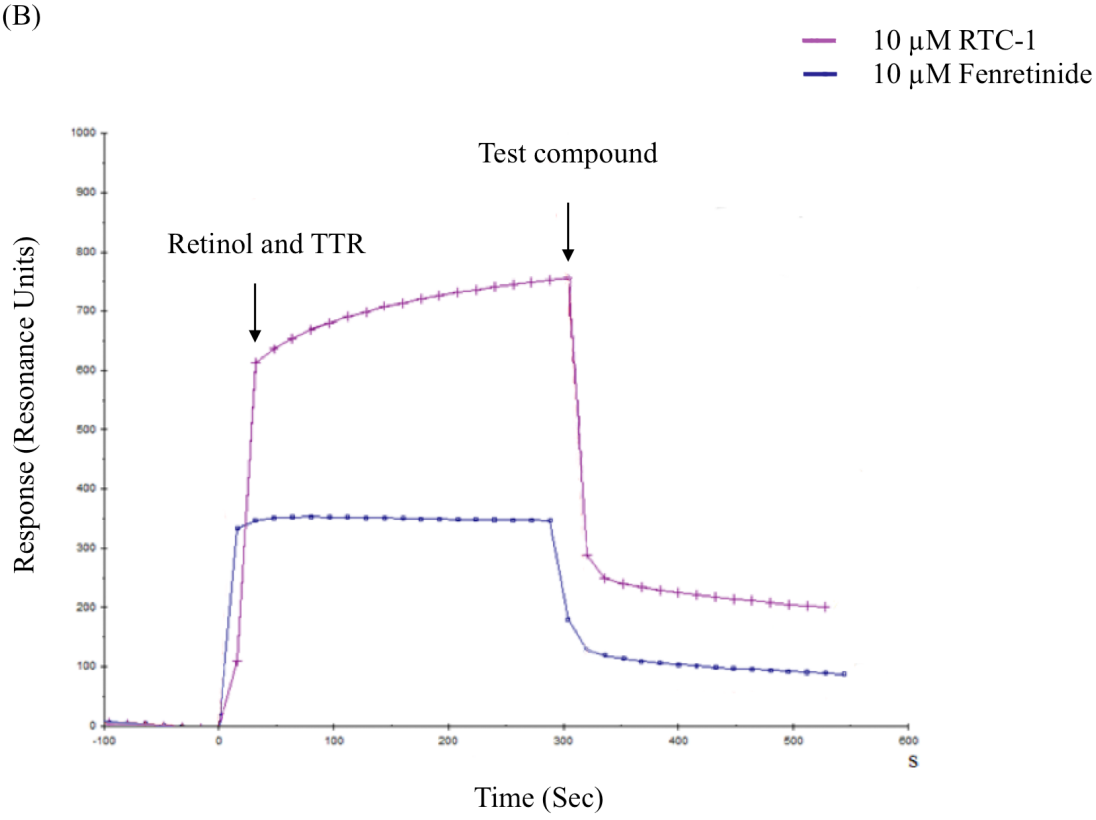

Figure 3.1 The effect of RTC-1 on RBP:TTR complex formation.

(A) Structure of RTC-1. (B) His-tagged RBP was immobilised on the surface of a sensor chip and exposed to retinol and TTR. The complex formation causes a change in the mass on the sensor chip resulting in a change in resonance units. The addition of 10 µM RTC-1 or fenretinide, both led to a decrease in this response, indicative of a disruption to the formation of the RBP:TTR complex. SPR analysis was carried out in the University of Leeds by Prof. Colin Fishwick's research group.

In an intervention study carried out by Dr. Clara Redondo, HFD-fed C57BL/6 mice exhibited reduced insulin sensitivity (Fig. 3.2A) and glucose tolerance (Fig. 3.2B), whereas HFD-fed mice that received 0.04 % (w/w) RTC-1 relative to the diet (~1 mg/mouse/day), displayed improved glucose handling, not significantly different to that of the chow fed control mice. Although there were no changes to food intake between mice on the HFD and the HFD supplemented with RTC-1, those receiving the novel compound maintained the bodyweight recorded at the time of RTC-1 administration, while those on the HFD alone continued to gain weight (Fig. 3.2C). Given this effect, *in vitro* analyses of RTC-1 were conducted to give further insight into the potential of the novel compound as a pharmacological strategy for the treatment of insulin resistance and type 2 diabetes. RTC-1 was found to dramatically increase glucose uptake in C2C12 muscle cells, an effect the action of the compound on RBP would not account for (Fig. 3.3).

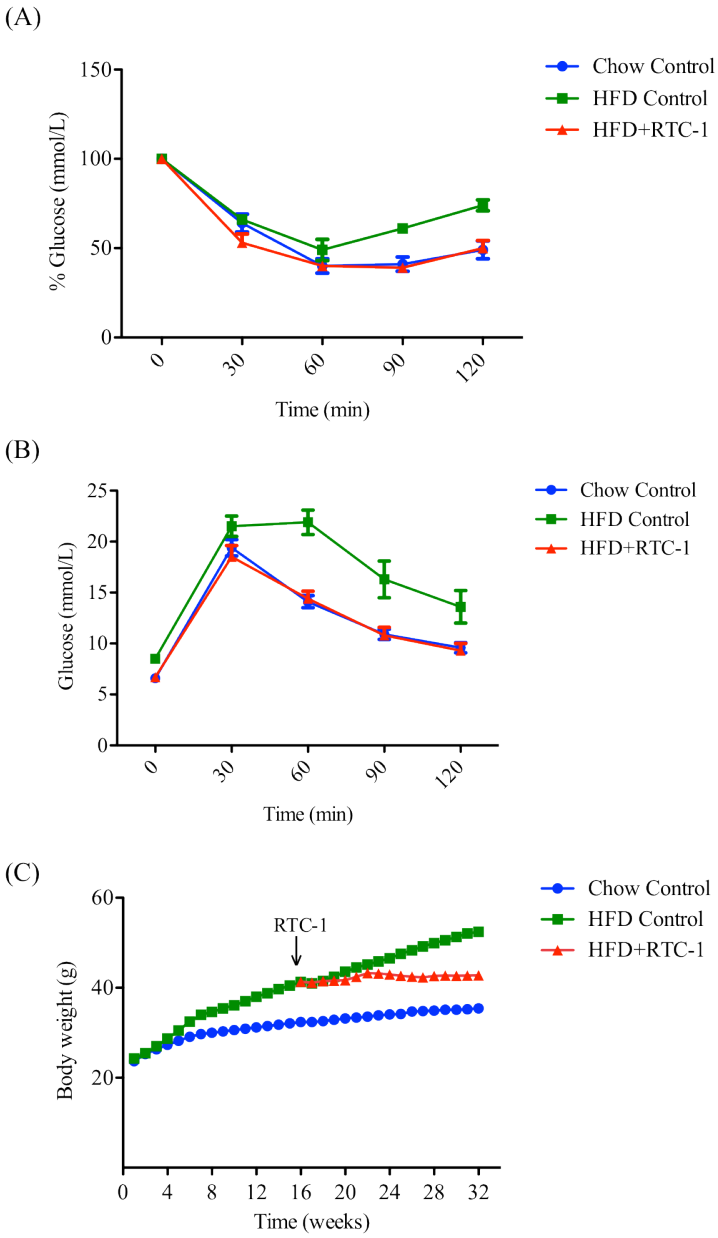

Figure 3.2 RTC-1 intervention study in a dietary-induced mouse model of type 2 diabetes.

Mice received a HFD of 5450 kcal/kg for 16 weeks (n=16). HFD-fed mice were then randomly divided into two groups with one cohort receiving a HFD supplemented with 0.04 % (w/w) RTC-1 for a further 16 weeks (n=8). (A) Mice fed either normal chow, HFD or HFD with RTC-1 were injected with a bolus of insulin and serum glucose levels were monitored for 2 hours. (B) Mice were also injected with a bolus of glucose and serum glucose clearance was monitored for 2 hours. (C) Total body weight was recorded for the duration of the experiment. Images were kindly provided by Dr. Darren Martin.

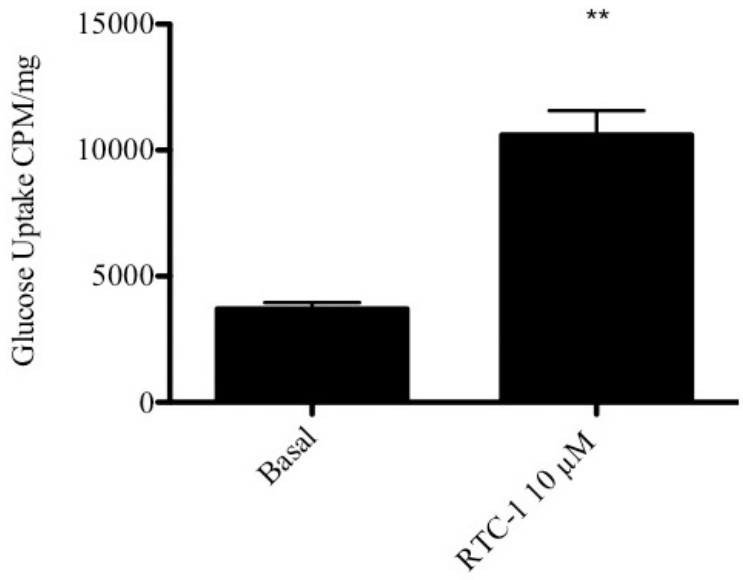

Figure 3.3 The direct effect of RTC-1 on glucose uptake in C2C12 muscle cells.

C2C12 myotubes were stimulated with 10 µM RTC-1 or an equal volume of the vehicle control, DMSO, in complete medium supplemented with 0.1 % (v/v) horse serum for 16 hours. Glucose uptake was measured via scintillation counting of cellular [^{3}H]-2-deoxyglucose. Data presented as mean ± SEM are representative of multiple independent experiments performed in triplicate. Using the unpaired Student's *t*-test GraphPad Prism® 5 software demonstrates significance at $p < 0.01$; **.

In an attempt to establish the mechanism of action of this compound, a variety of targets known to positively impact the type 2 diabetic phenotype were investigated. RTC-1 displayed no effect on well-known diabetic targets such as GLP-1R or PPARγ nor did it induce secretion of insulin or GLP-1 from INS-1e and NCI-H716 cell lines respectively (Martin *et al.,* 2016). In a cell toxicity profile RTC-1 demonstrated no adverse reaction *in vivo,* it did not induce cell death in rat hepatocytes nor did it affect the hERG channel, a recognised preclinical safety test (Priest *et al.*, 2008). These results highlighted RTC-1 as a promising anti-diabetic therapeutic, however in order to further develop this compound investigations into its precise mechanism of action were paramount.

The observed effect of RTC-1 on glucose handling, weight gain and potentially energy balance suggested that AMPK may be a prime candidate through which RTC-1 could exert its effects. AMPK is a central regulator of energy homeostasis that responds to increases in cellular AMP and ADP (Hardie *et al.,* 1998). Once activated, AMPK restores cellular energy balance by switching on ATP generating pathways such as glucose transport and fatty acid oxidation and by switching off ATP consuming pathways such as fatty acid synthesis and gluconeogenesis. As altered glucose and lipid metabolism are central to type 2 diabetes, several anti-diabetic drugs are thought to target AMPK to alleviate this pathophysiology, including metformin, the current standard for the treatment of this disease (Coughlan *et al.,* 2014, Inzucchi *et al.,* 2015).

3.2 Aims and Objectives

The current study aimed to elucidate the mechanism of action of RTC-1 and the consequential effects on glucose uptake, insulin resistance, adipogenesis and osteogenesis using various *in vitro* analysis approaches. In order to demonstrate a structure-activity relationship, a derivative of RTC-1, RTC-15, was analysed in the preliminary stages of this study. The effects of these novel compounds were also compared to that of metformin, the leading medication in the treatment of type 2 diabetes, to gain insight into their effectiveness as a novel pharmacological approach for the treatment of insulin resistance and type 2 diabetes.

3.3 Results

3.3.1 RTC-1 Demonstrates a Dramatic Effect on Glucose Uptake

As skeletal muscle accounts for up to 80 % of glucose uptake (Thiebaud *et al.,* 1982), the C2C12 myoblast cell line, isolated from mouse skeletal muscle, was chosen to compare the effect of RTC-1 on glucose transport to that of insulin and metformin. Stimulation of differentiated C2C12 myotubes for 16 hours with increasing concentrations of RTC-1 led to a progressively significant increase in glucose uptake, as determined by the cellular levels of [^{3}H]-2-deoxyglucose (Fig. 3.4A). [^{3}H]-2-deoxyglucose, a derivative of glucose was used to monitor glucose uptake, as unlike glucose, it cannot be metabolised by the cell. Following stimulations of cells with 1 μM, 10 μM and 100 μM RTC-1, a meaningful increase in glucose uptake was evident and comparable to that of an acute insulin challenge (30 minute incubation with 100 nM insulin). The action of metformin, although significant at 1 μM and 10 μM was only equivalent to a 100 nM insulin stimulation at concentrations above 100 μM (Fig. 3.4B). Based on these results optimal concentrations of RTC-1 (10 μM) and metformin (500 μM) were selected to examine the influence of the compounds on glucose uptake over time. Both RTC-1 (Fig. 3.5A) and metformin (Fig. 3.5B) led to an increase in glucose uptake, becoming significant at 4 hours, with the effect of RTC-1 surpassing that of metformin at the 6 hour time point. Given this dramatic impact of RTC-1 on glucose transport, the long-term response to the compound was then evaluated. Glucose uptake was stimulated in C2C12 myotubes with the addition of 10 μM RTC-1 for 16 hours. Cells were washed free of the compound and changes to glucose uptake were then examined. At 6 and 12 hours post RTC-1 removal a significant increase in glucose uptake was observed. Although this effect lessened at 24 and 48 hours, basal glucose levels were surpassed (Fig. 3.6).

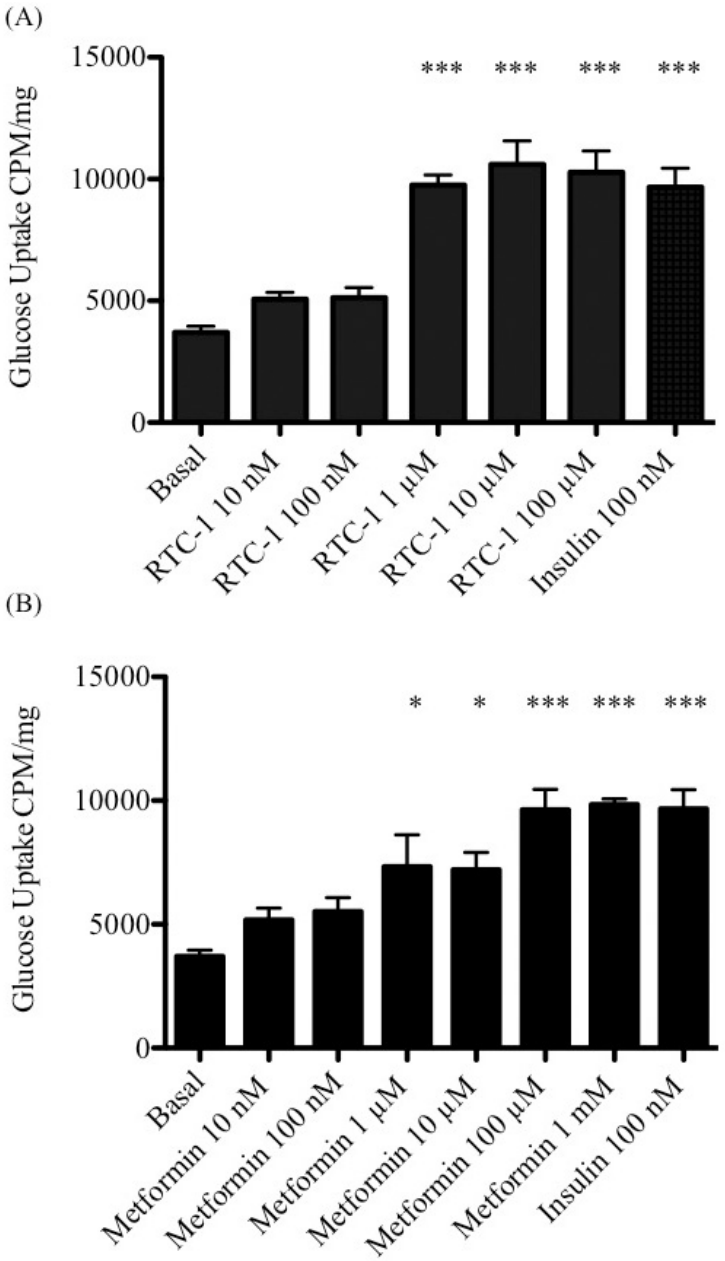

Figure 3.4 Concentration dependent effects of RTC-1 and metformin on glucose uptake.

C2C12 myotubes were stimulated with varying concentrations of (A) RTC-1 or (B) metformin for 16 hours in complete medium supplemented with 0.1 % (v/v) horse serum. As a positive control, cells were incubated with 100 nM insulin in KRBG for 30 minutes. Glucose uptake was measured via scintillation counting of cellular [^{3}H]-2-deoxyglucose. Data presented as mean ± SEM are representative of two independent experiments performed in triplicate. One-way ANOVA with a post-hoc Dunnett test using GraphPad Prism® 5 software demonstrates significance at $p < 0.05$; * and $p < 0.001$; ***.

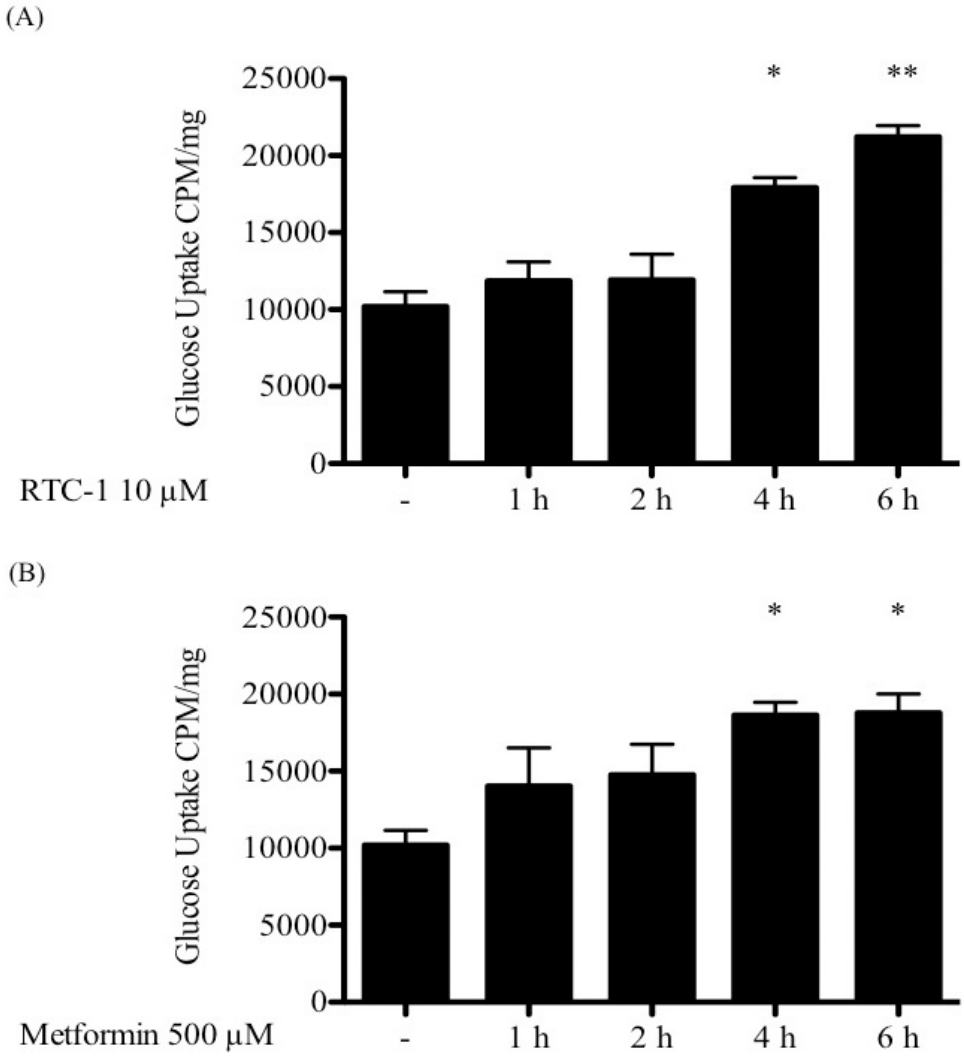

Figure 3.5 Time dependent effects of RTC-1 and metformin on glucose uptake.

C2C12 myotubes were stimulated for various times points ranging from 1 hour to 6 hours with optimal concentrations of (A) RTC-1 (10 µM) and (B) metformin (500 µM) in complete medium containing 0.1 % (v/v) horse serum. Changes in glucose uptake were evaluated via scintillation counting of cellular [^{3}H]-2-deoxyglucose. Data presented as mean ± SEM are representative of three independent experiments performed in triplicate each time. One-way ANOVA with a post-hoc Dunnett test using GraphPad Prism® 5 software demonstrates significance at $p < 0.05$; * and $p < 0.01$; **.

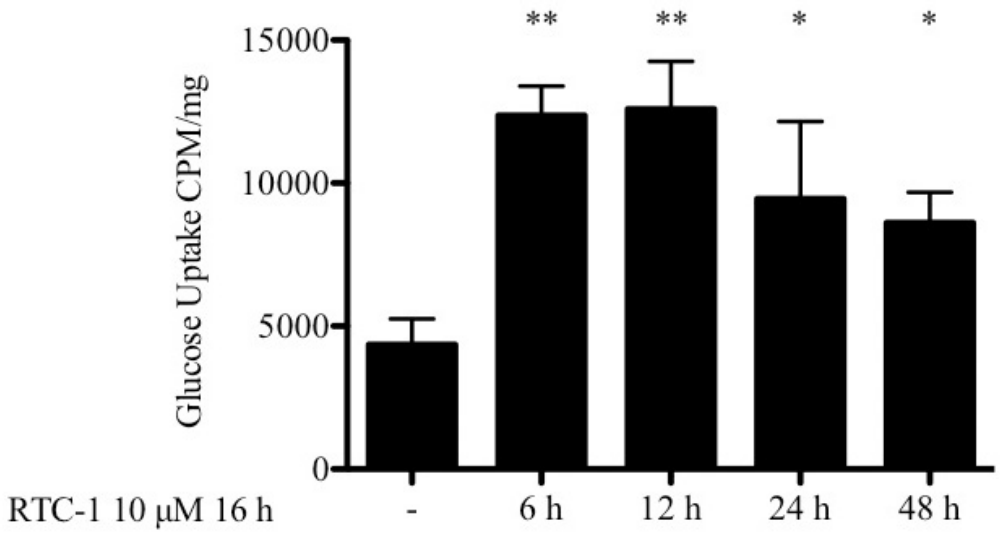

Figure 3.6 The long-term effects of RTC-1-stimulated glucose uptake in cells washed free of the compound.

C2C12 myotubes were stimulated with 10 μM RTC-1 in complete medium supplemented with 0.1 % (v/v) horse serum for 16 hours, then washed free of RTC-1 with DPBS and incubated with fresh medium. Changes in glucose uptake were evaluated via scintillation counting of cellular [^{3}H]-2-deoxyglucose at 6, 12, 24 and 48 hours post medium change. Data presented as mean ± SEM are representative of two independent experiments performed in triplicate each time. One-way ANOVA with a post-hoc Dunnett test using GraphPad Prism® 5 software demonstrates significance at $p < 0.05$; * and $p < 0.01$; **.

3.3.2 RTC-1 and its Derivative, RTC-15, Induce GLUT4 Translocation

In order to investigate the structure-activity relationship of RTC-1, a large number of compounds with alterations to the original structure of RTC-1 were tested for their capacity to induce glucose uptake. Stimulation of C2C12 myotubes with 10 μM of one derivative, RTC-15 (Fig. 3.7A), led to a significant increase in glucose uptake, similar to the action of 100 nM insulin. However, the response to RTC-15 did not exceed that observed with RTC-1 (Fig. 3.7B).

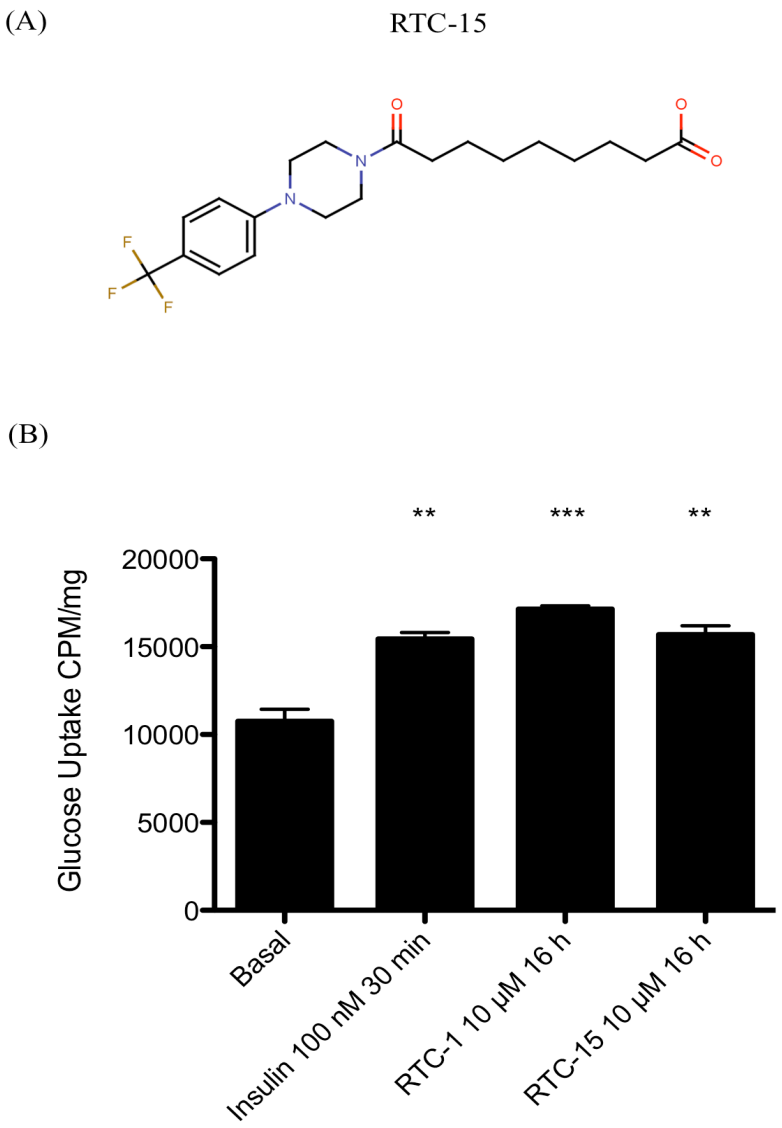

Figure 3.7 The effect of the RTC-1 derivative, RTC-15, on glucose uptake.

(A) Structure of RTC-15. (B) C2C12 myotubes were incubated with 10 µM RTC-1 or 10 µM RTC-15 in complete medium containing 0.1 % (v/v) horse serum for 6 hours. Cells were also stimulated with 100 nM insulin in KRBG for 30 minutes, as a positive control. Glucose uptake was measured via scintillation counting of cellular [^{3}H]-2-deoxyglucose. Data presented as mean ± SEM are representative of multiple experiments, performed in triplicate each time. One-way ANOVA with a post-hoc Dunnett test using GraphPad Prism® 5 software demonstrates significance at $p < 0.01$; ** and $p < 0.001$; ***.

As GLUT4 is the primary modulator of glucose uptake in response to insulin stimulation (Pessin *et al.,* 1999), and has also been implicated in AMPK-induced glucose transport (Kurth-Kraczek *et al.,* 1999), the effect of these novel compounds on GLUT4 translocation was investigated. Under basal conditions, GLUT4 resides in intracellular storage vesicles until signalled to redistribute to the plasma membrane to facilitate increased uptake of glucose (Larance *et al.,* 2008). Through flow cytometry analysis, a significant increase in plasma membrane associated GLUT4 was observed in C2C12 cells stimulated with 10 μM RTC-1 or 10 μM RTC-15. Cells incubated with 500 μM metformin exhibited a level of GLUT4 cell surface expression similar to those exposed to the vehicle control, DMSO (Fig. 3.8).

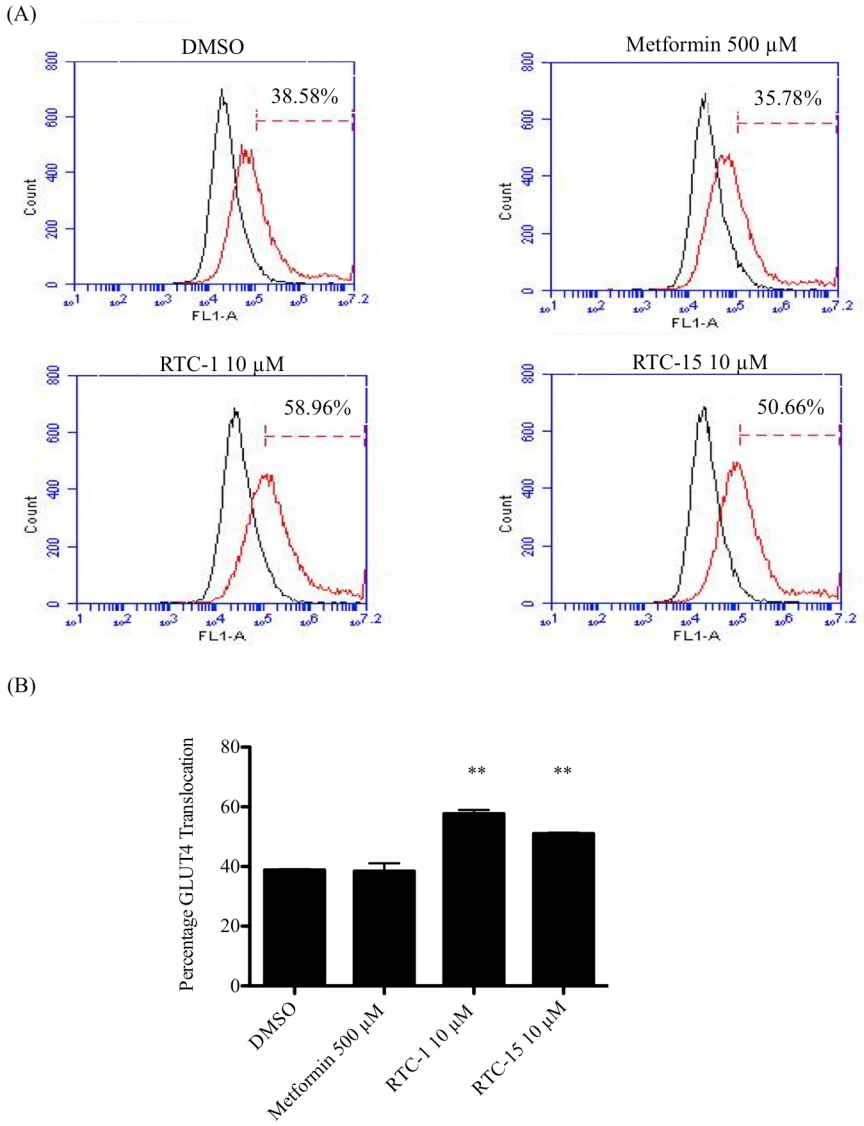

Figure 3.8 The effect of RTC-1, RTC-15 and metformin on GLUT4 translocation.

C2C12 myotubes were stimulated with 10 µM RTC-1, 10 µM RTC-15, 500 µM metformin or an equal volume of DMSO for 4 hours in complete medium containing 0.1 % (v/v) horse serum. Cells were incubated with a GLUT4 specific antibody followed by a FITC conjugated secondary antibody (red line). As a control, cells were stained with the secondary antibody alone (black line). Cells were analysed using flow cytometry with 10,000 events recorded. (A) Data are presented in histograms of mean fluorescence intensity, representing two separate experiments. (B) A bar chart represents the average percentage of membrane-associated GLUT4 relative to cells incubated with the fluorescent secondary antibody alone. One-way ANOVA with a post-hoc Dunnett test using GraphPad Prism® 5 software demonstrates significance at $p < 0.01$; **.

3.3.3 RTC-1 and RTC-15 Activate AMPK

Given the effects of RTC-1 and RTC-15 on GLUT4 translocation, the next step was to examine the activation status of AMPK (Mu *et al.,* 2001). Phosphorylation of the catalytic α-subunit of AMPK at Thr^{172} was investigated in response to RTC-1, RTC-15 and metformin, as phosphorylation at this residue is a recognised indicator of AMPK activation (Hawley *et al.,* 1996, Stein *et al.,* 2000). After a 15 minute incubation, 10 μM RTC-1 moderately induced the phosphorylation of AMPKα in C2C12 myotubes; this became amplified at 45 minutes and plateaued (Fig. 3.9A). An increase in the phosphorylation of AMPKα was observed at 45 minutes post stimulation in response to 10 μM RTC-15, this was augmented at 2 hours and the phosphorylation status of the kinase remained elevated for the duration of the time course (Fig. 3.9B). A 500 μM metformin incubation augmented AMPKα phosphorylation after 15 minutes, phosphorylation increased again at 45 minutes and was sustained throughout the remainder of the time course (Fig. 3.9C).

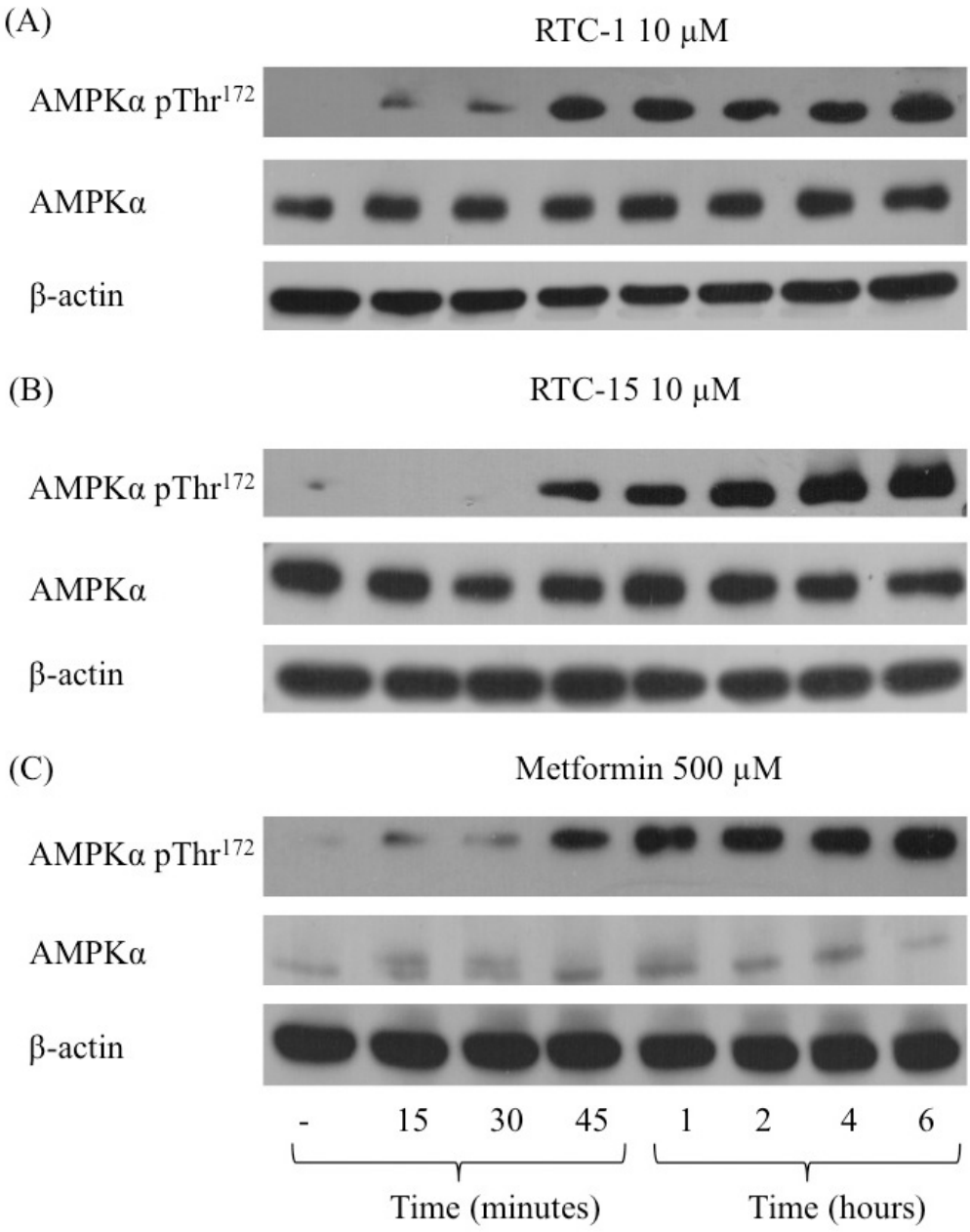

Figure 3.9 Time dependent effects of RTC-1, RTC-15 and metformin on AMPKα phosphorylation.

C2C12 myotubes were stimulated with (A) 10 μM RTC-1, (B) 10 μM RTC-15 or (C) 500 μM metformin for 15 minutes up to 6 hours in complete medium with 0.1 % (v/v) horse serum. Cells were lysed, subjected to SDS-PAGE and immunoblotted with antibodies against phospho-AMPKα Thr^{172} and native AMPKα. β-actin was used as a loading control. Data are representative of multiple independent experiments.

3.3.4 RTC-1 and RTC-15 Inhibit NADH:ubiquinone oxidoreductase Activity

To determine if the effect of these compounds was as a result of a direct interaction with AMPK or of a regulating mechanism upstream of the protein, the influence of RTC-1 and RTC-15 on the activity of NADH:ubiquinone oxidoreductase in mitochondria was investigated. As metformin is believed to instigate its influence on AMPK in this way (Owen *et al.,* 2000), the impact of the RTC compounds was again compared to that of metformin. Before each assay the activity of mitochondria isolated from rat liver was assessed ± the addition of rotenone, a potent NADH:ubiquinone oxidoreductase inhibitor that obstructs NADH oxidation by blocking the ubiquinone binding site of the enzyme (Degli Esposti, 1998). Using a temperature controlled spectrophotometer, NADH:ubiquinone oxidoreductase activity was initiated, and monitored, with the addition of 60 μM ubiquinone. As more NAD^+ was produced from NADH to generate a proton gradient a decrease in absorbance was observed, as NAD^+ does not absorb at 340 nm. With the addition of 1 μM rotenone, the solution began to absorb again at 340 nm, an indication of a decrease in NAD^+ production (Fig. 3.10A). The effect of a compound on NADH:ubiquinone oxidoreductase was determined by comparing activity before and after addition, relative to the vehicle control, DMSO (Fig. 3.10B).

Utilising the same method, the addition of RTC-1 (Fig. 3.11A) and RTC-15 (Fig. 3.11B) to disrupted mitochondria produced a dose-related inhibition of NADH:ubiquinone oxidoreductase activity. This assay also allowed the IC_{50} of the compounds to be calculated; 27 μM for RTC-1 and 104 μM for RTC-15. There was no apparent effect with metformin until the addition of the highest soluble concentration, 10 mM (Fig. 3.11C).

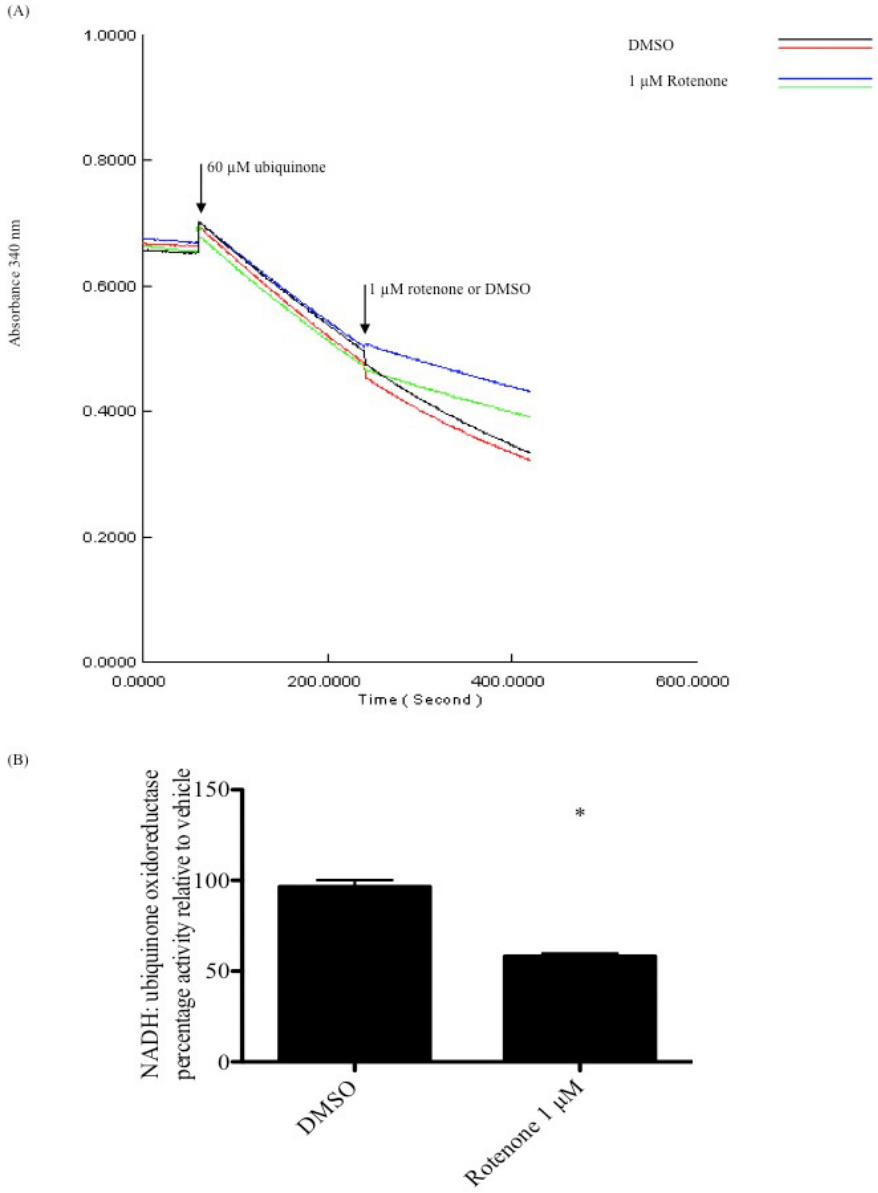

Figure 3.10 The effect of rotenone on NADH:ubiquinone oxidoreductase activity.

(A) Baseline activity of NADH:ubiquinone oxidoreductase in isolated mitochondria was measured at 340 nm for 1 minute. The addition of 60 µM ubiquinone led to the oxidation of NADH to NAD^+. DMSO (black and red lines) demonstrated little effect on this process, while 1 µM of the specific NADH:ubiquinone oxidoreductase inhibitor, rotenone (blue and green lines), prevented the oxidation of NADH. (B) A bar chart represents the average percentage activity of NADH:ubiquinone oxidoreductase relative to the vehicle control, DMSO. Using the unpaired Student's *t*-test GraphPad Prism® 5 software demonstrates a significant decrease in activity at $p < 0.05$; *.

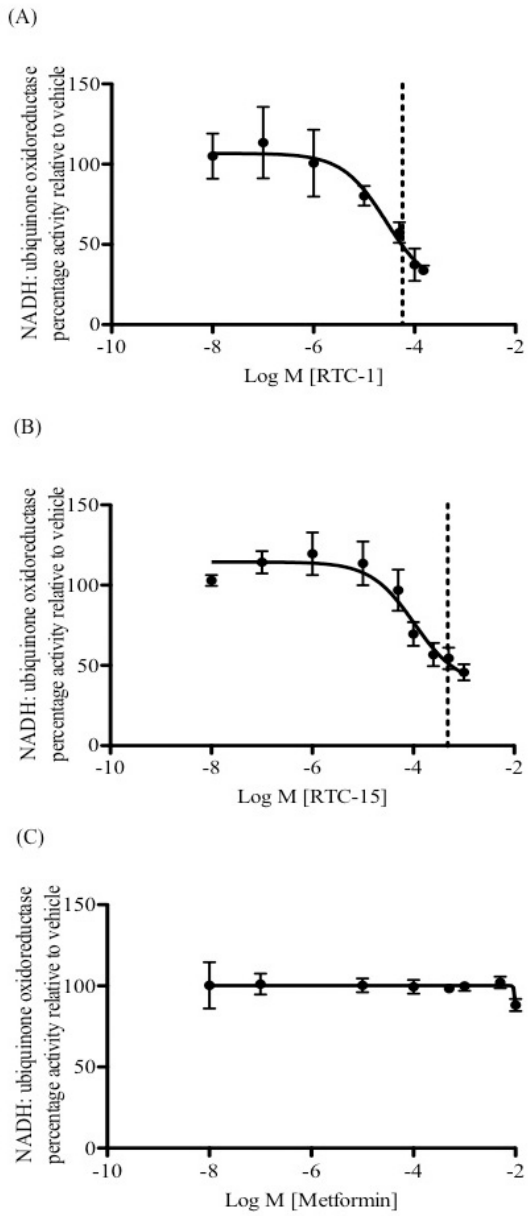

Figure 3.11 The effect of RTC-1, RTC-15 and metformin on NADH:ubiquinone oxidoreductase activity.

Mitochondria isolated from rat liver were incubated with (A) RTC-1, (B) RTC-15 and (C) metformin at various concentrations. The effect of the compounds on NADH:ubiquinone oxidoreductase was determined by comparing activity before and after addition, relative to the vehicle control, DMSO. Data are presented as mean ± SEM of at least three independent experiments. A nonlinear regression curve of log [inhibitor] v response was calculated using GraphPad Prism® 5 software. This estimated an IC_{50} value at 27 μM for RTC-1 and 104 μM for RTC-15, as indicated by the dashed line.

In a separate study carried out by Dr. Conor Breen, the effect of RTC-1 on oxygen consumption was examined to determine if the action of the compound was limited to NADH:ubiquinone oxidoreductase. Intact rat liver mitochondria were incubated with an air-saturated medium (20 mM Tris-HCl, 80 mM KCl, 5 mM $MgCl_2$, 0.5 M KH_2PO_4, pH 7.4) and oxygen consumption was monitored with a Clark electrode (Fig. 3.12). The complex I substrate (160 mM glutamate, 40 mM sodium malate) stimulated oxygen consumption as electrons from NADH entered the respiratory chain via NADH:ubiquinone oxidoreductase. This increase was augmented with the addition of ADP, however 10 μM RTC-1 inhibited the process. RTC-1 demonstrated no effect on complex II of the mitochondrial respiratory chain (succinate:ubiquinone oxidoreductase), as oxygen consumption was restored with the addition of 0.5 mM sodium succinate which provides electrons for succinate:ubiquinone oxidoreductase, bypassing NADH:ubiquinone oxidoreductase.

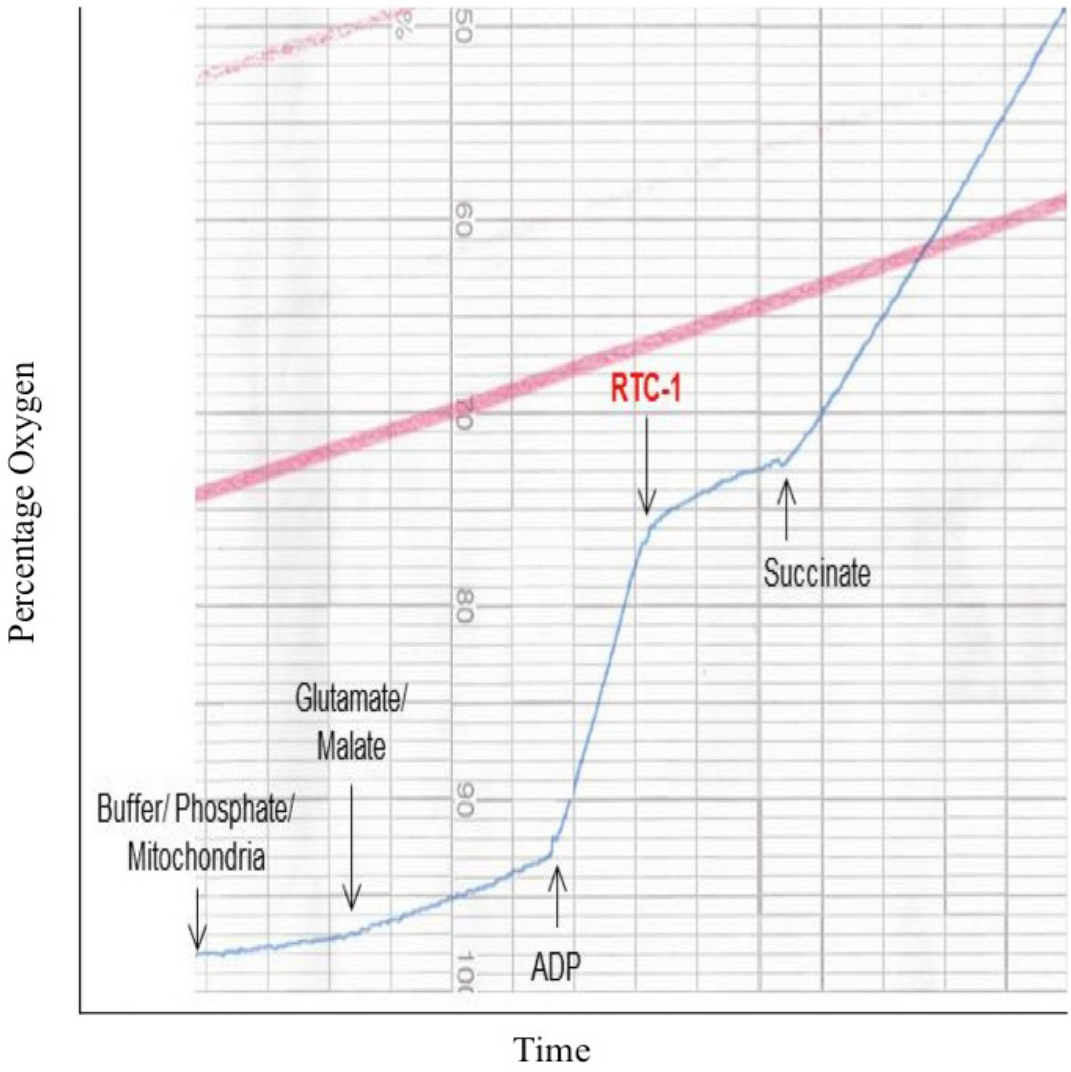

Figure 3.12 The effect of RTC-1 on oxygen consumption in isolated mitochondria.

Isolated rat liver mitochondria were monitored for changes in oxygen consumption using a Clark electrode. Glutamate/malate was used as a substrate to increase NADH levels. The addition of 10 μM RTC-1 resulted in a drop in oxygen consumption, which was rescued with the complex II substrate, succinate. Image kindly provided by Dr. Conor Breen.

As RTC-1 appeared to target NADH:ubiquinone oxidoreductase alone, the mode of action which impacts AMPK is believed to be due to the resultant decrease in ATP levels. Using a luminescent ATP detection kit to look at cellular ATP levels directly, there was no apparent effect with C2C12 muscle cells when exposed to rotenone, RTC-1, RTC-15 or metformin for 30 minutes (Fig. 3.13A). However after 1 hour, a dramatic reduction in cellular ATP was observed with the addition of 25 μM rotenone. A decrease in cellular ATP levels, although not significant, was also seen in cells incubated with 10 μM RTC-1 and 10 μM RTC-15, while 500 μM metformin demonstrated no effect on ATP levels (Fig. 3.13B). RTC-1, RTC-15 and metformin all provoked a modest decrease in cellular ATP 4 hours post stimulation, again not statistically different from basal concentrations (Fig. 3.13C).

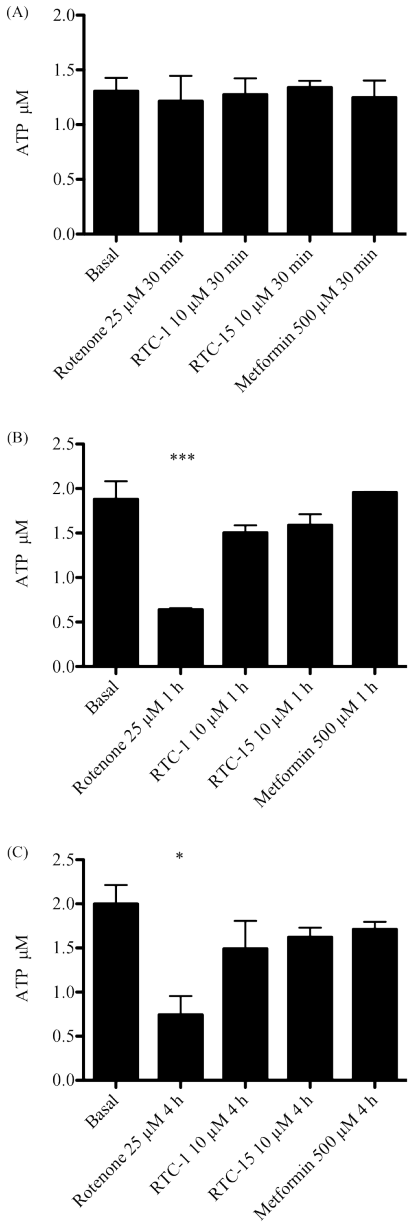

Figure 3.13 The impact of RTC-1, RTC-15 and metformin on cellular ATP levels.

C2C12 myotubes were stimulated with 10 µM RTC-1, 10 µM RTC-15, 500 µM metformin or 25 µM rotenone in complete medium with 0.1 % (v/v) horse serum for (A) 30 minutes, (B) 1 hour and (C) 4 hours. A luminescent ATP detection assay (Abcam, ab113849) was used according to the manufacturer's instructions to monitor changes in ATP levels. Data presented as mean ± SEM are representative of two independent experiments each performed in triplicate. One-way ANOVA with a post-hoc Dunnett test using GraphPad Prism® 5 software demonstrates significance at $p < 0.05$; * and $p < 0.001$; ***.

3.3.5 RTC-1 and RTC-15-Induced Glucose Uptake is Dependent on AMPK Activation

To confirm AMPK as the effector protein by which RTC-1 elicited its effects on glucose metabolism *in vivo,* C2C12 myotubes were incubated with the specific AMPK inhibitor, Compound C, at 10 μM for 1 hour prior to the addition of 10 μM RTC-1, 10 μM RTC-15 or 500 μM metformin. RTC-1, RTC-15 and metformin all significantly increased glucose uptake in C2C12 cells, the effect of which was dramatically attenuated by Compound C (Fig. 3.14). Compound C failed to inhibit insulin-induced glucose uptake, demonstrating the selectivity of the inhibitor.

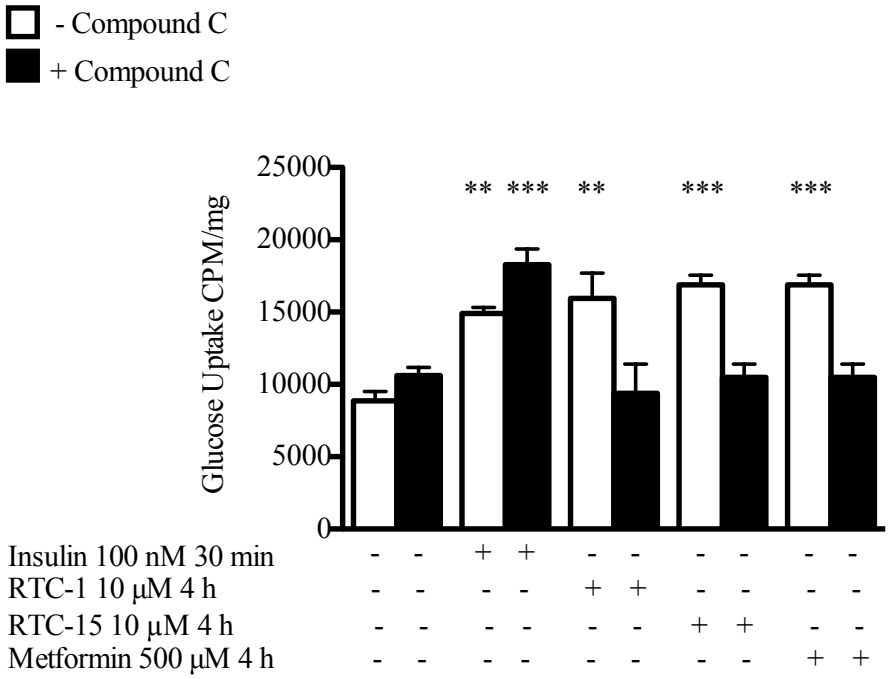

Figure 3.14 The effect of the AMPK inhibitor, Compound C, on insulin, RTC-1, RTC-15 and metformin-induced glucose uptake.

C2C12 myotubes were incubated with 10 μM Compound C or an equal volume of the vehicle control, DMSO, in complete medium supplemented with 0.1 % (v/v) horse serum for 1 hour. Cells were then stimulated with 100 nM insulin for 30 minutes or 10 μM RTC-1, 10 μM RTC-15 and 500 μM metformin for 4 hours. Glucose uptake was measured via scintillation counting of cellular [^{3}H]-2-deoxyglucose. Data presented as mean ± SEM are representative of three independent experiments performed in triplicate each time. One-way ANOVA with a post-hoc Dunnett test using GraphPad Prism® 5 software demonstrates significance at $p < 0.01$; ** and $p < 0.001$; ***.

3.3.6 RTC-1 and RTC-15 Activate the Downstream Effector Proteins of AMPK; AS160 and ACC

The activation of AMPK initiates a series of signalling events culminating in the uptake and oxidation of substrates important for ATP synthesis such as glucose. AS160 mediates GLUT4 translocation to facilitate glucose uptake when phosphorylated at a number of residues, with Thr^{642} and Ser^{588} of particular importance (Sano, 2003, Geraghty *et al.,* 2007, Schweitzer *et al.,* 2012). Activated AMPK also leads to a decrease in ATP-consuming biosynthetic processes such as lipid synthesis through the phosphorylation of ACC at Ser^{79} (Park *et al.,* 2002).

Downstream of AMPK activation, RTC-1 was found to influence these main effector proteins of cell metabolism. In a dose response experiment, a 16 hour stimulation of C2C12 muscle cells with 10 nM RTC-1 induced the phosphorylation of AMPKα and of AS160 at Thr^{642}, which was enhanced with increasing concentrations of the compound. Phosphorylation of AS160 at Ser^{588} was also seen to increase in response to a 10 nM stimulation, albeit to a lesser extent. RTC-1 triggered ACC phosphorylation moderately at 10 nM, with a more pronounced effect seen at concentrations of 100 nM and above (Fig. 3.15). In response to metformin, the phosphorylation of AMPKα was augmented by a 16 hour, 10 nM stimulation of C2C12 myotubes, with phosphorylation peaking in response to 1 mM. Metformin demonstrated little effect on the phosphorylation of AS160 at Thr^{642}, while phosphorylation at Ser^{588} increased with a 1 mM stimulation. An increase in ACC phosphorylation was also observed at concentrations above 10 nM metformin (Fig. 3.16).

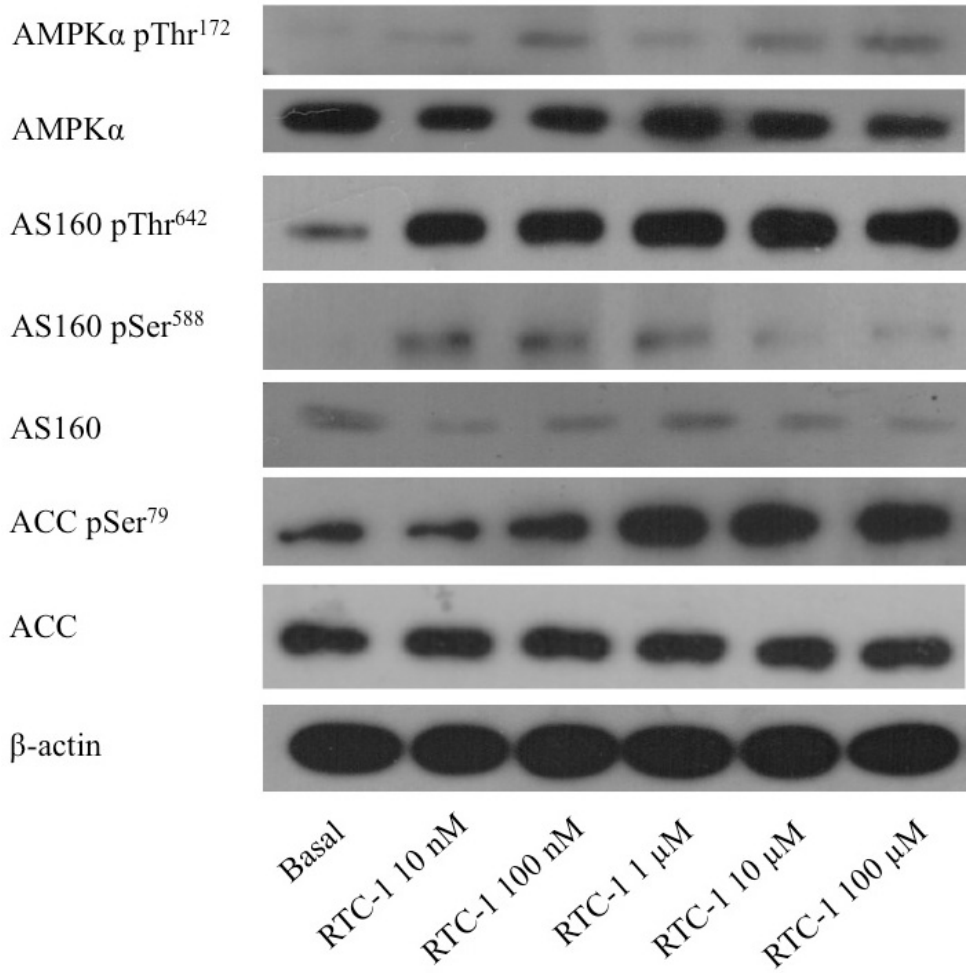

Figure 3.15 Concentration dependent effects of RTC-1 on AMPK signalling.

C2C12 myotubes were stimulated with varying concentrations of RTC-1 (10 nM – 100 μM) for 16 hours in complete medium containing 0.1 % (v/v) horse serum. Cells were lysed, subjected to SDS-PAGE and immunoblotted with antibodies against phospho-AMPKα Thr^{172}, phospho-AS160 Thr^{642} and Ser^{588}, phospho-ACC Ser^{79}, native AMPKα, AS160 and ACC. β-actin was used as a loading control. Data are representative of two independent experiments.

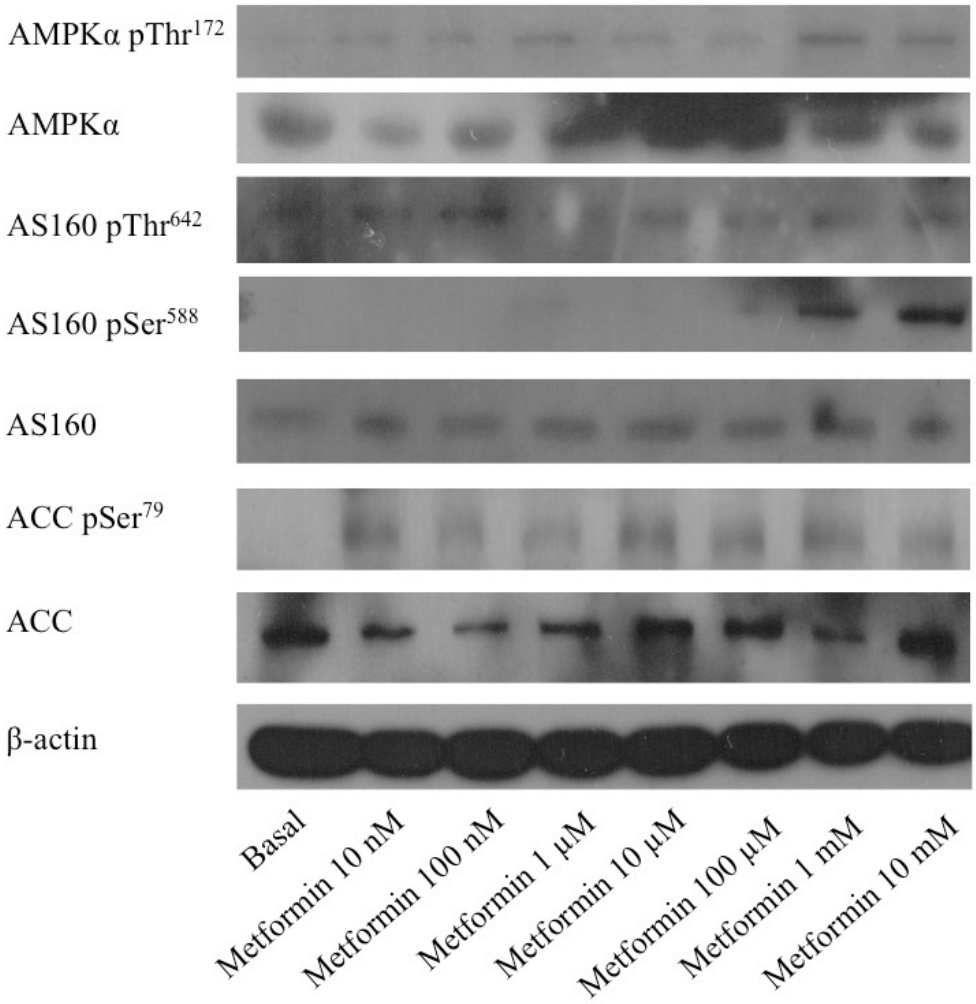

Figure 3.16 Concentration dependent effects of metformin on AMPK signalling.

C2C12 myotubes were stimulated with varying concentrations of metformin (10 nM – 10 mM) for 16 hours in complete medium containing 0.1 % (v/v) horse serum. Cells were lysed, subjected to SDS-PAGE and immunoblotted with antibodies against phospho-AMPKα Thr^{172}, phospho-AS160 Thr^{642} and Ser^{588}, phospho-ACC Ser^{79}, native AMPKα, AS160 and ACC. β-actin was used as a loading control. Data are representative of two independent experiments.

In a time course study, 10 μM RTC-1 (Fig. 3.17A), 10 μM RTC-15 (Fig. 3.17B) and 500 μM metformin (Fig. 3.17C) all led to an increase in ACC phosphorylation corresponding to the phosphorylation pattern of AMPKα (Fig. 3.9).

Time course analysis of AS160 demonstrated a 10 μM exposure to RTC-1 (Fig. 3.18A) to increase the phosphorylation status of AS160 at Thr^{642} within 15 minutes and at Ser^{588} at 45 minutes. Phosphorylation at both residues diminished to basal levels after 2 hours and increased again at the 6 hour time point. A similar, although less intense profile of phosphorylation was observed in cells stimulated with 10 μM RTC-15 (Fig. 3.18B). Conversely, 500 μM metformin increased the phosphorylation of AS160 at both residues maximally within 15 minutes. The phosphorylation at Thr^{642} diminished to basal levels at 2 hours, with the more pronounced phosphorylation at Ser^{588} resembling basal activity at 45 minutes (Fig. 3.18C). The pattern of AS160 phosphorylation associated with RTC-1 and RTC-15 did not reflect that of AMPKα at the early times points, suggesting that these compounds may influence another regulator of AS160, the obvious candidate being Akt.

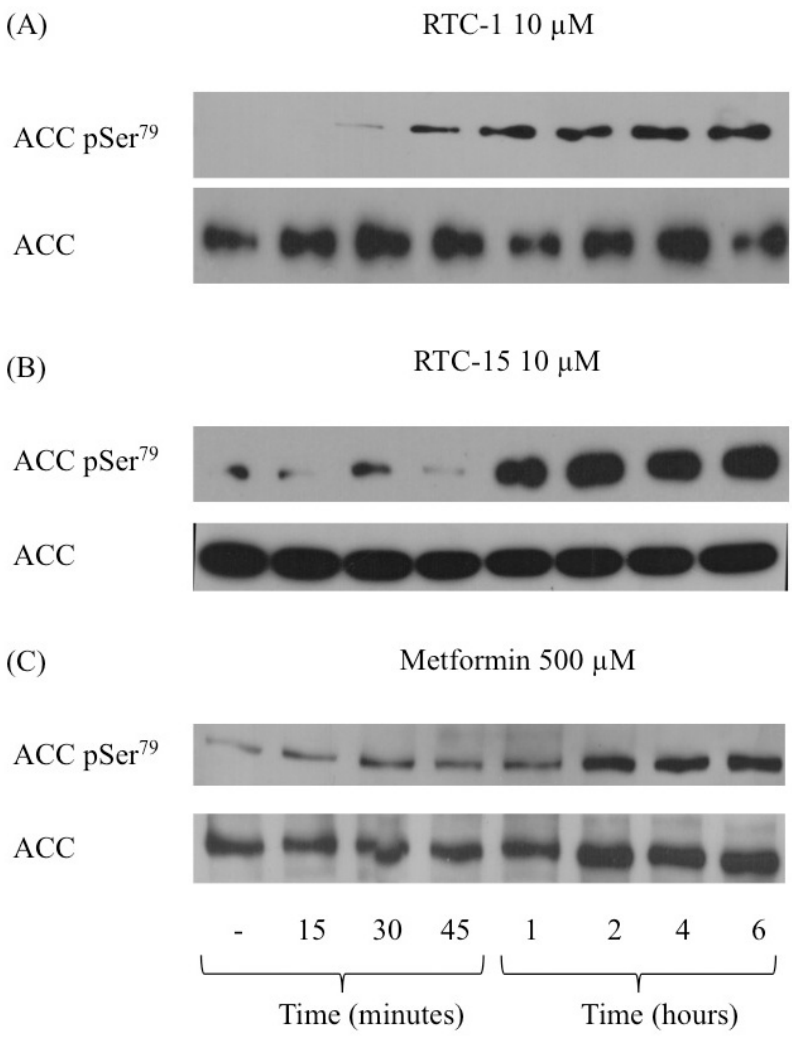

Figure 3.17 Time dependent effects of RTC-1, RTC-15 and metformin on ACC phosphorylation.

C2C12 myotubes were stimulated with (A) 10 μM RTC-1, (B) 10 μM RTC-15 or (C) 500 μM metformin for 15 minutes up to 6 hours in complete medium containing 0.1 % (v/v) horse serum. Cells were lysed, subjected to SDS-PAGE and immunoblotted with antibodies against phospho-ACC Ser^{79} and native ACC. Data are representative of three independent experiments.

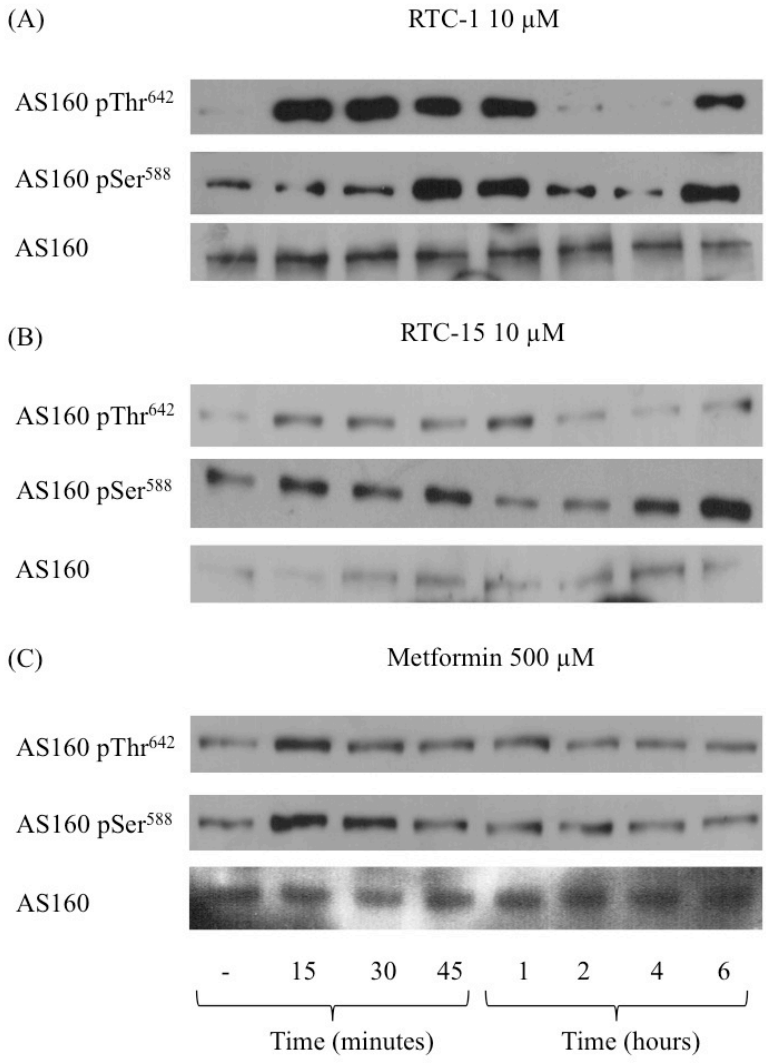

Figure 3.18 Time dependent effects of RTC-1, RTC-15 and metformin on AS160 phosphorylation.

C2C12 myotubes were stimulated with (A) 10 µM RTC-1, (B) 10 µM RTC-15 or (C) 500 µM metformin for 15 minutes up to 6 hours in complete medium containing 0.1 % (v/v) horse serum. Cells were lysed, subjected to SDS-PAGE and immunoblotted with antibodies against phospho-AS160 Thr^{642} and Ser^{588} and native AS160. Data are representative of three independent experiments.

3.3.7 RTC-1 and RTC-15 Activate Akt

The addition of 10 μM RTC-1 (Fig. 3.19A) to C2C12 myotubes resulted in a rapid increase in Akt phosphorylation within 15 minutes, this lessened after 30 minutes, subsiding to basal levels at 45 minutes and decreased further at 4 hours. Similarly, 10 μM RTC-15 (Fig. 3.19B) promptly increased Akt phosphorylation at 30 minutes, which sustained a high level of activity until the 4 hour time point. Conversely, 500 μM metformin led to a progressive decrease in Akt phosphorylation over time (Fig. 3.19C).

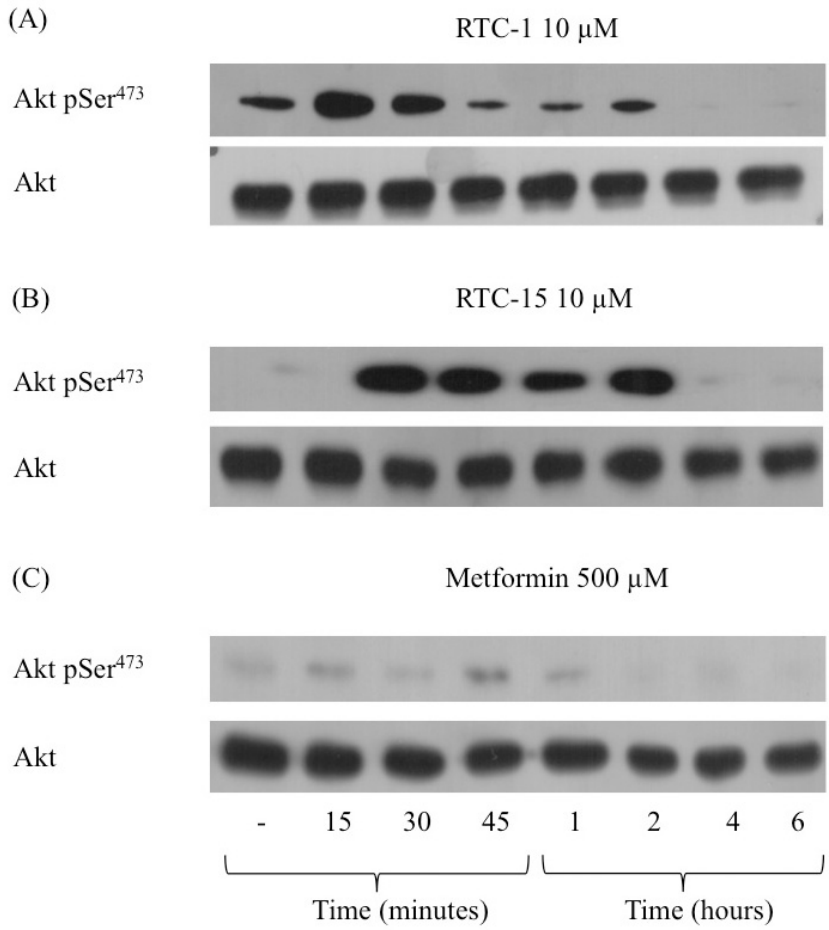

Figure 3.19 Time dependent effects of RTC-1, RTC-15 and metformin on Akt phosphorylation.

C2C12 myotubes were stimulated with (A) 10 µM RTC-1, (B) 10 µM RTC-15 or (C) 500 µM metformin for 15 minutes up to 6 hours in complete medium containing 0.1 % (v/v) horse serum. Cells were lysed, subjected to SDS-PAGE and immunoblotted with antibodies against phospho-Akt Ser^{473} and native Akt. Data are representative of three independent experiments.

In an extended time course study, stimulation of C2C12 cells with 10 μM RTC-1 (Fig. 3.20A) and 10 μM RTC-15 (Fig. 3.20B) led to a noticeable increase in Akt phosphorylation within 1 minute, which became saturated at 5 minutes and declined over the remainder of the time course. This pattern was also reflected in the phosphorylation of AS160 in response to RTC-1 and RTC-15. Both compounds led to an increase in AS160 phosphorylation after 1 minute, yet this effect began to diminish at Ser^{588} after 30 minutes and at Thr^{642} after 45 minutes in response to RTC-1. RTC-15-induced phosphorylation of AS160 subsided at Thr^{642} and at Ser^{588} after 45 minutes. Phosphorylation of AS160 at Thr^{642} returned at 6 hours and after 2 hours at Ser^{588} in response to RTC-1. RTC-15 restored AS160 phosphorylation at Thr^{642} after 4 hours, with phosphorylation of AS160 at Ser^{588} augmented once more at the 6 hour time point. Again 500 μM metformin led to a decrease in Akt phosphorylation over time, appearing inhibitory at 2 hours. Stimulation with metformin led to an increase in AS160 phosphorylation at Thr^{642} and at Ser^{588} to a lesser extent after 1 minute, which diminished over time (Fig. 3.20C).

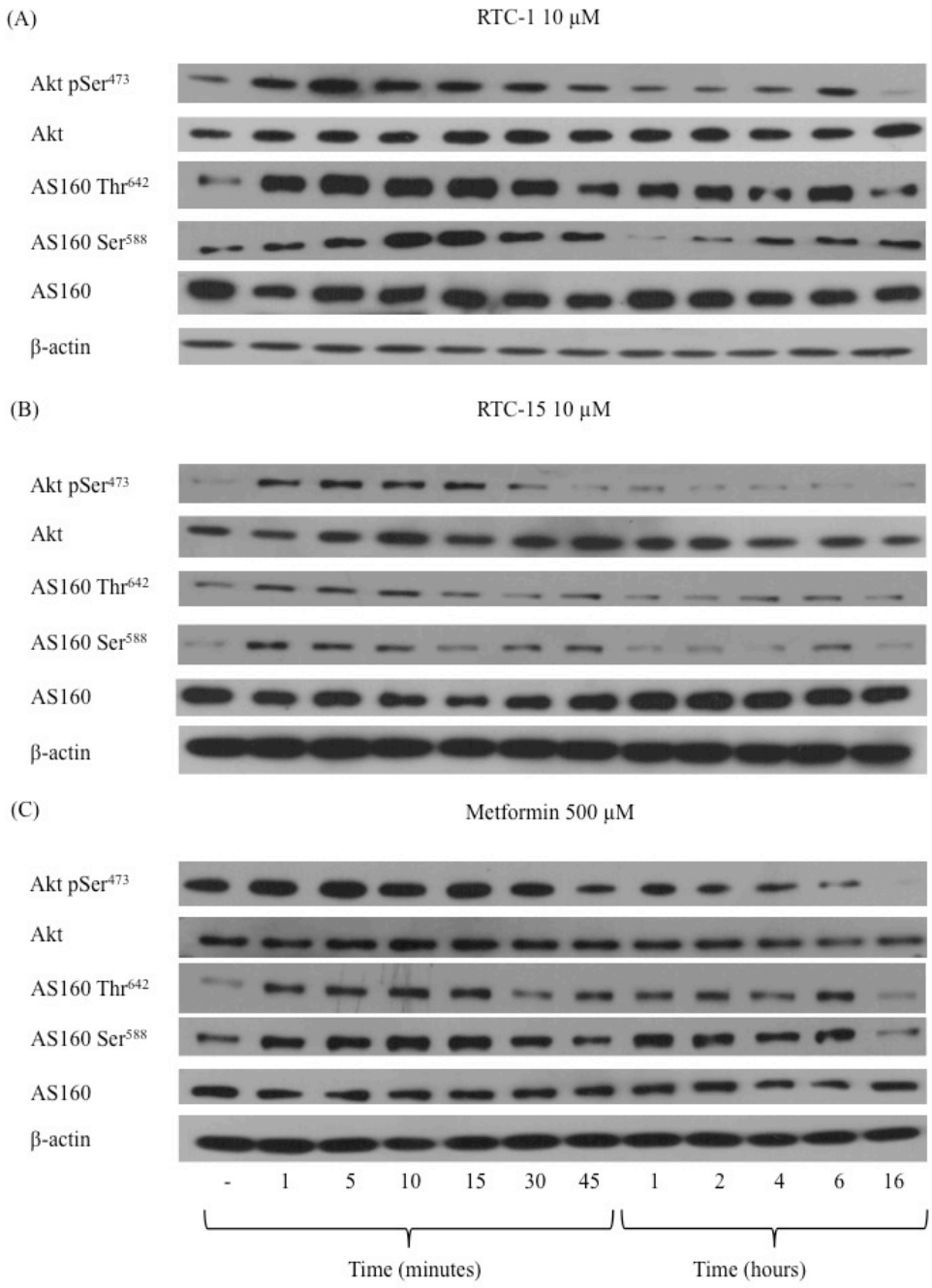

Figure 3.20 Time dependent effects of RTC-1, RTC-15 and metformin on Akt signalling.

C2C12 myotubes were stimulated with (A) 10 µM RTC-1, (B) 10 µM RTC-15 or (C) 500 µM metformin for 1 minute up to 16 hours in complete medium containing 0.1 % (v/v) horse serum. Cells were lysed, subjected to SDS-PAGE and immunoblotted with antibodies against phospho-Akt Ser^{473}, phospho-AS160 Thr^{642} and Ser^{588}, native Akt and AS160. β-actin was used as a loading control. Data are representative of two independent experiments.

In an attempt to understand the role of this early phosphorylation of Akt in RTC-1-stimulated glucose uptake, differentiated C2C12 cells were incubated with an inhibitor of Akt activity, wortmannin, for 1 hour prior to the addition of 10 μM RTC-1. As a control, the effect on insulin-induced glucose uptake was also evaluated. Pre-treatment with 1 μM wortmannin reduced basal glucose uptake and prevented insulin-stimulated glucose transport in C2C12 myotubes. Wortmannin appeared to attenuate RTC-1-induced glucose uptake at the early time point of 15 minutes, which corresponded to the activation of Akt. At 1 hour, RTC-1 overcame the effects of wortmannin, returning glucose uptake to basal levels. Glucose uptake increased again at 4 hours post RTC-1 stimulation in the presence of wortmannin, and significantly so at 16 hours (Fig. 3.21).

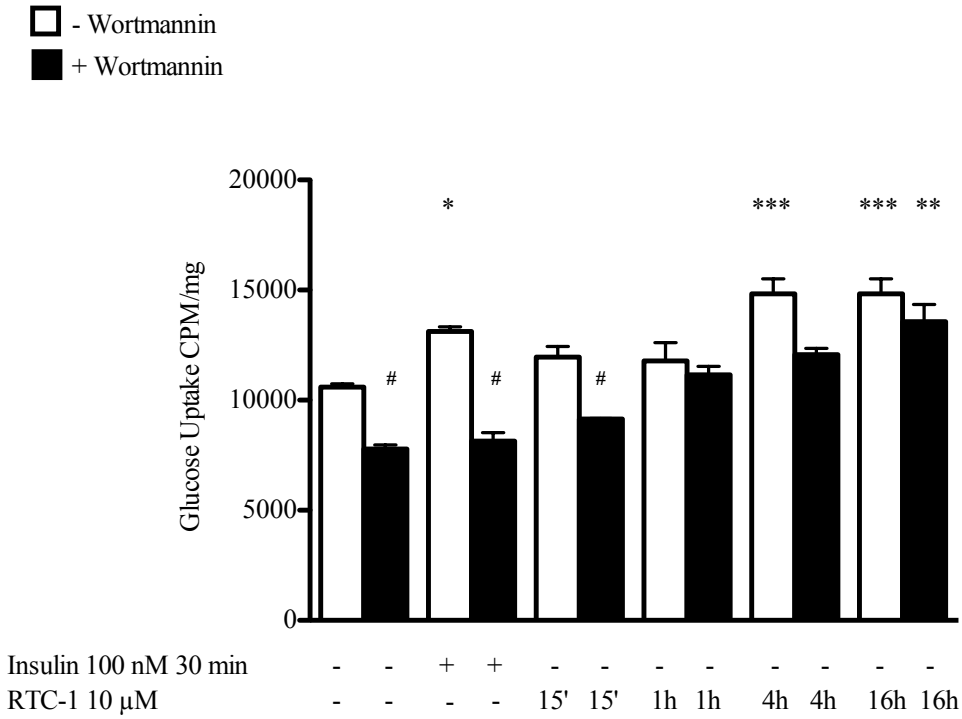

Figure 3.21 The effect of wortmannin on insulin- and RTC-1-induced glucose uptake.

C2C12 myotubes were treated with 1 µM wortmannin or an equal volume of the vehicle control, DMSO, in complete medium containing 0.1 % (v/v) horse serum for 1 hour. Control cells were incubated with 1 µM wortmannin for 17 hours to represent the effects of long-term exposure. Cells were then stimulated with 100 nM insulin for 30 minutes or 10 µM RTC-1 for 15 minutes up to 16 hours. Glucose uptake was measured via scintillation counting of cellular [^{3}H]-2-deoxyglucose. Data presented as mean ± SEM are representative of at least three experiments performed in triplicate each time. One-way ANOVA with a post-hoc Dunnett test using GraphPad Prism® 5 software demonstrates a significant increase in glucose uptake at $p < 0.05$; * $p < 0.01$; ** and $p < 0.001$; ***. A significant decrease in glucose uptake at $p < 0.05$ is indicated by $^{\#}$.

3.3.8 RTC-1 Does Not Directly Influence PI3K, the Major Regulator of Akt Activity

As PI3K lies directly upstream of Akt, the effect of the compounds on this regulator of Akt activation was evaluated. Using a PI3K ELISA, in which the capture protein, GRP-1, binds PIP_3 generated as part of the kinase reaction or the biotinylated-PIP_3 tracer, wherein a lower signal was indicative of increased PI3K activity. Wortmannin (1 μM), used as a control, diminished PI3K activity with p110α, p110δ and p120γ. However, RTC-1 (10 μM), RTC-15 (10 μM) and metformin (500 μM) did not alter PI3K activity with the four class I PI3Ks, p110α, p110β, p110δ and p120γ (Fig. 3.22).

As basal kinase activity appeared low in this assay, the direct effect of the compounds on PIP_3 production was next examined. Lipids were extracted from C2C12 myotubes stimulated with 1 μM wortmannin, 100 nM insulin, 10 μM RTC-1, 10 μM RTC-15 or 500 μM metformin and cellular PIP_3 abundance was determined using a HTRF PIP_3 assay. No change was detected upon exposure to RTC-1, RTC-15 or metformin. Insulin provoked an increase in PIP_3, while wortmannin significantly reduced cellular PIP_3 concentration (Fig. 3.23).

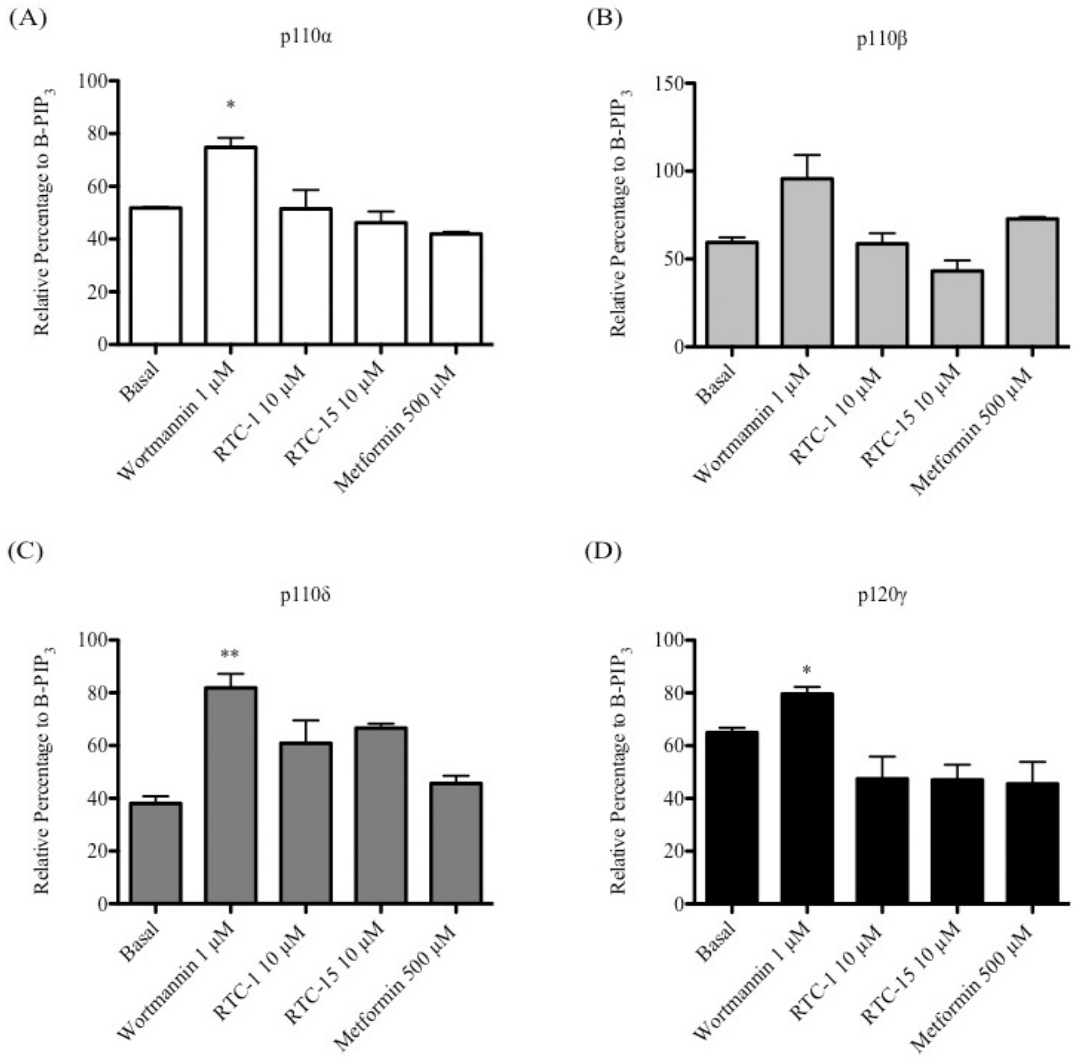

Figure 3.22 The effect of RTC-1, RTC-15 and metformin on PI3K activity.

Each kinase isoform (A) p110α, (B) p110β, (C) p110δ and (D) p120γ was incubated with each compound (1 μM wortmannin, 10 μM RTC-1, 10 μM RTC-15, 500 μM metformin) for 10 minutes at room temperature then processed according to PI3K ELISA (Merck Millipore, 17-493). Data are presented as mean ± SEM, n=4. One-way ANOVA with a post-hoc Dunnett test using GraphPad Prism® 5 software denotes significance at $p < 0.05$; *, with an increase in relative percentage to biotinylated-PIP_3 (B-PIP_3) characteristic of reduced kinase activity.

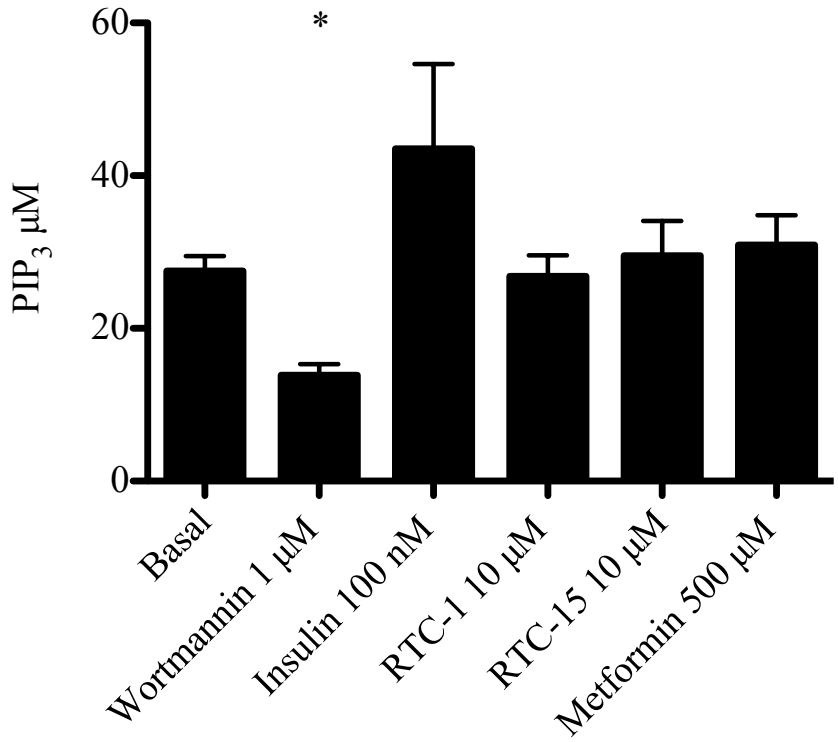

Figure 3.23 The effect of RTC-1, RTC-15 and metformin on PIP_3 production.

C2C12 myotubes were incubated with 1 µM wortmannin, 100 nM insulin, 10 µM RTC-1, 10 µM RTC-15 or 500 µM metformin for 1 hour. Lipids were extracted and cellular PIP_3 abundance was determined using a HTRF PIP_3 assay (Merck Millipore, 17-495). Data are presented as mean ± SEM, n=4. One-way ANOVA with a post-hoc Dunnett test using GraphPad Prism® 5 software denotes significance at $p < 0.05$; *.

3.3.9 RTC-1 Prevents TNF-α-Induced Insulin Resistance in C2C12 Muscle Cells

The powerful anti-diabetic effects of RTC-1 *in vivo* prompted exploration into the bearing this compound may have on an *in vitro* model of insulin resistance. Treatment of C2C12 myotubes with 40 ng/ml TNF-α prevented insulin-induced glucose uptake, a response that could be attenuated with the addition of 10 μM RTC-1 (Fig. 3.24A). 500 μM metformin improved glucose uptake following a 2 hour exposure to TNF-α, although not to the same extent as RTC-1 (Fig. 3.24B).

In parallel with this, TNF-α prevented insulin-induced phosphorylation of IRS1, Akt and AS160 at Thr^{642} and Ser^{588}, all of which were counteracted by the addition of 10 μM RTC-1 (Fig. 3.25A). Although the response of the insulin signalling pathway to TNF-α was modest, the effect of metformin on this system appeared weak, echoing the outcome of the glucose uptake assay (Fig. 3.25B).

As TNF-α is known to provoke the inhibition of insulin signalling through the action of JNK, the influence of the compounds on the phosphorylation of JNK and the other MAPKs was assessed. RTC-1 did not impede TNF-α-induced phosphorylation of JNK, Erk or p38 (Fig. 3.26A). In contrast, metformin counteracted the influence of TNF-α on the three MAPKs investigated (Fig. 3.26B).

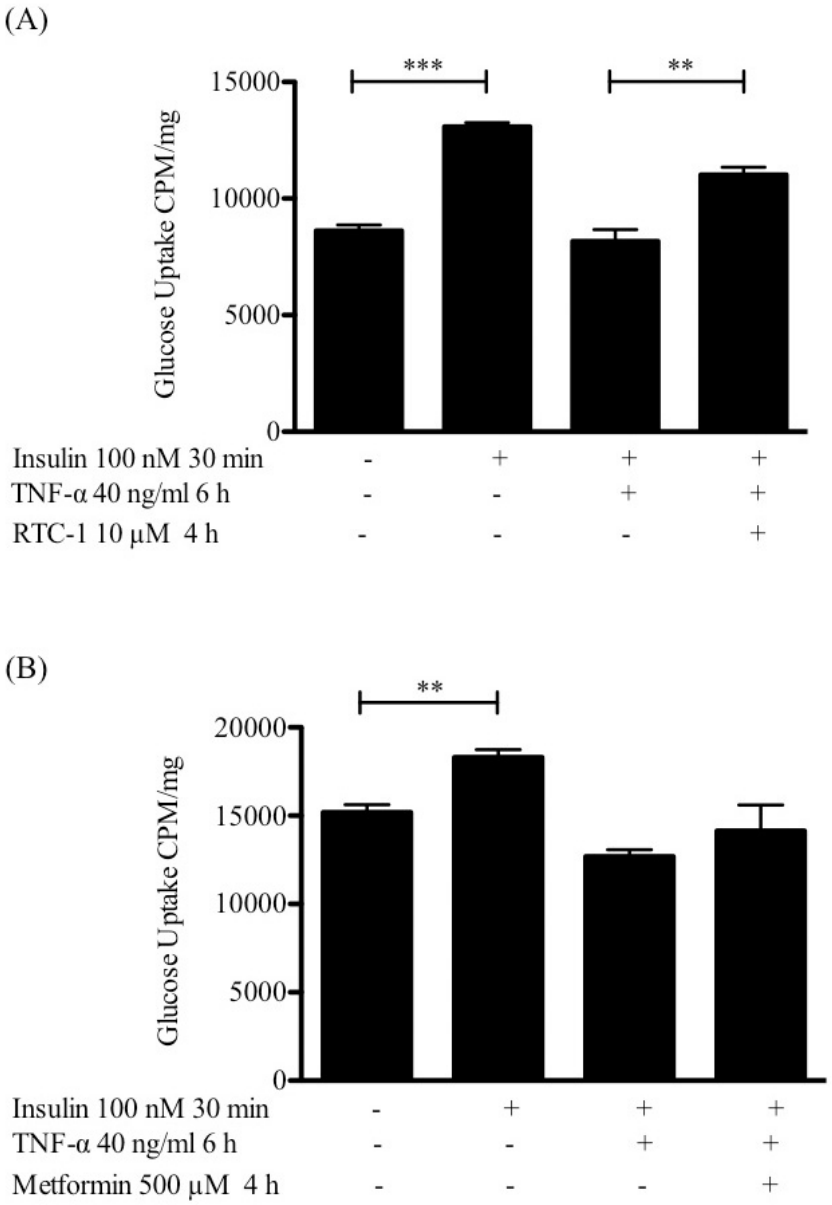

Figure 3.24 Glucose uptake analysis of the effect of RTC-1 and metformin on TNF-α-induced insulin resistance.

C2C12 myotubes were incubated with 40 ng/ml TNF-α for 2 hours in complete medium supplemented with 0.1 % (v/v) horse serum ± (A) 10 µM RTC-1 or (B) 500 µM metformin for a further 4 hours. Cells were then stimulated with 100 nM insulin for a final 30 minutes. Changes to glucose uptake were evaluated by measuring cellular [^{3}H]-2-deoxyglucose content. Data presented as mean ± SEM are representative of at least three experiments performed in triplicate. Using the unpaired Student's *t*-test GraphPad Prism® 5 software demonstrates a significant increase in glucose uptake at $p < 0.01$; ** and $p < 0.001$; ***.

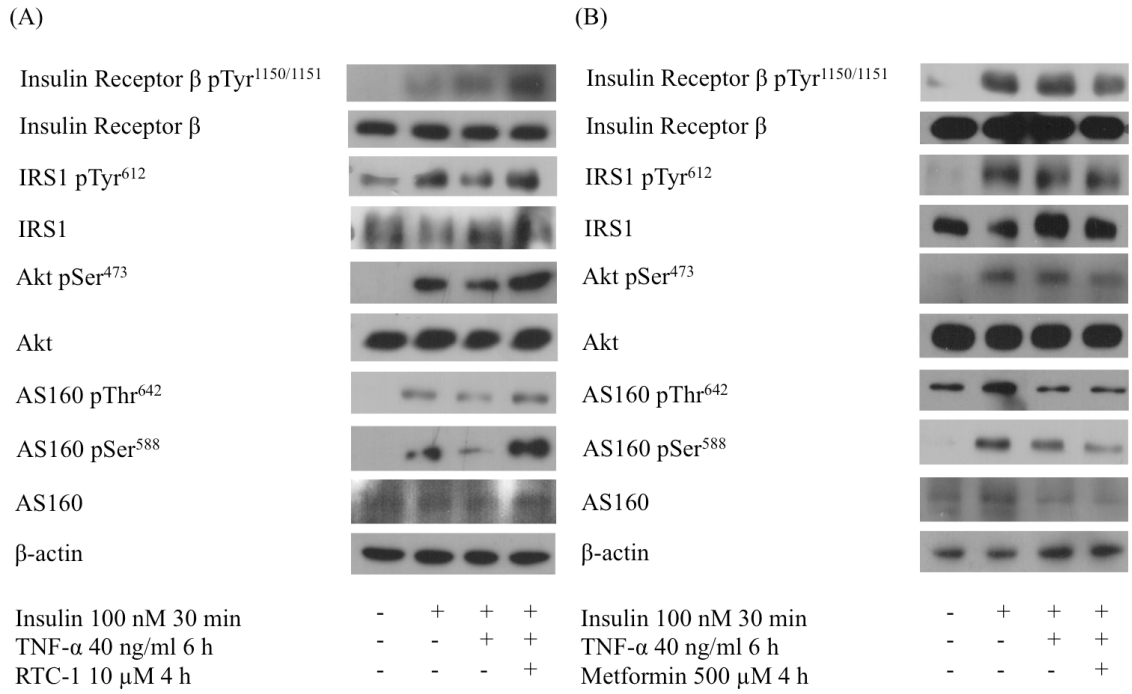

Figure 3.25 Western blot analysis of the effect of RTC-1 and metformin on TNF-α-induced insulin resistance.

C2C12 myotubes were incubated with 40 ng/ml TNF-α for 2 hours in complete medium supplemented with 0.1 % (v/v) horse serum ± (A) 10 μM RTC-1 or (B) 500 μM metformin for a further 4 hours. Cells were then stimulated with 100 nM insulin for a final 30 minutes. Cells were lysed, subjected to SDS-PAGE and immunoblotted with antibodies against phospho-insulin receptor β $Tyr^{1150/1151}$, phospho-IRS1 Tyr^{612}, phospho-Akt Ser^{473}, phospho-AS160 Thr^{642} and Ser^{588}, native insulin receptor β, IRS1, Akt and AS160. β-actin was used as a loading control. Data are representative of two independent experiments.

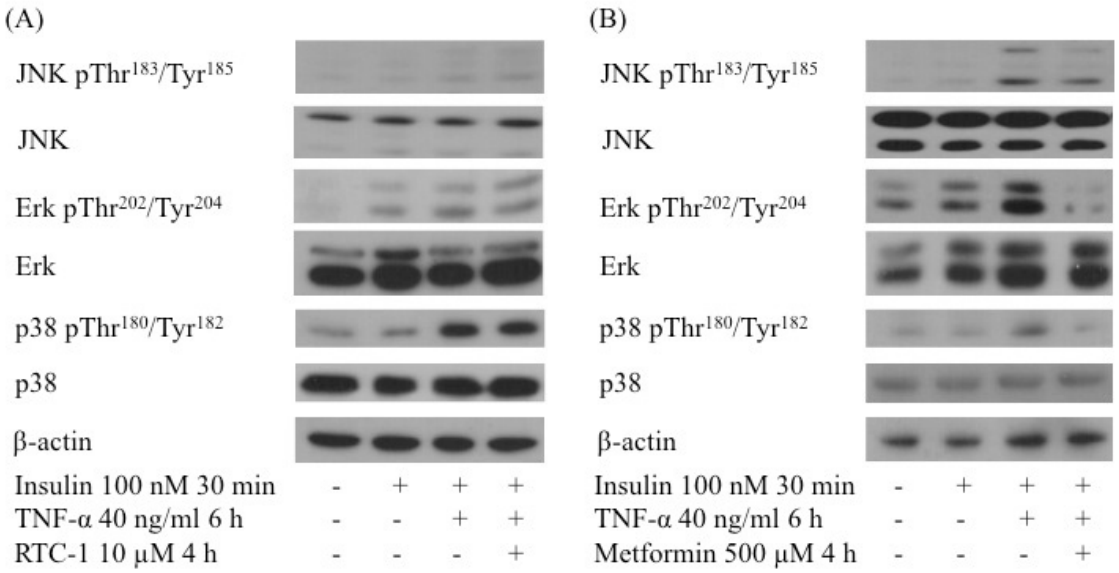

Figure 3.26 The effect of RTC-1, metformin and TNF-α on the phosphorylation of the MAPKs.

C2C12 myotubes were incubated with 40 ng/ml TNF-α for 2 hours in complete medium supplemented with 0.1 % (v/v) horse serum ± (A) 10 μM RTC-1 or (B) 500 μM metformin for a further 4 hours. Cells were then stimulated with 100 nM insulin for a final 30 minutes. Cells were lysed, subjected to SDS-PAGE and immunoblotted with antibodies against phospho-JNK Thr^{183}/Tyr^{185}, phospho-Erk Thr^{202}/Tyr^{204}, phospho-p38 Thr^{180}/Tyr^{182}, native JNK, Erk and p38. β-actin was used as a loading control. Data are representative of two independent experiments.

3.3.10 RTC-1 Compliments the Action of Insulin

In an effort to elucidate the mechanism by which RTC-1 ameliorated insulin-induced glucose transport in the presence of TNF-α, the effect of the compound on insulin-stimulated glucose uptake alone was evaluated. Both insulin and RTC-1 produced a marked increase in glucose uptake in C2C12 muscle cells. The combination of RTC-1 and insulin surpassed the response to these molecules alone (Fig. 3.27).

To determine if RTC-1 was demonstrating insulin sensitising properties, the impact of the compound on insulin-induced phosphorylation of the insulin signalling pathway was examined. As expected, insulin stimulation alone amplified the phosphorylation of the insulin receptor, IRS1, Akt and AS160 in C2C12 myotubes. There was no indication of RTC-1 altering the phosphorylation status of the insulin receptor, IRS1 or Akt in cells incubated with the compound alone. However, RTC-1 augmented AS160 phosphorylation at Thr^{642} and at Ser^{588}, presumably via AMPK activation at this later time point. In cells stimulated with RTC-1 followed by insulin, no significant change was seen in the phosphorylation of the insulin receptor or IRS1 when compared to the action of insulin. However, an increase in the phosphorylation of Akt and of AS160 at Thr^{642} and at Ser^{588}, beyond that of insulin stimulation alone, was seen following treatment with RTC-1 and insulin (Fig. 3.28).

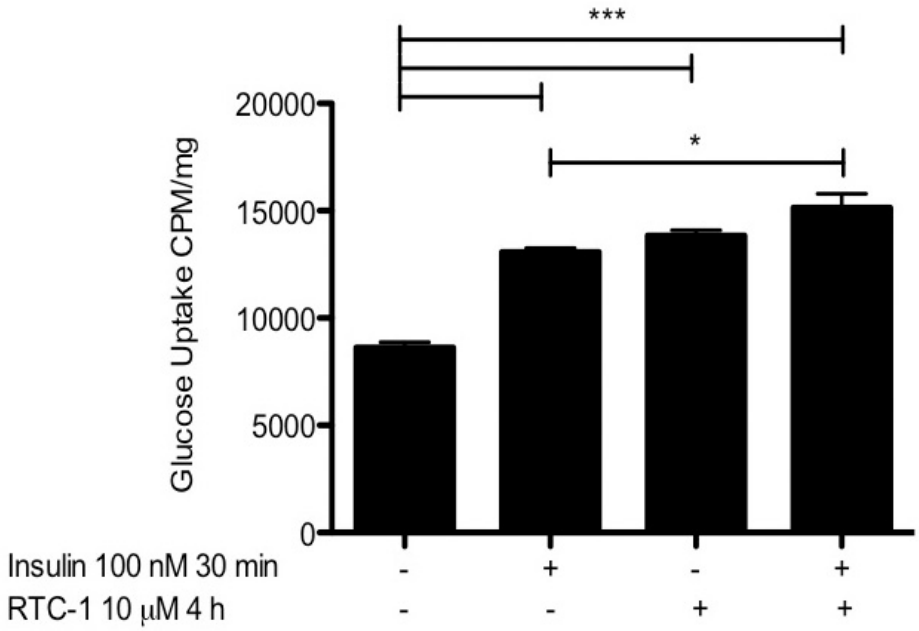

Figure 3.27 The effect of RTC-1 on insulin-induced glucose uptake.

C2C12 myotubes were stimulated with 10 μM RTC-1 for 4 hours in complete medium containing 0.1 % (v/v) horse serum, cells were then incubated with KRBG ± 100 nM insulin for 30 minutes. Changes to glucose uptake were established by measuring the cellular levels of [^{3}H]-2-deoxyglucose. Data are representative of two independent experiments presented as mean ± SEM. One-way ANOVA with a post-hoc Tukey test using GraphPad Prism® 5 software indicates a significant increase in glucose uptake at $p < 0.05$; * and $p < 0.001$; ***.

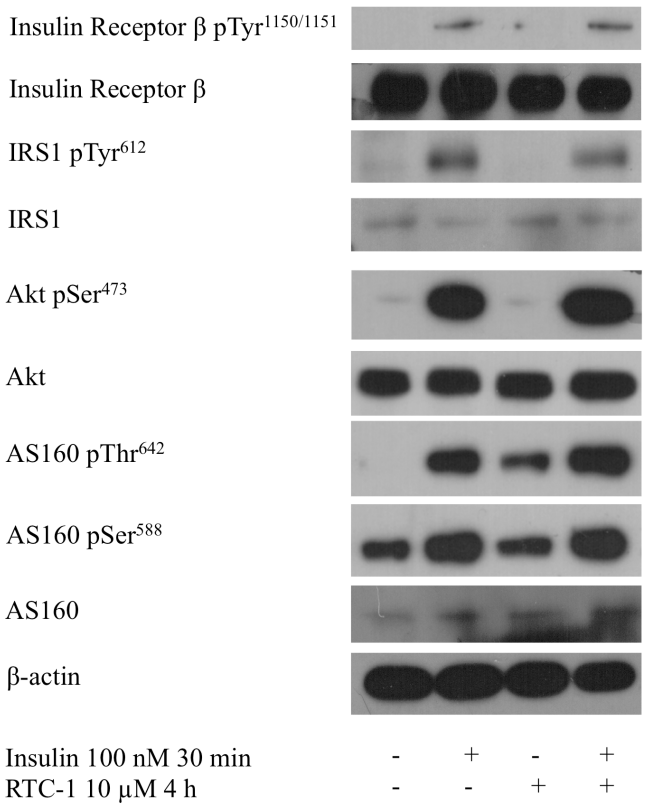

Figure 3.28 The effect of RTC-1 on insulin-induced phosphorylation of the insulin signalling pathway.

C2C12 myotubes were stimulated with 10 μM RTC-1 for 4 hours in complete medium containing 0.1 % (v/v) horse serum, cells were then incubated with KRBG ± 100 nM insulin for 30 minutes. Following this, cells were lysed, proteins separated by SDS-PAGE and immunoblotted with antibodies against phospho-insulin receptor β $Tyr^{1150/1151}$, phospho-IRS1 Tyr^{612}, phospho-Akt Ser^{473}, phospho-AS160 Thr^{642} and Ser^{588}, native insulin receptor β, IRS1, Akt and AS160. β-actin was used as a loading control. Data are representative of two independent experiments.

3.3.11 RTC-1 Prevents Adipogenesis

As RTC-1-treated mice exhibited a reduction in weight gain, the influence of the compound on the process of adipogenesis was examined *in vitro* to further explore this effect. In the 3T3L-1 preadipocyte cell line induction medium caused extensive morphological changes resulting in the accumulation of intracellular lipid droplets. Using Oil Red O as an aid to visualisation, RTC-1 was seen to potently inhibit the process of adipogenesis when added at the time of induction (Fig. 3.29A). Conversely, metformin demonstrated little effect on adipogenesis, which the quantification of the Oil Red O stain revealed to be insignificant (Fig. 3.29B). Western blot analysis was then employed to determine if AMPK played an influential role in this observation through the action of ACC, as inhibition of this regulator of fatty acid synthesis, which can be achieved through AMPK-induced phosphorylation, has been found to inhibit adipogenesis (Cordonier *et al.,* 2015). Incubation of 3T3-L1 cells with RTC-1 for the duration of the differentiation process augmented AMPKα and ACC phosphorylation. A moderate increase in the phosphorylation of AMPKα and a considerable increase in ACC phosphorylation was observed in cells stimulated with metformin (Fig. 3.30).

The influence of the compounds on fully differentiated 3T3-L1 adipocytes was then investigated. Both RTC-1 and metformin instigated a slight decrease in lipid accumulation as visualised by Oil Red O staining (Fig. 3.31A). However, quantification of the stain revealed no significant change in lipid content in response to the compounds when compared to the vehicle control, DMSO (Fig. 3.32B). At the protein level, the phosphorylation status of AMPKα and ACC, were marginally increased in response to RTC-1 and metformin when compared to differentiated 3T3-L1 adipocytes incubated with DMSO (Fig. 3.33).

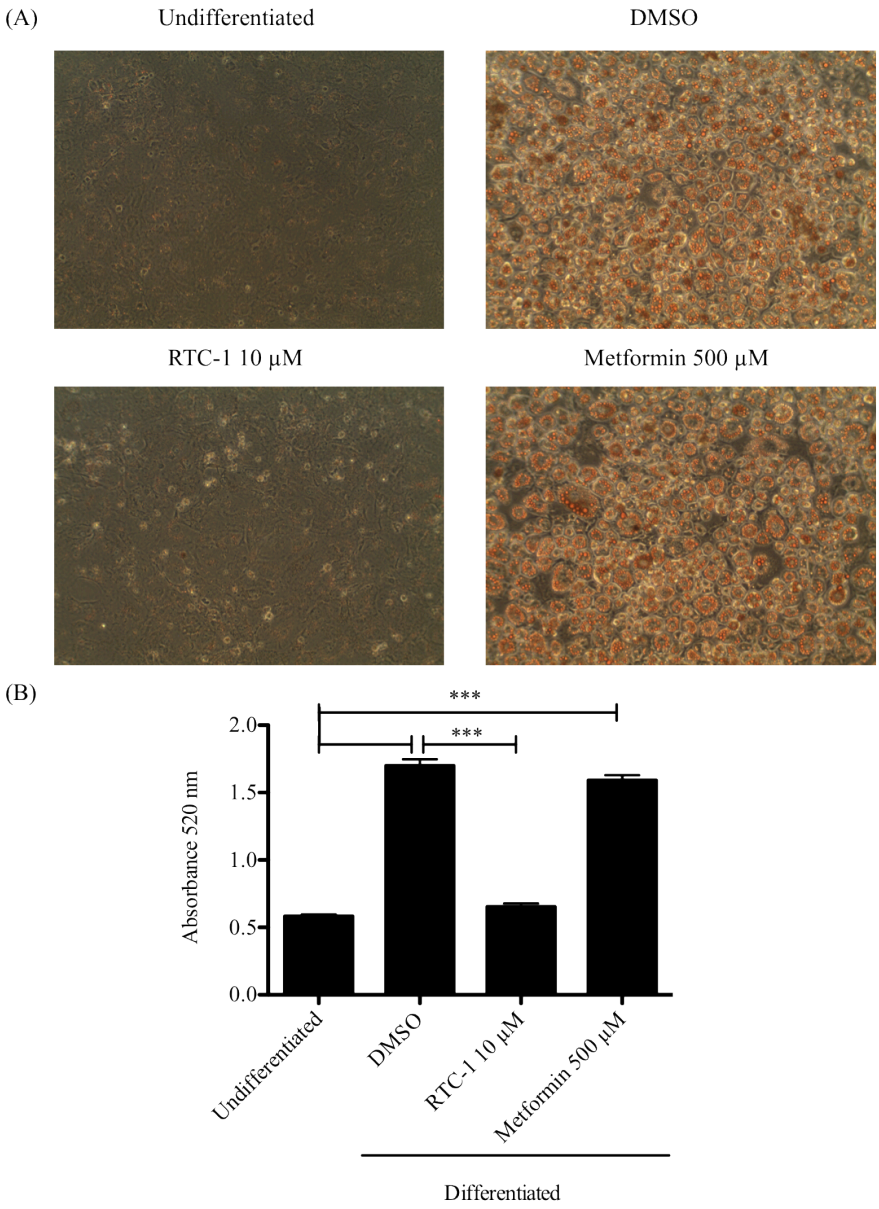

Figure 3.29 Visual analysis of the effect of RTC-1 and metformin on 3T3-L1 adipocyte differentiation.

3T3-L1 preadipocytes were cultured in control medium or adipogenic medium in the presence or absence of 10 µM RTC-1 or 500 µM metformin. Medium was changed every 48 hours. (A) Lipid accumulation was visualised after day 8 of differentiation by Oil Red O staining. Images are representative of two independent experiments. Cells were visualised with a x100 magnification. (B) Total lipid content was quantified by eluting the Oil Red O stain with isopropanol and measuring absorbance at 520 nm. One-way ANOVA with a post-hoc Tukey test using GraphPad Prism® 5 software denotes significance at $p < 0.001$; ***.

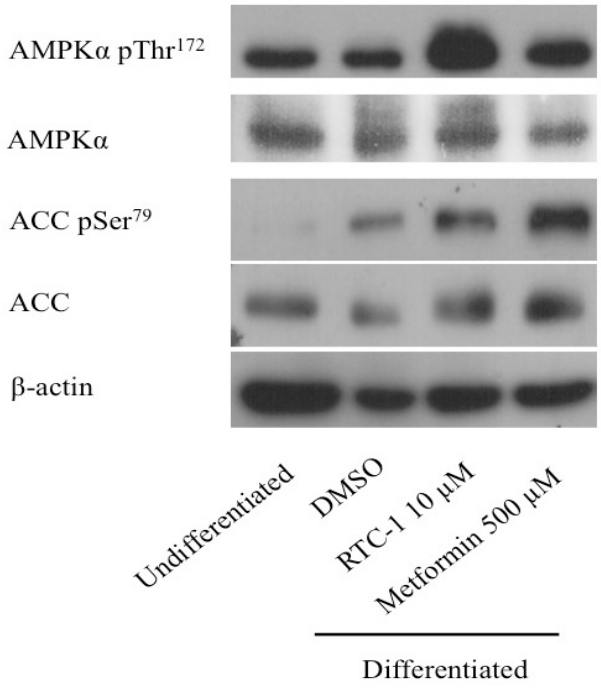

Figure 3.30 The effect of RTC-1 and metformin on AMPKα and ACC phosphorylation in 3T3-L1 adipocytes.

3T3-L1 preadipocytes were cultured in control medium or adipogenic medium in the presence or absence of 10 μM RTC-1 or 500 μM metformin. Medium was changed every 48 hours. On day 8, cells were lysed, subjected to SDS-PAGE and immunoblotted with antibodies against phospho-AMPKα Thr^{172}, phospho-ACC Ser^{79} and native AMPKα and ACC. β-actin was used as a loading control. Data are representative of two independent experiments.

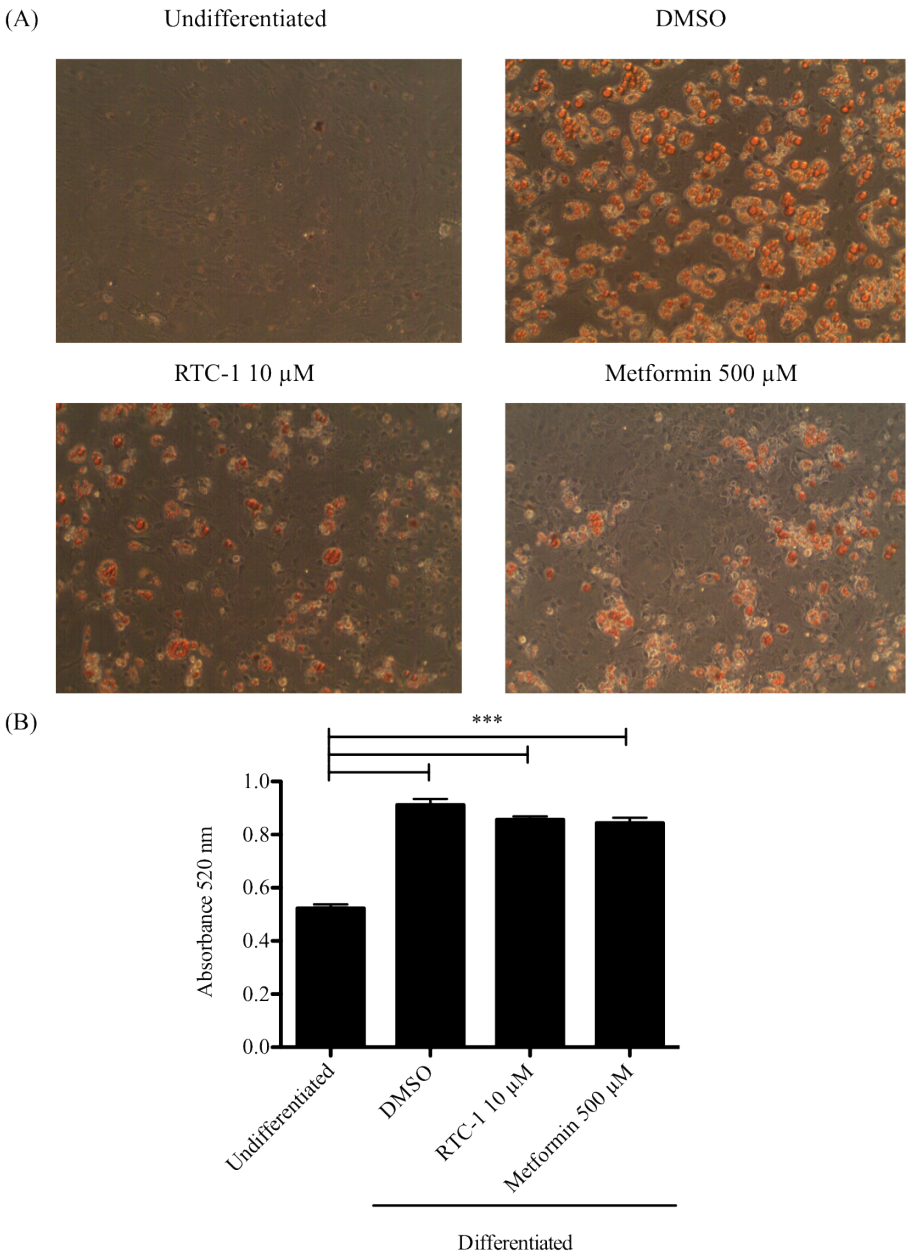

Figure 3.31 Visual analysis of the effect of RTC-1 and metformin on fully differentiated 3T3-L1 adipocytes.

Fully differentiated adipocytes were stimulated with 10 µM RTC-1 or 500 µM metformin. Medium was changed every 48 hours. (A) Lipid accumulation was visualised microscopically with a x100 magnification using an Oil Red O stain. Images are representative of two independent experiments. (B) Total lipid content was quantified by eluting the Oil Red O stain with isopropanol and measuring absorbance at 520 nm. One-way ANOVA with a post-hoc Tukey test using GraphPad Prism® 5 software denotes significance at $p < 0.001$; ***.

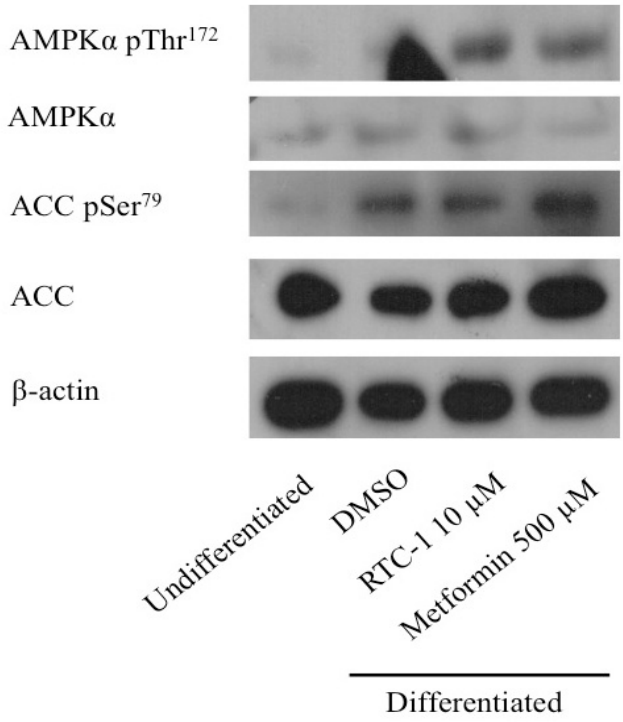

Figure 3.32 The effect of RTC-1 and metformin on AMPKα and ACC phosphorylation in fully differentiated 3T3-L1 adipocytes.

3T3-L1 preadipocytes were cultured in control medium or adipogenic medium. Fully differentiated adipocytes were stimulated with 10 μM RTC-1 or 500 μM metformin, with fresh medium added every 48 hours. On day 8, cells were lysed, subjected to SDS-PAGE and immunoblotted with antibodies against phospho-AMPKα Thr^{172}, phospho-ACC Ser^{79} and native AMPKα and ACC. β-actin was used as a loading control. Data are representative of two independent experiments.

To determine if this response translated into other cell types, murine MSC, which readily differentiate into fat cells given the appropriate conditions, were incubated with RTC-1 or metformin throughout the differentiation process. MSC incubated with adipogenic medium containing DMSO underwent morphogenesis with the formation of large intracellular lipid droplets. RTC-1 reduced the capacity of MSC to differentiate into adipocytes, while cells incubated with metformin exhibited intracellular lipid droplets similar to the control (Fig. 3.33A). Quantification of the stain demonstrated the significant influence of the adipogenic medium on MSC differentiation, an effect that RTC-1 markedly reduced, metformin however, demonstrated less force (Fig. 3.33B). Analysis of the AMPK pathway revealed that 10 μM RTC-1 impacted on the phosphorylation of both AMPKα and ACC substantially, while 500 μM metformin exhibited little effect (Fig. 3.34).

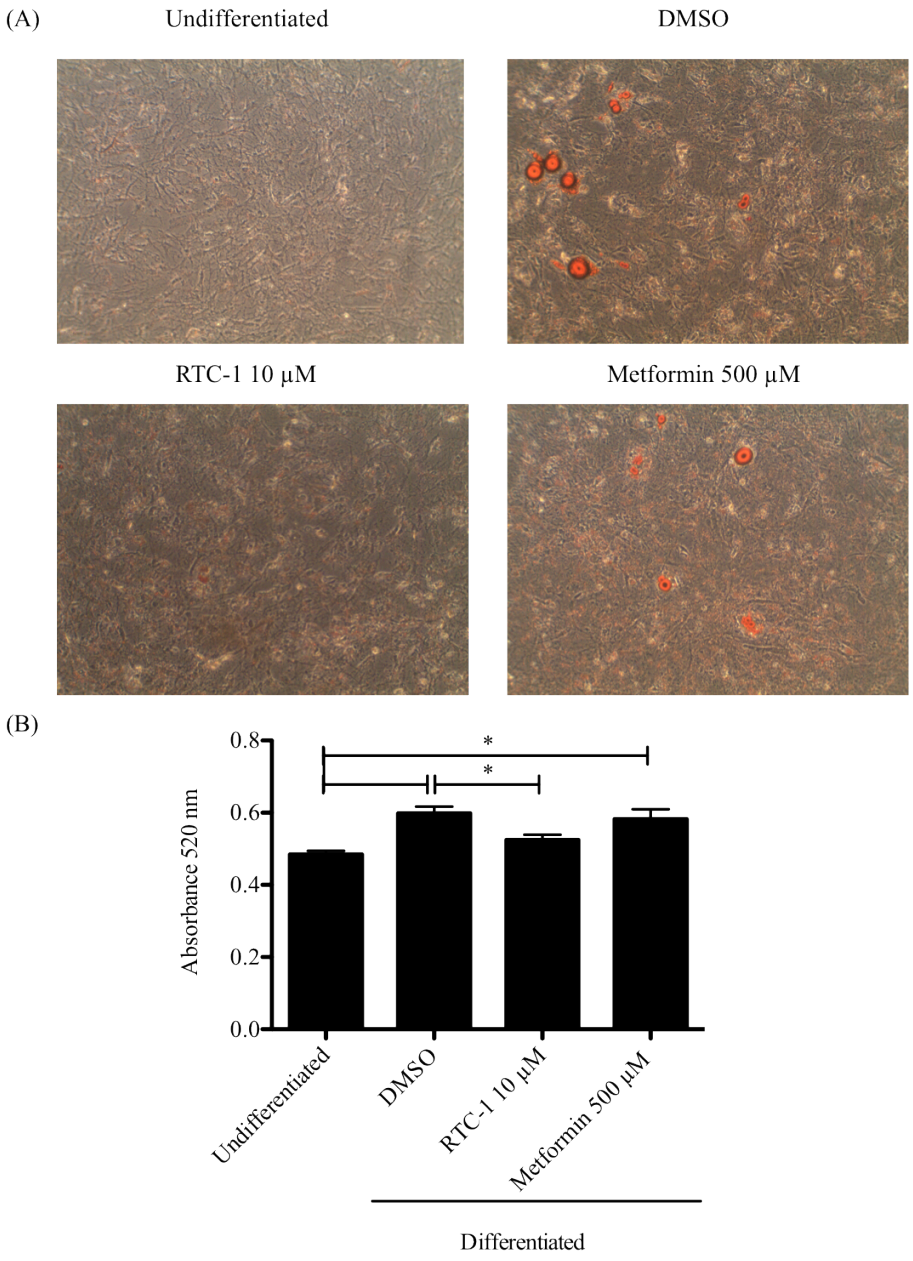

Figure 3.33 Visual analysis of the effect of RTC-1 and metformin on murine MSC adipogenesis.

MSC isolated from the femur and tibia of 6 – 8 week old female BALB/c mice were cultured in control medium or adipogenic medium in the presence or absence or 10 µM RTC-1 or 500 µM metformin for 21 days. (A) Lipid accumulation was visualised microscopically with a x100 magnification using an Oil Red O stain. Images are representative of three independent experiments. (B) Total lipid content was quantified as described in Section 2.2.1.2. One-way ANOVA with a post-hoc Tukey test using GraphPad Prism® 5 software denotes significance at $p < 0.05$; *.

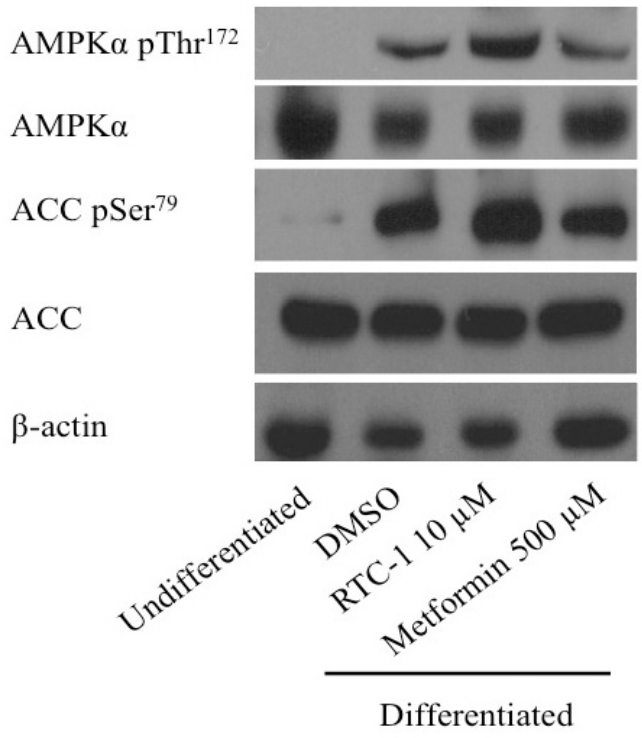

Figure 3.34 The effect of RTC-1 and metformin on AMPKα and ACC phosphorylation in murine MSC during adipogenesis.

Murine MSC were cultured in control medium or adipogenic medium in the presence or absence or 10 μM RTC-1 or 500 μM metformin for 21 days. Cells were lysed, subjected to SDS-PAGE and immunoblotted with antibodies against phospho-AMPKα Thr^{172}, phospho-ACC Ser^{79} and native AMPKα and ACC. β-actin was used as a loading control. Data are representative of two independent experiments.

3.3.12 RTC-1 Augments MSC Osteogenesis

To ensure RTC-1 did not negatively alter other lineages of cellular differentiation the effect of the compound on MSC bone differentiation was also examined. Visualisation of Alizarin Red S demonstrated the modest response of MSC to the process of osteoblast differentiation when compared to undifferentiated cells (Fig. 3.35A). However, quantification of the stain revealed a significant increase in mineralisation in cells incubated with the osteogenic medium (Fig. 3.35B). While metformin appeared to marginally increase the process of differentiation, cells incubated with RTC-1 assumed the osteogenic morphology more readily, which quantification of the stain revealed to be significant. As the activation of AMPK is known to positively regulate osteoblast mineralisation (Kanazawa *et al.,* 2009), the role of RTC-1 and metformin in augmenting the phosphorylation of this effector protein was investigated. Differentiated control cells displayed increased phosphorylation of AMPKα when compared to undifferentiated cells, while cells stimulated with metformin marginally improved the level of activity, RTC-1 was found to augment this response considerably (Fig. 3.36).

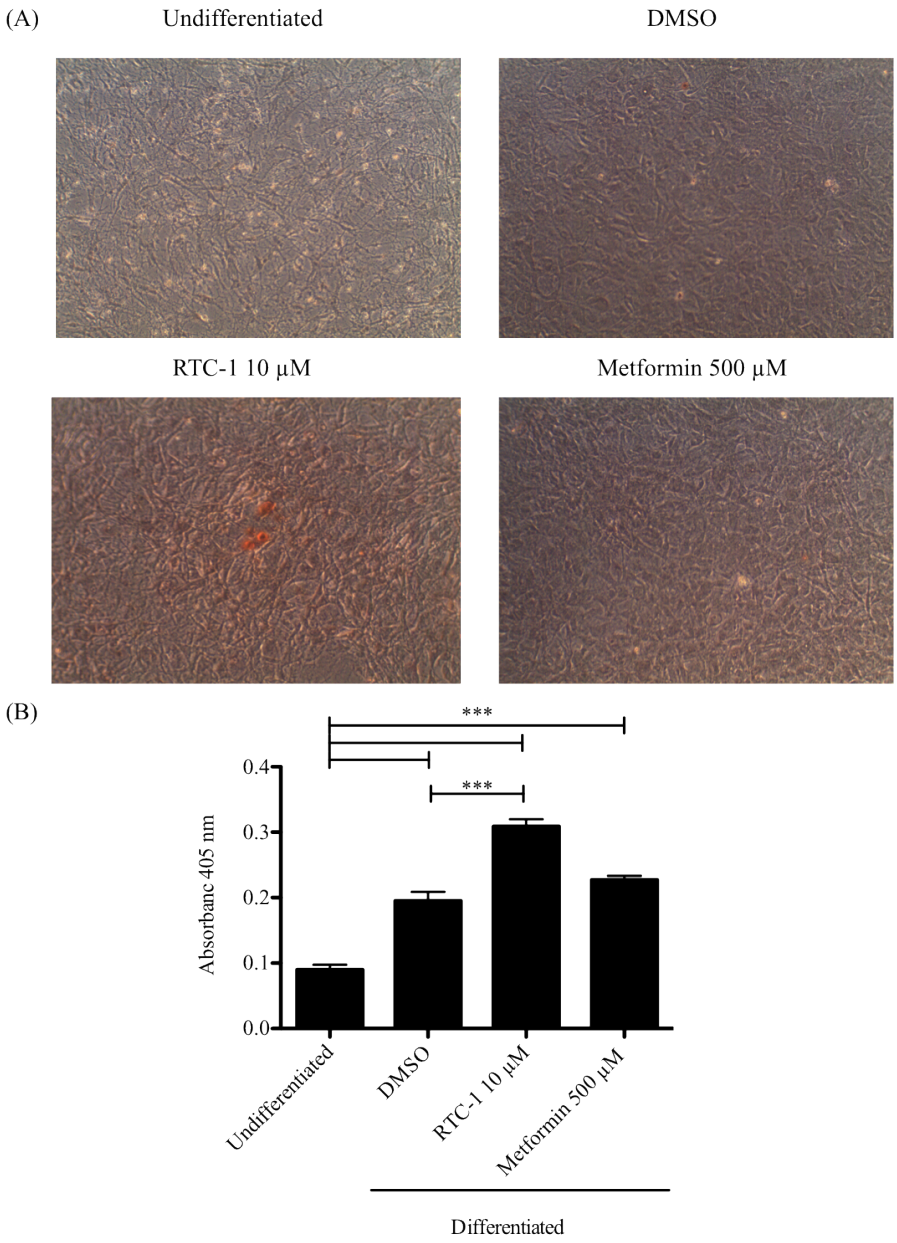

Figure 3.35 Visual analysis of the effect of RTC-1 and metformin on murine MSC osteogenesis.

Murine MSC were cultured in control medium or osteogenic medium in the presence or absence or 10 µM RTC-1 or 500 µM metformin for 21 days. (A) Calcium deposition stained with Alizarin Red S was visualised microscopically with a x100 magnification. (B) Total mineral deposition was quantified as described in Section 2.2.1.3. One-way ANOVA with a post-hoc Tukey test using GraphPad Prism® 5 software denotes significance at $p < 0.001$; ***, n=3.

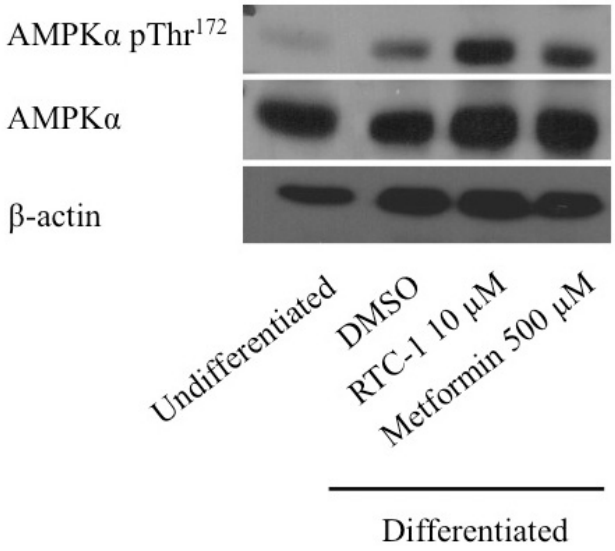

Figure 3.36 The effect of RTC-1 and metformin on AMPKα phosphorylation in murine MSC during osteogenesis.

Murine MSC were cultured in control medium or osteogenic medium in the presence or absence or 10 μM RTC-1 or 500 μM metformin for 21 days. Cells were lysed, subjected to SDS-PAGE and immunoblotted with antibodies against phospho-AMPKα Thr^{172} and native AMPKα. β-actin was used as a loading control. Data are representative of three independent experiments.

3.4 Discussion

This study has delved into the underlying mechanism by which RTC-1 restored normal glucose disposal, augmented insulin sensitivity and prevented weight gain in a murine diet-induced model of type 2 diabetes. The structure of this novel compound has been demonstrated to be central to its activity as a derivative of RTC-1, RTC-15, produced similar results to the parent compound *in vitro.* Comparing the action of this novel compound to that of metformin, RTC-1 demonstrated very superior effects in amending some of the many *in vitro* representations of the pathophysiology of type 2 diabetes.

3.4.1 Consequences of RTC-1-Induced Inhibition of NADH: ubiquinone oxidoreductase Activity

Both RTC-1 and RTC-15 have been found to inhibit NADH:ubiquinone oxidoreductase activity with respective IC_{50} values of 27 μM and 104 μM. Although metformin is believed to directly stimulate glucose uptake through AMPK, activated by the inhibition of NADH:ubiquinone oxidoreductase (Owen *et al.,* 2000), it failed to significantly alter NADH:ubiquinone oxidoreductase activity at the concentrations assayed. Studies carried out by Jenkins and colleagues (2013), found metformin to be a weak inhibitor of NADH:ubiquinone oxidoreductase, with an IC_{50} of 27 mM. In line with this finding, Bridges and colleagues (2014), observed metformin to be the weakest of the five pharmacologically relevant biguanides in attenuating complex I catalysis, demonstrating an IC_{50} of 19.4 ± 1.4 mM in bovine heart mitochondria, 22.6 ± 4.3 mM in *Pichia pastoris* mitochondria and 60.7 ± 8.5 mM in the mitochondria of *E. coli.* As these predicted IC_{50} values exceed the maximal soluble concentration possible in the assay employed in this study, it is unsurprising that metformin did not appear to perturb NADH:ubiquinone oxidoreductase activity.

The action of RTC-1 appears to be restricted to NADH:ubiquinone oxidoreductase as oxidative phosphorylation could be restored with the addition of succinate, the complex II substrate. This has also been observed to be true of metformin (Hinke *et al.,* 2007, Wheaton *et al.,* 2014). These compounds, incapable of uncoupling the energy harnessing process of mitochondria outright, appear to cause little detrimental damage to the cell. Nonetheless, any potential resultant transient decrease in cellular ATP and rise in cellular ADP and AMP could provoke the activation of AMPK.

RTC-1 and RTC-15 stimulate the phosphorylation of AMPKα, and its downstream effector proteins, AS160 and ACC in a more pronounced manner to metformin despite the 50-fold higher dose of the common anti-diabetic therapy, echoing the previous finding in terms of drug potency. The enhanced influence of RTC-1 and RTC-15 resonates through to their impact on glucose transport, with RTC-1 demonstrating signs of longevity as glucose uptake is elevated for some time after cells have been washed free of the compound. This may be due in part to the lipophilic properties of RTC-1, which also reflects its ability to provoke these effects at relatively low concentrations. As patients often demonstrate poor adherence to the multitude of daily doses required of metformin to effectively regulate glycaemic control (Donnan *et al.,* 2002, García-Pérez *et al.,* 2013)**,** the enhanced potency of RTC-1 should promote its use as a more manageable therapeutic regime, particularly when its low toxicity profile is also considered.

3.4.2 RTC-1-Induced Activation of Akt

Along with being almost 1,000-fold more efficacious than metformin in the inhibition of NADH:ubiquinone oxidoreductase, the enhanced effects of RTC-1 on a direct modulator of glucose uptake, AS160, may also lie with its influence on the activity of

Akt. RTC-1 was found to stimulate the phosphorylation of Akt and of AS160 in a superior manner to metformin, predominantly at Thr^{642}, a critical consensus site in facilitating GLUT4 translocation. As insulin-stimulated phosphorylation of AS160 at Thr^{642} is impaired in patients with type 2 diabetes (Middelbeek *et al.,* 2013), the multifaceted action of RTC-1 through Akt strengthens its potential as a promising anti-diabetic therapy. However, the direct role RTC-1 plays in the augmenting the phosphorylation of Akt remains obscure as this novel compound and its derivative demonstrated no impact on the major upstream regulator of Akt, PI3K. It is therefore likely the RTC compounds influence another aspect of Akt activation.

Although most modulators of Akt activity rely on PI3K dependent relocalisation of Akt to the plasma membrane via the PH domain (Toker and Marmiroli, 2014), diphosphoinositol pentakisphosphate (IP_7), synthesised by a family of three inositol hexaphosphate kinases (IP6Ks) (Stephens *et al.,* 1993), has recently emerged as an Akt regulator competing with this mechanism (Chakraborty *et al.,* 2010). In *Dictyostelium discoideum*, IP_7 has been shown to compete with PIP_3 at PH domains, preventing PIP_3 signalling (Luo *et al.,* 2003). Prasad and colleagues (2011), specifically demonstrated the ability of IP_7 to compete with PIP_3 at the PH domain of Akt, negatively regulating PIP_3-mediated cellular functions in neutrophils. Furthermore, IP6K1 knockout mice which have depleted IP_7 levels, demonstrate a lean phenotype and have elevated Akt activity in response to insulin stimulation (Chakraborty *et al.,* 2010).

IP6K's have a Km for ATP between 1 and 1.4 mM, making IP_7 synthesis very sensitive to fluctuations in ATP levels (Wunderberg and Mayr, 2012). The effect of the RTC compounds on NADH:ubiquinione oxidoreductase activity and subsequently intracellular ATP levels, may therefore, inhibit the function of IP6K to promote Akt

activation. Although further experimentation would be required to confirm this, it is instructive that the IP6K inhibitor TNP, which decreases IP_7 production to activate Akt, demonstrates similar effects to RTC-1 in that it also increases the phosphorylation of AMPKα and ACC (Sun *et al.,* 2015). While the activation of Akt appears promising to attenuate the symptoms of type 2 diabetes, stimulation of Akt as a therapeutic target must be tightly regulated as hyperactivation of this protein is thought to be involved in the development of many human cancers (Kumar *et al.,* 2013). The role of the RTC compounds is encouraging in this regard as RTC-induced activation of Akt and consequentially AS160, is very short lived and is rapidly replaced by AMPK-dependent activation of AS160 to further promote glucose uptake.

3.4.3 Akt and AMPK-Mediated Signalling

The action of the RTC compounds in stimulating glucose transport appears to be stringently regulated. The initial surge of RTC-1-induced glucose uptake is thought to be dependent on Akt activation, as wortmannin was seen to effectively inhibit glucose uptake after a 15 minute exposure of C2C12 myotubes to RTC-1, while this impact lessened at the later time points. This initial effect on Akt, whether through the inhibition of IP6K or by other means, is quickly attenuated, followed by the activation of AMPK, indicative of a feedback relationship between the two proteins. A reduction in ATP levels, such as that triggered by the inhibition of NADH:ubiquinone oxidoreductase is known to destabilise the phosphorylation state of Akt by exposing phosphorylated sites to phosphatases (Chan *et al.,* 2011, Lin *et al.,* 2012). Furthermore, Akt has been shown to phosphorylate rat AMPK at Ser^{485}, which renders the kinase inactive (Horman *et al.,* 2006). The intricate relationship between Akt and AMPK may be fundamental to the power of the RTC compounds in stimulating glucose uptake. As the initial activity of Akt subsides, so too does that of AS160, only to return under the

influence of AMPK. The latter surge in glucose uptake appears to be dependent on the action of AMPK as it was effectively attenuated with the addition of Compound C.

A proteomics study conducted by Dr. Pamela Young (Young *et al.*, 2016), reinforces the potent downstream effects of the RTC compounds in targeting metabolomic proteins to restore cellular energy balance. Notably, RTC-15 was found to increase the expression of triose phosphate isomerase, a protein that contributes to the process of glycolysis, of Annexin A2, a calcium binding protein involved in the fusion of plasma secretory vesicles, such as those of GLUT4, with the plasma membrane and of ECH1, an auxiliary enzyme of β-oxidation involved in preparing unsaturated fatty acids for fatty acid oxidation.

3.4.4 RTC-1-Induced Effects on Insulin Signalling

To better understand the anti-diabetic properties of RTC-1, the pro-inflammatory cytokine TNF-α was used to mimic an insulin resistant state *in vitro.* TNF-α prevented insulin-induced glucose uptake by increasing the phosphorylation of the MAPKs thus leading to the inhibition of key components of the insulin signalling pathway. Both RTC-1 and metformin overcame the influence of TNF-α, improving glucose uptake; RTC-1 elicited a more efficacious response at a much lower concentration. At the protein level, metformin did not noticeably attenuate the impact of TNF-α on the insulin signalling pathway. However, metformin markedly reduced the phosphorylation of JNK, Erk and p38. The modest impact of metformin on this system may lie with its ability to constrain the phosphorylation of the MAPKs, as small molecule inhibitors of JNK have been found to restore insulin sensitivity in a mouse model of type 2 diabetes (Stebbins *et al.,* 2008). Additionally, metformin has been reported to inhibit the action of the MAPKs (Isoda *et al.,* 2006, Simon-Szabó *et al.,* 2014). However, controversy

remains in this area as Kumar and Dey (2002), found that metformin increased p38 phosphorylation, having no effect on Erk or JNK. Furthermore, Lee and colleagues (2012) observed that metformin positively impacted on the phosphorylation of JNK. As metformin demonstrated little effect in restoring the signalling capabilities of insulin, the influence of metformin on AMPK alone may have led to the moderate increase in glucose uptake in the presence of TNF-α. Given the fact that metformin demonstrates no effect on the insulin signalling pathway in diabetic patients (Kim *et al.,* 2002, Karlsson *et al.,* 2005), nor does it act as an insulin sensitizer in mouse skeletal muscle (Turban *et al.,* 2012), it seems likely that the modest influence of metformin bypasses the insulin signalling pathway.

RTC-1 on the other hand, demonstrated no effect on the MAPKs yet restored insulin-induced glucose uptake in a much more successful and significant manner to metformin. As RTC-1 was found to augment the signalling capabilities of insulin in cells stimulated with TNF-α, the enhanced effect of this compound was postulated to lie in its ability to also act as an insulin sensitizer. Although RTC-1 demonstrated no direct effect on the insulin signalling pathway, in the presence of this compound the action of insulin significantly improved downstream of Akt. However, the longer-lasting potent effects of RTC-1 on AMPK may have given rise to the increase in AS160 phosphorylation which enhanced glucose uptake. Nonetheless, as RTC-1 was observed to restore insulin-induced phosphorylation of IRS1 in the presence of TNF-α, a protein it probably does not directly interact with, an unresolved element of the influence of RTC-1 remains. Analysis of other downstream targets of TNF-α that negatively impact on insulin signalling such as IKKβ and SOCS3, may give further insight into the regulatory effect of RTC-1 on TNF-α-induced insulin resistance. Given that the inhibition of

IP6K1 either through knockout studies or by pharmacological intervention has been suggested to increase insulin sensitivity (Mackenzie and Elliott, 2014), the proposed impact of RTC-1 on this system to regulate Akt activity may explain the apparent insulin sensitising effects of the compound.

3.4.5 The Anti-Adipogenic Effects of RTC-1

As obesity is a major contributor to the genesis of type 2 diabetes, the reduction in weight gain observed in RTC-1 HFD-fed mice warranted further exploration. RTC-1 was found to potently block adipogenesis in 3T3-L1 preadipocytes and murine MSC with a concurrent rise in AMPKα and ACC phosphorylation. Direct pharmacological attenuation of ACC (Levert *et al.,* 2002) or transient inhibition through the phosphorylation of Ser^{79} via AMPK (Ejaz *et al.,* 2009) has been found to attenuate the lipogenic activity of ACC and effectively inhibit adipogenesis. Although a significant decrease in adipogenesis was not observed with the addition of metformin, despite the increase in ACC phosphorylation, several studies have demonstrated the anti-adipogenic abilities of metformin and other AMPK activating molecules (Giri *et al.,* 2006, Ahn *et al.,* 2008, Zhou *et al.,* 2009, Molinuevo *et al.,* 2010, Vingtdeux *et al.,* 2011). RTC-1 and metformin were found to moderately reduce lipid accumulation in fully differentiated 3T3-L1 adipocytes with a modest increase in AMPKα and ACC phosphorylation. This finding correlates with the effects of RTC-1 *in vivo* as the compound prevented HFD-fed mice from gaining weight, yet it did not appear to reduce pre-established adipose tissue.

3.4.6 The Impact of RTC-1 on Osteogenesis

RTC-1-induced phosphorylation of AMPKα positively altered the osteogenic differentiation process of murine MSC. As patients with diabetes often present with

osteoporosis (Krakauer *et al.,* 1995), this result proves particularly meaningful given the fact that administration of the anti-diabetic, roziglitizone, results in significant bone loss (Rzonca *et al.,* 2004). In line with studies of osteoblastic differentiation in MC3T3-E1 cells (Kanazawa *et al.,* 2008) and rat bone marrow progenitor cells (Molinuevo *et al.,* 2010), quantification of Alizarin Red S also demonstrated a modest increase in osteogenesis associated with metformin-induced AMPK activation. Consistent with this, a role for AMPK signalling in skeletal physiology has been demonstrated by Shah and colleagues (2010). Primary rat calvaria osteoblasts cultured in the presence of AMPK activators, AICAR and metformin exhibit a dose-dependent increase in trabecular bone nodule formation, while AMPKα knockout mice demonstrate smaller cortical and trabecular bone compartments when compared to wild type mice. AMPK is believed to influence this process of differentiation by increasing the expression of eNOS and bone morphogenetic protein 2 (Kanazawa *et al.,* 2009), both of which are critical in the regulation of bone mass and bone turnover by modulating osteoblast function (Yamaguchii *et al.,* 2000, Armour *et al.,* 2001).

3.4.7 Summary

This study has established the basis for the anti-diabetic and anti-obesity effects a novel compound exhibited in a dietary-induced murine model of type 2 diabetes (Fig. 3.37). RTC-1-induced inhibition of NADH:ubiquinone oxidoreductase leads to a transient decrease in cellular ATP levels which may reduce IP6K-induced IP_7 production to promote Akt activation and sensitise the cell to the action of insulin. This transient alteration to cellular energy also facilitates the activation of AMPK with a successive decrease in Akt activity and increase in the phosphorylation of AS160 and ACC. The superior impact of RTC-1 on glucose transport, insulin resistance, adipogenesis and osteogenesis when compared to metformin, advocates this novel molecule as a powerful

therapy capable of regulating many facets of the pathophysiology of type 2 diabetes.

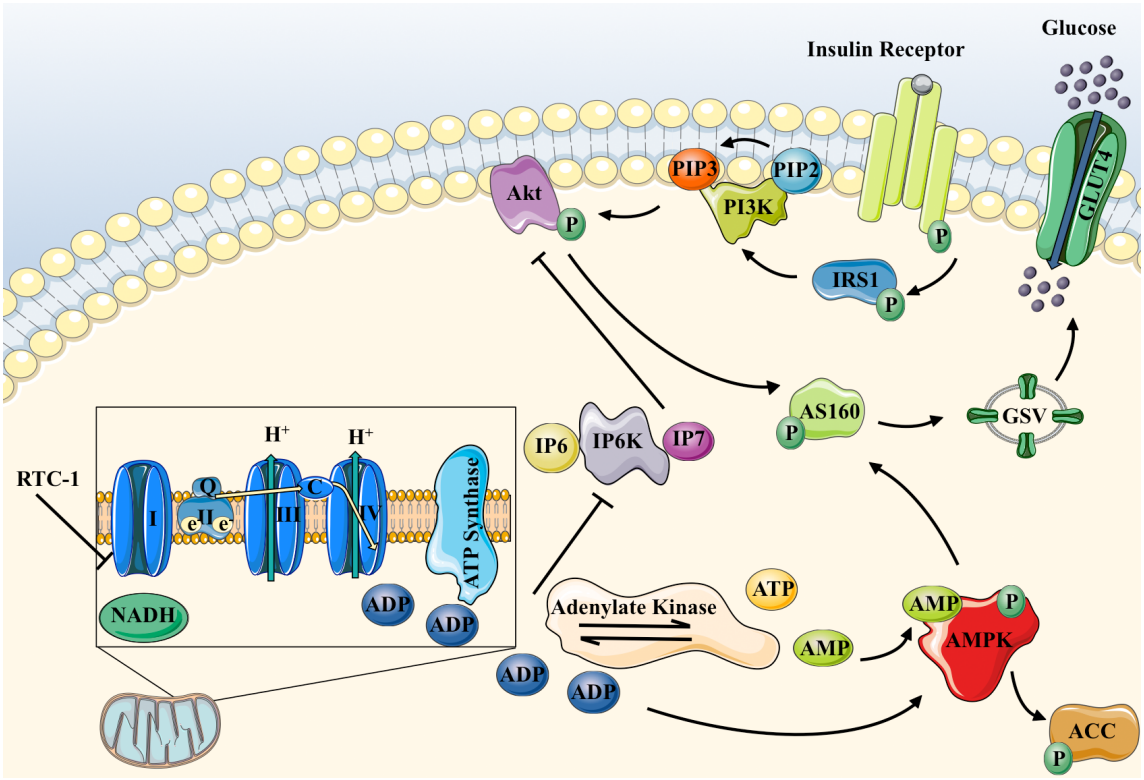

Figure 3.37 Proposed mechanism of action of RTC-1.

RTC-1 inhibits NADH:ubiquinone oxidoreductase activity, transiently decreasing cellular ATP levels. This may prevent IP6K-induced IP_7 synthesis, sensitising the cell to the action of insulin-stimulated PIP_3 production, which can promote glucose transport through Akt. The likely build up of ADP may then be sensed by adenylate kinase, which converts two molecules of ADP into one ATP and one AMP molecule. The rise cellular ADP and AMP promotes AMPK phosphorylation and leads to a decrease in Akt activity. Activated AMPK restores cellular energy balance by stimulating glucose transport through the action of AS160 and by reducing fatty acid synthesis as it inhibits ACC, thus preventing the conversion of acetyl-CoA to malonyl-CoA.

Chapter 4

GPR21, A Novel Target for Obesity-Associated Type 2 Diabetes

4.1 Introduction

Type 2 diabetes is primarily caused by a systemic insulin resistant state to which obesity is a major contributing factor. Increasing visceral adipose tissue provokes a chronic, low-grade, inflammatory response that negatively impacts on the insulin signalling pathway (Weyer *et al.,* 2001, Kahn *et al.,* 2006, Qatanani and Lazar, 2007, Emanuela *et al.,* 2012, Osborn and Olefsky, 2012). The rapidly rising incidence of type 2 diabetes, along with variable subject responses and the increasing limitations of current therapies, urge the need for innovative, effective strategies to prevent the development and progression of this condition (Rochester and Akiyode, 2014). GPCRs represent a rich source of drug targets for many disease states. These seven transmembrane receptors, the largest family of proteins in the genome, convey major external signals to the internal environment of the cell, with approximately 30 – 40 % of all marketed drugs targeting these versatile proteins (Ma and Zemmel, 2002, Lappano and Maggiolini, 2011, Tautermann, 2014).

GPR21, an orphan GPCR, has recently emerged as a potential novel target for the treatment of type 2 diabetes (Gardner *et al.,* 2012, Osborn *et al.,* 2012). GPR21 knockout mice fed on a HFD demonstrated increased insulin sensitivity, improved glucose tolerance and a reduction in pro-inflammatory markers when compared to wild type littermates. Both the identity of the ligand for this receptor and the precise mechanism by which it mediates this action remain unclear. Analysis of the G protein to which GPR21 couples to amplify signal potential is key to understanding the activity and downstream consequences of receptor activation. It has been suggested that GPR21 couples with $G\alpha_q$ (Bresnick *et al.,* 2003) and specifically $G\alpha_{15/16}$ (Xiao *et al.,* 2008). Selective GPCR coupling to $G\alpha_q$ proteins leads to the

activation of PLC, which cleaves PIP_2 into the secondary messengers, DAG and IP_3 (Fig. 4.1). The membrane-bound DAG activates PKC, whereas the soluble IP_3 binds to its receptor in the endoplasmic reticulum triggering the release of Ca^{2+}. Downstream of this, a wide range of intracellular pathways can be activated, including the MAPK cascade (Naor *et al.,* 2000, Chan and Wong, 2004, Goldsmith and Dhanasekaran, 2007), of which JNK is an established contributor to the development of insulin resistance (Aguirre *et al.,* 2000).

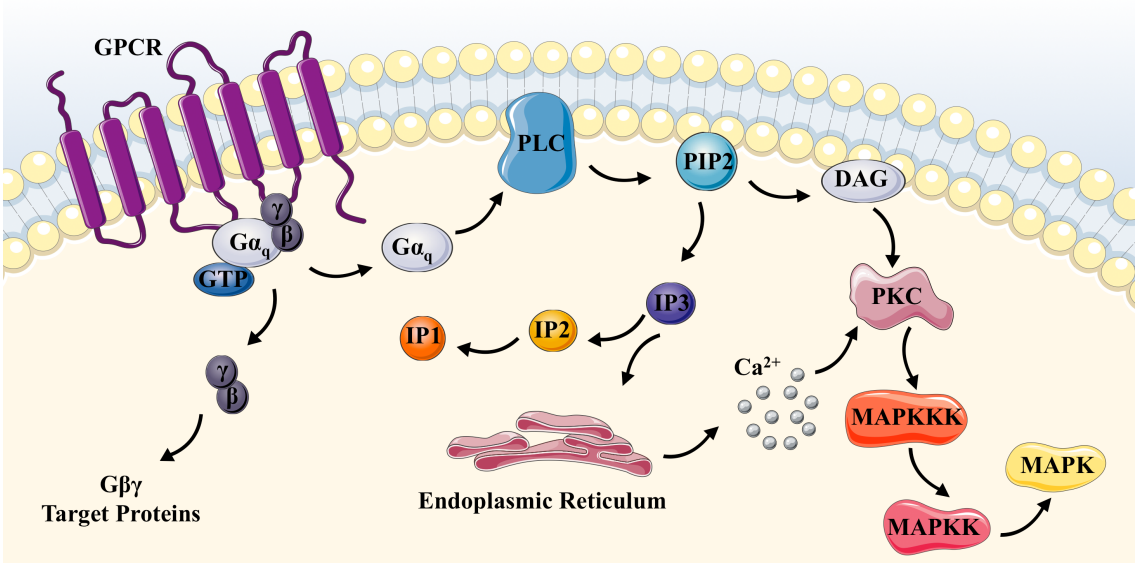

Figure 4.1 $G\alpha_q$ signalling.

Upon GPCR activation, a G protein binds to the receptor, which facilitates the exchange of bound GDP for GTP on the α-subunit. The active GTP bound G protein then dissociates from the receptor forming a Gα monomer and a Gβγ dimer to modulate downstream effector proteins. The $G\alpha_q$ family comprises four subtypes; $G\alpha_q$, $G\alpha_{q/11}$, $G\alpha_{14}$ and $G\alpha_{15/16}$ which activate PLC, an enzyme that catalysis the hydrolysis of PIP_2 into DAG and IP_3. DAG directly activates PKC while IP_3 released into the cytoplasm mobilises Ca^{2+} from intracellular stores to influence PKC before it is rapidly metabolised into IP_2 and subsequently IP_1. PKC signals to a variety of proteins including MAPKKKs, which phosphorylate MAPKKs; highly specific activators of the MAPKs; Erk, p38 and JNK.

4.2 Aims and Objectives

This study aimed to elucidate the signalling mechanisms of GPR21 and the role it may play in obesity-associated type 2 diabetes. Given the impact of knocking out this receptor *in vivo* and the potential role it may play in the development of insulin resistance, moderating the effects of GPR21 with novel compounds may hold great promise as a prospective therapy for type 2 diabetes. As the structure of GPR21 is unknown, homology modelling and ligand docking studies were employed to identify potential small molecules capable of binding GPR21 and attenuating the downstream effects of the receptor.

4.3 Results

4.3.1 Increased Expression of GPR21 is Observed in the Adipose Tissue of HFHS-Fed Mice

Western blot analysis of the epididymal fat pads of wild type C57BL/6J mice, a meaningful indicator of obesity-related diabetes, revealed a substantial increase in GPR21 expression in HFHS-fed mice when compared to chow fed control mice (Fig. 4.2A). A concurrent increase in the content of the macrophage marker F4/80 was also observed in HFHS-fed mice (Fig. 4.2B). As the epididymal fat pads of the mice demonstrated differential expression of standard housekeeping proteins such as β-actin, Coomassie brilliant blue was used to confirm equal protein loading between groups (Fig. 4.2C). A rise in F4/80 expression was also seen at the mRNA level (Fig. 4.2D) along with a notable increase in the pro-inflammatory cytokine TNF-α in HFHS-fed mice (Fig. 4.2E).

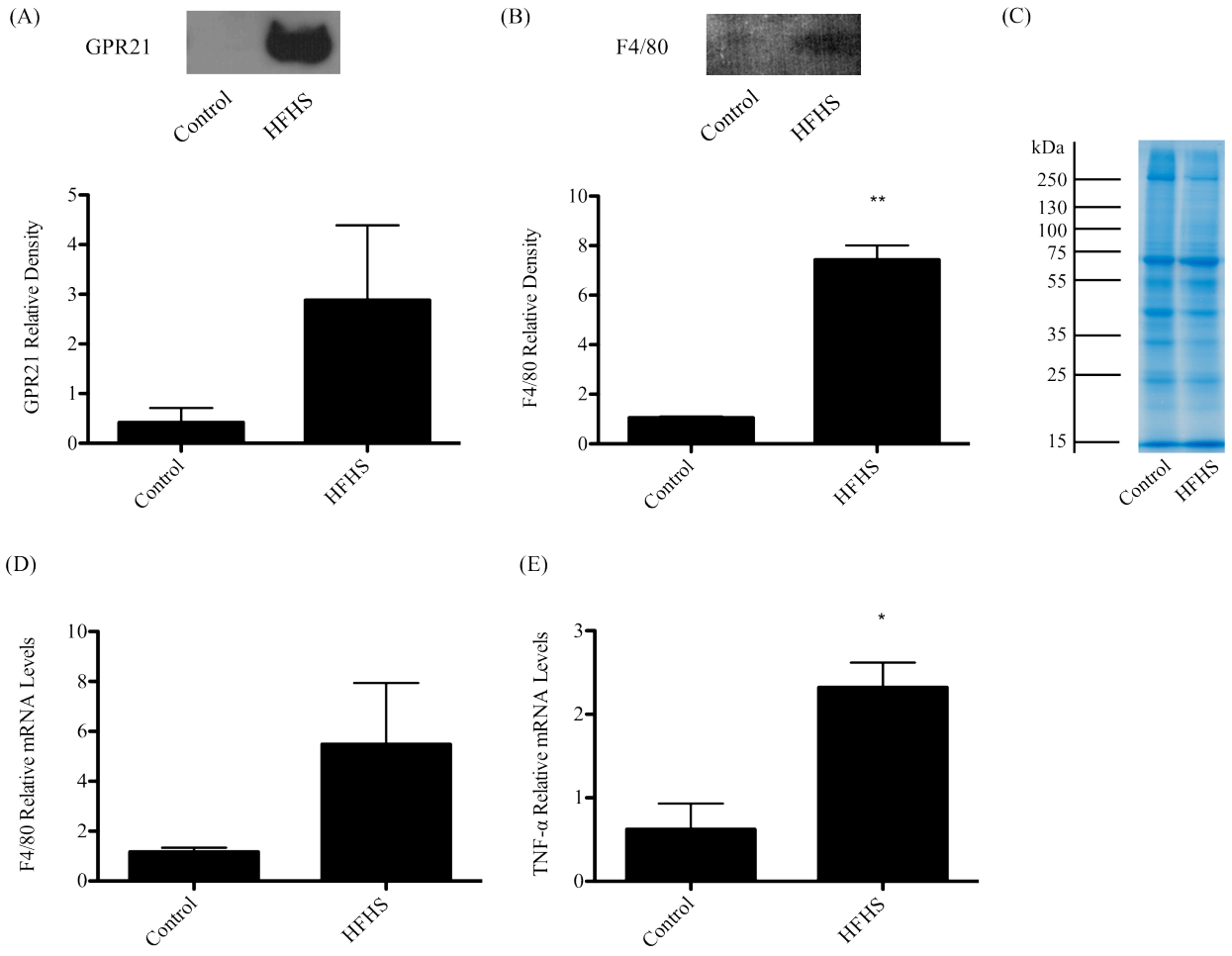

Figure 4.2 Analysis of the epididymal fat pads of chow fed and HFHS-fed mice.

Epididymal fat pads of chow fed and HFHS-fed C57BL/6J mice were lysed, proteins separated by SDS-PAGE and expression of (A) GPR21 and (B) the macrophage marker F4/80, were evaluated by Western blotting. Representative Western blots are shown along with relative densities obtained with ImageJ software, presented as mean ± SEM, n=3. (C) A representative Coomassie brilliant blue stained gel was used to confirm equal loading of the extracted proteins. qRT-PCR was also used to assess the mRNA levels of (D) F4/80 and (E) TNF-α, relative to the housekeeping control, HPRT. Using the unpaired Student's *t*-test, GraphPad Prism® 5 software demonstrates significance at $p < 0.05$; * and $p < 0.01$; **.

4.3.2 GPR21 is a Ubiquitously Expressed Protein

In an attempt to better understand this receptor, the expression profile of GPR21 in various cell lines was analysed through Western blotting (Fig. 4.3). Upon short immunoblotting exposure, GPR21 was not detected in C2C12 muscle cells, in THP-1 monocytes or in the macrophage cell lines J774, RAW 264.7 and BMDM. Relatively low levels of the receptor were observed in A549 alveolar basal epithelial lung cells, CHO cells and SH-SY5Y neuroblastoma cells. COS-1 and HEK293T kidney cells expressed a greater amount of GPR21, with more again detected in HepG2 liver cells. The greatest abundance of GPR21 by far was found in differentiated 3T3-L1 adipocytes. However, with a longer exposure time it was clear the monocytes and various macrophage cell lines were not completely devoid of the receptor, with C2C12 muscle cells also potentially exhibiting expression of GPR21.

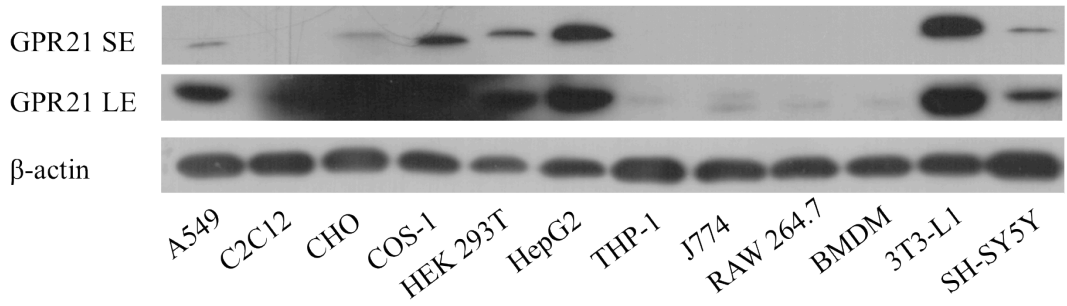

Figure 4.3 Western blot analysis of GPR21 expression in various cell lines.

The indicated cell lines were grown to confluency, lysed, subjected to SDS-PAGE and immunoblotted with antibodies against GPR21 with short (SE) and long (LE) exposures. β-actin was used as a loading control. Data presented are representative of two independent experiments.

4.3.3 GPR21 cDNA can be effectively Transfected into HEK293T, RAW 264.7 and 3T3-L1 cells

In order to explore the potential of an increase in GPR21 levels, overexpression of the receptor in a cell line was carried out. HEK293T cells were selected as the primary cell for this study, as this human cell line expresses the SV40 large T antigen, which can bind to SV40 enhancers of expression vectors, yielding increased protein production. Given the differential expression profile of GPR21 in adipocytes and macrophages, resident cells of the epididymal fat pads, transfection efficiencies with RAW 264.7 macrophages and 3T3-L1 adipocytes were also investigated. To determine optimal transfection conditions HEK293T cells were transiently transfected with eGFP using Lipofectamine® 2000, whereas RAW 264.7 macrophages and 3T3-L1 preadipocytes were transfected with eGFP using Lipofectamine® 3000 (Fig. 4.4A). Cells transiently transfected under the indicated conditions were found to successfully express GPR21 as confirmed by Western blotting for the myc tag incorporated into the C-terminus of the receptor (Fig. 4.4B).

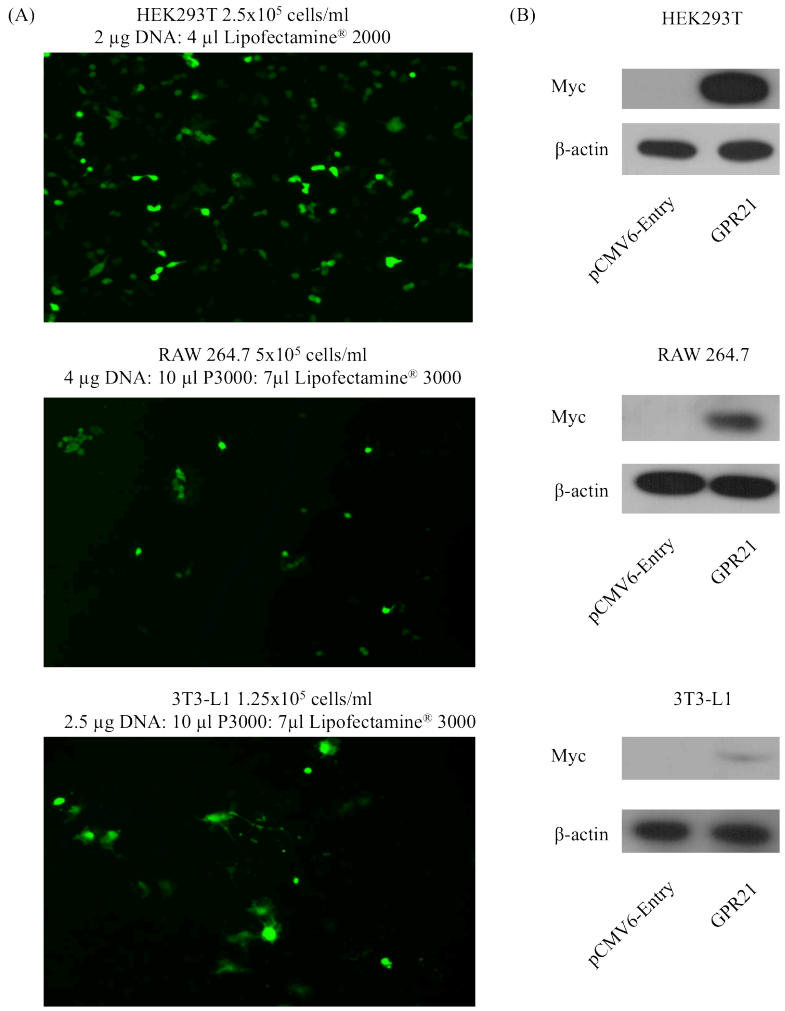

Figure 4.4 Optimisation of cell line transfection.

HEK293T, RAW 264.7 and 3T3-L1 cells were seeded at the indicated densities and left to adhere for 24 hours. Cells were then transfected with various ratios of eGFP: Lipofectamine® 2000 or Lipofectamine® 3000 as outlined in the manufacturer's instructions. (A) HEK293T and RAW 264.7 cells were left for 24 hours at 37 °C then imaged with an inverted Olympus CKX41 fluorescent microscope. 3T3-L1 cells demonstrating expression of the plasmid after 24 hours were differentiated as outlined in Section 2.2.1.2. Cells were visualised microscopically every two days and imaged on day six of the differentiation process. (B) Using the outlined, optimised conditions, cells were transfected with GPR21 or the empty vector pCMV6-Entry. After 24 hours, or at the end of the differentiation process in the case of 3T3-L1 adipocytes, cells were lysed, subjected to SDS-PAGE and immunoblotted for the myc tag incorporated into the C-terminus of GPR21 to confirm expression. β-actin was used as a loading control.

4.3.4 GPR21 is a Constitutively Active Receptor, Signalling Preferentially Through $G\alpha_{15/16}$

As HEK293T cells transiently expressed GPR21 with the greatest efficiency, they were selected to investigate the G protein to which GPR21 couples, to give further insight into the consequences of an increase in receptor expression. HEK293T cells were transiently transfected with GPR21 along with the cDNAs of the α-subunits of the G_q family members; $G\alpha_q$, $G\alpha_{14}$, and $G\alpha_{15/16,}$ as these effector proteins have been suggested to couple with the receptor (Bresnick *et al.,* 2003, Xiao *et al.,* 2008). Mammalian receptors activating $G\alpha_q$ family members apparently do not discriminate between $G\alpha_q$ and $G\alpha_{q/11}$ (Offermanns *et al.,* 1994), therefore, the influence of $G\alpha_{q/11}$ on GPR21 activity was not investigated.

Analysis of IP_1 production with a FRET based IP-one assay was used as a surrogate of the transient $G\alpha_q$ secondary messenger IP_3, since the degradation of this metabolite of IP_3 can be prevented with the addition of lithium chloride (Trinquet *et al.,* 2006). An increase in endogenous IP_1 was observed in HEK293T cells transfected with GPR21 alone and in the absence of a ligand when compared to cells transfected with the empty vector, an indication of a constitutively active receptor. Each of the $G\alpha_q$ subtypes led to an increase in basal IP_1 production when co-transfected with the empty vector pCMV6-Entry. When GPR21 was coupled with $G\alpha_q$ a significant increase in IP_1 was observed. Although transfection with $G\alpha_q$ stimulated the greatest production of IP_1, $G\alpha_{15/16}$ was found to significantly augment GPR21-induced release of IP_1. $G\alpha_{14}$ did not appear to markedly influence GPR21-induced production of IP_1 (Fig. 4.5).

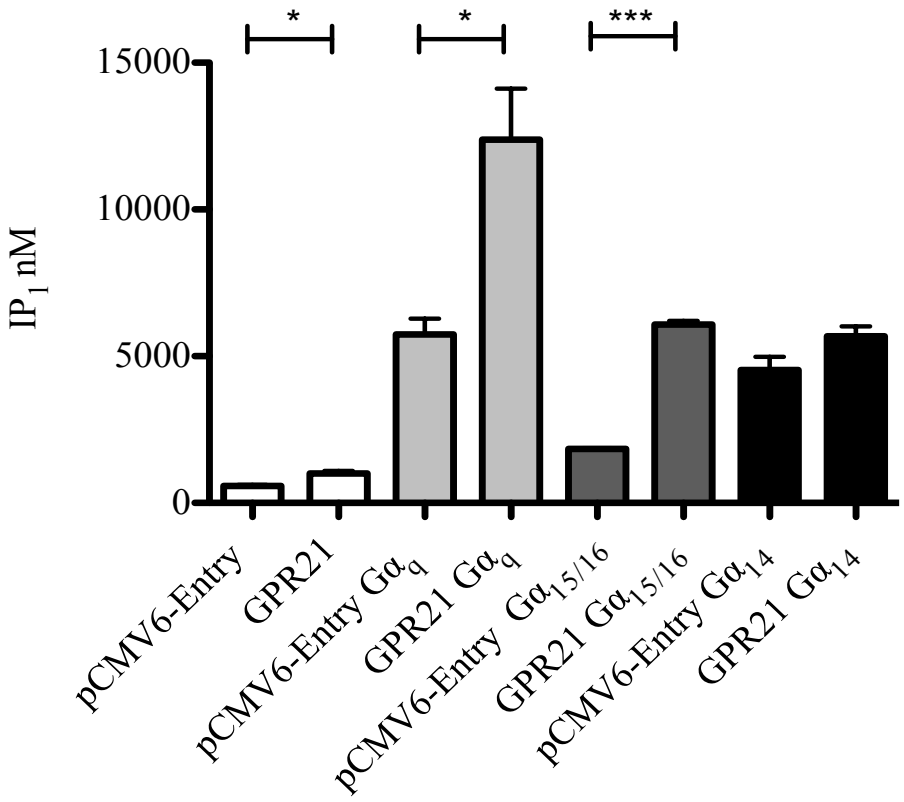

Figure 4.5 GPR21 activity in HEK293T cells.

HEK293T cells were seeded at $2.5x10^5$ cells/ml in a 6 well plate, after 24 hours cells were transiently transfected with 4 µl Lipofectamine® 2000: 2 µg GPR21 plasmid DNA or the empty vector pCMV6-Entry. When co-transfecting cells with $G\alpha_q$, $G\alpha_{15/16}$ and $G\alpha_{14}$, 1 µg of each plasmid DNA was used. After 24 hours cells were trypsinised, resuspended at a density of $6x10^6$ cells/ml in IP-one stimulation buffer and processed according to the IP-one assay protocol (Cisbio, 62IPAPEC). IP_1 concentrations were then extrapolated from an IP_1 standard curve. One-way ANOVA with a post-hoc Tukey test using GraphPad Prism® 5 software denotes significance at $p < 0.05$; * and $p < 0.001$; ***. Data presented as mean ± SEM are representative of at least three independent experiments.

To confirm GPR21 was explicitly signalling through $G\alpha_q$, HEK293T cells overexpressing GPR21 were incubated with increasing concentrations of the PLC inhibitor U73122 (Smith *et al.,* 1990), as PLC is the crucial intermediate protein between $G\alpha_q$ signalling and the production of IP_3. Since the receptor appeared most active when co-expressed with $G\alpha_{15/16}$, the effect of the inhibitor on GPR21 when coupled with $G\alpha_{15/16}$ was concurrently investigated. Cells transfected with pCMV6-Entry and pCMV6-Entry coupled with $G\alpha_{15/16}$ were also stimulated with U73122 as a control. The PLC inhibitor demonstrated little effect on endogenous IP_1 production in these control cells. However, in cells overexpressing GPR21, a dose dependent decrease in IP_1 production was observed (Fig. 4.6A), a response more evident when GPR21 was coupled with $G\alpha_{15/16}$ (Fig. 4.6B).

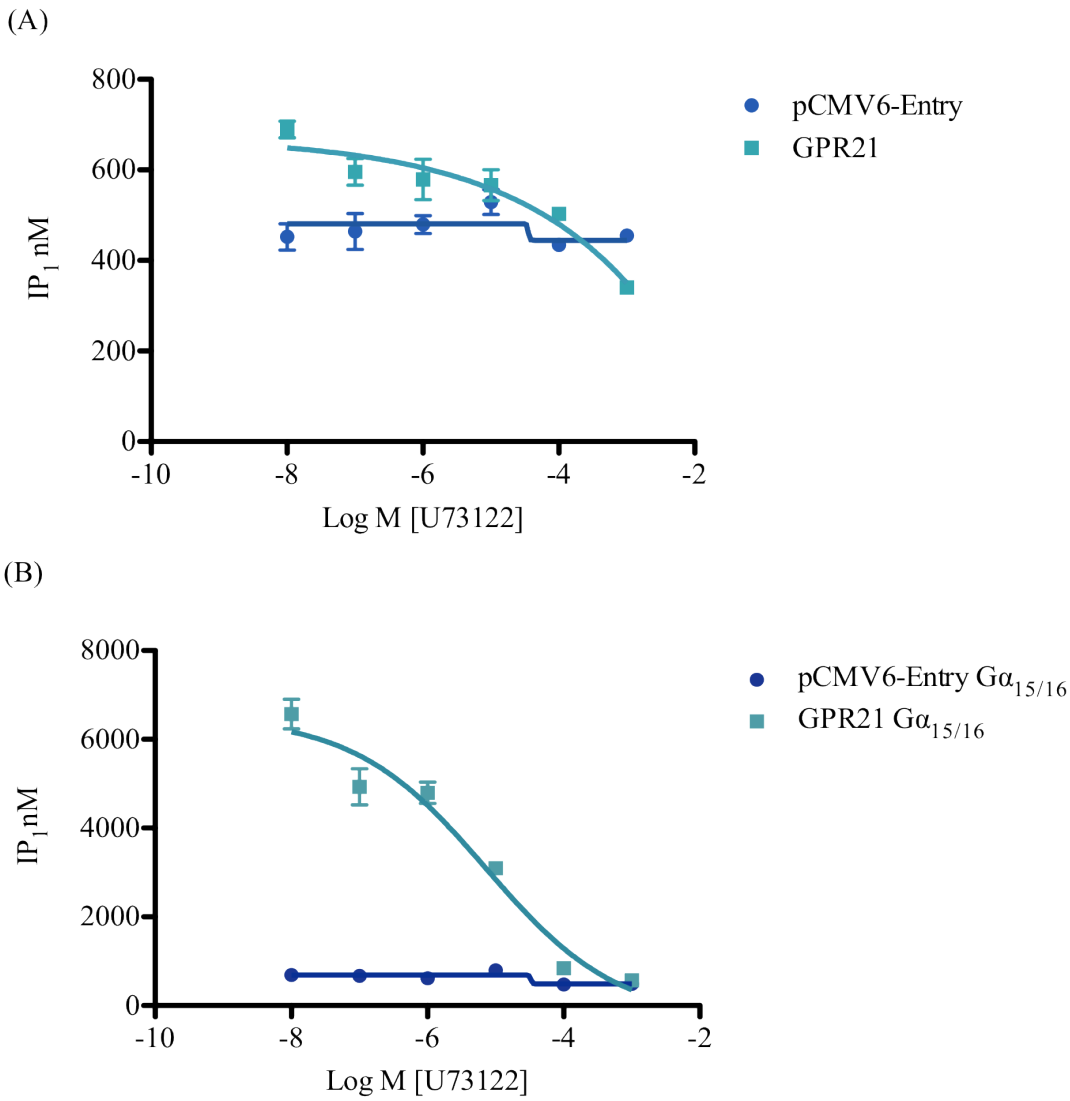

Figure 4.6 The effect of the PLC inhibitor, U73122, on GPR21-induced IP_1 production in HEK293T cells.

HEK293T cells were transiently transfected with (A) pCMV6-Entry or GPR21 and (B) pCMV6-Entry coupled with $G\alpha_{15/16}$ or GPR21 coupled with $G\alpha_{15/16}$. After 24 hours cells were trypsinised and resuspended at a density of $6x10^6$ cells/ml in IP-one stimulation buffer. Cells were then incubated with the PLC inhibitor U73122 (Sigma-Aldrich, U6756) in IP-one stimulation buffer and processed according to the IP-one assay protocol. IP_1 concentrations were extrapolated from an IP_1 standard curve and GraphPad Prism® 5 software was used to generate a non-linear sigmoidal dose response curve. Data presented as mean ± SEM are representative of two independent experiments performed in triplicate each time.

4.3.5 Overexpression of GPR21 leads to the Activation of the MAPKs

Downstream of the $G\alpha_q$ secondary messenger PLC, a wide range of intracellular pathways can be activated, including the MAPK cascade. Overexpression of GPR21 led to a significant increase in the phosphorylation of the MAPKs Erk, p38 and JNK when compared to cells transfected with pCMV6-Entry. The effect of GPR21 on the MAPKs was reduced in cells incubated with complete medium containing 10 % (v/v) FBS in comparison to serum starved cells (Fig. 4.7A). When coupled with $G\alpha_{15/16}$ (Fig. 4.7B), GPR21 again led to an increase in the phosphorylation of Erk, p38 and JNK. In the presence of 10 % (v/v) FBS, the phosphorylation status of the MAPKs was unaltered.

To determine if the activation of the MAPKs was dependent on GPR21 signalling through $G\alpha_q$ to activate PLC, HEK293T cells overexpressing GPR21 were incubated with 10 μM U73122 in serum free complete medium. The PLC inhibitor reduced the effect of the receptor on the MAPKs, with the influence of U73122 on JNK phosphorylation slightly inferior to that of the JNK inhibitor SP600125 (Fig. 4.8).

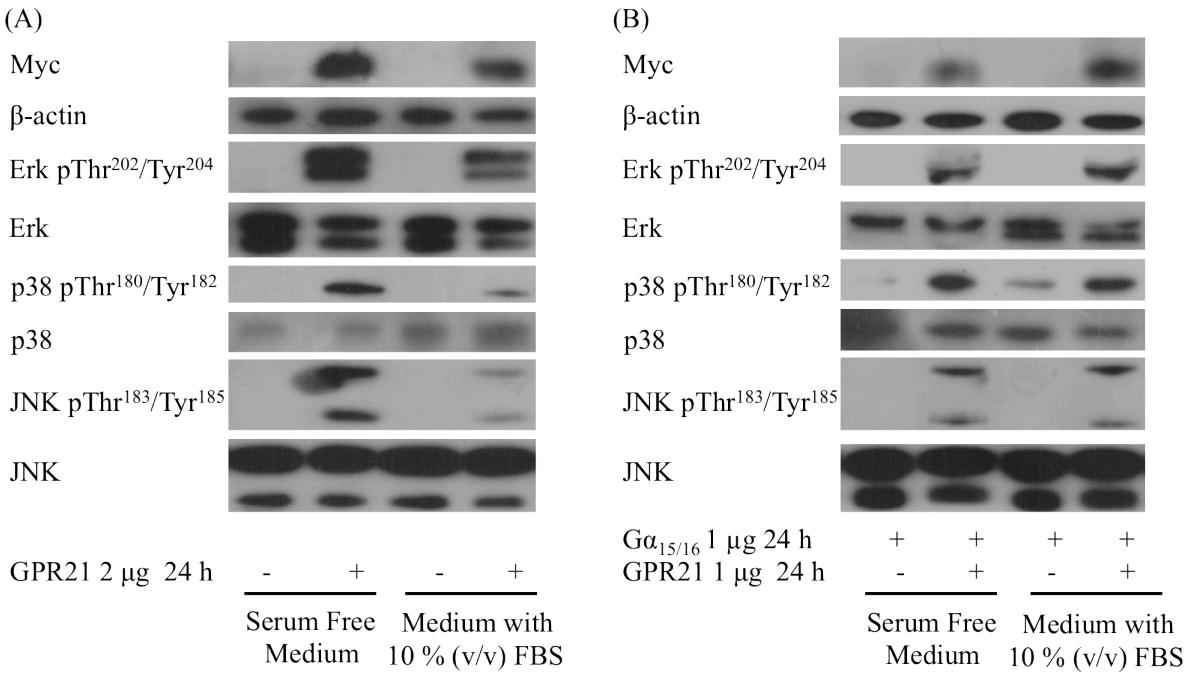

Figure 4.7 The effect of GPR21 overexpression on the phosphorylation of the MAPKs in HEK293T cells.

HEK293T cells transiently transfected with (A) pCMV6-Entry or GPR21 and (B) pCMV6-Entry coupled with $G\alpha_{15/16}$ or GPR21 coupled with $G\alpha_{15/16}$ were incubated for 24 hours in complete medium in the presence or absence of 10 % (v/v) FBS. Cells were lysed and subjected to SDS-PAGE followed by immunoblotting with antibodies against phospho-Erk Thr^{202}/Tyr^{204}, phospho-p38 Thr^{180}/Tyr^{182}, phospho-JNK Thr^{183}/Tyr^{185}, native Erk, p38 and JNK. Myc was used to confirm GPR21 expression and β-actin was used as a loading control. Data are representative of two independent experiments.

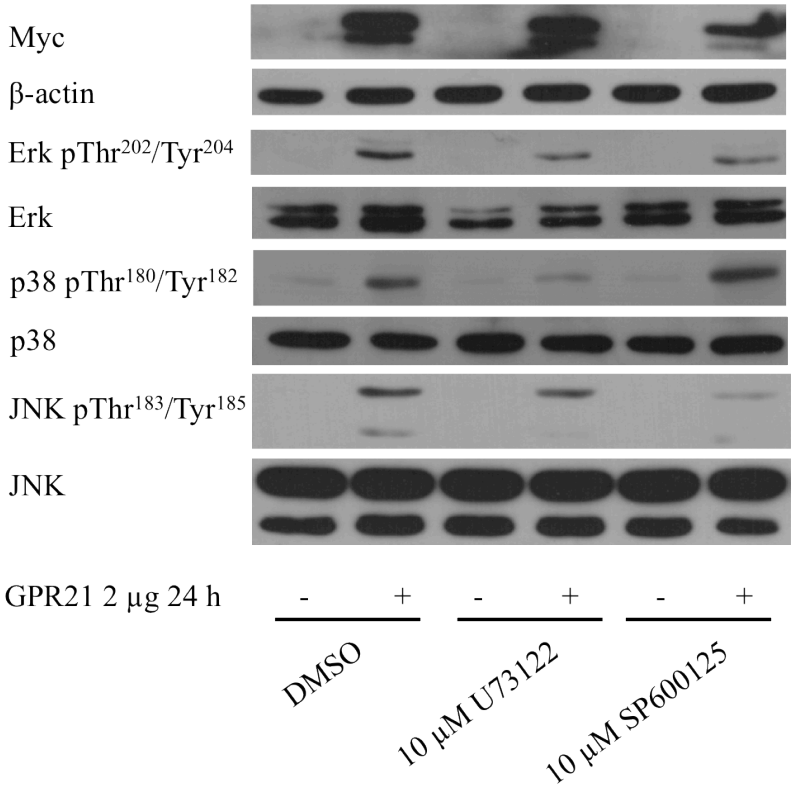

Figure 4.8 The effect of U73122 on GPR21-induced phosphorylation of the MAPKs in HEK293T cells.

HEK293T cells were transiently transfected with the empty vector pCMV6-Entry or GPR21 and left for 24 hours to incorporate plasmid DNA. Cells were then stimulated with 10 µM U73122, a PLC inhibitor, 10 µM SP600125, a JNK inhibitor (Sigma-Aldrich, S5567) or an equal volume of the vehicle control, DMSO for 24 hours in serum free complete medium. Cells were lysed and subjected to SDS-PAGE followed by immunoblotting with antibodies against phospho-Erk Thr^{202}/Tyr^{204}, phospho-p38 Thr^{180}/Tyr^{182}, phospho-JNK Thr^{183}/Tyr^{185}, native Erk, p38 and JNK. Myc was used to confirm GPR21 expression and β-actin was used as a loading control. Data are representative of two independent experiments.

4.3.6 GPR21 Negatively Impacts the Insulin Signalling Pathway

As overexpression of GPR21 in HEK293T cells led to a significant increase in JNK phosphorylation, an acknowledged negative regulator of the insulin signalling cascade, the direct effect of receptor overexpression on this pathway was investigated (Fig. 4.9A). HEK293T cells transfected with the empty vector pCMV6-Entry as a control, exhibited basal phosphorylation of the principal proteins of the insulin signalling pathway. Control cells also responded to the 1 hour 100 nM insulin stimulation, leading to an increase in the phosphorylation of the insulin receptor, IRS1, Akt and AS160 at both residues, Thr^{642} and Ser^{588} critical for GLUT4 translocation to facilitate glucose transport. Conversely, cells overexpressing GPR21 demonstrated reduced basal phosphorylation of Akt and AS160. Furthermore, cells did not respond to insulin-induced stimulation of the insulin receptor itself, diminishing the activity of the signalling pathway.

Incubation of cells transfected with the empty vector with complete medium containing 10 % (v/v) FBS, increased the phosphorylation of AS160 at Thr^{642} marginally, yet had little bearing on the activation of the other proteins of the signalling cascade. However, the effect of GPR21 overexpression on this pathway was curtailed in the presence of FBS. The phosphorylation of the insulin receptor, IRS1, Akt and AS160 were seen to increase when compared to GPR21-expressing cells incubated with serum free medium. Nonetheless, the phosphorylation status of these proteins remained below that of cells transfected with pCMV6-Entry.

A similar result was observed when GPR21 was coupled with $G\alpha_{15/16}$ (Fig. 4.9B), while cells co-expressing pCMV6-Entry and $G\alpha_{15/16}$ responded to the action of insulin. Additionally, the impact of serum containing complete medium in weakening the effect of GPR21 on the insulin signalling pathway was less effective when the receptor was coupled with $G\alpha_{15/16}$.

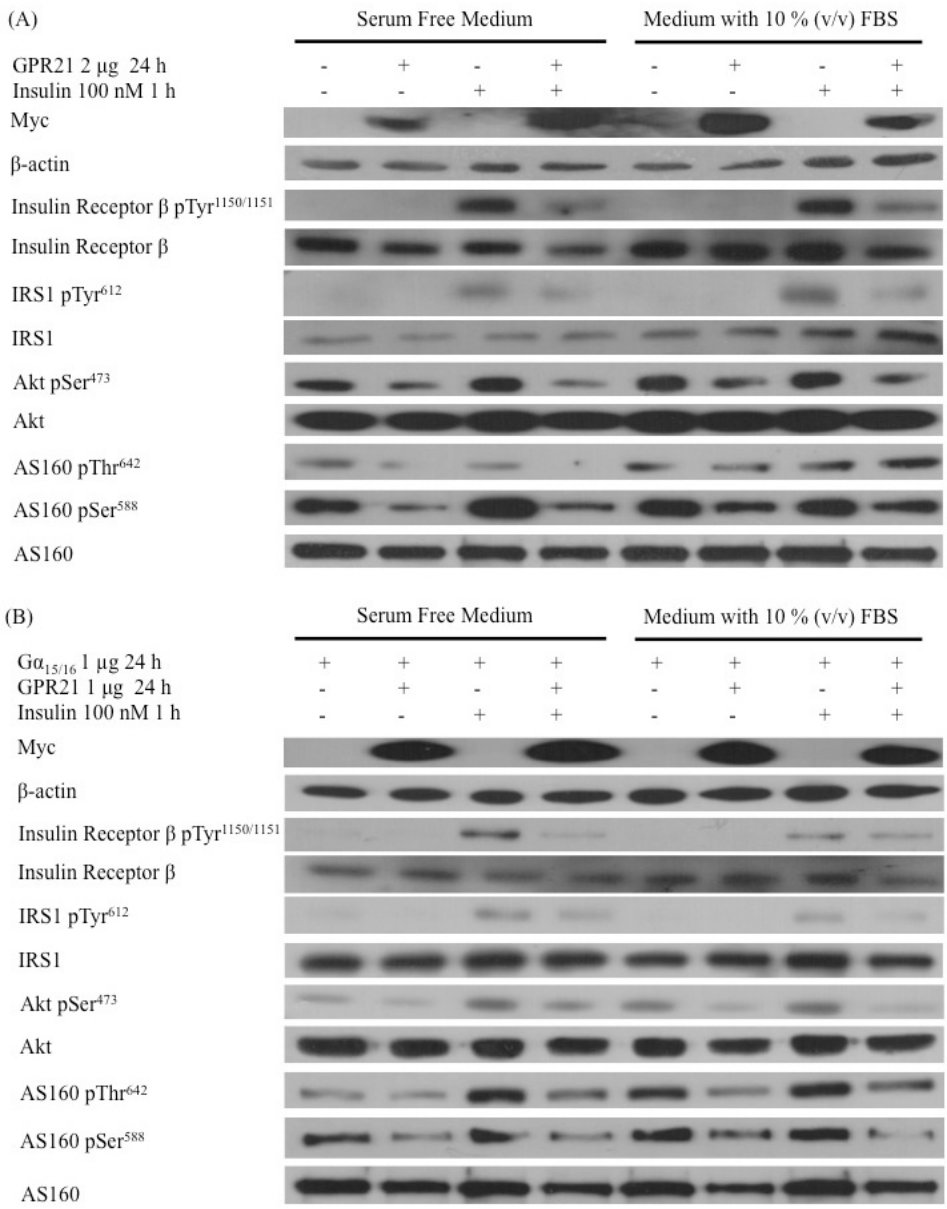

Figure 4.9 Western blot analysis of the effect of GPR21 on insulin signalling in HEK293T cells.

HEK293T cells transiently transfected with (A) pCMV6-Entry or GPR21 and (B) pCMV6-Entry coupled with $G\alpha_{15/16}$ or GPR21 coupled with $G\alpha_{15/16}$ were incubated for 24 hours in complete medium in the presence or absence of 10 % (v/v) FBS, then stimulated with 100 nM insulin for 1 hour in KRBG. Cells were lysed and subjected to SDS-PAGE followed by immunoblotting with antibodies against phospho-insulin receptor β $Tyr^{1150/1151}$, phospho-IRS1 Tyr^{612}, phospho-Akt Ser^{473}, phospho-AS160 Thr^{642} and Ser^{588}, native insulin receptor β, IRS1, Akt and AS160. Myc was used to confirm GPR21 expression and β-actin was used as a loading control. Data are representative of two independent experiments.

As a consequence of a hindered insulin signalling pathway, overexpression of GPR21 also led to a significant decrease in glucose uptake both basally and under insulin stimulation. Although this response was weakened in cells incubated with complete medium supplemented with 10 % (v/v) FBS, glucose uptake did not return to the level of counterpart cells transfected with the empty vector. Complete medium supplemented with 10 % (v/v) FBS demonstrated no effect in augmenting glucose uptake in control cells transfected with pCMV6-Entry (Fig. 4.10A). HEK293T cells expressing GPR21 coupled with $G\alpha_{15/16}$ also displayed a reduction in basal and insulin-induced glucose uptake when compared to cells transfected with pCMV6-Entry coupled with $G\alpha_{15/16}$. Similarly, complete medium supplemented with 10 % (v/v) FBS undermined the impact of GPR21 coupled with $G\alpha_{15/16}$, while exhibiting no effect on glucose uptake in control cells transfected with pCMV6-Entry and $G\alpha_{15/16}$ (Fig. 4.10B).

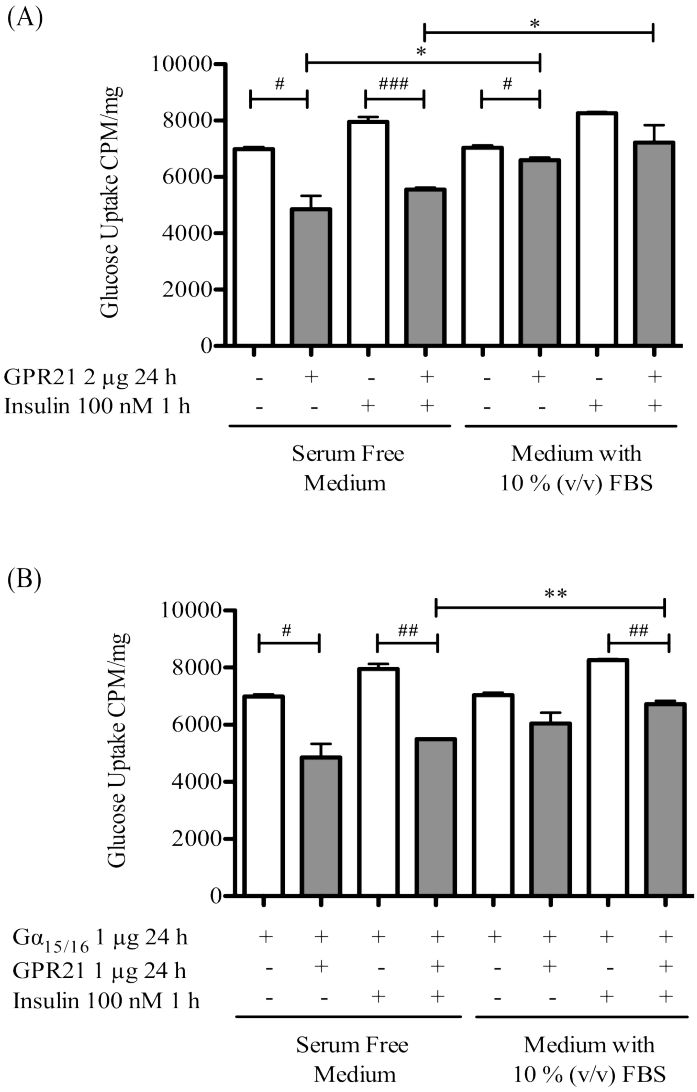

Figure 4.10 The effect of serum on glucose uptake in HEK293T cells overexpressing GPR21.

HEK293T cells transiently transfected with (A) pCMV6-Entry or GPR21 and (B) pCMV6-Entry coupled with $G\alpha_{15/16}$ or GPR21 coupled with $G\alpha_{15/16}$ were incubated for 24 hours in the presence or absence of 10 % (v/v) FBS, then stimulated with 100 nM insulin for 1 hour in KRBG. The effect on glucose uptake was established by measuring cellular levels of [^{3}H]-2-deoxyglucose. Data presented as mean ± SEM are representative of two independent experiments. One-way ANOVA with a post-hoc Tukey test using GraphPad Prism® 5 software conveys a significant increase in glucose uptake at $p < 0.05$; * and $p < 0.01$; **. A significant decrease in glucose uptake is denoted at $p < 0.05$; $^{\#}$, $p < 0.01$; $^{\#\#}$ and $p < 0.001$; $^{\#\#\#}$.

4.3.7 The Constituents of FBS may Influence GPR21 Activity

To further explore the effect of FBS on the phosphorylation events observed in response to GPR21 overexpression, transfected HEK293T cells were incubated with complete medium containing increasing concentrations of FBS for 24 hours prior to insulin stimulation (Fig. 4.11). In serum free medium and medium containing 6 % (v/v) FBS, overexpression of GPR21 reduced insulin-induced phosphorylation of the insulin receptor. When GPR21 transfected cells were incubated with complete medium containing 12 % (v/v), 25 % (v/v) and 50 % (v/v) FBS the effect of GPR21 on the insulin receptor was abated. In serum free medium, overexpression of GPR21 led to an obvious decrease in insulin-induced phosphorylation of IRS1, an effect that was attenuated with increasing concentrations of FBS. GPR21 also lessened insulin-induced phosphorylation of Akt in serum free medium, however with increasing concentrations of FBS the response to insulin became augmented. Further down the signalling pathway, the inhibitory effect of GPR21 on AS160 at Thr^{642} was evident both basally and upon insulin stimulation in serum starved cells. However, this response was reduced in GPR21-expressing cells incubated with complete medium containing 6 % (v/v) FBS. While cells expressing GPR21 incubated with 12 % (v/v) and 25 % (v/v) FBS demonstrated a reduction in basal AS160 phosphorylation at Thr^{642}, insulin-induced phosphorylation was comparable to cells transfected with the empty vector. The phosphorylation status of AS160 at Thr^{642} was also equivalent to the basal levels observed with control cells when incubated in complete medium supplemented with 50 % (v/v) serum. Insulin-induced phosphorylation of AS160 at Thr^{642} appeared to be reduced under these conditions, although the band present may have bleached due to the intensity. Overall the overexpression GPR21 demonstrated little effect on the phosphorylation of AS160 at Ser^{588}.

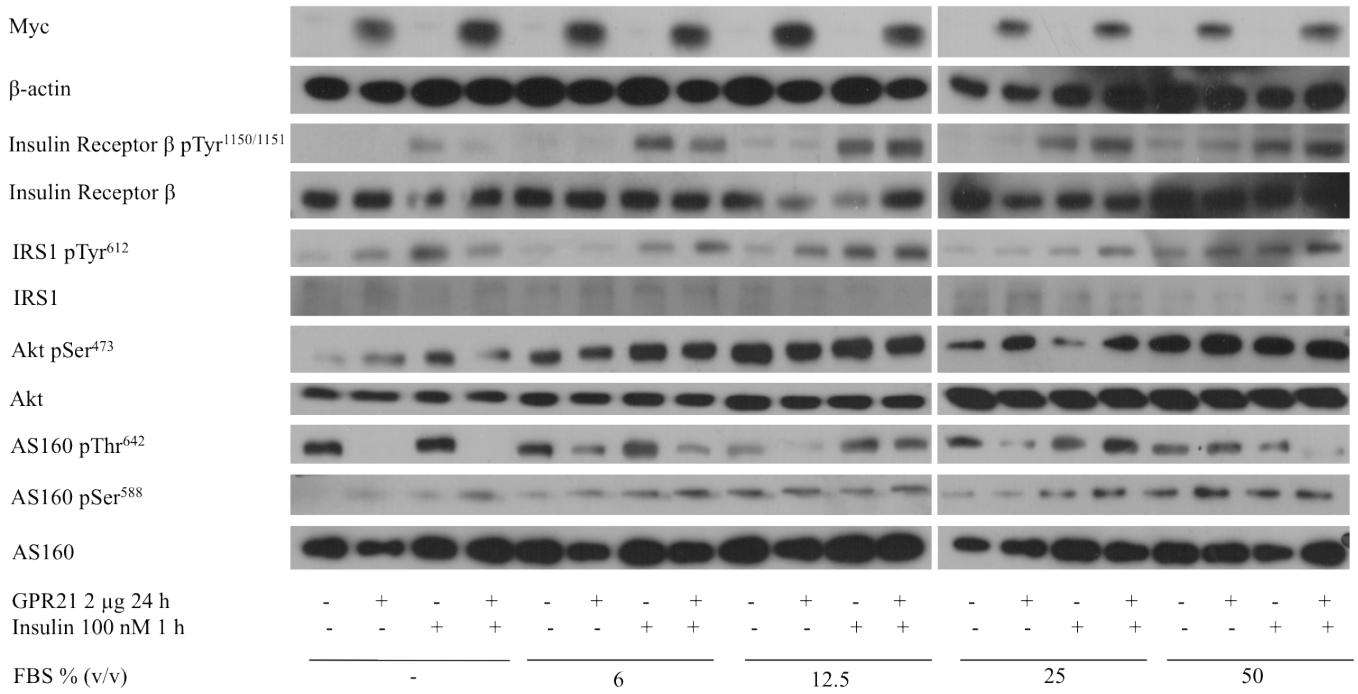

Figure 4.11 Western blot analysis of the effect of serum on insulin signalling in HEK293T cells overexpressing GPR21 in HEK293T cells.

HEK293T cells transiently transfected with pCMV6-Entry or GPR21 were incubated for 24 hours with complete medium containing concentrations of FBS ranging from 0 – 50 % (v/v). Cells were then stimulated with 100 nM insulin for 1 hour in KRBG, lysed and subjected to SDS-PAGE. Membranes were immunoblotted with antibodies against phospho-insulin receptor β $Tyr^{1150/1151}$, phospho-IRS1 Tyr^{612}, phospho-Akt Ser^{473}, phospho-AS160 Thr^{642} and Ser^{588}, native insulin receptor β, IRS1, Akt and AS160. Myc was used to confirm GPR21 expression and β-actin was used as a loading control. Data are representative of two independent experiments.

The direct effect of FBS on GPR21 activity was then assessed through the impact on the activation of the MAPKs and IP_1 production, to determine if the influence on the insulin signalling pathway was merely as a result of residual serum derived insulin present in the medium.

Looking at the same sample set, phosphorylation of Erk was markedly increased in cells transfected with GPR21 in the presence and absence of insulin, yet only in serum free medium. Basal phosphorylation of Erk in cells transfected with pCMV6-Entry also subsided with increasing serum concentrations. Transfection of HEK293T cells with GPR21 led to a considerable increase in the phosphorylation of p38 in serum free medium and medium supplemented with 6 % (v/v) and 12.5 % (v/v) FBS. However GPR21-induced phosphorylation of p38 was reduced in cells incubated with concentrations of FBS above 25 %. HEK293T cells overexpressing GPR21 incubated with serum free medium demonstrated an increase in JNK phosphorylation, while phosphorylated JNK remained undetected in cells transfected with the empty vector. The effect of GPR21 on JNK diminished gradually when cells were incubated with medium containing increasing concentrations of FBS (Fig. 4.12).

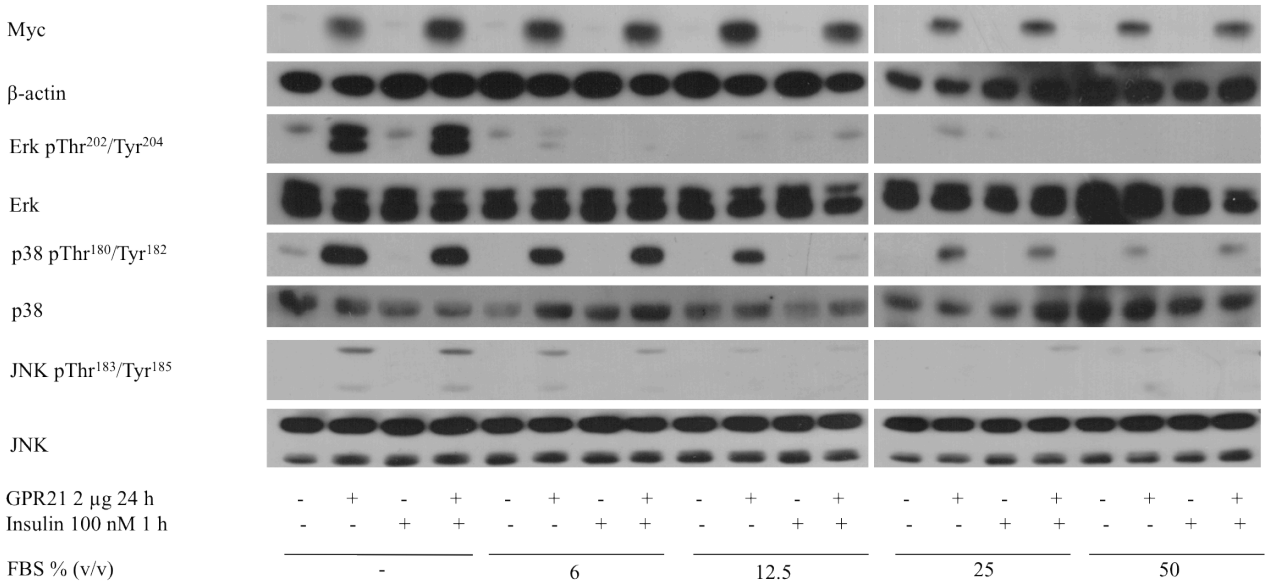

Figure 4.12 Western blot analysis of the effect of increasing serum concentration of GPR21 activation of the MAPKs in HEK293T cells.

HEK293T cells transiently transfected with pCMV6-Entry or GPR21 were incubated for 24 hours in complete medium containing FBS at concentrations ranging from 0 – 50 % (v/v). Cells were then stimulated with 100 nM insulin for 1 hour in KRBG, lysed and subjected to SDS-PAGE with antibodies against phospho-Erk Thr^{202}/Tyr^{204}, phospho-p38 Thr^{180}/Tyr^{182}, phospho-JNK Thr^{183}/Tyr^{185}, native Erk, p38 and JNK. Myc was used to confirm GPR21 expression and β-actin was used as a loading control. Data are representative of two independent experiments.

Table 4.1 Summarising the influence of GPR21 overexpression on protein phosphorylation.

Phospho-Protein	-	6 % (v/v) FBS	12.5 % (v/v) FBS	25 % (v/v) FBS	50 % (v/v) FBS
Insulin Signalling Cascade					
Insulin Receptor	-	+	++	++	+++
IRS1	+	++	++	+	++
Akt	+	++	+++	+++	+++
AS160 Thr^{642}	-	+	+	++	++
MAPKs					
Erk	+++	+	-	-	-
p38	+++	+++	++	+	+
JNK	++	+	-	-	-

With regards to IP_1 levels, GPR21-induced IP_1 production decreased significantly when cells were incubated FBS (Fig. 4.13A). In HEK293T cells overexpressing GPR21 coupled with $G\alpha_{15/16}$ IP_1 production decreased gradually with increasing concentrations of serum and markedly so at 50 % (v/v) FBS (Fig. 4.13B).

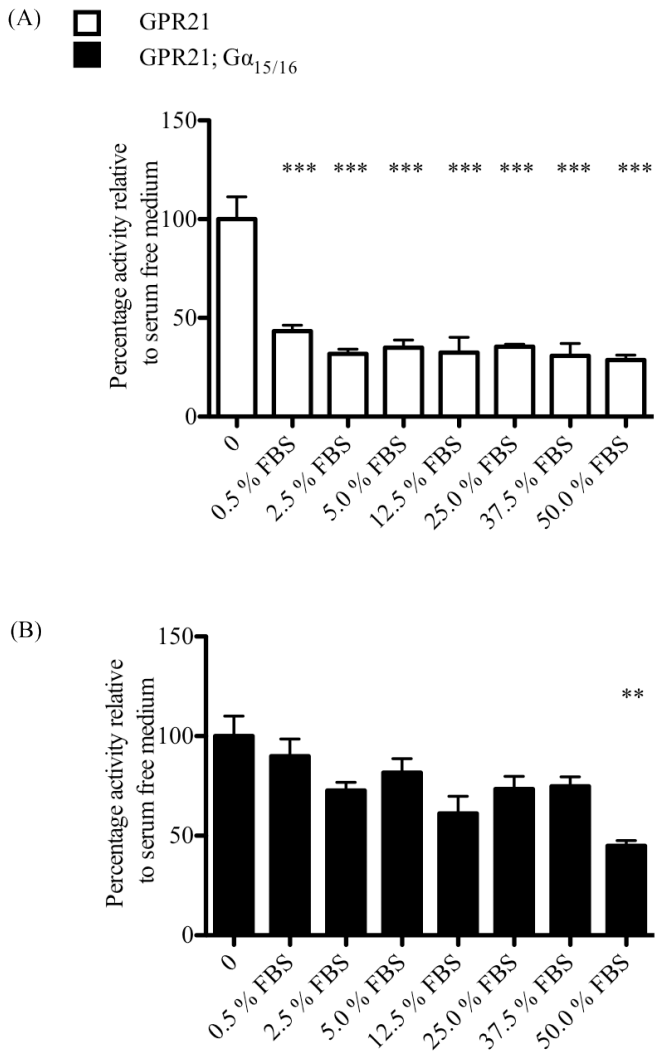

Figure 4.13 IP_1 production in HEK293T cells overexpressing GPR21 in response to FBS.

HEK293T cells were transiently transfected with (A) pCMV6-Entry or GPR21 and (B) pCMV6-Entry coupled with $G\alpha_{15/16}$ or GPR21 coupled with $G\alpha_{15/16}$. After 24 hours cells were trypsinised and resuspended at a density of $6x10^6$ cells/ml in IP-one stimulation buffer. Cells were then incubated with IP-one stimulation buffer containing FBS at concentrations ranging from 0 – 50 % (v/v) and processed according to the IP-one assay protocol. IP_1 concentrations were extrapolated from an IP_1 standard curve and GPR21 activity was determined by dividing the concentration of IP_1 produced in cells expressing GPR21 by the concentration of IP_1 produced in cells transfected with the empty vector. The effect of the compounds was defined relative to cells incubated with serum free medium. Data presented as mean ± SEM are representative of two independent experiments, n=2. One-way ANOVA with a post-hoc Dunnett test using GraphPad Prism® 5 software denotes significance at $p < 0.01$; ** and $p < 0.001$; ***.

4.3.8 A Novel Compound, GRA2, Reduces the Activity of GPR21

As the crystal structure of GPR21 remains unknown and no native interacting ligands for the orphan receptor have been identified to date, the development of a structural homology model was undertaken to design novel, small molecule ligands to bind GPR21 to modulate its downstream effects. Dr. Gemma Kinsella developed the GPR21 homology model (Fig. 4.14) using the Modeller software embedded in Biovia Discovery Studio (Biovia Software Inc.). A sequence alignment was constructed between the amino acid sequence of the GPCR templates 2RH1 (Cherezov *et al.,* 2007) and 4GBR (Zou *et al.,* 2012), with human GPR21 (Swissprot accession code Q99679). Using this alignment, 1,000 different models were generated with a refinement protocol applied to the loop regions (Fiser and Sali, 2003a, 2003b) and disulphide bonds were formed between Cys^{102} and Cys^{181}. The final model was selected using the Modeller objective score and a selection of protein assessment tools (http://services.mbi.ucla.edu/SAVES/, Laskowski *et al.*, 1996, Wiederstein and Sippl, 2007).

Utilising the developed model, Dr. Gemma Kinsella screened large compound databases such as Specs (www.specs.net) *in silico* through molecular docking studies using the FRED docking engine and OMEGA conformational databases from OpenEye Scientific Software (Perola and Charifson, 2004, McGaughey *et al.*, 2007, Hawkins *et al.*, 2010, McGann, 2011). From the ranked list of 11 compounds, 8 were screened experimentally *in vitro* for their ability to alter GPR21-induced production of IP_1 (Fig. 4.15). Although the hit compounds did not significantly modify GPR21-induced production of IP_1 at the concentrations assayed, one compound, GRA2 appeared to negatively influence the effect of GPR21.

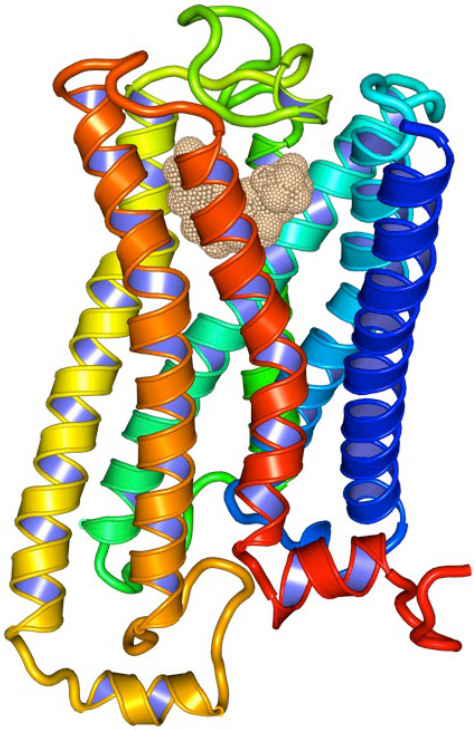

Figure 4.14 Homology model of GPR21 incorporating the predicted binding site of a lead compound, GRA2.

A Homology Model of GPR21 was designed using the Modeller software embedded in Biovia Discovery Studio based on its amino acid sequence and a template protein structure of related homologous proteins. Image kindly generated by Dr. Gemma Kinsella using PyMOL (www.pymol.org).

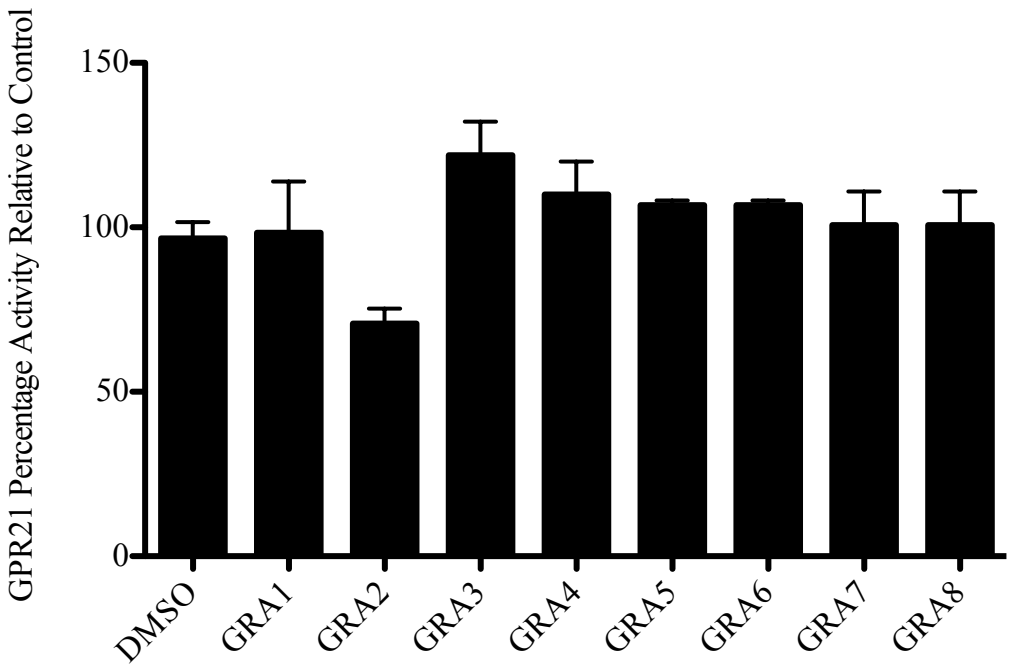

Figure 4.15 The effect of hit compounds on IP_1 production in HEK293T cells overexpressing GPR21.

HEK293T cells were transiently transfected with the empty vector pCMV6-Entry or GPR21 plasmid DNA. After 24 hours cells were trypsinised and resuspended at a density of $6x10^6$ cells/ml in IP-one stimulation buffer. Cells were then incubated with the hit compounds at a final concentration of 10 μM or an equal volume of vehicle control, DMSO, in IP-one stimulation buffer for 2 hours at 37 °C. IP_1 concentrations were extrapolated from an IP_1 standard curve and GPR21 activity was determined by dividing the concentration of IP_1 produced in cells expressing GPR21 by the concentration of IP_1 produced in cells transfected with the empty vector. The effect of the compounds was defined relative to the DMSO control. Data presented as mean ± SEM are representative of two independent experiments performed in triplicate each time.

In a dose response assay, the reaction to GRA2 was not significant in HEK293T cells transfected with GPR21 alone, with a mild decrease in cellular IP_1 observed at 1 mM only (Fig. 4.16A). However, in cells overexpressing GPR21 coupled with $G\alpha_{15/16}$, the more pronounced IP_1 production was markedly inhibited by GRA2 at 100 nM, an effect which plateaued at 1 μM supressing the activity of GPR21 (Fig. 4.16B). GRA2 did not influence basal IP_1 levels of control cells transfected with pCMV6-Entry or pCMV6-Entry coupled with $G\alpha_{15/16}$.

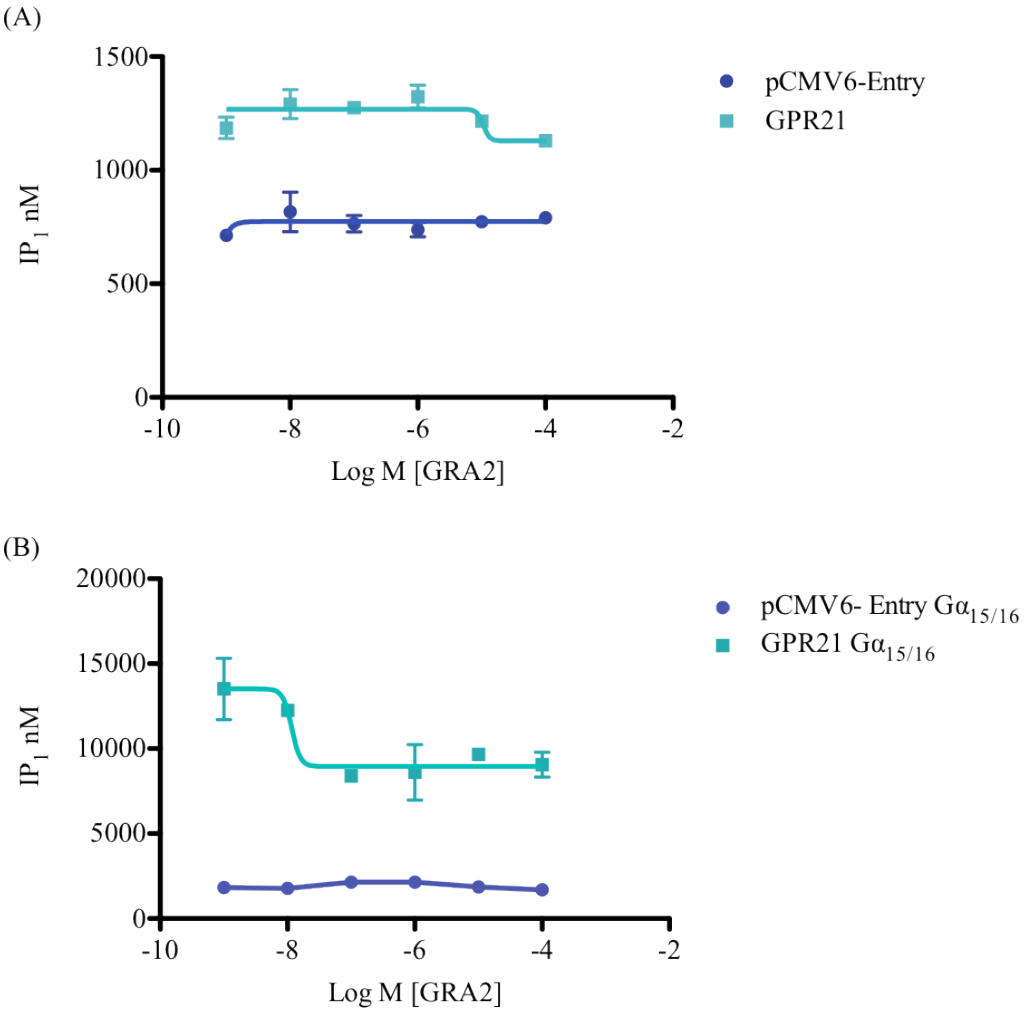

Figure 4.16 Dose response analysis of GRA2 on IP_1 production in HEK293T cells overexpressing GPR21.

HEK293T cells were transiently transfected with (A) GPR21 or pCMV6-Entry and (B) pCMV6-Entry coupled with $G\alpha_{15/16}$ or GPR21 coupled with $G\alpha_{15/16}$. After 24 hours cells were trypsinised and resuspended at a density of $6x10^6$ cells/ml in IP-one stimulation buffer. Cells were then incubated with the lead compound, GRA2 at various concentrations in IP-one stimulation buffer. IP_1 concentrations were extrapolated from an IP_1 standard curve and GraphPad Prism® 5 software was used to generate a non-linear sigmoidal dose response curve. Data presented as mean ± SEM are representative of two independent experiments performed in triplicate each time.

4.3.9 GRA2 Protects Against the Effects of GPR21 on the Insulin Signalling Pathway

To determine if the impact of this compound resonated through to the downstream effects of GPR21 on insulin signalling, transfected HEK293T cells were incubated with GRA2 for 24 hours followed by an acute insulin stimulation. In the presence of the vehicle control DMSO, HEK293T cells overexpressing GPR21 demonstrated significantly reduced phosphorylation of the insulin receptor in response to insulin when compared to cells transfected with the empty vector. Overexpression of GPR21 also diminished basal and insulin-stimulated phosphorylation of IRS1, Akt and AS160 at Thr^{642} and at Ser^{588} when compared to cells transfected with pCMV6-Entry. Conversely, cells overexpressing GPR21 incubated with 10 μM GRA2, demonstrated no negative impact on insulin-stimulated phosphorylation of its receptor, with the effect of insulin comparable to that of cells transfected with the empty vector. Cells overexpressing GPR21 treated with GRA2 also demonstrated a level of IRS1 and Akt activity similar to that displayed by cells transfected with pCMV6-Entry. Although treatment with GRA2 attenuated the effect of GPR21 on AS160 when compared to the DMSO control, the phosphorylation status of the protein at Thr^{642} and at Ser^{588} was still below that of cells transfected with the empty vector. HEK293T cells transfected with pCMV6-Entry also demonstrated a slight response to GRA2, in that phosphorylation of the components of the insulin signalling cascade increased somewhat (Fig. 4.17A).

A similar effect was observed in HEK293T cells co-transfected with GPR21 and $G\alpha_{15/16}$ (Fig. 4.17B). Phosphorylation of the insulin receptor, IRS1, Akt and AS160 at both critical residues were decreased in HEK293T cells expressing GPR21 coupled with $G\alpha_{15/16}$. In the presence of 10 μM GRA2, the effect of GPR21 on the insulin receptor, IRS1, Akt and AS160 at Thr^{642} was reduced. GRA2 also exhibited a positive action on control cells, marginally increasing the phosphorylation of the insulin receptor, IRS1 and AS160 at Thr^{642} in cells transfected with pCMV6-Entry coupled with $G\alpha_{15/16}$.

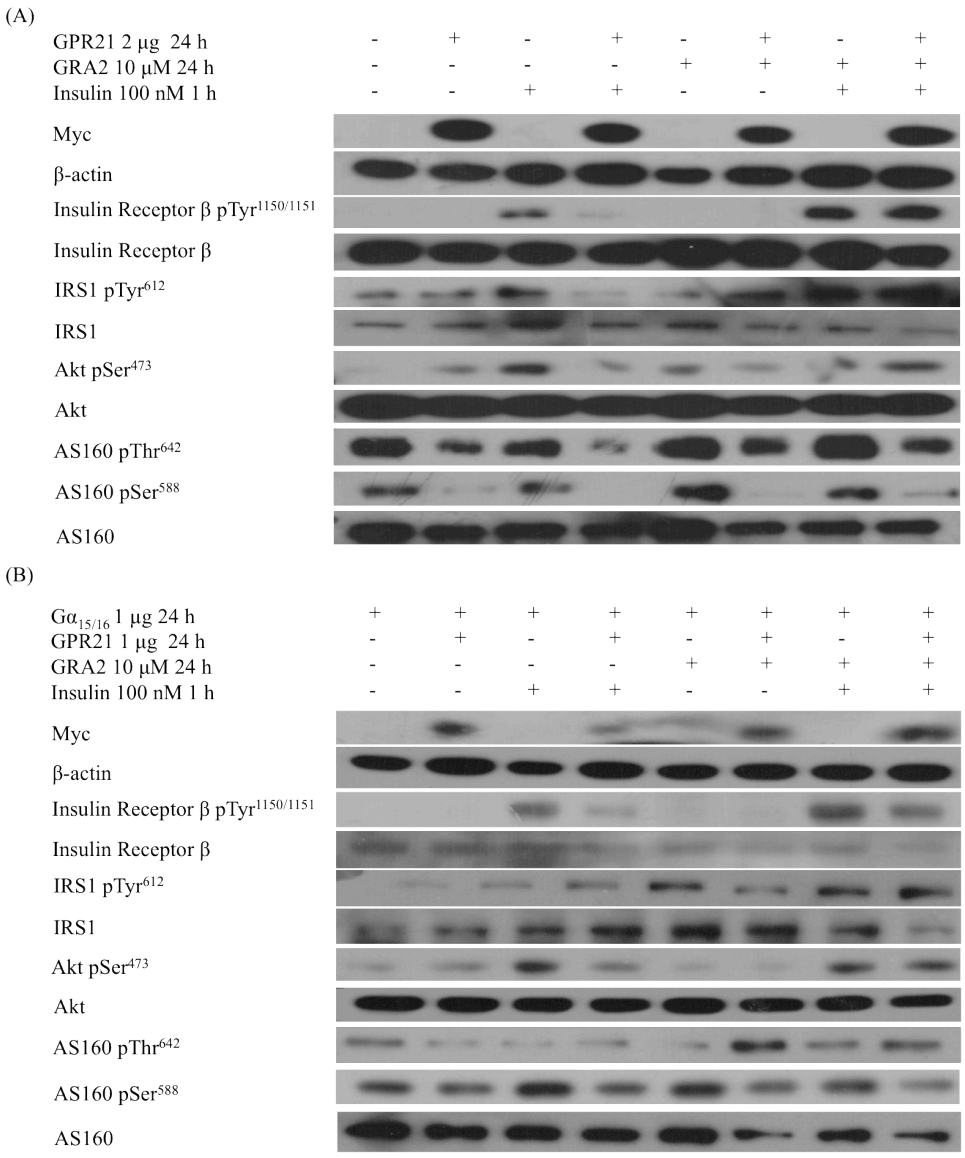

Figure 4.17 Western blot analysis of the effect of GRA2 on the insulin signalling pathway in HEK293T cells overexpressing GPR21.

HEK293T cells transiently transfected with (A) GPR21 or (B) GPR21 coupled with $G\alpha_{15/16.}$ Cells were stimulated with 10 µM GRA2 or an equal volume of DMSO in serum free complete medium for 24 hours. Cells were then stimulated with 100 nM insulin for 1 hour in KRBG, lysed and subjected to SDS-PAGE followed by immunoblotting with antibodies against phospho-insulin receptor β $Tyr^{1150/1151}$, phospho-IRS1 Tyr^{612}, phospho-Akt Ser^{473}, phospho-AS160 Thr^{642} and Ser^{588}, native insulin receptor β, IRS1, Akt and AS160. Myc was used to confirm GPR21 expression and β-actin was used as a loading control. Data are representative of two independent experiments.

These effects carried through to the downstream glucose uptake response. HEK293T cells transfected with pCMV6-Entry reacted positively to a 100 nM insulin stimulation with a comparable increase in glucose uptake observed in the presence of DMSO and 10 μM GRA2 (Fig. 4.18A). Conversely, cells expressing GPR21 demonstrated a reduction in basal glucose uptake in the presence of DMSO, and a reduced response to insulin. Treatment of HEK293T cells expressing GPR21 with 10 μM GRA2 for 24 hours led to a significant improvement in basal and insulin-stimulated glucose uptake.

In cells transfected with pCMV6-Entry coupled with $G\alpha_{15/16}$ a comparable outcome to the empty vector alone was detected. Cells overexpressing GPR21 with $G\alpha_{15/16}$ demonstrated reduced basal and insulin-stimulated glucose uptake. While 10 μM GRA2 improved glucose uptake in cells overexpressing GPR21 with $G\alpha_{15/16}$, the effect was not significant (Fig. 4.18B).

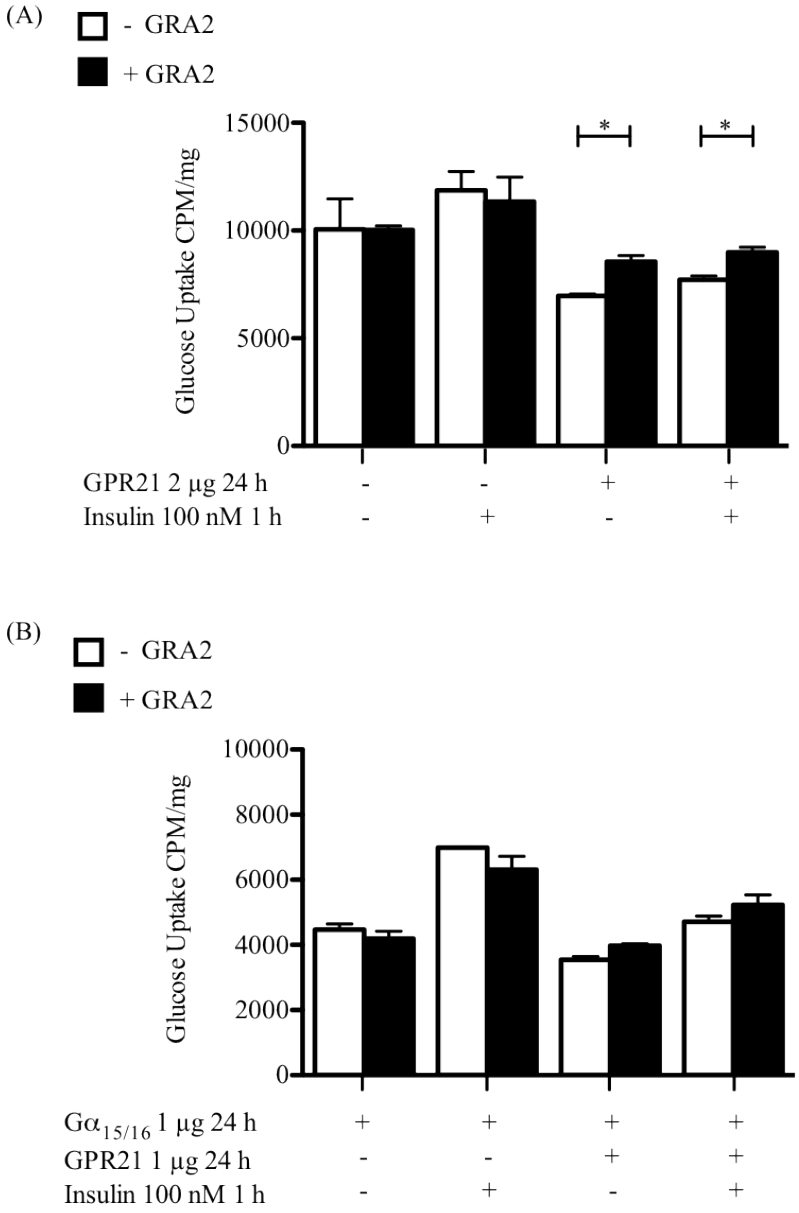

Figure 4.18 The effect of GRA2 on glucose uptake in HEK293T cells overexpressing GPR21.

HEK293T cells transiently transfected with (A) GPR21 or (B) GPR21 coupled with $G\alpha_{15/16}$ were incubated with 10 µM GRA2 or an equal volume of DMSO in serum free complete medium for 24 hours. Cells were then stimulated with 100 nM insulin for 1 hour in KRBG. The effect on glucose uptake was established by measuring cellular levels of [^{3}H]-2-deoxyglucose. Data presented as mean ± SEM are representative of two independent experiments. One-way ANOVA with a post-hoc Tukey test using GraphPad Prism® 5 software denotes significance at $p < 0.05$; *.

4.3.10 GPR21 induces Macrophage Migration

As GPR21 has been implicated in the promotion of macrophage infiltration into adipose tissue to encourage the genesis of type 2 diabetes (Osborn *et al.,* 2012), the effect of GPR21 overexpression in 3T3-L1 adipocytes and RAW 264.7 macrophages was investigated. Since 3T3-L1 adipocytes exhibited the highest native level of GPR21, the effect of augmented expression, through transfection, on 3T3-L1 conditioned medium to induce macrophage migration was investigated. Conditioned medium was harvested from 3T3-L1 adipocytes transfected with pCMV6-Entry, GPR21, and pCMV6-Entry or GPR21 coupled with $G\alpha_{15/16}$ in the presence and absence of GRA2. RAW 264.7 macrophages did not demonstrate a significant increase in migratory capacity in response to conditioned medium from 3T3-L1 adipocytes transfected with GPR21 or GPR21 coupled with $G\alpha_{15/16}$ (Fig. 4.19). The novel compound GRA2 similarly produced no effect on the migratory ability of the macrophages in this system.

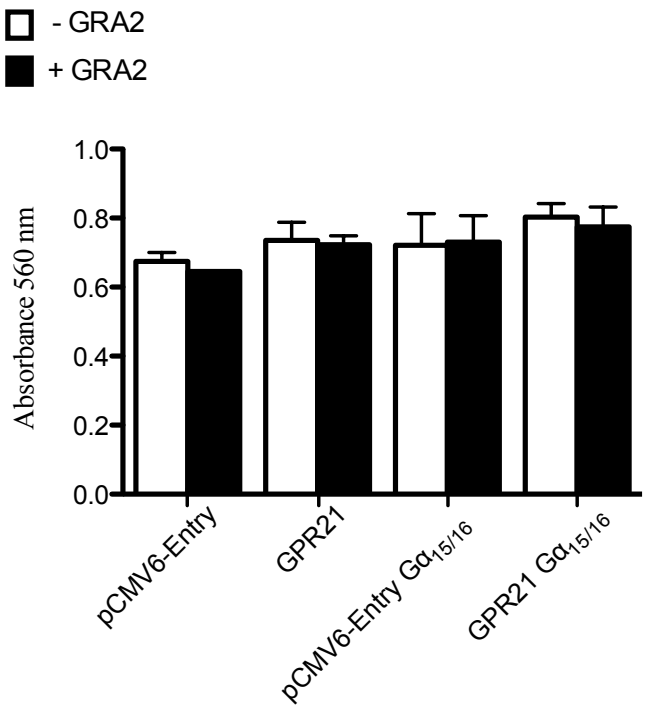

Figure 4.19 The effect of GPR21 on RAW 264.7 migration towards 3T3-L1 adipocyte conditioned medium.

3T3-L1 adipocytes were transiently transfected with pCMV6-Entry, GPR21, pCMV6-Entry coupled with $G\alpha_{15/16}$ or GPR21 coupled with $G\alpha_{15/16}$. Fully differentiated adipocytes were incubated with 10 µM GRA2 or DMSO for 24 hours to generate conditioned medium. RAW 264.7 macrophages were placed in a 5.0 µm Transwell® insert at a density of $5x10^5$ cells/ml in complete medium supplemented with 2 % (v/v) FBS and equilibrated in a 24 well plate with complete medium containing 2 % (v/v) FBS for 1 hour at 37 °C. Untransfected RAW 264.7 were allowed to migrate towards conditioned medium generated from transfected 3T3-L1 adipocytes displaying large lipid droplets ± 10 µM GRA2. After a 4 hour incubation at 37 °C, migratory cells were quantified as described in Section 2.7.5.

Given that GPR21 did not appear to influence the production of soluble factors to promote macrophage chemotaxis, the direct effect of the receptor on RAW 264.7 migration towards 3T3-L1 conditioned medium was evaluated. RAW 264.7 macrophages overexpressing GPR21 demonstrated an increased aptitude for migration, as did cells overexpressing GPR21 coupled with $G\alpha_{15/16}$. When RAW 264.7 cells were exposed to GRA2, the compound provoked a minor curtailment of GPR21-induced migration, whilst a significant decrease was observed in cells expressing GPR21 coupled with $G\alpha_{15/16}$ (Fig. 4.20A).

As JNK has been implicated in the process of macrophage accumulation in adipose tissue (Han *et al.,* 2013) and can be activated downstream of proteins involved in the promotion of cytoskeletal reorganisation to facilitate macrophage migration, the effect of GRA2 on GPR21-induced phosphorylation of JNK in RAW 264.7 macrophages was examined and was found to decrease in the presence of the novel compound (Fig. 4.20B).

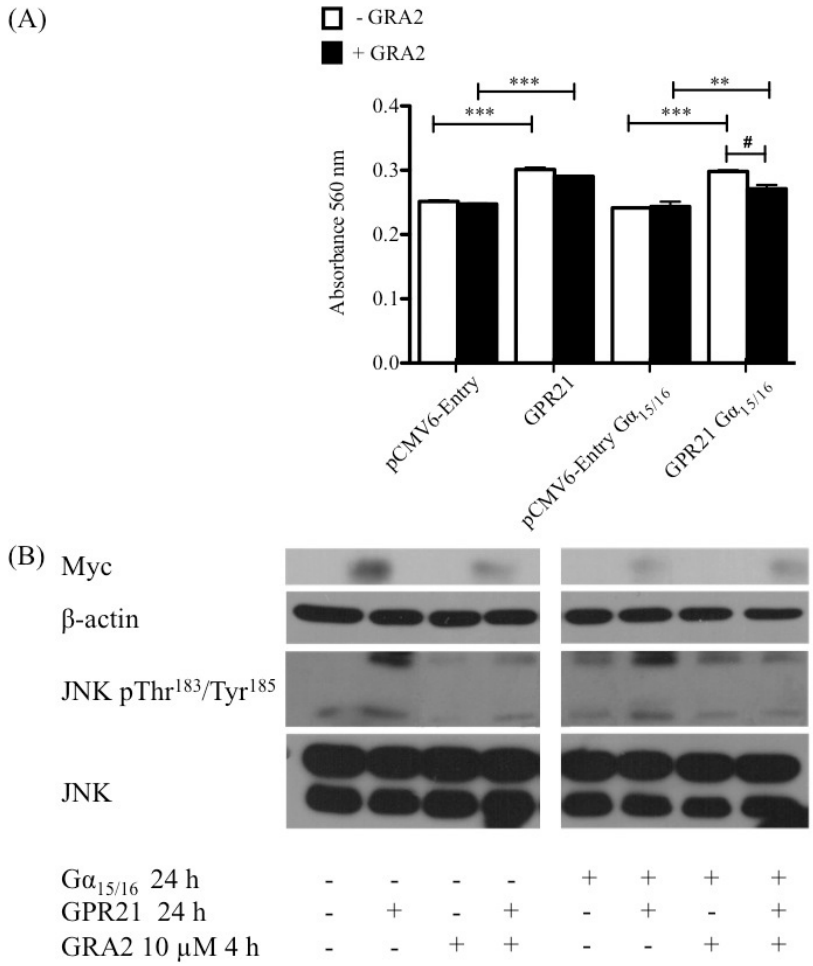

Figure 4.20 The direct effect of GRA2 on the migratory capacity of RAW 264.7 cells overexpressing GPR21.

RAW 264.7 macrophages were transfected with pCMV6-Entry, GPR21, pCMV6-Entry coupled with $G\alpha_{15/16}$ or GPR21 coupled with $G\alpha_{15/16}$. (A) After 24 hours cells were transferred into a 5.0 μm Transwell® insert and stimulated with 10 μM GRA2 in complete medium supplemented with 2 % (v/v) FBS then positioned into a 24 well plate containing 3T3-L1 conditioned medium. After a 4 hour incubation at 37 °C, migratory cells were quantified as described in Section 2.7.5. One-way ANOVA with a post-hoc Tukey test using GraphPad Prism® 5 software denotes a significant increase in migration at $p < 0.01$; ** and $p < 0.001$; ***. A significant decrease in migration is indicated at $p < 0.05$; $^{\#}$, n=3. (B) Alternatively, cells incubated with 10 μM GRA2 for 4 hours were lysed, subjected to SDS-PAGE and immunoblotted with antibodies against phospho-JNK Thr^{183}/Tyr^{185} and native JNK. Myc was used to confirm GPR21 expression and β-actin was used as a loading control.

4.4 Discussion

Analysis of the expression profile and signalling capabilities of GPR21 has given further insight into mechanisms by which this orphan GPCR may contribute to the development of the type 2 diabetic phenotype.

4.4.1 The Effects of Enhanced GPR21 Expression

Increased expression of GPR21 in the epididymal fat pads of wild type HFHS-fed mice was found to correlate with a rise in the macrophage marker F4/80, along with an increase in TNF-α expression. As well as being a marker gene for pro-inflammatory M1 type macrophages, TNF-α is known to contribute to the development of insulin resistance (Uysal *et al.,* 1997, Lumeng *et al.,* 2007). Western blot analysis of various cell lines demonstrated an abundance of GPR21 present in adipocytes whilst reduced expression of the receptor was found in the three macrophage cell lines tested. Although the adipocytes displayed the highest levels of GPR21, macrophages cannot be discounted as a source of the increased receptor expression in the epididymal fat pads of HFHS-fed mice as the macrophage cell lines investigated were not specifically polarised into either the M1 or M2 type subset. This differentiation may be significant as Osborn and colleagues (2012), observed a marked increase in GPR21 mRNA levels in M1 type macrophages when compared to M2 type macrophages. As the macrophage cell lines investigated were not polarised into either subset it is not possible to ratify unambiguously the source of the increased GPR21 expression in the HFHS-fed mice.

Confirming the signalling capabilities of GPR21 was fundamental to understanding the consequence of the observed increase in receptor expression. As studies indicate that GPR21 may signal through G_q type G protein α-subunits (Bresnick *et al.,* 2003, Xiao *et*

al., 2008), the effect of the receptor on IP_1 production was investigated. Analysis of this stable downstream metabolite of IP_3, which accumulates upon $G\alpha_q$ receptor activation, suggests that GPR21 overexpressed in HEK293T cells can adopt the active conformation necessary to couple and activate $G\alpha_q$ type G proteins. GPR21 was observed to stimulate this signal transduction in the absence of a ligand, a hallmark of a constitutively active receptor. Co-expression with the specific members of the $G\alpha_{q,}$ family revealed a functional interaction between GPR21 and $G\alpha_{15/16}$, as receptor-induced IP_1 production increased most significantly when co-transfected with $G\alpha_{15/16}$. Although the greatest increase in cellular IP_1 was observed in cells co-expressing GPR21 and $G\alpha_q$, this is believed to be a consequence of $G\alpha_q$ expression alone, as this protein provoked a significant increase in cellular IP_1 when expressed without the receptor. Incubation of transfected HEK293T cells with the PLC inhibitor, U73122, blocked GPR21-induced production of IP_1, confirming the selectivity of the effect of GPR21 on this signalling cascade.

4.4.2 The Downstream Consequences of $G\alpha_q$ Activation

The $G\alpha_q$ class of G proteins play a pivotal role in the regulation of many proteins central to the development of insulin resistance. In 3T3-L1 adipocytes $G\alpha_{q/11}$ has been shown to increase insulin-induced glucose uptake in a potentially PI3K dependent manner (Imamura *et al.,* 1999), while β-cell specific inactivation of the genes encoding $G\alpha_q$ and $G\alpha_{q/11}$ results in impaired glucose tolerance and insulin secretion in mice (Sassmann *et al.,* 2010). However, stimulation of the $G\alpha_q$ pathway by the prostaglandin receptor EP1, leads to MAPK activation and the production of pro-inflammatory cytokines involved in the genesis of insulin resistance such as IL-6 and TNF-α (Sun and Ye, 2012). Furthermore, studies with $G\alpha_{q/11}$ have demonstrated reduced insulin-induced

phosphorylation of Akt in HeLa cells overexpressing this G protein α-subunit (Ueda *et al.,* 2004). These results demonstrate that the influence of $G\alpha_q$ type G proteins on glucose homeostasis is not only receptor, but also cell specific.

Downstream of PLC, distinctive $G\alpha_q$ signalling systems have been found to activate the MAPKs; Erk, p38 and JNK (Naor *et al.,* 2000). Focusing on this pathway, GPR21 was found to significantly increase the phosphorylation of Erk, p38 and JNK in a PLC-dependent manner. However, in the presence of complete medium containing increasing concentrations of FBS, GPR21-induced phosphorylation of the MAPKs was attenuated, intimating the possibility of a native inverse agonist for the constitutively active receptor in the serum. JNK is known to negatively regulate insulin signalling and is abnormally elevated in dietary and genetic murine models of obesity (Hirosumi *et al.,* 2002). Possibly as a consequence of increased JNK activity, HEK293T cells overexpressing GPR21 displayed an impaired insulin signalling pathway, both basally and under insulin stimulation. The regulatory effect of FBS on GPR21 activity was carried through to this signalling cascade and the consequential effect on glucose uptake. In cells overexpressing both GPR21 and $G\alpha_{15/16}$ the effect of serum was reduced, suggesting that the increased activity of GPR21 when coupled with $G\alpha_{15/16}$ may lead to a "hyper activated" signalling pathway that may not easily subside in the presence of any potential regulatory factor in the serum. As increasing serum concentrations led to a decrease in IP_1 production and a decline in MAPK phosphorylation, it is possible that a regulatory ligand for GPR21 present in the serum also led to the reduced impact of the receptor on the insulin signalling pathway rather than it arising as a consequence of residual serum derived insulin.

4.4.3 The Potential of a Ligand for GPR21

The prospect of an endogenous inverse agonist suggests that the effect of GPR21 may be tightly regulated under normal physiological conditions and only becomes deleterious when uncontrolled, as in a state of obesity. The identification of natural ligands for orphan receptors, such as GPR21 may provide insight into the regulatory mechanism of the receptor as well as lead to the discovery of novel molecules not previously recognised as extracellular mediators. So-called reverse pharmacology has led to the deorphanisation of about 300 GPCRs and the discovery of several novel ligands (Chung, Funakoshi and Civelli, 2008). However, as this method can prove to be a lengthy and demanding endeavor, the onset of homology modelling and ligand docking studies has revitalised the drug discovery field, enabling high throughput screening of receptors (Flohr *et al.,* 2002, Evers and Klabunde, 2005, Kufareve *et al.,* 2011). Given the influence of GPR21 on insulin signalling, a molecule that binds GPR21 and blocks its constitutive activity in a similar manner to the prospective native ligand could be a very powerful new anti-diabetic therapy.

Constitutively active orphan GPCRs, such as GPR21 provide a direct route to drug discovery as their functionality can be understood without the need to identify endogenous ligands (Chalmers and Behan, 2002). Virtual screening of an in house model of GPR21 identified 11 hit compounds with the potential to bind the receptor. Of the 8 compounds screened *in vitro*, GRA2, demonstrated prospective abilities as an inverse agonist of GPR21 as it reduced IP_1 accumulation in HEK293T cells overexpressing the receptor. Unfortunately, this compound displayed reduced solubility at higher concentrations and the effect on IP_1 waned. The diminished effect on IP_1 production could also arise through β-arrestin-mediated internalisation of the ligand

bound-receptor, following prolonged incubation with a high concentration of the compound. Nevertheless, at the more soluble concentration of 10 μM GRA2 improved the signalling responses to insulin in cells overexpressing GPR21 and GPR21 coupled with $G\alpha_{15/16}$, following through to a modest restoration of glucose uptake. Cells transfected with the empty vector also displayed enhanced phosphorylation of the proteins involved in the insulin signalling cascade in response to GRA2. This may be as a consequence of the compound acting on native GPR21 expressed in HEK293T cells, obstructing the dampening effects of the receptor on the insulin signalling pathway.

4.4.4 The Role of GPR21 in Macrophage Migration

The marked effect of GPR21 on JNK activity was noteworthy, as increased expression of this MAPK in macrophage cells has been reported to promote HFD-induced accumulation of adipose tissue macrophages. Macrophage specific deletion of JNK has been observed to decrease the expression of macrophage marker genes, Cd68 and F4/80 in the adipose tissue of HFD-fed mice (Han *et al.,* 2013). Furthermore, Osborn and colleagues (2012), found markedly fewer adipose tissue macrophages in GPR21 knockout mice than in wild type counterparts, while GPR21 knockout macrophages also displayed reduced migration towards chemokine rich medium. Complementing this study, RAW 264.7 macrophages overexpressing GPR21 displayed an enhanced migratory capacity towards 3T3-L1 conditioned medium. Although Osborn and colleagues (2012), discovered fewer macrophages to migrate towards conditioned medium harvested from GPR21 knockout adipocytes, conditioned medium generated from 3T3-L1 adipocytes overexpressing GPR21 did not influence macrophage migration. The latter finding suggests GPR21 might not control macrophage migration

by upregulating the production of classical chemoattractants such as MCP-1 and LTB4 (Kamei *et al.,* 2006, Li *et al.,* 2015). It may therefore be plausible to speculate that GPR21 could be a novel control point coordinating, amongst other possibilities, the rearrangement of the actin cytoskeleton to promote macrophage migration into adipose tissue.

A range of extracellular signals are known to induce cytoskeletal reorganisation to mediate cellular chemotaxis through GPCRs, receptor tyrosine kinases, PI3K isoforms and small GTPases (Jones, 2000). The activation of small GTPases controls cell migration through the regulation of the actin cytoskeleton and the MAPK pathways (Hall, 1998). The MAPKs JNK, Erk and p38 have all been observed play crucial roles in cell migration as the inhibition of these proteins can prevent migration in many cell types (Huang, Jacobson and Schaller, 2004). Notably, the Rho family of small GTPases have been found to signal downstream of $G\alpha_q$ (Seasholtz, Majumdar and Brown, 1999, Chikumi *et al.*, 2002, Vogt *et al.*, 2003). Moreover, $G\alpha_q$ deficient neutrophils and dendritic cells display reduced chemotactic responses (Shi *et al.,* 2007). PKC isoforms, which can be activated downstream of the $G\alpha_q$ family, have been found to directly associate with microfilaments (Larsson, 2006) and regulate focal adhesion components (Fogh *et al.,* 2014), to mediate cytoskeleton changes that facilitate cell migration. It may be plausible to speculate that GPR21 could promote cytoskeletal reorganisation through its action on $G\alpha_{15/16}$, leading to the observed increase in RAW 264.7 migration. This reinforces the findings of Osborn and colleagues (2012), who demonstrated that GPR21 knockout macrophages did not undergo crucial cytoskeletal rearrangements to promote transmigration.

The direct effect of GRA2 in attenuating GPR21-promoted migration reinforces the

hypothesis that it may have the ability to act as an anti-diabetic therapy. Strengthening the potential of GRA2-related inhibition of GPR21-induced JNK activation, macrophage specific JNK deficiency has been shown to prevent the accumulation of adipose tissue macrophages expressing the M1 surface markers $CD11c^+$ and $CD206^-$ and to reduce the expression of genes associated with M1 polarisation; CD11c, IL-1β, Il-6, NOS2, TNF-α (Han *et al.,* 2013). Analysis of macrophage cell surface markers following GPR21 overexpression and GRA2 treatment may give further insight into whether the receptor may also influence macrophage polarisation to the pro-inflammatory M1 subset and if this novel compound may have a regulatory impact. Taken together, these results demonstrate the pivotal role GPR21 signal transduction through $G\alpha_{15/16}$ may play in the development of type 2 diabetes, giving insight into a novel means of controlling adipose tissue macrophage accumulation.

4.4.5 Summary

Under normal physiological conditions, this constitutively active GPCR may be tightly regulated to facilitate macrophage migration in reaction to an antigen driven immune response. However, obesity-induced type 2 diabetes potentially dysregulates GPR21; an increase in GPR21 expression, an increase in an endogenous agonist or a reduction in an inverse agonist could all exacerbate the effects of this receptor. Downstream of $G\alpha_{15/16}$, the potentiated pro-inflammatory signal activates the MAPKs, inhibits the insulin signalling pathway and may promote macrophage migration through the induction of cytoskeletal reorganisation (Fig. 4.21). Whatever the primary cause of the GPR21 effect *in vivo*, an inverse agonist such as the one identified in this study could restore the signalling potential of insulin to reinstate normal glucose homeostasis. Structure-activity relationship studies of the identified compound should yield

compounds with increased affinity for the receptor and hence increased biological efficacy to curtail the development of type 2 diabetes.

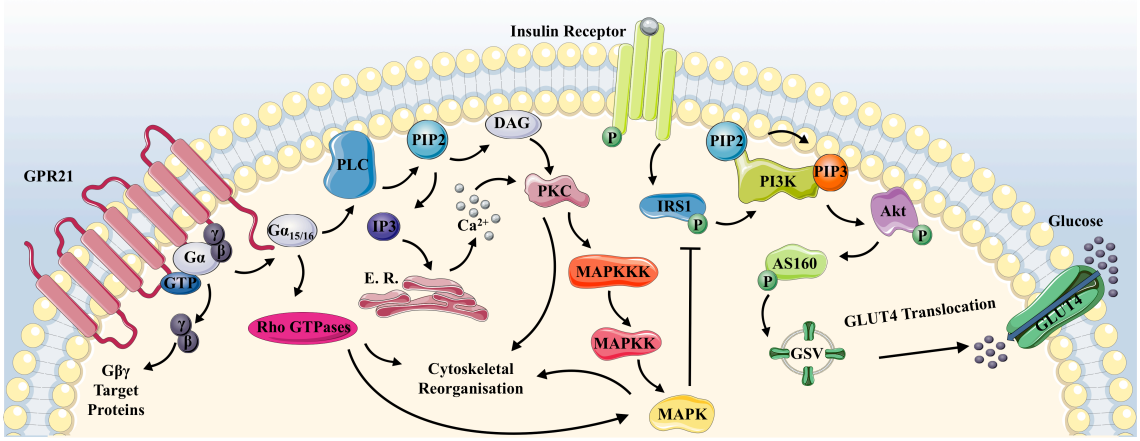

Figure 4.21 Proposed role of GPR21 in the development of type 2 diabetes.

The constitutively active GPR21 recruits and activates $G\alpha_{15/16}$, which facilitates the hydrolysis of PIP_2 into DAG and IP_3 through the action of PLC. Both DAG and IP_3 activate PKC, which signals to and activates the MAPK cascade. PKC has also been implicated in the promotion of cytoskeletal reorganisation to stimulate cell migration. $G\alpha_q$ proteins have been found to activate the Rho family of small GTPases that stimulate the activity of the MAPKs and regulate intracellular actin dynamics to promote cell migration, among other functions. Activated JNK has been proposed to promote macrophage accumulation in adipose tissue and is known to phosphorylate IRS1 of the insulin signalling cascade at Ser^{307} preventing insulin-induced tyrosine phosphorylation of its substrate. Due to the potential of a native inverse agonist in serum, the pro-inflammatory signal transduction of GPR21 is believed to be tightly regulated under normal physiological conditions. However in a state of obesity, GPR21 activity is uncontrolled and becomes deleterious, promoting macrophage migration into adipose tissue and insulin resistance, potentially through the action of JNK.

Chapter 5

Discussion

5.1 Synopsis

Type 2 diabetes is a complex metabolic condition provoked primarily by obesity-induced insulin resistance. Distinct routes may be taken to attenuate the pathophysiology of this condition, such as augmenting key metabolic regulators to overturn the damaging effects of insulin resistance and directly targeting the root cause, which many believe to be obesity-induced inflammation. The work undertaken in this project has aided in resolving the mechanism of action of a successful anti-diabetic compound, RTC-1 and has given insight into the underlying mechanisms by which the novel diabetic target, GPR21 exerts its effects. Although the original aims of this project were achieved, several questions surfaced over the course of this study, which warrant further investigation.

5.2 Cellular Effects of RTC-1

The ability of RTC-1 to inhibit RBP binding, the purpose for which it was designed, may have contributed to the dramatic effect of the compound on insulin sensitivity *in vivo*. However, as a result of this study the anti-diabetic and anti-obesity effects of RTC-1 have been largely attributed to the activation of AMPK as a consequence of the inhibition of NADH:ubiquinone oxidoreductase. Although the inhibition of the mitochondrial respiratory chain was traditionally believed to be detrimental to the cell (Degli Esposti, 1998), more recent studies have illustrated over-activation of mitochondria as a potential risk for insulin resistance, suggesting the protective benefits of inhibition (Pospisilik *et al.,* 2007, Vernochet *et al.,* 2012, Quintens *et al.,* 2013). RTC-1 demonstrated a superior effect to metformin in this regard, which may lie with the structural differences of the compounds. Metformin is largely hydrophilic and reliant on organic cation transporters to enter the cell (Rena *et al.,* 2013), while the

lipophilic properties of RTC-1 allow easier target engagement. The compounds may also occupy distinctive regions of the mitochondrial respiratory chain to alter cellular energy balance. Studies by Wheaton and colleagues (2014), found metformin to reversibly inhibit mitochondrial NADH:ubiquinone oxidoreductase. Although the exact binding site remains unknown, this group have speculated that metformin does not act on the same site as the irreversible NADH:ubiquinone oxidoreductase inhibitor rotenone, as metformin did not substantially increase H_2O_2 release from mitochondria, whereas rotenone augmented this significantly. Recently, Madiraju and colleagues (2014), observed that metformin bound non-competitively to an intermediate mitochondrial respiratory chain component, mitochondrial glycerophosphate dehydrogenase (mGPD). mGPD controls cytoplasmic NADH levels and is involved in lipid and glucose synthesis (Mráček *et al.,* 2013), thereby providing an alternative mode by which metformin may exert its downstream effects. Based on some structural similarities to ubiquinone, RTC-1 could possibly bind the ubiquinone cleft of NADH:ubiquinone oxidoreductase to reduce the activity of the complex. Molecular docking and binding simulations may give further insight into the binding capacity of RTC-1. In addition to the observed consequential effects on glucose uptake and lipid synthesis, RTC-1 may also elicit long-term beneficial effects on dysregulated pancreatic β-cells through AMPK-induced autophagy (Quan *et al.,* 2012, Rubinsztein *et al.,* 2012). Analysis of an autophagy marker, such as the microtubule-associated protein 1 light chain 3, may help to ascertain whether RTC-1-induced activation of AMPK also promotes autophagy.

Although more potent than metformin, the prospect of RTC-1 inducing the rare, yet most damaging physiological condition associated with metformin, lactic acidosis, is

unlikely. RTC-1 does not impair the process of oxidative phosphorylation entirely, as oxygen consumption can be restored with the addition of the succinate:ubiquinone oxidoreductase substrate. Free protons resulting from ATP hydrolysis can, therefore, be processed, albeit less efficiently, reducing the possibility of acidosis. Furthermore, metformin-induced lactic acidosis may not exclusively arise as a consequence of NADH:ubiquinone oxidoreductase inhibition. The effect of metformin on mGPD may contribute to the development of lactic acidosis, as this disrupts the conversion of lactate to glucose. Moreover, high therapeutic levels of metformin have been observed to reduce lactate clearance by the liver (Lalau *et al.,* 2015). Nevertheless, the effect of RTC-1 on lactate production should be investigated as this compound is explored as a novel anti-diabetic therapy.

While the superior effect of RTC-1 on glucose uptake may be attributed to the enhanced action on NADH:ubiquinone oxidoreductase to promote AMPK activation, the influence of RTC-1-induced phosphorylation of Akt cannot be discounted as a contributory factor. As RTC-1 demonstrated no effect on the major regulator of Akt activity, PI3K, it is possible that RTC-1-stimulated decreases in ATP levels may prevent IP6K-induced IP_7 synthesis to relieve the inhibitory effect of this inositol pyrophosphate on Akt activation. The effects of the IP6K inhibitor, TNP, further support this concept, as it has been observed to enhance Akt, AMPK and ACC phosphorylation, however, this compound demonstrates no inhibitory effect on NADH:ubiquinone oxidoreductase activity (Sun *et al.,* 2015). TNP also reduces 3T3-L1 adipogenesis (Chakraborty *et al.,* 2010), although this impact does not approach the effectiveness of RTC-1, emphasising the potential of this novel compound. HPLC analysis of cellular IP_7 levels will give further insight as to whether this is a mechanism

by which RTC-1 may augment Akt activation and improve insulin sensitivity (Saiardi *et al.,* 2002). Furthermore, the inhibition of IP_7 associated with the IP6K inhibitor, TNP, has been observed to improve cardiac function, a notable outcome as mitochondrial dysfunction associated with insulin resistance can promote the development of cardiovascular diseases, the leading cause of death among patients with diabetes (Sun *et al.,* 2015). If studies demonstrate that RTC-1 modulates intracellular IP_7 levels, it would be interesting to determine if cardiomyocyte apoptosis can also be regulated.

5.3 GPR21 Signal Transduction

Although G_q coupled GPCRs are usually stimulatory towards insulin, it is clear the influence of these proteins cannot be generalised, given that the G_q coupled gonadotropin releasing hormone receptor has been observed to inhibit insulin release from rat islets (Amisten *et al.,* 2013). In this study the G_q coupled GPCR, GPR21, was found to be a constitutively active receptor that promoted macrophage migration and the activation of the MAPKs, which can negatively impact on the insulin signalling pathway. Expression of this receptor was observed to be upregulated in HFHS-fed mice and correlated with an increase in epididymal fat pad macrophages, consistent with a role for this receptor in obesity-associated type 2 diabetes. Intriguingly, the effects of GPR21 on MAPK activation and insulin signalling could be attenuated with increasing concentrations of serum, advocating the potential of an endogenous regulatory ligand for the receptor. Employing GPR21 induced IP_1 production as a functional screen for fractionated serum samples, followed by mass spectrometry analysis of those that attenuate GPR21 activity may assist in the identification of this regulatory ligand. Furthermore, analysis of the effects of diabetic serum on GPR21 activity may give insight into the role of this receptor in the development of type 2 diabetes.

The adverse contributions of visceral adipose tissue inflammation to the progression of type 2 diabetes are stark. Unsurprisingly, therefore, the prospect of targeting inflammatory mediators to arrest the pathogenesis of this condition has gained significant attention. Initial studies with the IL-1 receptor antagonist, anakinra, demonstrated the beneficial effects of an anti-inflammatory agent on insulin resistance as a reduction in inflammatory markers correlated with an extended improvement in insulin action. Although adverse effects occurred with the daily injections of anakinra, the benefits of targeting inflammation to regulate insulin resistance have been realised and antagonists for IL-1β are currently under investigation (Donath, 2014).

Virtual screening of an in house homology model of GPR21 led to the identification a novel compound, GRA2, with potential anti-diabetic properties as it was found to attenuate the downstream effects of the constitutively active GPCR on macrophage migration and JNK activation. Targeting macrophage infiltration into adipose tissue has the potential to slow the progressive decline in insulin secretion and responsiveness associated with type 2 diabetes. In a phase 2 clinical trial, Hanefeld and colleagues (2012), found promise with the MCP-1 receptor antagonist in this regard, as glycated haemoglobin levels were seen to decrease in obese type 2 diabetic patients. It remains unclear if GPR21-related JNK activation promotes migration or if it could be activated as a consequence of another mediator of cytoskeletal reorganisation. F-actin staining of GPR21-overexpressing RAW 264.7 macrophages may reveal if GPR21-induced signal transduction promotes cytoskeletal reorganisation to form the branched morphology necessary for migration. Furthermore, treatment of macrophages overexpressing GPR21 with specific inhibitors for proteins downstream of $G\alpha_q$ signalling that have been found to regulate cell migration, such as PKC (Inhibitor-calphostin C) may give further insight into the role GPR21 plays in macrophage migration.

Nevertheless, GRA2 holds promise as an anti-diabetic agent, as along with regulating migration and JNK phosphorylation in RAW 264.7 macrophages, it also counteracted the effects of GPR21 to augment insulin signalling and glucose uptake. Although there are currently no anti-diabetic therapies marketed to regulate JNK activity, the effects of the insulin sensitising thiazolidinedione, rosiglitazone may also involve the modulation of this kinase. Díaz-Delfín, Morales and Caelles (2007), found rosiglitazone to inhibit the elevated JNK activity associated with obesity to restore insulin-induced IRS1 tyrosine phosphorylation. Modulating JNK activity to restore insulin sensitivity is therefore a promising tactic to target type 2 diabetes and may account for the underlying *in vitro* effects of GRA2 on GPR21-induced insulin resistance. Analysis of the effects of GPR21 overexpression in JNK deficient cells may reveal if the impact of the receptor on migration and insulin signalling are dependent on the MAPK. Furthermore, the analysis of other key negative regulators of insulin signalling, namely IKKβ and SOCS3, in response to GPR21 overexpression would help consolidate the influence of this receptor in the development of insulin resistance.

5.4 Conclusion

The work presented in this thesis has contributed to a better understanding of the ways in which the type 2 diabetic phenotype may be regulated. Given the complexity of the factors contributing to the development of this condition, an amalgamation of therapies directed at versatile targets, such as those discussed in this study, may be the best approach to treat type 2 diabetes.

Chapter 6

Bibliography

Aguirre, V., Uchida, T., Yenush, L., Davis, R., and White, M. F., 2000. The c-Jun NH_2-terminal kinase promotes insulin resistance during association with insulin receptor substrate-1 and phosphorylation of Ser^{307}. *The Journal of Biological Chemistry*, 275 (12), 9047–9054.

Ahmed, K., Tunaru, S., Langhans, C. D., Hanson, J., Michalski, C. W., Kölker, S., Jones, P. M., Okun, J. G., and Offermanns, S., 2009. Deorphanization of GPR109B as a receptor for the β-oxidation intermediate 3-OH-octanoic acid and its role in the regulation of lipolysis. *The Journal of Biological Chemistry*, 284 (33), 21928–21933.

Ahn, J., Lee, H., Kim, S., Park, J., and Ha, T., 2008. The anti-obesity effect of quercetin is mediated by the AMPK and MAPK signaling pathways. *Biochemical and Biophysical Research Communications*, 373 (4), 545–549.

Alers, S., Loffler, A. S., Wesselborg, S., and Stork, B., 2012. Role of AMPK-mTOR-Ulk1/2 in the Regulation of Autophagy: Cross Talk, Shortcuts, and Feedbacks. *Molecular and Cellular Biology*, 32 (1), 2–11.

Altschul, S. F., Gish, W., Miller, W., Myers, E. W., and Lipman, D. J., 1990. Basic local alignment search tool. *Journal of Molecular Biology*, 215 (3), 403–410.

Amisten, S., Salehi, A., Rorsman, P., Jones, P. M., and Persaud, S. J., 2013. An atlas and functional analysis of G-protein coupled receptors in human islets of Langerhans. *Pharmacology and Therapeutics*, 139 (3), 359–391.

Armour, K. E., Armour, K. J., Gallagher, M. E., Gödecke, A., Helfrich, M. H., Reid, D. M., and Ralston, S. H., 2001. Defective bone formation and anabolic response to exogenous estrogen in mice with targeted disruption of endothelial nitric oxide synthase. *Endocrinology*, 142 (2), 760–766.

Aronoff, S. L., Berkowitz, K., Shreiner, B., and Want, L., 2004. Glucose Metabolism and Regulation: Beyond Insulin and Glucagon. *Diabetes Spectrum*, 17 (3), 183–190.

Ayala, J. E., Bracy, D. P., James, F. D., Burmeister, M. A., Wasserman, D. H., and Drucker, D. J., 2010. Glucagon-like peptide-1 receptor knockout mice are protected from high-fat diet-induced insulin resistance. *Endocrinology*, 151 (10), 4678–4687.

Bailey, C. J., Path, M. R. C., and Turner, R. C., 1996. Metformin. *The New England Journal of Medicine*, 334 (9), 547–579.

Bando, H., 2005. Phosphorylation of the 6-Phosphofructo-2-Kinase/Fructose 2,6-Bisphosphatase/PFKFB3 Family of Glycolytic Regulators in Human Cancer. *Clinical Cancer Research*, 11 (16), 5784–5792.

Bechtold, D. A., Sidibe, A., Saer, B. R. C., Li, J., Hand, L. E., Ivanova, E. A., Darras, V. M., Dam, J., Jockers, R., Luckman, S. M., and Loudon, A. S. I., 2012. A role for the melatonin-related receptor GPR50 in leptin signaling, adaptive thermogenesis, and torpor. *Current Biology*, 22 (1), 70–77.

Becker-Zimmermann, K., Berger, M., Berchtold, P., Gries, F. A., Herberg, L., and Schwenen, M., 1982. Treadmill training improves intravenous glucose tolerance and insulin sensitivity in fatty Zucker rats. *Diabetologia*, 22 (6), 468–474.

van Bennekum, A. M., Wei, S., Gamble, M. V, Vogel, S., Piantedosi, R., Gottesman, M., Episkopou, V., and Blaner, W. S., 2001. Biochemical Basis for Depressed Serum Retinol Levels in Transthyretin-deficient Mice. *The Journal of Biological Chemistry*, 276 (2), 1107–1113.

Berridge, M. J. and Irvine, R. F., 1984. Inositol trisphosphate, a novel second messenger

in cellular signal transduction. *Nature*, 312 (5992), 315–321.

Berry, D. C. and Noy, N., 2012. Signaling by vitamin A and retinol-binding protein in regulation of insulin responses and lipid homeostasis. *Biochimica et Biophysica Acta*, 1821 (1), 168–76.

Bhattacharya, S., Lam, A. R., Li, H., Balaraman, G., Niesen, M. J. M., and Vaidehi, N., 2013. Critical Analysis of the Successes and Failures of Homology Models of G-protein coupled receptors: Homology modeling of GPCRs: Success and failures. *Proteins*, 81 (5), 729–739.

Biovia Software Inc., Discovery Studio Modeling Environment, Release 2.5, San Diego: Accelrys Software Inc., 2007.

Birnbaumer, L., Abramowitz, J., and Brown, A. M., 1990. Receptor-effector coupling by G proteins. *Biochimica et Biophysica Acta*, 1031 (2), 163–224.

Bjursell, M., Gerdin, A. K., Jönsson, M., Surve, V. V., Svensson, L., Huang, X. F., Törnell, J., and Bohlooly-Y, M., 2006a. G protein-coupled receptor 12 deficiency results in dyslipidemia and obesity in mice. *Biochemical and Biophysical Research Communications*, 348 (2), 359–366.

Bjursell, M., Gerdin, A., Ploj, K., Svensson, D., Svensson, L., Oscarsson, J., Snaith, M., Törnell, J., and Bohlooly-Y, M., 2006b. Malanin-Concentrating Hormone Receptor 1 deficiency Increases Insulin Sensitivity in Obese Leptin Defieient Mice Without Affecting Body Weight. *Diabetes*, 55 (3), 725–733.

Bouvier, M., 2013. Unraveling the structural basis of GPCR activation and inactivation. *Nature Structural and Molecular Biology*, 20 (5), 539–41.

Bresnick, J. N., Skynner, H. A., Chapman, K. L., Jack, A. D., Zamiara, E., Negulescu,

P., Beaumont, K., Patel, S., and McAllister, G., 2003. Identification of signal transduction pathways used by orphan G protein-coupled receptors. *Assay Drug Dev Technol*, 1 (2), 239–249.

Bridges, H. R., Jones, A. J. Y., Pollak, M. N., and Hirst, J., 2014. Effects of metformin and other biguanides on oxidative phosphorylation in mitochondria. *The Biochemical Journal*, 487, 475–487.

Bultot, L., Guigas, B., Von Wilamowitz-Moellendorff, A., Maisin, L., Vertommen, D., Hussain, N., Beullens, M., Guinovart, J. J., Foretz, M., Viollet, B., Sakamoto, K., Hue, L., and Rider, M. H., 2012. AMP-activated protein kinase phosphorylates and inactivates liver glycogen synthase. *The Biochemical Journal*, 443 (1), 193–203.

Cai, D., Yuan, M., Frantz, D. F., Melendez, P. A., Hansen, L., Lee, J., and Shoelson, S. E., 2005. Local and systemic insulin resistance resulting from hepatic activation of IKK-β and NF-κB. *Nature Medicine*, 11 (2), 183–90.

Cai, T. Q., Ren, N., Jin, L., Cheng, K., Kash, S., Chen, R., Wright, S. D., Taggart, A. K. P., and Waters, M. G., 2008. Role of GPR81 in lactate-mediated reduction of adipose lipolysis. *Biochemical and Biophysical Research Communications*, 377 (3), 987–991.

Campos-Sandoval, J. A., Redondo, C., Kinsella, G. K., Pal, A., Jones, G., Eyre, G. S., Hirst, S. C., and Findlay, J. B. C., 2011. Fenretinide derivatives act as disrupters of interactions of serum retinol binding protein (sRBP) with transthyretin and the sRBP receptor. *Journal of Medicinal Chemistry*, 54, 4378–4387.

Carbone, F., La Rocca, C., and Matarese, G., 2012. Immunological functions of leptin and adiponectin. *Biochimie*, 94 (10), 2082–2088.

Carey, A. L., Steinberg, G. R., Macaulay, S. L., Thomas, W. G., Holmes, A. G.,

Ramm, G., Prelovsek, O., Hohnen-Behrens, C., Watt, M. J., James, D. E., Kemp, B. E., Pedersen, B. K., and Febbraio, M. A., 2006. Interleukin-6 Increases Insulin-Stimulated Glucose Disposal in Humans and Glucose Uptake and Fatty Acid Oxidation *In Vitro* via AMP-Activated Protein Kinase. *Diabetes*, 55 (10), 2688–2697.

Carling, D. and Viollet, B., 2015. Beyond Energy Homeostasis: the Expanding Role of AMP-Activated Protein Kinase in Regulating Metabolism. *Cell Metabolism*, 21 (6), 799–804.

Chakraborty, A., Koldobskiy, M. A., Bello, N. T., Maxwell, M., Potter, J. J., Juluri, K. R., Maag, D., Kim, S., Huang, A. S., Dailey, M. J., Saleh, M., Snowman, A. M., Moran, T. H., Mezey, E., and Snyder, S. H., 2010. Inositol pyrophosphates inhibit Akt signaling, thereby regulating insulin sensitivity and weight gain. *Cell*, 143 (6), 897–910.

Chalmers, D. T. and Behan, D. P., 2002. The use of constitutively active GPCRs in drug discovery and functional genomics. *Nature Reviews Drug Discovery*, 1 (8), 599–608.

Chamorro, S., Della-Zuana, O., Fauchere, J. L., Feletou, M., Galizzi, J. P., and Levens, N., 2002. Appetite suppression based on selective inhibition of NPY receptors. *International Journal of Obesity*, 26 (3), 281–298.

Chan, A. S. L. and Wong, Y. H., 2004. Gβγ signaling and Ca^{2+} mobilization co-operate synergistically in a Sos and Rac-dependent manner in the activation of JNK by Gq-coupled receptors. *Cellular Signalling*, 16 (7), 823–836.

Chan, T. O., Zhang, J., Rodeck, U., Pascal, J. M., Armen, R. S., Spring, M., Dumitru, C. D., Myers, V., Li, X., Cheung, J. Y., and Feldman, A. M., 2011. Resistance of Akt

kinases to dephosphorylation through ATP-dependent conformational plasticity. *Proceedings of the National Academy of Sciences of the United States of America*, 108 (46), E1120–E1127.

Chappell, J. B. and Hansford, R. G., 1972. Preparation of mitochondria from animal tissues and yeasts. *Subcellular Components: Preparation and Fractionation*, 77–91.

Chawla, A., Nguyen, K. D., and Goh, Y. P. S., 2012. Macrophage-mediated inflammation in metabolic disease. *Nature Reviews Immunology*, 11 (11), 738.

Chen, D., Liu, X., Zhang, W., and Shi, Y., 2012. Targeted inactivation of GPR26 leads to hyperphagia and adiposity by activating AMPK in the hypothalamus. *PLoS ONE*, 7 (7), 1–10.

Chen, L., Magliano, D. J., and Zimmet, P. Z., 2012. The worldwide epidemiology of type 2 diabetes mellitus-present and future perspectives. *Nature Reviews Endocrinology*, 8 (4), 228–236.

Cherezov, V., Rosenbaum, D. M., Hanson, M. A., Rasmussen, S. G. F., Thian, F. S., Kobilka, T. S., Choi, H. J., Kuhn, P., Weis, W. I., Kobilka, B. K., and Stevens, R. C., 2007. High-resolution crystal structure of an engineered human β2-adrenergic G protein-coupled receptor. *Science*, 318 (5854), 1258–1265.

Chidiac, P., Hebert, T. E., Valiquette, M., Dennis, M., and Bouvier, M., 1994. Inverse agonist activity of β-adrenergic antagonists. *Molecular Pharmacology*, 45, 490–499.

Chikumi, H., Vázquez-Prado, J., Servitja, J. M., Miyazaki, H., and Silvio Gutkind, J., 2002. Potent activation of RhoA by Gαq and Gq-coupled receptors. *The Journal of Biological Chemistry*, 277 (30), 27130–27134.

Chruscinski, A. J., Rohrer, D. K., Schauble, E., Desai, K. H., Bernstein, D., and Kobilka, B. K., 1999. Targeted disruption of the β2 adrenergic receptor gene. *The Journal of Biological Chemistry*, 274 (24), 16694–16700.

Chung, S., Funakoshi, T., and Civelli, O., 2008. Orphan GPCR research. *British Journal of Pharmacology*, 153, S339–S346.

Codoñer-Franch, P. and Alonso-Iglesias, E., 2015. Resistin: Insulin resistance to malignancy. *Clinica Chimica Acta*, 438, 46–54.

Colca, J. R., McDonald, W. G., Cavey, G. S., Cole, S. L., Holewa, D. D., Brightwell-Conrad, A. S., Wolfe, C. L., Wheeler, J. S., Coulter, K. R., Kilkuskie, P. M., Gracheva, E., Korshunova, Y., Trusgnich, M., Karr, R., Wiley, S. E., Divakaruni, A. S., Murphy, A. N., Vigueira, P. A., Finck, B. N., and Kletzien, R. F., 2013. Identification of a Mitochondrial Target of Thiazolidinedione Insulin Sensitizers (mTOT)—Relationship to Newly Identified Mitochondrial Pyruvate Carrier Proteins. *PLoS ONE*, 8 (5), e61551.

Colca, J. R., McDonald, W. G., and Kletzien, R. F., 2014. Mitochondrial target of thiazolidinediones. *Diabetes, Obesity and Metabolism*, 16 (11), 1048–1054.

Contreras-Alcantara, S., Baba, K., and Tosini, G., 2010. Removal of melatonin receptor type 1 induces insulin resistance in the mouse. *Obesity*, 18 (9), 1861–1863.

Cordonier, E., Jarecke, S., Hollinger, F., and Zempleni, J., 2015. Inhibition of acetyl-CoA carboxylase activity prevents adipocyte differentiation in 3T3-L1 cells. *The FASEB Journal*, 29, 750-753.

Corton, J. M., Gillespie, J. G., and Hardie, D. G., 1994. Role of the AMP-activated protein kinase in the cellular stress response. *Current Biology*, 4 (4), 315–324.

Corton, J. M., Gillespie, J. G., Hawley, S. A., and Hardie, D. G., 1995. 5-aminoimidazole-4-carboxamide ribonucleoside. A specific method for activating AMP-activated protein kinase in intact cells? *European Journal of Biochemistry*, 229 (2), 558–565.

Coughlan, K. A., Valentine, R. J., Ruderman, N. B., and Saha, A. K., 2014. AMPK activation: a therapeutic target for type 2 diabetes? *Diabetes, Metabolic Syndrome and Obesity : Targets and Therapy*, 7, 241–53.

Daaka, Y., Pitcher, J. A., Richardson, M., Stoffel, R. H., Robishaw, J. D., and Lefkowitz, R. J., 1997. Receptor and G βγ isoform-specific interactions with G protein-coupled receptor kinases. *Proceedings of the National Academy of Sciences of the United States of America*, 94 (6), 2180–2185.

Davies, S. P., Helps, N. R., Cohen, P. T. W., and Hardie, D. G., 1995. 5'-AMP inhibits dephosphorylation, as well as promoting phosphorylation, of the AMP-activated protein kinase. Studies using bacterially expressed human protein phosphatase-2C-α and native bovine protein phosphatase-2Ac. *FEBS Letters*, 377 (3), 421–425.

Defronzo, R. A., 2011. Bromocriptine: A Sympatholytic, D2-Dopamine Agonist for the Treatment of Type 2 Diabetes. *Diabetes*, 34, 789–794.

Degli Esposti, M., 1998. Inhibitors of NADH-ubiquinone reductase: An overview. *Biochimica et Biophysica Acta*, 1364 (2), 222–235.

Deveaux, V., Cadoudal, T., Ichigotani, Y., Teixeira-Clerc, F., Louvet, A., Manin, S., Nhieu, J. T. Van, Belot, M. P., Zimmer, A., Even, P., Cani, P. D., Knauf, C., Burcelin, R., Bertola, A., Le Marchand-Brustel, Y., Gual, P., Mallat, A., and Lotersztajn, S., 2009. Cannabinoid CB2 receptor potentiates obesity-associated inflammation, insulin resistance and hepatic steatosis. *PLoS ONE*, 4 (6).

Díaz-Delfín, J., Morales, M., and Caelles, C., 2007. Hypoglycemic Action of Thiazolidinediones/Peroxisome Proliferator–Activated Receptor γ by Inhibition of the c-Jun NH2-Terminal Kinase Pathway. *Diabetes*, 56, 1865–1871.

Doménech, E., Maestre, C., Esteban-martínez, L., Partida, D., Pascual, R., Fernández-miranda, G., Seco, E., Campos-Olivas, R., Pérez, M., Megias, D., Allen, K., López, M., Saha, A. K., Velasco, G., Rial, E., and Méndez, R., 2015. AMPK and PFKFB3 mediate glycolysis and survival in response to mitophagy during mitotic arrest. *Nature Cell Biology*, 17 (10), 1304.

Donath, M. Y., 2014. Targeting inflammation in the treatment of type 2 diabetes: time to start. *Nature Reviews Drug Discovery*, 13 (6), 465–476.

Dong, X., Zhao, Y., Huang, X., Lin, K., Chen, J., Wei, E., Liu, T., and Hu, Y., 2013. Structure-based drug design using GPCR homology modeling: toward the discovery of novel selective CysLT2 antagonists. *European Journal of Medicinal Chemistry*, 62, 754–763.

Donnan, P. T., MacDonald, T. M., and Morris, A. D., 2002. Adherence to prescribed oral hypoglycaemic medication in a population of patients with Type 2 diabetes: A retrospective cohort study. *Diabetic Medicine*, 19 (4), 279–284.

Downes, G. B. and Gautam, N., 1999. The G protein subunit gene families. *Genomics*, 62 (3), 544–552.

Efremov, R. G., Baradaran, R., and Sazanov, L. A., 2010. The architecture of respiratory complex I. *Nature*, 465 (7297), 441–445.

Ehlting, C., Lai, W. S., Schaper, F., Brenndorfer, E. D., Matthes, R. J., Heinrich, P. C., Ludwig, S., Blackshear, P. J., Gaestel, M., Haussinger, D., and Bode, J. G., 2007. Regulation of suppressor of cytokine signaling 3 (SOCS3) mRNA stability by

TNF-alpha involves activation of the MKK6/p38MAPK/MK2 cascade. *Journal of Immunology*, 178 (5), 2813–2826.

Ejaz, A., Wu, D., Kwan, P., and Meydani, M., 2009. Curcumin inhibits adipogenesis in 3T3-L1 adipocytes and angiogenesis and obesity in C57/BL mice. *The Journal of Nutrition*, 139 (5), 919–925.

Emanuela, F., Grazia, M., Marco, D. R., Maria Paola, L., Giorgio, F., and Marco, B., 2012. Inflammation as a Link between Obesity and Metabolic Syndrome. *Journal of Nutrition and Metabolism*, 2012, 476380.

Evers, A. and Klabunde, T., 2005. Structure-based drug discovery using GPCR homology modeling: Successful virtual screening for antagonists of the α1A adrenergic receptor. *Journal of Medicinal Chemistry*, 48 (4), 1088–1097.

Fanelli, F. and De Benedetti, P. G., 2011. Update 1 of: computational modeling approaches to structure-function analysis of G protein-coupled receptors. *Chemical Reviews*, 111 (12), PR438–535.

Fernández-Vizarra, E., Tiranti, V., and Zeviani, M., 2009. Assembly of the oxidative phosphorylation system in humans: What we have learned by studying its defects. *Biochimica et Biophysica Acta*, 1793 (1), 200–211.

Fiser, A. and Sali, A., 2003a. Modeller: generation and refinement of homology-based protein structure models. *Methods in Enzymology*, 374, 461–491.

Fiser, A. and Sali, A., 2003b. ModLoop: automated modeling of loops in protein structures. *Bioinformatics*, 19 (18), 2500–2501.

Flohr, S., Kurz, M., Kostenis, E., Brkovich, A., Fournier, A., and Klabunde, T., 2002. Identification of nonpeptidic urotensin II receptor antagonists by virtual screening

based on a pharmacophore model derived from structure-activity relationships and nuclear magnetic resonance studies on urotensin II. *Journal of Medicinal Chemistry*, 45 (9), 1799–1805.

Fogh, B. S., Multhaupt, H. A. B., and Couchman, J. R., 2014. Protein Kinase C, Focal Adhesions and the Regulation of Cell Migration. *Journal of Histochemistry and Cytochemistry*, 62 (3), 172–184.

FRED. 2.2.4 ed., www.eyesopen.com, OpenEye Scientific Software, Santa Fe, NM, USA.

Fredriksson, R., Lagerström, M. C., Lundin, L. G., and Schiöth, H. B., 2003. The G-protein-coupled receptors in the human genome form five main families. Phylogenetic analysis, paralogon groups, and fingerprints. *Molecular Pharmacology*, 63 (6), 1256–1272.

Fredriksson, R. and Schio, H. B., 2005. The Repertoire of G-Protein–Coupled Receptors in Fully Sequenced Genomes. *Molecular Pharmacology*, 67 (5), 1414–1425.

Fröjdö, S., Vidal, H., and Pirola, L., 2009. Alterations of insulin signaling in type 2 diabetes: A review of the current evidence from humans. *Biochimica et Biophysica Acta*, 1792 (2), 83–92.

Gage, D., 2012. Weight loss/maintenance as an effective tool for controlling type 2 diabetes: novel methodology to sustain weight reduction. *Diabetes/Metabolism Research and Reviews*, 28, 214–218.

Gao, Z., Hwang, D., Bataille, F., Lefevre, M., York, D., Quon, M. J., and Ye, J., 2002. Serine Phosphorylation of Insulin Receptor Substrate 1 by Inhibitor B Kinase Complex. *The Journal of Biological Chemistry*, 277 (50), 48115–48121.

Garber, A. J., 2011. Long-Acting Glucagon-Like Peptide 1 Receptor Agonists: A review of their efficacy and tolerability. *Diabetes Care*, 34, S279–S284.

García-Pérez, L. E., Alvarez, M., Dilla, T., Gil-Guillén, V., and Orozco-Beltrán, D., 2013. Adherence to therapies in patients with type 2 diabetes. *Diabetes Therapy*, 4 (2), 175–94.

Gardner, J., Wu, S., Ling, L., Danao, J., Li, Y., Yeh, W. C., Tian, H., and Baribault, H., 2012. G-protein-coupled receptor GPR21 knockout mice display improved glucose tolerance and increased insulin response. *Biochemical and Biophysical Research Communications*, 418 (1), 1–5.

Ge, H., Li, X., Weiszmann, J., Wang, P., Baribault, H., Chen, J. L., Tian, H., and Li, Y., 2008. Activation of G protein-coupled receptor 43 in adipocytes leads to inhibition of lipolysis and suppression of plasma free fatty acids. *Endocrinology*, 149 (9), 4519–4526.

Genova, M. L. and Lenaz, G., 2014. Functional role of mitochondrial respiratory supercomplexes. *Biochimica et Biophysica Acta*, 1837 (4), 427–443.

Geraghty, K. M., Chen, S., Harthill, J. E., Ibrahim, A. F., Toth, R., Morrice, N. A., Vandermoere, F., Moorhead, G. B., Hardie, D. G., and MacKintosh, C., 2007. Regulation of multisite phosphorylation and 14-3-3 binding of AS160 in response to IGF-1, EGF, PMA and AICAR. *The Biochemical Journal*, 407 (2), 231–41.

Gerich, J. E., 1993. Control of glycaemia. *Bailliere's Clinical Endocrinology and Metabolism*, 7 (3), 551–586.

Giri, S., Rattan, R., Haq, E., Khan, M., Yasmin, R., Won, J., Key, L., Singh, A. K., and Singh, I., 2006. AICAR inhibits adipocyte differentiation in 3T3L1 and restores metabolic alterations in diet-induced obesity mice model. *Nutrition and*

Metabolism, 3, 31.

Goldsmith, Z. G., and Dhanasekaran, D. N., 2007. G Protein regulation of MAPK . networks. *Oncogene,* 26 (22), 3122–3142.

Gonzalez, C. D., Lee, M. S., Marchetti, P., Pietropaolo, M., Towns, R., Vaccaro, M. I., Watada, H., and Wiley, J. W., 2011. The emerging role of autophagy in the pathophysiology of diabetes mellitus. *Autophagy*, 7 (1), 2–11.

Goodman D.S., 1984, Overview of current knowledge of metabolism of vitamin A and carotenoids, *The Journal of the National Cancer Institute,* 73 (6), 1375-1379.

Goodman Jr, O. B., Krupnick, J. G., Santini, F., Gurevich, V. V, Penn, R., Gagnon, A. W., Keen, J. H., and Benovic, J. L., 1996. β-arrestin acts as a clathrin adaptor in endocytosis of the β2-adrenergic receptor. *Nature*, 383, 447–450.

Graham, T. E., Yang, Q., Blurt, M., Hammarstedt, A., Ciaraldi, T. P., Henry, R. R., Wason, C. J., Oberbach, A., Jansson, P. A., Smith, U., and Kahn, B. B., 2006. Retinol-Binding Protein 4 and Insulin Resistance in Lean, Obese, and Diabetic Subjects. *The New England Journal of Medicine*, 354, 2552–2563.

Gwinn, D. M., Shackelford, D. B., Egan, D. F., Mihaylova, M. M., Mery, A., Vasquez, D. S., Turk, B. E., and Shaw, R. J., 2008. AMPK Phosphorylation of Raptor Mediates a Metabolic Checkpoint. *Molecular Cell*, 30 (2), 214–226.

Hall, A., 1998. Rho GTPases and the actin cytoskeleton. *Science*, 279 (5350), 509–514.

Hamm, H. E., 1998. The Many Faces of G Protein Signaling. *The Journal of Biological Chemistry*, 273 (21), 669–672.

Han, M. S., Jung, D. Y., Morel, C., Lakhani, S. A., Kim, J. K., Flavell, R. A., and Davis, R. J., 2013. JNK Expression by Macrophages Promotes Obesity-induced

Insulin Resistance and Inflammation. *Science*, 339 (7405), 109–113.

Hanefeld, M., Schell, E., Gouni-Berthold, Ioanna Melichar, M., Vesela, I., Johnson, D., Miao, S., Sullivan, T. J., Jaen, J. C., Schall, T. J., and Pirow, B., 2012. Orally-Administered Chemokine Receptor CCR2 Antagonist CCX140-B in Type 2 Diabetes: A Pilot Double-Blind, Randomized Clinical Trial. *Diabetes and Metabolism*, 3 (225), doi: 10.4172/2155–6156.1000225.

Hansen, M., Sonne, D. P., and Knop, F. K., 2014. Bile Acid Sequestrants: Glucose-Lowering Mechanisms and Efficacy in Type 2 Diabetes. *Current Diabetes Reports*, 14 (5), 482.

Hardie, D. G., Carling, D., and Sim, A. T. R., 1989. The AMP-activated protein kinase: a multisubstrate regulator of lipid metabolism. *Trends in Biochemical Sciences*, 14 (1), 20–23.

Hardie, D. G., Carling, D., and Carlson, M., 1998. The AMP-activated/SNF1 protein kinase subfamily: metabolic sensors of the eukaryotic cell? *Annual Review of Biochemistry*, 67, 821–55.

Hardie, D. G., 2011. AMP-activated protein kinase — an energy sensor that regulates all aspects of cell function. *Genes and Development*, 25, 1895–1908.

Hardie, D. G., Ross, F. A., and Hawley, S. A., 2012. AMPK: a nutrient and energy sensor that maintains energy homeostasis. *Nature Reviews Molecular Cell Biology*, 13 (4), 251–262.

Hart, M. J., Jiang, X., Kozasa, T., Roscoe, W., Singer, W. D., Gilman, A. G., Sternweis, P. C., and Bollag, G., 1998. Direct stimulation of the guanine nucleotide exchange activity of p115 RhoGEF by Gα13. *Science*, 280 (5372), 2112–2114.

Hawkins, P. C. D., Skillman, A. G., Warren, G. L., Ellingson, B. A., and Stahl, M. T., 2010. Conformer generation with OMEGA: Algorithm and validation using high quality structures from the protein databank and cambridge structural database. *Journal of Chemical Information and Modeling*, 50 (4), 572–584.

Hawley, S. A., Davison, M., Woods, A., Davies, S. P., Beri, R. K., Carling, D., and Hardie, D. G., 1996. Characterization of the AMP-activated Protein Kinase Kinase from Rat Liver and Identification of Threonine 172 as the Major Site at Which It Phosphorylates AMP-activated Protein Kinase. *The Journal of Biological Chemistry*, 271 (44), 27879–27887.

Hawley, S. A., Boudeau, J., Reid, J. L., Mustard, K. J., Udd, L., Mäkelä, T. P., Alessi, D. R., and Hardie, D. G., 2003. Complexes between the LKB1 tumor suppressor, STRAD alpha/beta and MO25 alpha/beta are upstream kinases in the AMP-activated protein kinase cascade. *Journal of Biology*, 2 (4), 28.

Hawley, S. A., Pan, D. A., Mustard, K. J., Ross, L., Bain, J., Edelman, A. M., Frenguelli, B. G., and Hardie, D. G., 2005. Calmodulin-dependent protein kinase kinase-β is an alternative upstream kinase for AMP-activated protein kinase. *Cell Metabolism*, 2 (1), 9–19.

Hawley, S. A., Fullerton, M. D., Ross, F. A., Schertzer, J. D., Chevtzoff, C., Walker, K. J., Peggie, M. W., Zibrova, D., Green, K. A., Mustard, K. J., Kemp, B. E., Sakamoto, K., Steinberg, G. R., and Hardie, D. G., 2012. The Ancient Drug Salicylate Directly Activates AMP-Activated Protein Kinase. *Science*, 336, 918–922.

Hay, D. L., Chen, S., Lutz, T. A., Parkes, D. G., and Roth, J. D., 2015. Amylin: Pharmacology, Physiology, and Clinical Potential. *Pharmacological Reviews*, 67

(3), 564–600.

Heinrich, P. C., Behrmann, I., Müller-Newen, G., Schaper, F., and Graeve, L., 1998. Interleukin-6-type cytokine signalling through the gp130/Jak/STAT pathway. *The Biochemical Journal*, 334 (2), 297–314.

Heller, J., 1975. Interactions of plasma retinol-binding protein with its receptor. Specific binding of bovine and human retinol-binding protein to pigment epithelium cells from bovine eyes. *The Journal of Biological Chemistry*, 250 (10), 3613-3619.

Hemi, R., Yochananov, Y., Barhod, E., Kasher-Meron, M., Karasik, A., Tirosh, A., and Kanety, H., 2011. p38 Mitogen-Activated Protein Kinase-Dependent Transactivation of ErbB Receptor Family: A Novel Common Mechanism for Stress-Induced IRS-1 Serine Phosphorylation and Insulin Resistance. *Diabetes*, 60 (4), 1134–1145.

Henriksen, E. J., 2002. Exercise Effects of Muscle Insulin Signaling and Action Invited Review: Effects of acute exercise and exercise training on insulin resistance. *Journal of Applied Physiology*, 93, 788–796.

Higashijima, T., Ferguson, K. M., Sternweis, P. C., Smigel, M. D., and Gilman, A. G., 1987. Effects of Mg^{2+} and the βγ-subunit complex on the interactions of guanine nucleotides with G proteins. *The Journal of Biological Chemistry*, 262 (2), 762–766.

Hinke, S. A., Martens, G. A., Cai, Y., Finsi, J., Heimberg, H., Pipeleers, D., and Van de Casteele, M., 2007. Methyl succinate antagonises biguanide-induced AMPK-activation and death of pancreatic β-cells through restoration of mitochondrial electron transfer. *British Journal of Pharmacology*, 150 (8), 1031–1043.

Hirosumi, J., Tuncman, G., Chang, L., Görgün, C. Z., Uysal, K. T., Maeda, K., Karin, M., and Hotamisligil, G. S., 2002. A central role for JNK in obesity and insulin resistance. *Nature*, 420 (6913), 333–336.

Holst, B., Egerod, K. L., Jin, C., Petersen, P. S., Østergaard, M. V., Hald, J., Sprinkel, A. M. E., Størling, J., Mandrup-Poulsen, T., Holst, J. J., Thams, P., Ørskov, C., Wierup, N., Sundler, F., Madsen, O. D., and Schwartz, T. W., 2009. G protein-coupled receptor 39 deficiency is associated with pancreatic islet dysfunction. *Endocrinology*, 150 (6), 2577–2585.

Hood, D. A., 2009. Mechanisms of exercise-induced mitochondrial biogenesis in skeletal muscle. *Applied Physiology, Nutrition, and Metabolism*, 34 (3), 465–472.

Hoppe, S., Bierhoff, H., Cado, I., Weber, A., Tiebe, M., Grummt, I., and Voit, R., 2009. AMP-activated protein kinase adapts rRNA synthesis to cellular energy supply. *Proceedings of the National Academy of Sciences of the United States of America*, 106 (42), 17781–17786.

Horman, S., Vertommen, D., Heath, R., Neumann, D., Mouton, V., Woods, A., Schlattner, U., Wallimann, T., Carling, D., Hue, L., and Rider, M. H., 2006. Insulin antagonizes ischemia-induced Thr 172 phosphorylation of AMP-activated protein kinase α-subunits in heart via hierarchical phosphorylation of Ser 485/491. *The Journal of Biological Chemistry*, 281 (9), 5335–5340.

Hotamisligil, G. S. and Spiegelman, B. M., 1994. Tumor necrosis factor α: a key component of the obesity-diabetes link. *Diabetes*, 43 (11), 1271–1278.

Huang, C., Jacobson, M., and Schaller, M. D., 2004. MAP Kinases and cell migration. *Journal of Cell Science*, 117 (20), 4619-4628.

Hubbard, S. R., 2013. The insulin receptor: Both a prototypical and atypical receptor

tyrosine kinase. *Cold Spring Harbor Perspectives in Biology*, 5 (3), a008946.

Hurley, R. L., Barre, L. K., Wood, S. D., Anderson, K. A., Kemp, B. E., Means, A. R., and Witters, L. A., 2006. Regulation of AMP-activated protein kinase by multisite phosphorylation in response to agents that elevate cellular cAMP. *The Journal of Biological Chemistry*, 281 (48), 36662–36672.

Huszar, D., Lynch, C. A., Fairchild-Huntress, V., Dunmore, J. H., Fang, Q., Berkemeier, L. R., Gu, W., Kesterson, R. A., Boston, B. A., Cone, R. D., Smith, F. J., Campfield, L. A., Burn, P., and Lee, F., 1997. Targeted disruption of the melanocortin-4 receptor results in obesity in mice. *Cell*, 88 (1), 131–141.

Hutagalung, A. H. and Novick, P. J., 2011. Role of Rab GTPases in Membrane Traffic and Cell Physiology. *Physiological Reviews*, 91 (1), 119–149.

Idris, I. and Donnelly, R., 2009. Sodium-glucose co-transporter-2 inhibitors: an emerging new class of oral antidiabetic drug. *Diabetes, Obesity and Metabolism*, 11 (2), 79–88.

Imamura, T., Vollenweider, P., Egawa, K., Clodi, M., Ishibashi, K., Nakashima, N., Ugi, S., Adams, J. W., Brown, J. H., and Olefsky, J. M., 1999. G alpha-q/11 protein plays a key role in insulin-induced glucose transport in 3T3-L1 adipocytes. *Molecular and Cellular Biology*, 19 (10), 6765–6774.

Inoki, K., Zhu, T., and Guan, K. L., 2003. TSC2 mediates cellular energy response to control cell growth and survival. *Cell*, 115 (5), 577–590.

Inzucchi, S. E., Bergenstal, R. M., Buse, J. B., Diamant, M., Ferrannini, E., Nauck, M., Peters, A. L., Tsapas, A., Wender, R., and Matthews, D. R., 2015. Management of hyperglycemia in type 2 diabetes, 2015: A patient-centered approach: Update to a Position statement of the American Diabetes Association (ADA) and the European

Association for the Study of Diabetes (EASD). *Diabetes Care*, 38 (6), 140–149.

Ishii, M., Fei, H., and Friedman, J. M., 2003. Targeted disruption of GPR7, the endogenous receptor for neuropeptides B and W, leads to metabolic defects and adult-onset obesity. *Proceedings of the National Academy of Sciences of the United States of America*, 100 (18), 10540–10545.

Isoda, K., Young, J. L., Zirlik, A., MacFarlane, L. A., Tsuboi, N., Gerdes, N., Schönbeck, U., and Libby, P., 2006. Metformin inhibits proinflammatory responses and nuclear factor-κB in human vascular wall cells. *Arteriosclerosis, Thrombosis, and Vascular Biology*, 26 (3), 611–7.

Jacobson, K. A., 2013. Structure-Based Approaches to Ligands for G Protein-Coupled Adenosine and P2Y Receptors, From Small Molecules to Nanoconjugates. *Journal of Medicinal Chemistry*, 56 (10), 3749–3767.

Jager, J., Grémeaux, T., Cormont, M., Le Marchand-Brustel, Y., and Tanti, J. F., 2007. Interleukin-1β-Induced Insulin Resistance in Adipocytes through Down-Regulation of Insulin Receptor Substrate-1 Expression. *Endocrinology*, 148 (1), 241–251.

Jäger, S., Handschin, C., St-Pierre, J., and Spiegelman, B. M., 2007. AMP-activated protein kinase (AMPK) action in skeletal muscle via direct phosphorylation of PGC-1alpha. *Proceedings of the National Academy of Sciences of the United States of America*, 104 (29), 12017–22.

Jeffrey, K. L., Camps, M., Rommel, C., and Mackay, C. R., 2007. Targeting dual-specificity phosphatases: manipulating MAP kinase signalling and immune responses. *Nature Reviews Drug Discovery*, 6 (5), 391–403.

Jenkins, Y., Sun, T. Q., Markovtsov, V., Foretz, M., Li, W., Nguyen, H., Li, Y., Pan,

A., Uy, G., Gross, L., Baltgalvis, K., Yung, S. L., Gururaja, T., Kinoshita, T., Owyang, A., Smith, I. J., McCaughey, K., White, K., Godinez, G., Alcantara, R., Choy, C., Ren, H., Basile, R., Sweeny, D. J., Xu, X., Issakani, S. D., Carroll, D. C., Goff, D. A., Shaw, S. J., Singh, R., Boros, L. G., Laplante, M. A., Marcotte, B., Kohen, R., Viollet, B., Marette, A., Payan, D. G., Kinsella, T. M., and Hitoshi, Y., 2013. AMPK activation through mitochondrial regulation results in increased substrate oxidation and improved metabolic parameters in models of diabetes. *PLoS ONE*, 8 (12), 1–19.

Jones, G. E., 2000. Cellular signaling in macrophage migration and chemotaxis. *Journal of Leukocyte Biology*, 68 (5), 593–602.

Jorgensen, S. B., O'Neill, H. M., Sylow, L., Honeyman, J., Hewitt, K. A., Palanivel, R., Fullerton, M. D., Oberg, L., Balendran, A., Galic, S., van der Poel, C., Trounce, I. A., Lynch, G. S., Schertzer, J. D., and Steinberg, G. R., 2013. Deletion of Skeletal Muscle SOCS3 Prevents Insulin Resistance in Obesity. *Diabetes*, 62 (1), 56–64.

Kahn, B. B., Alquier, T., Carling, D., and Hardie, D. G., 2005. AMP-activated protein kinase: ancient energy gauge provides clues to modern understanding of metabolism. *Cell Metabolism*, 1 (1), 15–25.

Kahn, S. E., Hull, R. L., and Utzschneider, K. M., 2006. Mechanisms linking obesity to insulin resistance and type 2 diabetes. *Nature*, 444 (7121), 840–6.

Kamei, N., Tobe, K., Suzuki, R., Ohsugi, M., Watanabe, T., Kubota, N., Ohtsuka-Kowatari, N., Kumagai, K., Sakamoto, K., Kobayashi, M., Yamauchi, T., Ueki, K., Oishi, Y., Nishimura, S., Manabe, I., Hashimoto, H., Ohnishi, Y., Ogata, H., Tokuyama, K., Tsunoda, M., Ide, T., Murakami, K., Nagai, R., and Kadowaki, T., 2006. Overexpression of monocyte chemoattractant protein-1 in adipose tissues

causes macrophage recruitment and insulin resistance. *The Journal of Biological Chemistry*, 281 (36), 26602–26614.

Kanai, M., Raz, A., and Goodman, D. S., 1968. Retinol-binding protein: the transport protein for vitamin A in human plasma. *The Journal of Clinical Investigation*, 47 (9), 2025–2044.

Kanazawa, I., Yamaguchi, T., Yano, S., Yamauchi, M., and Sugimoto, T., 2008. Metformin enhances the differentiation and mineralization of osteoblastic MC3T3-E1 cells via AMP kinase activation as well as eNOS and BMP-2 expression. *Biochemical and Biophysical Research Communications*, 375 (3), 414–419.

Kanazawa, I., Yamaguchi, T., Yano, S., Yamauchi, M., and Sugimoto, T., 2009. Activation of AMP kinase and inhibition of Rho kinase induce the mineralization of osteoblastic MC3T3-E1 cells through endothelial NOS and BMP-2 expression. *The American Journal of Physiology Endocrinology and Metabolism*, 296 (1), E139–E146.

Kandadi, M. R., Rajanna, P. K., Unnikrishnan, M. K., Boddu, S. P., Hua, Y., Li, J., Du, M., Ren, J., and Sreejayan, N., 2010. 2-(3,4-Dihydro-2H-pyrrolium-1-yl)-3oxoindan-1-olate (DHPO), a novel, synthetic small molecule that alleviates insulin resistance and lipid abnormalities. *Biochemical Pharmacology*, 79 (4), 623–31.

Kanneganti, T. D. and Dixit, V. D., 2012. Immunological complications of obesity. *Nature Immunology*, 13 (8), 707–712.

Karik, K., Weissman, D., and Welsh, F. A., 2004. Inhibition of Toll-like Receptor and Cytokine Signaling-A Unifying Theme in Ischemic Tolerance. *Journal of Cerebral Blood Flow and Metabolism*, 1288–1304.

Karlsson, H. K. R., Hällsten, K., Björnholm, M., Tsuchida, H., Chibalin, A. V, Virtanen, K. A., Heinonen, O. J., Lönnqvist, F., Nuutila, P., and Zierath, J. R., 2005. Effects of metformin and rosiglitazone treatment on insulin signaling and glucose uptake in patients with newly diagnosed type 2 diabetes: a randomized controlled study. *Diabetes*, 54 (5), 1459–67.

Kawaguchi, R., Yu, J., Honda, J., Hu, J., Whitelegge, J., Ping, P., Wiita, P., Bok, D., and Sun, H., 2007. A Membrane Receptor for Retinol Binding Protein Mediates Cellular Uptake of Vitamin A. *Science*, 820, 820–826.

Kebede, M., Alquier, T., Latour, M. G., Semache, M., Tremblay, C., and Poitout, V., 2008. The Fatty Acid Receptor GPR40 Plays a Role in Insulin Secretion In Vivo After High-Fat Feeding. *Diabetes*, 57 (9), 2432–2437.

Kelly, M., Keller, C., Avilucea, P. R., Keller, P., Luo, Z., Xiang, X., Giralt, M., Hidalgo, J., Saha, A. K., Pedersen, B. K., and Ruderman, N. B., 2004. AMPK activity is diminished in tissues of IL-6 knockout mice: the effect of exercise. *Biochemical and Biophysical Research Communications*, 320 (2), 449–454.

Kemp, B. E., 2004. Bateman domains and adenosine derivatives form a binding contract. *Journal of Clinical Investigation*, 113 (2), 182–184.

Kenakin, T., 2003. Ligand-selective receptor conformations revisited: the promise and the problem. *Trends in Pharmacological Sciences*, 24 (7), 346–354.

Kern, P. A., Ranganathan, S., Li, C., Wood, L., and Ranganathan, G., 2001. Adipose tissue tumor necrosis factor and interleukin-6 expression in human obesity and insulin resistance. *The American Journal of Physiology Endocrinology and Metabolism*, 280 (5), 745–751.

Khan, S. M., Sleno, R., Gora, S., Zylbergold, P., Laverdure, J., Labbé, J., and Miller, G.

J., 2013. The Expanding Roles of G βγ Subunits in G Protein – Coupled Receptor Signaling and Drug Action. *Pharmacological Reviews*, 545–577.

Kim, J. H., Park, J. M., Kim, E. K., Lee, J. O., Lee, S. K., Jung, J. H., You, G. Y., Park, S. H., Suh, P. G., and Kim, H. S., 2010. Curcumin stimulates glucose uptake through AMPK-p38 MAPK pathways in L6 myotube cells. *Journal of Cellular Physiology*, 223 (3), 771–8.

Kim, M. S., Hur, H. J., Kwon, D. Y., and Hwang, J.T., 2012. Tangeretin stimulates glucose uptake via regulation of AMPK signaling pathways in C2C12 myotubes and improves glucose tolerance in high-fat diet-induced obese mice. *Molecular and Cellular Endocrinology*, 358 (1), 127–34.

Kimple, M. E., Neuman, J. C., Linnemann, A. K., and Casey, P. J., 2014. Inhibitory G proteins and their receptors: emerging therapeutic targets for obesity and diabetes. *Experimental and Molecular Medicine*, 46 (6), e102.

Kishimoto, A., Takai, Y., Mori, T., Kikkawa, U., and Nishizuka, Y., 1980. Activation of Calcium and Phospholipid-dependent Protein Kinase By Diacylglycerol, Its Possiblr Relation to Phosphatidylinositol Turnover. *The Journal of Biological Chemistry*, 255 (11), 2273–2276.

Klok, M. D., Jakobsdottir, S., and Drent, M. L., 2007. The role of leptin and ghrelin in the regulation of food intake and body weight in humans: A Review. *Obesity Reviews*, 8 (1), 21–34.

Knall, C. and Johnson, G. L., 1998. G-protein regulatory pathways: rocketing into the twenty-first century. *Journal of Cellular Biochemistry Supplements*, 30-31, 137–146.

Kobilka, B. K., 2002. Agonist-induced conformational changes in the β2 adrenergic

receptor. *The Journal of Peptide Research*, 60 (6), 317–321.

Kobilka, B. K., 2007. G protein coupled receptor structure and activation. *Biochimica et Biophysica Acta*, 1768 (4), 794–807.

Koo, S. H., Flechner, L., Qi, L., Zhang, X., Screaton, R. A., Jeffries, S., Hedrick, S., Xu, W., Boussouar, F., Brindle, P., Takemori, H., and Montminy, M., 2005. The CREB coactivator TORC2 is a key regulator of fasting glucose metabolism. *Nature*, 437 (7062), 1109–1111.

Kopin, A. S., Mathes, W. F., McBride, E. W., Nguyen, M., Al-Haider, W., Schmitz, F., Bonner-Weir, S., Kanarek, R., and Beinborn, M., 1999. The cholecystokinin-A receptor mediates inhibition of food intake yet is not essential for the maintenance of body weight. *The Journal of Clinical Investigation*, 103 (3), 383–391.

Kopp, H. P., Krzyzanowska, K., Möhlig, M., Spranger, J., Pfeiffer, A. F. H., and Schernthaner, G., 2005. Effects of marked weight loss on plasma levels of adiponectin, markers of chronic subclinical inflammation and insulin resistance in morbidly obese women. *International Journal of Obesity*, 29 (7), 766–771.

Krakauer, J. C., McKenna, M. J., Buderer, N. F., Rao, D. S., Whitehouse, F. W., and Parfitt, A. M., 1995. Bone loss and bone turnover in diabetes. *Diabetes*, 44 (7), 775–782.

Krebs, E. G., 1989. The Albert Lasker Medical Awards. Role of the cyclic AMP-dependent protein kinase in signal transduction. *JAMA*, 262 (13), 1815–1818.

Kufareve, I., Rueda, M., Katritch, V., Stevens, R., and Abagyan, R., 2011. Status of GPCR modelling and docking as reflected by community-wide GPCR Dock 2010 assessment. *Structure*, 19 (8), 1108–1126.

Kumar, A., Rajendran, V., Sethumadhavan, R., and Purohit, R., 2013. AKT kinase pathway: A leading target in cancer research. *The Scientific World Journal*, 2013.

Kumar, N. and Dey, C. S., 2002. Metformin enhances insulin signalling in insulin-dependent and-independent pathways in insulin resistant muscle cells. *British Journal of Pharmacology*, 137 (3), 329–336.

Kuri-Harcuch, W., and Green, H., 1978. Adipose conversion of 3T3 cells depends on a serum factor. *Proceedings of the National Academy of Sciences of the United States of America*, 75 (12), 6107–6109.

Kurth-Kraczek, E. J., Hirshman, M. F., Goodyear, L. J., and Winder, W. W., 1999. 5' AMP-activated protein kinase activation causes GLUT4 translocation in skeletal muscle. *Diabetes*, 48 (8), 1667–1671.

Ladenheim, E. E., Hampton, L. L., Whitney, A. C., White, W. O., Battey, J. F., and Moran, T. H., 2002. Disruptions in feeding and body weight control in gastrin-releasing peptide receptor deficient mice. *The Journal of Endocrinology*, 174 (2), 273–281.

Laemmli, U. K., 1970. Cleavage of structural proteins during the assembly of the head of bacteriophage T4. *Nature*, 227 (5259), 680–685.

Lalau, J. D., Arnouts, P., Sharif, A., and De Broe, M. E., 2015. Metformin and other antidiabetic agents in renal failure patients. *Kidney International*, 87 (2), 308–322.

Lan, F., Cacicedo, J. M., Ruderman, N., and Ido, Y., 2008. SIRT1 Modulation of the Acetylation Status, Cytosolic Localization, and Activity of LKB1: Possible Role in AMP-Activated Protein Kinase Activation. *The Journal of Biological Chemistry*, 283 (41), 27628–27635.

Lan, H., Vassileva, G., Corona, A., Liu, L., Baker, H., Golovko, A., Abbondanzo, S. J., Hu, W., Yang, S., Ning, Y., Del Vecchio, R. A., Poulet, F., Laverty, M., Gustafson, E. L., Hedrick, J. A., and Kowalski, T. J., 2009. GPR119 is required for physiological regulation of glucagon-like peptide-1 secretion but not for metabolic homeostasis. *Journal of Endocrinology*, 201 (2), 219–230.

Lantier, L., Fentz, J., Mounier, R., Leclerc, J., Treebak, J. T., Pehmoller, C., Sanz, N., Sakakibara, I., Saint-Amand, E., Rimbaud, S., Maire, P., Marette, A., Ventura-Clapier, R., Ferry, A., Wojtaszewski, J. F. P., Foretz, M., and Viollet, B., 2014. AMPK controls exercise endurance, mitochondrial oxidative capacity, and skeletal muscle integrity. *The FASEB Journal*, 28 (7), 3211–3224.

Lappano, R. and Maggiolini, M., 2011. G protein-coupled receptors: novel targets for drug discovery in cancer. *Nature Reviews Drug Discovery*, 10 (1), 47–60.

Larance, M., Ramm, G., Stöckli, J., Van Dam, E. M., Winata, S., Wasinger, V., Simpson, F., Graham, M., Junutula, J. R., Guilhaus, M., and James, D. E., 2005. Characterization of the role of the Rab GTPase-activating protein AS160 in insulin-regulated GLUT4 trafficking. *The Journal of Biological Chemistry*, 280 (45), 37803–37813.

Larance, M., Ramm, G., and James, D. E., 2008. The GLUT4 code. *Molecular Endocrinology*, 22 (2), 226–233.

Larkin, M. A., Blackshields, G., Brown, N. P., Chenna, R., McGettigan, P. A., McWilliam, H., Valentin, F., Wallace, I. M., Wilm, A., Lopez, R., Thompson, J. D., Gibson, T. J., and Higgins, D. G., 2007. Clustal W and Clustal X version 2.0. *Bioinformatics*, 23 (21), 2947–2948.

Larsson, C., 2006. Protein kinase C and the regulation of the actin cytoskeleton.

Cellular Signalling, 18 (3), 276–284.

Laskowski, R., Rullmann, J. A., MacArthur, M., Kaptein, R., and Thornton, J., 1996. AQUA and PROCHECK-NMR: Programs for checking the quality of protein structures solved by NMR. *Journal of Biomolecular NMR*, 8 (4), 477–486.

Latek, D., Pasznik, P., Carlomagno, T., and Filipek, S., 2013. Towards Improved Quality of GPCR Models by Usage of Multiple Templates and Profile-Profile Comparison. *PLoS ONE*, 8 (2), 1–10.

LeBrasseur, N. K., Kelly, M., Tsao, T. S., Farmer, S. R., Saha, A. K., Ruderman, N. B., and Tomas, E., 2006. Thiazolidinediones can rapidly activate AMP-activated protein kinase in mammalian tissues. *The American Journal of Physiology Endocrinology and Metabolism*, 291 (1), E175–E181.

Lee, B. and Shao, J., 2012. Adiponectin and lipid metabolism in skeletal muscle. *Acta Pharmaceutica Sinica B*, 2 (4), 335–340.

Lee, J. O., Lee, S. K., Kim, J. H., Kim, N., You, G. Y., Moon, J. W., Kim, S. J., Park, S. H., and Kim, H. S., 2012. Metformin regulates glucose transporter 4 (GLUT4) translocation through AMP-activated protein kinase (AMPK)-mediated Cbl/CAP signaling in 3T3-L1 preadipocyte cells. *The Journal of Biological Chemistry*, 287 (53), 44121–9.

Lee, M. S., 2014. Role of islet β cell autophagy in the pathogenesis of diabetes. *Trends in Endocrinology and Metabolism*, 25 (12), 620–627.

Lee, Y. S., Kok-Seng Poh, L., and Loke, K. Y., 2002. A Novel Melanocortin 3 Receptor Gene (MC3R) Mutation Associated with Severe Obesity. *The Journal of Endochrinology and Metabolism*, 87, 1423–1426.

Leff, P., 1995. The two-state model of receptor activation. *Trends in Pharmacological Sciences*, 16 (3), 89–97.

Leff, P., Scaramellini, C., Law, C., and McKechnie, K., 1997. A three-state receptor model of agonist action. *Trends in Pharmacological Sciences*, 18 (10), 355–362.

Levert, K. L., Waldrop, G. L., and Stephens, J. M., 2002. A biotin analog inhibits acetyl-CoA carboxylase activity and adipogenesis. *The Journal of Biological Chemistry*, 277 (19), 16347–16350.

Li, J., Spletter, M. L., Johnson, D. A., Wright, L. S., Svendsen, C. N., and Johnson, J. A., 2005. Rotenone-induced caspase 9/3-independent and -dependent cell death in undifferentiated and differentiated human neural stem cells. *Journal of Neurochemistry*, 92 (3), 462–476.

Li, P., Oh, D. Y., Bandyopadhyay, G., Lagakos, W. S., Osborn, O., Johnson, A., Chung, H., Maris, M., Ofrecio, M., Taguchi, S., Lu, M., and Olefsky, J. M., 2015. LTB4 causes macrophage-mediated inflammation and directly induces insulin resistance in obesity. *Nature Medicine*, 21 (3), 239–247.

Li, Y., Xu, S., Mihaylova, M. M., Zheng, B., Hou, X., Jiang, B., Park, O., Luo, Z., Lefai, E., Shyy, J. Y. J., Gao, B., Wierzbicki, M., Verbeuren, T. J., Shaw, R. J., Cohen, R. A., and Zang, M., 2011. AMPK Phosphorylates and Inhibits SREBP Activity to Attenuate Hepatic Steatosis and Atherosclerosis in Diet-Induced Insulin-Resistant Mice. *Cell Metabolism*, 13 (4), 376–388.

Lin, K., Lin, J., Wu, W. I., Ballard, J., Lee, B. B., Gloor, S. L., Vigers, G. P. A., Morales, T. H., Friedman, L. S., Skelton, N., and Brandhuber, B. J., 2012. An ATP-site on-off switch that restricts phosphatase accessibility of Akt. *Science Signaling*, 5 (223), ra37.

Liu, Z. G., Hsu, H., Goeddel, D. V., and Karin, M., 1996. Dissection of TNF receptor 1 effector functions: JNK activation is not linked to apoptosis while NF-κB activation prevents cell death. *Cell*, 87 (3), 565–576.

Lohse, M. J., Benovic, J. L., Codina, J., Caron, M. G., and Lefkowitz, R. J., 1990. β-arrestin: a protein that regulates β-adrenergic receptor function. *Science*, 248, 1547–1550.

Lopez-Castejon, G. and Brough, D., 2011. Understanding the mechanism of IL-1β secretion. *Cytokine and Growth Factor Reviews*, 22 (1), 189–195.

Lumeng, C. N., Bodzin, J. L., and Saltiel, A. R., 2007. Obesity induces a phenotypic switch in adipose tissue macrophage polarization. *The Journal of Clinical Investigation*, 117 (1), 175–184.

Luo, H. R., Huang, Y. E., Chen, J. C., Saiardi, A., Iijima, M., Ye, K., Huang, Y., Nagata, E., Devreotes, P., and Snyder, S. H., 2003. Inositol Pyrophosphates Mediate Chemotaxis in Dictyostelium via Pleckstrin Homology Domain-PtdIns(3,4,5)P3 Interactions. *Cell*, 114, 559–572.

Ma, P. and Zemmel, R., 2002. Value of novelty? *Nature Reviews Drug Discovery*, 1 (8), 571–572.

Mackenzie, R. W. and Elliott, B. T., 2014. Akt/PKB activation and insulin signaling: a novel insulin signaling pathway in the treatment of type 2 diabetes. *Diabetes, Metabolic Syndrome and Obesity : Targets and Therapy*, 7, 55–64.

Madiraju, A. K., Erion, D. M., Rahimi, Y., Zhang, X. M., Braddock, D. T., Albright, R. A., Prigaro, B. J., Wood, J. L., Bhanot, S., MacDonald, M. J., Jurczak, M. J., Camporez, J. P., Lee, H. Y., Cline, G. W., Samuel, V. T., Kibbey, R. G., and Shulman, G. I., 2014. Metformin suppresses gluconeogenesis by inhibiting

mitochondrial glycerophosphate dehydrogenase. *Nature*, 510 (7506), 542–546.

Marsin, A. S., Bertrand, L., Rider, M. H., Deprez, J., Beauloye, C., Vincent, M. F., Van den Berghe, G., Carling, D., and Hue, L., 2000. Phosphorylation and activation of heart PFK-2 by AMPK has a role in the stimulation of glycolysis during ischaemia. *Current Biology*, 10 (20), 1247–1255.

Marsin, A. S., Bouzin, C., Bertrand, L., and Hue, L., 2002. The stimulation of glycolysis by hypoxia in activated monocytes is mediated by AMP-activated protein kinase and inducible 6-phosphofructo-2-kinase. *The Journal of Biological Chemistry*, 277 (34), 30778–30783.

Martin, D. S. D., Leonard, S., Devine, R., Redondo, C., Kinsella, G. K., Breen, C. J., McEneaney, V., Rooney, M., Porter, R. K., Sivaprasadarao, A., Stephens, J. C., and Findlay, J. B. C., 2016. Novel mitochondrial complex I inhibitors restore glucose-handling abilities of high-fat fed mice. *Journal of Molecular Endocrinology,* DOI: 10.1530/JME-15-0225

Martinon, F., Burns, K., and Tschopp, J., 2002. The inflammasome: a molecular platform triggering activation of inflammatory caspases and processing of proIL-β. *Molecular Cell*, 10 (2), 417–426.

Matsuda, I. and Aiba, A., 2004. Receptor knock-out and knock-in strategies. *Methods in Molecular Biology*, 259, 379–390.

Matsuzaki, S. and Humphries, K. M., 2015. Selective Inhibition of Deactivated Mitochondrial Complex I by Biguanides. *Biochemistry*, 54 (11), 2011–2021.

McArdle, M. A., Finucane, O. M., Connaughton, R. M., McMorrow, A. M., and Roche, H. M., 2013. Mechanisms of Obesity-Induced Inflammation and Insulin Resistance: Insights into the Emerging Role of Nutritional Strategies. *Frontiers in*

Endocrinology, 4 (May), 1–23.

McGann, M., 2011. FRED pose prediction and virtual screening accuracy. *Journal of Chemical Information and Modeling*, 51 (3), 578–596.

McGaughey, G. B., Sheridan, R. P., Bayly, C. I., Culberson, J. C., Kreatsoulas, C., Lindsley, S., Maiorov, V., Truchon, J. F., and Cornell, W. D., 2007. Comparison of topological, shape, and docking methods in virtual screening. *Journal of Chemical Information and Modeling*, 47 (4), 1504–1519.

Meister, J., Le Duc, D., Ricken, A., Burkhardt, R., Thiery, J., Pfannkuche, H., Polte, T., Grosse, J., Schoneberg, T., and Schulz, A., 2014. The G Protein-coupled Receptor P2Y14 Influences Insulin Release and Smooth Muscle Function in Mice. *The Journal of Biological Chemistry*, 289, 23353–23366.

Merrill, G. F., Kurth, E. J., Hardie, D. G., and Winder, W. W., 1997. AICA riboside increases AMP-activated protein kinase, fatty acid oxidation, and glucose uptake in rat muscle. *The American Journal of Physiology*, 273, 1107–1112.

Michalsky, E., Goede, A., and Preissner, R., 2003. Loops In Proteins (LIP)-a comprehensive loop database for homology modelling. *Protein Engineering*, 16 (12), 979–985.

Middelbeek, R. J. W., Chambers, M. A., Tantiwong, P., Treebak, J. T., An, D., Hirshman, M. F., Musi, N., and Goodyear, L. J., 2013. Insulin stimulation regulates AS160 and TBC1D1 phosphorylation sites in human skeletal muscle. *Nutrition and Diabetes*, 3, e74.

Mihaylova, M. M., Vasquez, D. S., Ravnskjaer, K., Denechaud, P. D., Yu, R. T., Alvarez, J. G., Downes, M., Evans, R. M., Montminy, M., and Shaw, R. J., 2011. Class IIa Histone Deacetylases are Hormone-activated regulators of FOXO and

Mammalian Glucose Homeostasis. *Cell*, 145 (4), 607–621.

Miller, R. A., Chu, Q., Xie, J., Foretz, M., Viollet, B., and Birnbaum, M. J., 2013. Biguanides suppress hepatic glucagon signalling by decreasing production of cyclic AMP. *Nature*, 494 (7436), 256–260.

Minokoshi, Y., Kim, Y. B., Peroni, O. D., Fryer, L. G. D., Muller, C., Carling, D., and Kahn, B. B., 2002. Leptin stimulates fatty-acid oxidation by activating AMP-activated protein kinase. *Nature*, 415 (6869), 339–343.

Miyawaki, K., Yamada, Y., Ban, N., Ihara, Y., Tsukiyama, K., Zhou, H., Fujimoto, S., Oku, A., Tsuda, K., Toyokuni, S., Hiai, H., Mizunoya, W., Fushiki, T., Holst, J. J., Makino, M., Tashita, A., Kobara, Y., Tsubamoto, Y., Jinnouchi, T., Jomori, T., and Seino, Y., 2002. Inhibition of gastric inhibitory polypeptide signaling prevents obesity. *Nature Medicine*, 8 (7), 738–742.

Molinuevo, M. S., Schurman, L., McCarthy, A. D., Cortizo, A. M., Tolosa, M. J., Gangoiti, M. V., Arnol, V., and Sedlinsky, C., 2010. Effect of metformin on bone marrow progenitor cell differentiation: in vivo and in vitro studies. *Journal of Bone and Mineral Research*, 25 (2), 211–221.

Momcilovic, M., Hong, S. P., and Carlson, M., 2006. Mammalian TAK1 Activates Snf1 Protein Kinase in Yeast and Phosphorylates AMP-activated Protein Kinase in Vitro. *The Journal of Biological Chemistry*, 281 (35), 25336–25343.

Mráček, T., Drahota, Z., and Houštěk, J., 2013. The function and the role of the mitochondrial glycerol-3-phosphate dehydrogenase in mammalian tissues. *Biochimica et Biophysica Acta*, 1827 (3), 401–410.

Mu, J., Brozinick, J. T., Valladares, O., Bucan, M., and Birnbaum, M. J., 2001. A role for AMP-activated protein kinase in contraction- and hypoxia-regulated glucose

transport in skeletal muscle. *Molecular Cell*, 7 (5), 1085–1094.

Muenzner, M., Tuvia, N., Deutschmann, C., Witte, N., Tolkachov, A., Valai, A., Henze, A., Sander, L. E., Raila, J., and Schupp, M., 2013. Retinol-binding protein 4 and its membrane receptor STRA6 control adipogenesis by regulating cellular retinoid homeostasis and retinoic acid receptor α activity. *Molecular and cellular biology*, 33 (20), 4068–82.

Munday, M. R., Campbell, D. G., Carling, D., and Hardie, D. G., 1988. Identification by amino acid sequencing of three major regulatory phosphorylation sites on rat acetyl-CoA carboxylase. *European Journal of Biochemistry*, 175 (2), 331–338.

Nagata, A., Ito, M., Iwata, N., Kuno, J., Takano, H., Minowa, O., Chihara, K., Matsui, T., and Noda, T., 1996. G protein-coupled cholecystokinin-B/gastrin receptors are responsible for physiological cell growth of the stomach mucosa in vivo. *Proceedings of the National Academy of Sciences of the United States of America*, 93 (21), 11825–11830.

Naor, Z., Benard, O., and Seger, R., 2000. Activation of MAPK cascades by G-protein-coupled receptors: The case of gonadotropin-releasing hormone receptor. *Trends in Endocrinology and Metabolism*, 11 (3), 91–99.

Nauck, M. A. and Friedrich, N., 2013. Do GLP-1-Based Therapies Increase Cancer Risk? *Diabetes Care*, 36, S245–S252.

Neer, E. J., 1995. Heterotrimeric G proteins: organizers of transmembrane signals. *Cell*, 80 (2), 249–257.

Nguyen, M. T. A., Favelyukis, S., Nguyen, A. K., Reichart, D., Scott, P. A., Jenn, A., Liu-Bryan, R., Glass, C. K., Neels, J. G., and Olefsky, J. M., 2007. A Subpopulation of Macrophages Infiltrates Hypertrophic Adipose Tissue and Is

Activated by Free Fatty Acids via Toll-like Receptors 2 and 4 and JNK-dependent Pathways. *The Journal of Biological Chemistry*, 282 (48), 35279–35292.

Nie, T., Hui, X., Gao, X., Li, K., Lin, W., Xiang, X., Ding, M., Kuang, Y., Xu, A., Fei, J., Wang, Z., and Wu, D., 2012. Adipose tissue deletion of Gpr116 impairs insulin sensitivity through modulation of adipose function. *FEBS Letters*, 586 (20), 3618–3625.

Norseen, J., Hosooka, T., Hammarstedt, A., Yore, M. M., Kant, S., Aryal, P., Kiernan, U. A., Phillips, D. A., Maruyama, H., Kraus, B. J., Usheva, A., Davis, R. J., Smith, U., and Kahn, B. B., 2012. Retinol-Binding Protein 4 Inhibits Insulin Signaling in Adipocytes by Inducing Proinflammatory Cytokines in Macrophages through a c-Jun N-Terminal Kinase- and Toll-Like Receptor 4-Dependent and Retinol-Independent Mechanism. *Molecular and Cellular Biology*, 32 (10), 2010–2019.

OMEGA, www.eyesopen.com, OpenEye Scientific Software, Santa Fe, NM, USA.

O'Neill, H. M., Holloway, G. P., and Steinberg, G. R., 2013. AMPK regulation of fatty acid metabolism and mitochondrial biogenesis: Implications for obesity. *Molecular and Cellular Endocrinology*, 366 (2), 135–151.

O'Neill, H. M., Maarbjerg, S. J., Crane, J. D., Jeppesen, J., Jørgensen, S. B., Schertzer, J. D., Shyroka, O., Kiens, B., van Denderen, B. J., Tarnopolsky, M. A., Kemp, B. E., Richter, E. A., and Steinberg, G. R., 2011. AMP-activated protein kinase (AMPK) β1β2 muscle null mice reveal an essential role for AMPK in maintaining mitochondrial content and glucose uptake during exercise. *Proceedings of the National Academy of Sciences of the United States of America*, 108 (38), 16092–7.

O'Rourke, R. and Metcalf, M., 2009. Depot-specific differences in inflammatory mediators and a role for NK cells and IFN-γ in inflammation in human adipose

tissue. *International Journal of Obesity*, 33 (9), 978–990.

O'Sullivan, L. A., Liongue, C., Lewis, R. S., Stephenson, S. E. M., and Ward, A. C., 2007. Cytokine receptor signaling through the Jak–Stat–Socs pathway in disease. *Molecular Immunology*, 44 (10), 2497–2506.

Offermanns, S., 2003. G-proteins as transducers in transmembrane signalling. *Progress in Biophysics and Molecular Biology*, 83 (2), 101–130.

Offermanns, S., Heiler, E., Spicher, K., and Schultz, G., 1994. Gq and G11 are concurrently activated by bombesin and vasopressin in Swiss 3T3 cells. *FEBS Letters*, 349 (2), 201–204.

Oh, D. Y., Talukdar, S., Bae, E. J., Imamura, T., Morinaga, H., Fan, W., Li, P., Lu, W. J., Watkins, S. M., and Olefsky, J. M., 2010. GPR120 Is an Omega-3 Fatty Acid Receptor Mediating Potent Anti-inflammatory and Insulin-Sensitizing Effects. *Cell*, 142 (5), 687–698.

Ohki-Hamazaki, H., Watase, K., Yamamoto, K., Ogura, H., Yamano, M., Yamada, K., Maeno, H., Imaki, J., Kikuyama, S., Wada, E., and Wada, K., 1997. Mice lacking bombesin receptor subtype-3 develop metabolic defects and obesity. *Nature*, 390 (6656), 165–169.

Oldham, W. M. and Hamm, H. E., 2006. Structural basis of function in heterotrimeric G proteins. *Quarterly Reviews of Biophysics*, 39 (2), 117–166.

Oldham, W. M. and Hamm, H. E., 2008. Heterotrimeric G protein activation by G-protein-coupled receptors. *Nature Reviews Molecular Cell Biology*, 9 (1), 60–71.

Osborn, O., Oh, D. Y., Mcnelis, J., Sanchez-alavez, M., Talukdar, S., Lu, M., Li, P., Thiede, L., Morinaga, H., Kim, J. J., Heinrichsdorff, J., Nalbandian, S., Ofrecio, J.

M., Scadeng, M., Schenk, S., Hadcock, J., Bartfai, T., and Olefsky, J. M., 2012. G protein – coupled receptor 21 deletion improves insulin sensitivity in diet-induced obese mice. *The Journal of Clinical Investigation*, 122 (7), 2444–2453.

Osborn, O. and Olefsky, J. M., 2012. The cellular and signaling networks linking the immune system and metabolism in disease. *Nature Medicine*, 18 (3), 363–374.

van der Ouweland, A. M. W., Dressen, J. C. F. M., Verdijk, M., Knoers, N. V. A. M., Monnens, L. A. H., Rocchi, M., and van Oost, B. A., 1992. Mutations in the vasopressin type 2 rebeptor gene (AVPR2) associated with nephrogenic diabetes insipidus. *Nature*, 2, 99–102.

Owen, M. R., Doran, E., and Halestrap, A. P., 2000. Evidence that metformin exerts its anti-diabetic effects through inhibition of complex 1 of the mitochondrial respiratory chain. *Biochemical Society*, 614, 607–614.

Pang, T., Zhang, Z. S., Gu, M., Qiu, B. Y., Yu, L. F., Cao, P. R., Shao, W., Su, M. B., Li, J. Y., Nan, F. J., and Li, J., 2008. Small Molecule Antagonizes Autoinhibition and Activates AMP-activated Protein Kinase in Cells. *The Journal of Biological Chemistry*, 283 (23), 16051–16060.

Pappalardo, M., Shachaf, N., Basile, L., Milardi, D., Zeidan, M., Raiyn, J., Guccione, S., and Rayan, A., 2014. Sequential Application of Ligand and Structure Based Modeling Approaches to Index Chemicals for Their hH4R Antagonism. *PLoS ONE*, 9 (10), e109340.

Park, S. H., Gammon, S. R., Knippers, J. D., Paulsen, S. R., Rubink, D. S., and Winder, W. W., 2002. Phosphorylation-activity relationships of AMPK and acetyl-CoA carboxylase in muscle. *Journal of Applied Physiology,* 92 (6), 2475-2482.

Park, S. H., Ryu, S. Y., Yu, W. J., Han, Y. E., Ji, Y. S., Oh, K., Sohn, J. W., Lim, A.,

Jeon, J. P., Lee, H., Lee, K. H., Lee, S. H., Berggren, P. O., Jeon, J. H., and Ho, W. K., 2013. Leptin promotes KATP channel trafficking by AMPK signaling in pancreatic-cells. *Proceedings of the National Academy of Sciences of the United States of America*, 110 (31), 12673–12678.

Patsouris, D., Li, P. P., Thapar, D., Chapman, J., Olefsky, J. M., and Neels, J. G., 2008. Ablation of CD11c-positive cells normalizes insulin sensitivity in obese insulin resistant animals. *Cell Metabolism*, 8 (4), 301–309.

Paula, G. S. M., Souza, L. L., Cabanelas, A., Bloise, F. F., Mello-Coelho, V., Wada, E., Ortiga-Carvalho, T. M., Oliveira, K. J., and Pazos-Moura, C. C., 2010. Female mice target deleted for the neuromedin B receptor have partial resistance to diet-induced obesity. *The Journal of Physiology*, 588 (Pt 9), 1635–1645.

Pedroso, J. A. B., Buonfiglio, D. C., Cardinali, L. I., Furigo, I. C., Ramos-Lobo, A. M., Tirapegui, J., Elias, C. F., and Donato, J., 2014. Inactivation of SOCS3 in leptin receptor-expressing cells protects mice from diet-induced insulin resistance but does not prevent obesity. *Molecular Metabolism*, 3 (6), 608–618.

Pernicova, I. and Korbonits, M., 2014. Metformin-mode of action and clinical implications for diabetes and cancer. *Nature Reviews Endocrinology*, 10 (3), 143–156.

Perola, E. and Charifson, P. S., 2004. Conformational analysis of drug-like molecules bound to proteins: an extensive study of ligand reorganization upon binding. *Journal of Medicinal Chemistry*, 47 (10), 2499–2510.

Pessin, J. E., Thurmond, D. C., Elmendorf, J. S., Coker, K. J., and Okada, S., 1999. Molecular Basis of Insulin- stimulated GLUT4 Vesicle Trafficking. *The Journal of Biological Chemistry*, 274 (5), 2593–2596.

Pierce, K. L. and Lefkowitz, R. J., 2001. Classical and new roles of β-arrestins in the regulation of G-protein-coupled receptors. *Nature Reviews Neuroscience*, 2 (10), 727–733.

Pierce, K. L., Premont, R. T., and Lefkowitz, R. J., 2002. Seven-transmembrane receptors. *Nature Reviews Molecular Cell Biology*, 3 (9), 639–650.

Pirola, L., Johnston, A. M., and Van Obberghen, E., 2004. Modulation of insulin action. *Diabetologia*, 47 (2), 170–184.

Pospisilik, J. A., Knauf, C., Joza, N., Benit, P., Orthofer, M., Cani, P. D., Ebersberger, I., Nakashima, T., Sarao, R., Neely, G., Esterbauer, H., Kozlov, A., Kahn, C. R., Kroemer, G., Rustin, P., Burcelin, R., and Penninger, J. M., 2007. Targeted Deletion of AIF Decreases Mitochondrial Oxidative Phosphorylation and Protects from Obesity and Diabetes. *Cell*, 131 (3), 476–491.

Prasad, A., Jia, Y., Chakraborty, A., Li, Y., Jain, S. K., Zhong, J., Roy, S. G., Loison, F., Mondal, S., Sakai, J., Blanchard, C., Snyder, S. H., and Luo, H. R., 2011. Inositol hexakisphosphate kinase 1 regulates neutrophil function in innate immunity by inhibiting phosphatidylinositol-(3,4,5)-trisphosphate signaling. *Nature immunology*, 12 (8), 752–760.

Premont, R. T., Inglese, J., and Lefkowitz, R. J., 1995. Protein kinases that phosphorylate activated G protein-coupled receptors. *The FASEB Journal*, 9 (2), 175–182.

Priest, B. T., Bell, I. M., and Garcia, M. L., 2008. Role of hERG potassium channel assays in drug development. *Channels*, 2 (2), 87–93.

Qatanani, M. and Lazar, M. A., 2007. Mechanisms of obesity-associated insulin resistance: Many choices on the menu. *Genes and Development*, 21 (12), 1443–

1455.

Quan, W., Lim, Y. M., and Lee, M. S., 2012. Role of autophagy in diabetes and endoplasmic reticulum stress of pancreatic β-cells. *Experimental and Molecular Medicine*, 44 (2), 81–88.

Quintens, R., Singh, S., Lemaire, K., De Bock, K., Granvik, M., Schraenen, A., Vroegrijk, I. O. C. M., Costa, V., Van Noten, P., Lambrechts, D., Lehnert, S., Van Lommel, L., Thorrez, L., De Faudeur, G., Romijn, J. A., Shelton, J. M., Scorrano, L., Lijnen, H. R., Voshol, P. J., Carmeliet, P., Mammen, P. P. A., and Schuit, F., 2013. Mice Deficient in the Respiratory Chain Gene Cox6a2 Are Protected against High-Fat Diet-Induced Obesity and Insulin Resistance. *PLoS ONE*, 8 (2), e56719.

Ravinet Trillou, C., Delgorge, C., Menet, C., Arnone, M., and Soubrié, P., 2004. CB1 cannabinoid receptor knockout in mice leads to leanness, resistance to diet-induced obesity and enhanced leptin sensitivity. *International Journal of Obesity*, 28 (4), 640–648.

Rayasam, G. V., Tulasi, V. K., Sodhi, R., Davis, J. A., and Ray, A., 2009. Glycogen synthase kinase 3: more than a namesake. *British Journal of Pharmacology*, 156 (6), 885–898.

Rehm, A., 1997. Assembly and Intracellular Targeting of the βγ Subunits of Heterotrimeric G Proteins. *The Journal of Cell Biology*, 137 (2), 305–317.

Reinehr, T., 2013. Type 2 diabetes mellitus in children and adolescents. *World Journal of Diabetes*, 4 (6), 270.

Rena, G., Pearson, E. R., and Sakamoto, K., 2013. Molecular mechanism of action of metformin: Old or new insights? *Diabetologia*, 56 (9), 1898–1906.

Rhee, S. G., 2001. Regulation of Phosphoinositide-specific Phospholipase C. *Annual Review of Biochemistry*, 70, 281–312.

Richter, E. A. and Ruderman, N. B., 2009. AMPK and the Biochemistry of Exercise: Implications for Human Health and Disease. *The Biochemical Journal*, 2 (418), 261–275.

Robertson, R. P., Halter, J. B., and Porte, D., 1976. A role for α-adrenergic receptors in abnormal insulin secretion in diabetes mellitus. *The Journal of Clinical Investigation*, 57 (3), 791–795.

Rochester, C. D. and Akiyode, O., 2014. Novel and emerging diabetes mellitus drug therapies for the type 2 diabetes patient. *World Journal of Diabetes*, 5 (3), 305–15.

Rodgers, R. J., Ishii, Y., Halford, J. C. G., and Blundell, J. E., 2002. Orexins and appetite regulation. *Neuropeptides*, 36 (5), 303–325.

Romero-Zerbo, S. Y., Rafacho, A., Díaz-Arteaga, A., Suárez, J., Quesada, I., Imbernon, M., Ross, R. A., Dieguez, C., de Fonseca, F. R., Nogueiras, R., Nadal, A., and Bermúdez-Silva, F. J., 2011. Role for the putative cannabinoid receptor GPR55 in the islets of Langerhans. *Journal of Endocrinology*, 211 (2), 177–185.

Rosenbaum, D. M., Rasmussen, S. G. F., and Kobilka, B. K., 2009. The structure and function of G-protein-coupled receptors. *Nature*, 459, 356–363.

Rosengren, A. H., Jokubka, R., Tojjar, D., Granhall, C., Hansson, O., Li, D. Q., Nagaraj, V., Reinbothe, T. M., Tuncel, J., Eliasson, L., Groop, L., Rorsman, P., Salehi, A., Lyssenko, V., Luthman, H., and Renström, E., 2010. Overexpression of α2A-adrenergic receptors contributes to type 2 diabetes. *Science*, 327 (5962), 217–220.

Rubinsztein, D. C., Codogno, P., and Levine, B., 2012. Autophagy modulation as a potential therapeutic target for diverse diseases. *Nature Reviews Drug Discovery*, 11 (9), 709–730.

Ruderman, N. B., Saha, A. K., Vavvas, D., and Witters, L. A., 1999. Malonyl-CoA, fuel sensing, and insulin resistance. *The American Journal of Physiology Endocrinology and Metabolism*, 276 (1), E1–E18.

Rzonca, S. O., Suva, L. J., Gaddy, D., Montague, D. C., and Lecka-Czernik, B., 2004. Bone Is a Target for the Antidiabetic Compound Rosiglitazone. *Endocrinology*, 145 (1), 401–406.

Sabio, G. and Davis, R. J., 2014. TNF and MAP kinase signaling pathways. *Seminars in Immunology*, 26 (3), 237–245.

Sachithanandan, N., Fam, B. C., Fynch, S., Dzamko, N., Watt, M. J., Wormald, S., Honeyman, J., Galic, S., Proietto, J., Andrikopoulos, S., Hevener, A. L., Kay, T. W. H., and Steinberg, G. R., 2010. Liver-specific suppressor of cytokine signaling-3 deletion in mice enhances hepatic insulin sensitivity and lipogenesis resulting in fatty liver and obesity. *Hepatology*, 52 (5), 1632–1642.

Saiardi, A., Sciambi, C., McCaffery, J. M., Wendland, B., and Snyder, S. H., 2002. Inositol pyrophosphates regulate endocytic trafficking. *Proceedings of the National Academy of Sciences of the United States of America*, 99 (22), 14206–14211.

Samuel, B. S., Shaito, A., Motoike, T., Rey, F. E., Backhed, F., Manchester, J. K., Hammer, R. E., Williams, S. C., Crowley, J., Yanagisawa, M., and Gordon, J. I., 2008. Effects of the gut microbiota on host adiposity are modulated by the short-chain fatty-acid binding G protein-coupled receptor, Gpr41. *Proceedings of the*

National Academy of Sciences of the United States of America, 105 (43), 16767–16772.

Sanders, M. J., Grondin, P. O., Hegarty, B. D., Snowden, M. A., and Carling, D., 2007. Investigating the mechanism for AMP activation of the AMP-activated protein kinase cascade. *The Biochemical Journal*, 403 (1), 139–148.

Sano, H., 2003. Insulin-stimulated Phosphorylation of a Rab GTPase-activating Protein Regulates GLUT4 Translocation. *The Journal of Biological Chemistry*, 278 (17), 14599–14602.

Sassmann, A., Gier, B., Gröne, H. J., Drews, G., Offermanns, S., and Wettschureck, N., 2010. The Gq/G11-mediated signaling pathway is critical for autocrine potentiation of insulin secretion in mice. *The Journal of Clinical Investigation*, 120 (6), 2184–2193.

Schweitzer, G. G., Arias, E. B., and Cartee, G. D., 2012. Sustained postexercise increases in AS160 Thr^{642} and Ser^{588} phosphorylation in skeletal muscle without sustained increases in kinase phosphorylation. *Journal of Applied Physiology*, 113 (12), 1852–61.

Scott, J. W., van Denderen, B. J. W., Jorgensen, S. B., Honeyman, J. E., Steinberg, G. R., Oakhill, J. S., Iseli, T. J., Koay, A., Gooley, P. R., Stapleton, D., and Kemp, B. E., 2008. Thienopyridone Drugs Are Selective Activators of AMP-Activated Protein Kinase β1-Containing Complexes. *Chemistry and Biology*, 15 (11), 1220–1230.

Seasholtz, T. M., Majumdar, M., and Brown, J. H., 1999. Rho as a mediator of G protein-coupled receptor signaling. *Molecular Pharmacology*, 55 (6), 949–956.

Senn, J. J., Klover, P. J., Nowak, I. A., and Mooney, R. A., 2002. Interleukin-6 induces

cellular insulin resistance in hepatocytes. *Diabetes*, 51 (12), 3391–3399.

Shackelford, D. B. and Shaw, R. J., 2009. The LKB1-AMPK pathway: metabolism and growthcontrol in tumor suppression. *Nature Reviews Cancer*, 9 (8), 563–575.

Shah, M., Kola, B., Bataveljic, A., Arnett, T. R., Viollet, B., Saxon, L., Korbonits, M., and Chenu, C., 2010. AMP-activated protein kinase (AMPK) activation regulates in vitro bone formation and bone mass. *Bone*, 47 (2), 309–319.

Shapiro, H., Shachar, S., Sekler, I., Hershfinkel, M., and Walker, M. D., 2005. Role of GPR40 in fatty acid action on the β cell line INS-1E. *Biochemical and Biophysical Research Communications*, 335 (1), 97–104.

Sharma, G. and Prossnitz, E. R., 2011. Mechanisms of estradiol-induced insulin secretion by the G protein-coupled estrogen receptor GPR30/GPER in pancreatic β-cells. *Endocrinology*, 152 (8), 3030–3039.

Shenoy, S. K., Drake, M. T., Nelson, C. D., Houtz, D. A., Xiao, K., Madabushi, S., Reiter, E., Premont, R. T., Lichtarge, O., and Lefkowitz, R. J., 2006. β-arrestin-dependent, G protein-independent ERK1/2 activation by the β2 adrenergic receptor. *The Journal of Biological Chemistry*, 281 (2), 1261–1273.

Shepherd, P. R., Withers, D. J., and Siddle, K., 1998. Phosphoinositide 3-kinase: the key switch mechanism in insulin signalling. *The Biochemical Journal*, 333 (3), 471–490.

Shi, G., Partida-Sánchez, S., Misra, R. S., Tighe, M., Borchers, M. T., Lee, J. J., Simon, M. I., and Lund, F. E., 2007. Identification of an alternative Gαq-dependent chemokine receptor signal transduction pathway in dendritic cells and granulocytes. *The Journal of Experimental Medicine*, 204 (11), 2705–2718.

Siderovski, D. P. and Willard, F. S., 2005. The GAPs, GEFs, and GDIs of heterotrimeric G-protein α-subunits. *International Journal of Biological Sciences*, 1 (2), 51–66.

Siehler, S., 2009. Regulation of RhoGEF proteins by G12/13-coupled receptors. *British Journal of Pharmacology*, 158 (1), 41–49.

Silha, J. V., Krsek, M., Skrha, J. V., Sucharda, P., Nyomba, B. L. G., and Murphy, L. J., 2003. Plasma resistin, adiponectin and leptin levels in lean and obese subjects: Correlations with insulin resistence. *European Journal of Endocrinology*, 149 (4), 331–335.

Simon-Szabó, L., Kokas, M., Mandl, J., Kéri, G., and Csala, M., 2014. Metformin attenuates palmitate-induced endoplasmic reticulum stress, serine phosphorylation of IRS-1 and apoptosis in rat insulinoma cells. *PLoS ONE*, 9 (6), E978–7.

Singh, A. S., Mulder, C., Twisk, J. W. R., van Mechelen, W., and Chinapaw, M. J. M., 2008. Tracking of childhood overweight into adulthood: a systematic review of the literature. *Obesity Reviews*, 9 (5), 474–488.

Sivaprasadarao, A., and Findlay, J. B., 1988a. The interaction of retinol-binding protein with its plasma-membrane receptor, *The Biochemical Journal,* 255 (2), 561-569.

Sivaprasadarao, A., and Findlay, J. B, 1988b. The mechanism of uptake of retinol by plasma-membrane vesicles, *The Biochemical Journal*, 255 (2), 571-9.

Smith, P. K., Krohn, R. I., Hermanson, G. T., Mallia, A. K., Gartner, F. H., Provenzano, M. D., Fujimoto, E. K., Goeke, N. M., Olson, B. J., and Klenk, D. C., 1985. Measurement of protein using bicinchoninic acid. *Analytical Biochemistry*, 150 (1), 76–85.

Smith, R. J., Sam, L. M., Justen, J. M., Bundy, G. L., Bala, G. A., and Bleasdale, J. E., 1990. Receptor-coupled signal transduction in human polymorphonuclear neutrophils: effects of a novel inhibitor of phospholipase C-dependent processes on cell responsiveness. *The Journal of Pharmacology and Experimental Therapeutics*, 253 (2), 688–697.

Smrcka, A. V., 2008. G protein βγ subunits: Central mediators of G protein-coupled receptor signalling. *Cellular and Molecular Life Sciences*, 65 (14), 2191–2214.

Solinas, G. and Karin, M., 2010. JNK1 and IKKβ : molecular links between obesity and metabolic dysfunction. *The FASEB Journal*, 24 (8), 2596–2611.

Sommer, U., Schmid, C., Sobota, R. M., Lehmann, U., Stevenson, N. J., Johnston, J. A., Schaper, F., Heinrich, P. C., and Haan, S., 2005. Mechanisms of SOCS3 Phosphorylation upon Interleukin-6 Stimulation: Contributions if Src- and Receptor-Tyrosine Kinases. *The Journal of Biological Chemistry*, 280 (36), 31478–31488.

Sørensen, H., Winzell, M. S., Brand, C. L., Fosgerau, K., Gelling, R. W., Nishimura, E., and Ahren, B., 2006. Glucagon receptor knockout mice display increased insulin sensitivity and impaired beta-cell function. *Diabetes*, 55 (12), 3463–3469.

Spinazzi, M., Casarin, A., Pertegato, V., Salviati, L., and Angelini, C., 2012. Assessment of mitochondrial respiratory chain enzymatic activities on tissues and cultured cells. *Nature Protocols*, 7 (6), 1235–1246.

Stebbins, J. L., De, S. K., Machleidt, T., Becattini, B., Vazquez, J., Kuntzen, C., Chen, L. H., Cellitti, J. F., Riel-Mehan, M., Emdadi, A., Solinas, G., Karin, M., and Pellecchia, M., 2008. Identification of a new JNK inhibitor targeting the JNK-JIP interaction site. *Proceedings of the National Academy of Sciences of the United*

States of America, 105 (43), 16809–16813.

Stein, S. A., Lamos, E. M., and Davis, S. N., 2013. A review of the efficacy and safety of oral antidiabetic drugs. *Expert Opinion on Drug Safety*, 12 (2), 153–175.

Stein, S. C., Woods, A., Jones, N. A., Davison, M. D., and Carling, D., 2000. The regulation of AMP-activated protein kinase by phosphorylation. *The Biochemical Journal*, 345 (3), 437–443.

Steinberg, G. R. and Kemp, B. E., 2009. AMPK in Health and Disease. *Physiological Reviews*, 89 (3), 1025–1078.

Steneberg, P., Rubins, N., Bartoov-Shifman, R., Walker, M. D., and Edlund, H., 2005. The FFA receptor GPR40 links hyperinsulinemia, hepatic steatosis, and impaired glucose homeostasis in mouse. *Cell Metabolism*, 1 (4), 245–258.

Stephens, L., Radenberg, T., Thiel, U., Vogel, G., Khoo, K. H., Dell, A., Jackson, T. R., Hawkins, P. T., and Mayr, G. W., 1993. The detection, purification, structural characterization, and metabolism of diphosphoinositol pentakisphosphate(s) and bisdiphosphoinositol tetrakisphosphate(s). *The Journal of Biological Chemistry*, 268 (6), 4009–4015.

Stevens, R. C., Cherezov, V., Katritch, V., Abagyan, R., Kuhn, P., Rosen, H., and Wüthrich, K., 2013. The GPCR Network: a large-scale collaboration to determine human GPCR structure and function. *Nature Reviews Drug Discovery*, 12 (1), 25–34.

Stockert, J. A. and Devi, L. A., 2015. Advancements in therapeutically targeting orphan GPCRs. *Frontiers in Pharmacology*, 6, 1–8.

Strathmann, M. P. and Simon, M. I., 1991. Gα 12 and Gα 13 subunits define a fourth

class of G protein alpha subunits. *Proceedings of the National Academy of Sciences of the United States of America*, 88 (13), 5582–5586.

Strowski, M. Z., Kohler, M., Chen, H. Y., Trumbauer, M. E., Li, Z., Szalkowski, D., Gopal-Truter, S., Fisher, J. K., Schaeffer, J. M., Blake, A. D., Zhang, B. B., and Wilkinson, H. A., 2003. Somatostatin receptor subtype 5 regulates insulin secretion and glucose homeostasis. *Molecular Endocrinology*, 17 (1), 93–106.

Sullivan, J. E., Brocklehurst, K. J., Marley, A. E., Carey, F., Carling, D., and Beri, R. K., 1994. Inhibition of lipolysis and lipogenesis in isolated rat adipocytes with AICAR, a cell-permeable activator of AMP-activated protein kinase. *FEBS Letters*, 353 (1), 33–36.

Sumara, G., Formentini, I., Collins, S., Sumara, I., Windak, R., Bodenmiller, B., Ramracheya, R., Caille, D., Jiang, H., Platt, K. A., Meda, P., Aebersold, R., Rorsman, P., and Ricci, R., 2009. Regulation of PKD by the MAPK p38δ in Insulin Secretion and Glucose Homeostasis. *Cell*, 136 (2), 235–248.

Sun, D., Li, S., Wu, H., Zhang, M., Zhang, X., Wei, L., Qin, X., and Gao, E., 2015. Oncostatin M (OSM) protects against cardiac ischaemia/reperfusion injury in diabetic mice by regulating apoptosis, mitochondrial biogenesis and insulin sensitivity. *Journal of Cellular and Molecular Medicine*, 19 (6), 1296–1307.

Sun, L. and Ye, R. D., 2012. Role of G protein-coupled receptors in inflammation. *Acta Pharmacologica Sinica*, 33 (3), 342–350.

Sun, Y., Butte, N. F., Garcia, J. M., and Smith, R. G., 2008. Characterization of adult ghrelin and ghrelin receptor knockout mice under positive and negative energy balance. *Endocrinology*, 149 (2), 843–850.

Sundaram, M., Sivaprasadarao, A., DeSousa, M. M., and Findlay, J. B., 1998. The

transfer of retinol from serum retinol-binding protein to cellular retinol-binding protein is mediated by a membrane receptor. *The Journal of Biological Chemistry*, 273 (6), 3336–42.

Taggart, A. K. P., Kero, J., Gan, X., Cai, T. Q., Cheng, K., Ippolito, M., Ren, N., Kaplan, R., Wu, K., Wu, T. J., Jin, L., Liaw, C., Chen, R., Richman, J., Connolly, D., Offermanns, S., Wright, S. D., and Waters, M. G., 2005. (D)-β-Hydroxybutyrate inhibits adipocyte lipolysis via the nicotinic acid receptor PUMA-G. *The Journal of Biological Chemistry*, 280 (29), 26649–26652.

Tan, Y., Ichikawa, T., Li, J., Si, Q., Yang, H., Chen, X., Goldblatt, C. S., Meyer, C. J., Li, X., Cai, L., and Cui, T., 2011. Diabetic Downregulation of Nrf2 Activity via ERK Contributes to Oxidative Stress-Induced Insulin Resistance in Cardiac Cells In Vitro and In Vivo. *Diabetes*, 60 (2), 625–633.

Tang, X., Wang, Y., Li, D., Luo, J., and Liu, M., 2012. Orphan G protein-coupled receptors (GPCRs): biological functions and potential drug targets. *Acta Pharmacologica Sinica*, 33 (3), 363–371.

Tao, Y. X., 2008. Constitutive activation of G protein-coupled receptors and diseases: Insights into mechanisms of activation and therapeutics. *Pharmacology and Therapeutics.* 120 (2), 129-148.

Tautermann, C. S., 2014. GPCR structures in drug design, emerging opportunities with new structures. *Bioorganic and Medicinal Chemistry Letters*, 24 (17), 4073–4079.

Tavakol, S., Kashani, I. R., Azami, M., Khoshzaban, A., Tavakol, B., Kharrazi, S., Ebrahimi, S., and Sorkhabadi, S. M. R., 2012. *In vitro* and *in vivo* investigations on bone regeneration potential of laminated hydroxyapatite/gelatin nanocomposite scaffold along with DBM. *Journal of Nanoparticle Research*, 14 (1265), doi:

10.1007/s11051-012-1265-y

Tecott, L. H., Sun, L. M., Akana, S. F., Strack, A. M., Lowenstein, D. H., Dallman, M. F., and Julius, D., 1995. Eating disorder and epilepsy in mice lacking 5-HT2c serotonin receptors. *Nature*, 374 (6522), 542–546.

Thiebaud, D., Jacot, E., DeFronzo, R. A., Maeder, E., Jequier, E., and Felber, J. P., 1982. The effect of graded doses of insulin on total glucose uptake, glucose oxidation, and glucose storage in man. *Diabetes*, 31 (11), 957–963.

Thompson, P. E. and Findlay, J. B., 1984. Phosphorylation of ovine rhodopsin. Identification of the phosphorylated sites. *The Biochemical Journal*, 220 (3), 773–80.

Thulé, P. M. and Umpierrez, G., 2014. Sulfonylureas: A New Look at Old Therapy. *Current Diabetes Reports*, 14 (4), 473.

Tobin, A. B., 2008. G-protein-coupled receptor phosphorylation: where, when and by whom. *British Journal of Pharmacology*, 153, S167–S176.

Toker, A. and Marmiroli, S., 2014. Signaling specificity in the Akt pathway in biology and disease. *Advances in Biological Regulation*, 55, 28–38.

Tolson, K. P., Garcia, C., Yen, S., Simonds, S., Stefanidis, A., Lawrence, A., Smith, J. T., and Kauffman, A. S., 2014. Impaired kisspeptin signaling decreases metabolism and promotes glucose intolerance and obesity. *The Journal of Clinical Investigation*, 124 (7), 3075–3079.

Tomkin, G. H., 2014. Treatment of type 2 diabetes, lifestyle, GLP1 agonists and DPP4 inhibitors. *World Journal of Diabetes*, 5 (5), 636–650.

Tornqvist, H. E., Pierce, M. W., Frackelton, A. R., Nemenoff, R. A., and Avruch, J.,

1987. Identification of insulin receptor tyrosine residues autophosphorylated in vitro. *The Journal of Biological Chemistry*, 262 (21), 10212–9.

Tournier, C., Dong, C., Turner, T. K., Jones, S. N., Flavell, R. A., and Davis, R. J., 2001. MKK7 is an essential component of the JNK signal transduction pathway activated by proinflammatory cytokines. *Genes and Development*, 15 (11), 1419–1426.

Treebak, J. T., Glund, S., Deshmukh, A., Klein, D. K., Long, Y. C., Jensen, T. E., Jørgensen, S. B., Viollet, B., Andersson, L., Neumann, D., Wallimann, T., Richter, E. A., Chibalin, A. V, Zierath, J. R., and Wojtaszewski, J. F. P., 2006. AMPK-mediated AS160 phosphorylation in skeletal muscle is dependent on AMPK catalytic and regulatory subunits. *Diabetes*, 55 (7), 2051–8.

Tremblay, F., Perreault, M., Klaman, L. D., Tobin, J. F., Smith, E., and Gimeno, R. E., 2007. Normal food intake and body weight in mice lacking the G protein-coupled receptor GPR39. *Endocrinology*, 148 (2), 501–506.

Trinquet, E., Fink, M., Bazin, H., Grillet, F., Maurin, F., Bourrier, E., Ansanay, H., Leroy, C., Michaud, A., Durroux, T., Maurel, D., Malhaire, F., Goudet, C., Pin, J. P., Naval, M., Hernout, O., Chrétien, F., Chapleur, Y., and Mathis, G., 2006. D-myo-Inositol 1-phosphate as a surrogate of D-myo-inositol 1,4,5-tris phosphate to monitor G protein-coupled receptor activation. *Analytical Biochemistry*, 358 (1), 126–135.

Tsutsumi, C., Okuno, M., Tannous, L., Piantedosi, R., Allan, M., Goodman, D. S., and Blaner, W. S., 1992. Retinoids and retinoid-binding protein expression in rat adipocytes. *The Journal of Biological Chemistry*, 267, 1805–1810.

Tuncman, G., Hirosumi, J., Solinas, G., Chang, L., Karin, M., and Hotamisligil, G. S.,

2006. Functional in vivo interactions between JNK1 and JNK2 isoforms in obesity and insulin resistance. *Proceedings of the National Academy of Sciences of the United States of America*, 103 (28), 10741–6.

Turban, S., Stretton, C., Drouin, O., Green, C. J., Watson, M. L., Gray, A., Ross, F., Lantier, L., Viollet, B., Hardie, D. G., Marette, A., and Hundal, H. S., 2012. Defining the contribution of AMP-activated protein kinase (AMPK) and protein kinase C (PKC) in regulation of glucose uptake by metformin in skeletal muscle cells. *The Journal of Biological Chemistry*, 287 (24), 20088–99.

Turner, N., Li, J., Gosby, A., To, S. W. C., Cheng, Z., Miyoshi, H., Taketo, M. M., Cooney, G. J., Kraegen, E. W., James, D. E., Hu, L., and Li, J., 2008. Berberine and Its More Biologically Available Derivative Dihyroberberine, Inhibit Mitochondrial Respiration. *Diabetes*, 57 (May), 1414–1418.

Ueda, H., Morishita, R., Narumiya, S., Kato, K., and Asano, T., 2004. Gαq/11 signaling induces apoptosis through two pathways involving reduction of Akt phosphorylation and activation of RhoA in HeLa cells. *Experimental Cell Research*, 298 (1), 207–217.

Ueki, K., Kondo, T., and Kahn, C. R., 2004. Suppressor of cytokine signaling 1 (SOCS-1) and SOCS-3 cause insulin resistance through inhibition of tyrosine phosphorylation of insulin receptor substrate proteins by discrete mechanisms. *Molecular and Cellular Biology*, 24 (12), 5434–46.

Uysal, K. T., Wiesbrock, S. M., Marino, M. W., and Hotamisligil, G. S., 1997. Protection from obesity-induced insulin resistance in mice lacking TNF-α function. *Nature*, 389 (6651), 610–614.

Vadlakonda, L., Dash, A., Pasupuleti, M., Anil Kumar, K., and Reddanna, P., 2013. The

Paradox of Akt-mTOR Interactions. *Frontiers in Oncology*, 3 (June), 165.

Vandanmagsar, B., Youm, Y., Ravussin, A., Galgani, J. E., Stadler, K., Mynatt, R. L., Ravussin, E., and Stephens, J. M., 2011. The NALP3/NLRP3 Inflammasome Instigates Obesity-Induced Autoinflammation and Insulin Resistance. *Nature Medicine*, 17 (2), 179–188.

Venkataraman, C. and Kuo, F., 2005. The G-protein coupled receptor, GPR84 regulates IL-4 production by T lymphocytes in response to CD3 crosslinking. *Immunology Letters*, 101 (2), 144–153.

Vernochet, C., Mourier, A., Bezy, O., Macotela, Y., Boucher, J., Rardin, M. J., An, D., Lee, K. Y., Ilkayeva, O. R., Zingaretti, C. M., Emanuelli, B., Smyth, G., Cinti, S., Newgard, C. B., Gibson, B. W., Larsson, N. G., and Kahn, C. R., 2012. Adipose-Specific Deletion of TFAM Increases Mitochondrial Oxidation and Protects Mice against Obesity and Insulin Resistance. *Cell Metabolism*, 16 (6), 765–776.

Vingtdeux, V., Chandakkar, P., Zhao, H., Davies, P., and Marambaud, P., 2011. Small-Molecule Activators of AMP-Activated Protein Kinase (AMPK), RSVA314 and RSVA405, Inhibit Adipogenesis. *Molecular Medicine*, 17 (9-10), 1022–1030.

Viollet, B., Horman, S., Leclerc, J., Lantier, L., Foretz, M., Billaud, M., Giri, S., and Andreelli, F., 2010. AMPK inhibition in health and disease. *Critical Reviews in Biochemistry and Molecular Biology*, 45 (4), 276–295.

Vogt, S., Grosse, R., Schultz, G., and Offermanns, S., 2003. Receptor-dependent RhoA activation in G12/G13-deficient cells. Genetic evidence for an involvement of Gq/G11. *The Journal of Biological Chemistry*, 278 (31), 28743–28749.

Voigt, J. P., Schade, R., Fink, H., and Hörtnagl, H., 2002. Role of 5-HT1A receptors in the control of food intake in obese Zucker rats of different ages. *Pharmacology,*

Biochemistry, and Behavior, 72 (2), 403–409.

Wallenius, V., Wallenius, K., Ahren, B., Rudling, M., Carlsten, H., Dickson, S. L., Ohlsson, C., and Jansson, J. O., 2002. Interleukin-6-deficient mice develop mature-onset obesity. *Nature Medicine*, 8 (1), 75–79.

Wess, J., 1997. G-protein-coupled receptors: molecular mechanisms involved in receptor activation and selectivity of G-protein recognition. *The FASEB Journal*, 11 (5), 346–54.

Weyer, C., Funahashi, T., Tanaka, S., Hotta, K., Matsuzawa, Y., Pratley, R. E., and Tataranni, P. A., 2001. Hypoadiponectinemia in Obesity and Type 2 Diabetes : Close Association with Insulin Resistance and Hyperinsulinemia. *The Journal of Endochrinology and Metabolism*, 86 (5), 1930–1935.

Wheaton, W. W., Weinberg, S. E., Hamanaka, R. B., Soberanes, S., Sullivan, L. B., Anso, E., Glasauer, A., Dufour, E., Mutlu, G. M., Scott Budigner, G. R., and Chandel, N. S., 2014. Metformin inhibits mitochondrial complex I of cancer cells to reduce tumorigenesis. *eLife*, (3), 1–18.

White, M. F., 1997. The insulin signalling system and the IRS proteins. *Diabetologia*, 40 (2), 2–17.

Wiederstein, M. and Sippl, M. J., 2007. ProSA-web: interactive web service for the recognition of errors in three-dimensional structures of proteins. *Nucleic Acids Research*, 35 (Web Server issue), W407–10.

Wikström, M., 1984. Two protons are pumped from the mitochondrial matrix per electron transferred between NADH and ubiquinone. *FEBS Letters*, 169 (2), 300–304.

Wilcox, G., 2005. Insulin and insulin resistance. *The Clinical Biochemist Reviews*, 26 (2), 19–39.

Winder, W. W. and Hardie, D. G., 1996. Inactivation of acetyl-CoA carboxylase and activation of AMP-activated protein kinase in muscle during exercise. *The American Journal of Physiology*, 270 (2), 299–304.

Winer, S., Chan, Y., Paltser, G., Truong, D., Tsui, H., Dorfman, R., Wang, Y., Zielenski, J., Mastronardi, F., Maezawa, Y., Drucker, D., Engleman, E., and Winer, D., 2009. Normalization of Obesity-Associated Insulin Resistance through Immunotherapy: CD4+ T Cells Control Glucose Homeostasis. *Nature Medicine*, 15 (8), 921–929.

Woods, A., Johnstone, S. R., Dickerson, K., Leiper, F. C., Fryer, L. G. D., Neumann, D., Schlattner, U., Wallimann, T., Carlson, M., and Carling, D., 2003. LKB1 Is the Upstream Kinase in the AMP-Activated Protein Kinase Cascade. *Current Biology*, 13 (22), 2004–2008.

World Health Organization, 2014. Global status report on noncommunicable diseases 2014. *Geneva, World Health Organization*.

Wundenberg T., and Mayr, G. W., 2012. Synthesis and biological actions of diphosphoinositol phosphates (inositol pyrophosphates), regulators of cell homeostasis. *Biological Chemistry,* 393 (9), 979–998.

Xiang, Z., 2006. Advances in homology protein structure modeling. *Current Protein and Peptide Science*, 7 (3), 217–227.

Xiao, B., Sanders, M. J., Underwood, E., Heath, R., Mayer, F. V, Carmena, D., Jing, C., Walker, P. A., Eccleston, J. F., Haire, L. F., Saiu, P., Howell, S. A., Aasland, R., Martin, S. R., Carling, D., and Gamblin, S. J., 2011. Structure of mammalian

AMPK and its regulation by ADP. *Nature*, 472 (7342), 230–233.

Xiao, B., Sanders, M. J., Carmena, D., Bright, N. J., Haire, L. F., Underwood, E., Patel, B. R., Heath, R. B., Walker, P. A., Hallen, S., Giordanetto, F., Martin, S. R., Carling, D., and Gamblin, S. J., 2013. Structural basis of AMPK regulation by small molecule activators. *Nature Communications*, 4, 1–10.

Xiao, S. H., Reagan, J. D., Lee, P. H., Fu, A., Schwandner, R., Zhao, X., Knop, J., Beckmann, H., and Young, S. W., 2008. High throughput screening for orphan and liganded GPCRs. *Combinatorial Chemistry and High Throughput Screening*, 11 (3), 195–215.

Xu, J., Morinaga, H., Oh, D., Li, P., Chen, A., Talukdar, S., Lazarowski, E., Olefsky, J. M., and Kim, J. J., 2012. GPR105 Ablation Prevents Inflammation and Improves Insulin Sensitivity in Mice with Diet-Induced Obesity. *The Journal of Immunology*, 189 (4), 1992–1999.

Yamada, M., Miyakawa, T., Duttaroy, A., Yamanaka, A., Moriguchi, T., Makita, R., Ogawa, M., Chou, C. J., Xia, B., Crawley, J. N., Felder, C. C., Deng, C. X., and Wess, J., 2001. Mice lacking the M3 muscarinic acetylcholine receptor are hypophagic and lean. *Nature*, 410 (6825), 207–212.

Yamaguchii, A., Suda, T., and Komori, T., 2000. Regulation of Osteoblast Differentiation Mediated by. *Endocrine Reviews*, 21, 393–411.

Yang, L., Li, P., Fu, S., Calay, E. S., and Hotamisligil, G. S., 2010. Defective Hepatic Autophagy in Obesity Promotes ER Stress and Causes Insulin Resistance. *Cell Metabolism*, 11 (6), 467–478.

Yang, Q., Graham, T. E., Mody, N., Preitner, F., Peroni, O. D., Zabolotny, J. M., Kotani, K., Quadro, L., and Kahn, B. B., 2005. Serum retinol binding protein 4

contributes to insulin resistance in obesity and type 2 diabetes. *Nature*, 436 (7049), 356–362.

Yang, Z., Hulver, M., McMillan, R. P., Cai, L., Kershaw, E. E., Yu, L., Xue, B., and Shi, H., 2012. Regulation of Insulin and Leptin Signaling by Muscle Suppressor of Cytokine Signaling 3 (SOCS3). *PLoS ONE*, 7 (10), e47493.

Young, P. A., Leonard, S., Martin, D. S. D., and Findlay, J. B. C., 2015. The effect of Retinol Binding Protein on the Proteome of C2C12 muscle cells. *Diabetes/Metabolism Research and Reviews,* DOI: 10.1002/dmrr.2764.

Young, P. A., Leonard, S., Martin, D. S. D., and Findlay, J. B. C., 2016. Analysis of the effect of a novel therapeutic for Type II Diabetes on the proteome of a muscle cell line. *Proteomics*. 16 (**1**), 70–79.

Yu, X., McCorkle, S., Wang, M., Lee, Y., Li, J., Saha, A. K., Unger, R. H., and Ruderman, N. B., 2004. Leptinomimetic effects of the AMP kinase activator AICAR in leptin-resistant rats: prevention of diabetes and ectopic lipid deposition. *Diabetologia*, 47 (11), 2012–2021.

Yuan, M., Konstantopoulos, N., Lee, J., Hansen, L., Li, Z. W., Karin, M., and Shoelson, S. E., 2001. Reversal of obesity- and diet-induced insulin resistance with salicylates or targeted disruption of Ikkβ. *Science*, 293 (5535), 1673–1677.

Yue, J. T. Y., Burdett, E., Coy, D. H., Giacca, A., Efendic, S., and Vranic, M., 2012. Somatostatin receptor type 2 antagonism improves glucagon and corticosterone counterregulatory responses to hypoglycemia in streptozotocin-induced diabetic rats. *Diabetes*, 61 (1), 197–207.

Yun, J., Rago, C., Cheong, I., Pagliarini, R., Angenendt, P., Rajagopalan, H., Schmidt,

K., Willson, J. K., Markowitz, S., Zhou, S., Diaz Jr, L. A., Velculescu, V. E., Lengauer, C., Kinzler, K. W., Vogelstein, B., and Papadopoulos, N., 2009. Glucose deprivation contributes to the development of KRAS pathway mutations in tumor cells. *Science*, 325 (5947), 1555–1559.

Zeleznikar, R. J., Heyman, R. A., Graeff, R. M., Walseth, T. F., Dawis, S. M., Butz, E. A., and Goldberg, N. D., 1990. Evidence for compartmentalized adenylate kinase catalysis serving a high energy phosphoryl transfer function in rat skeletal muscle. *The Journal of Biological Chemistry*, 265 (1), 300–311.

Zeqiraj, E., Filippi, B. M., Deak, M., Alessi, D. R., and van Aalten, D. M. F., 2009. Structure of the LKB1-STRAD-MO25 complex reveals an allosteric mechanism of kinase activation. *Science*, 326 (5960), 1707–1711.

Zhang, W., Patil, S., Chauhan, B., Guo, S., Powell, D. R., Le, J., Klotsas, A., Matika, R., Xiao, X., Franks, R., Heidenreich, K. A., Sajan, M. P., Farese, R. V., Stolz, D. B., Tso, P., Koo, S. H., Montminy, M., and Unterman, T. G., 2006. FoxO1 Regulates Multiple Metabolic Pathways in the Liver: Effects on Gluconeogenic, Glycolytic and Lipogenic Gene Expression. *The Journal of Biological Chemistry*, 281 (15), 10105–10117.

Zhang, W., Thompson, B. J., Hietakangas, V., and Cohen, S. M., 2011. MAPK/ERK Signaling Regulates Insulin Sensitivity to Control Glucose Metabolism in Drosophila. *PLoS Genetics*, 7 (12), e1002429.

Zheng, J. and Ramirez, V. D., 2000. Inhibition of mitochondrial proton F0F1-ATPase/ATP synthase by polyphenolic phytochemicals. *British Journal of Pharmacology*, 130 (5), 1115–1123.

Zhou, Y., Wang, D., Zhu, Q., Gao, X., Yang, S., Xu, A., and Wu, D., 2009. Inhibitory

effects of A-769662, a novel activator of AMP-activated protein kinase, on 3T3-L1 adipogenesis. *Biological and Pharmaceutical Bulletin*, 32 (6), 993–998.

Zinzalla, V., Stracka, D., Oppliger, W., and Hall, M. N., 2011. Activation of mTORC2 by Association with the Ribosome. *Cell*, 144 (5), 757–768.

Zou, Y., Weis, W. I., and Kobilka, B. K., 2012. N-terminal T4 lysozyme fusion facilitates crystallization of a G protein coupled receptor. *PLoS ONE*, 7 (10), e46039.